A STUDY OF PREFABRICATED SANDWICH-PANEL BUILDING STRUCTURES

Santi Rizzo

A Thesis

in

the Centre for Building Studies,

Presented in Partial Fulfillment of the Requirements
for the degree of Doctor of Philosophy at
Concordia University
Montreal, Quebec, Canada

June 1979

ABSTRACT

A STUDY OF PREFABRICATED SANDWICH-PANEL BUILDING STRUCTURES

Santi Rizzo, Ph.D.
Concordia University, 1979

The structural behaviour of a half-scale building model made up of prefabricated light-weight aluminum frame sandwich panels and assembled with stapled connections is investigated theoretically and experimentally.

The behaviour of the stapled joints showed nonlinear shear-slippage characteristics which were simulated by stepwise polygonal within the theory.

The "Equivalent Frame Method", for the analysis of shear-wall structures, was extended to model the behaviour of sandwich shear-walls such as used in the building model.

Results from a set of four tests of the building model were compared with theoretical results. This comparison shows that the "Frame Equivalent Method" is suitable for the analysis of sandwich shear-wall structures with 2-dimensional nonlinear joint behaviour.

A comprehensive strength analysis of framed sandwich panels is shown to favourably compare with the results obtained from a set of tests. The study also shows the relative contribution of the edge-frames of the panels to the overall stiffness of the system.

The behaviour of the building model at failure was also

studied. The sequence and modes of panel failures are described. Early stages of the structural behaviour during failure may be predicted by the proposed theory.

ACKNOWLEDGEMENTS

The author is indebted to his supervisor, Dr. P. Fazio, for his encouragement and advice during the course of this study.

The author also expresses his appreciation to Profs. K.H. Ha and C. Marsh for helpful discussions and comments on this project.

Concordia University and the Centre for Building Studies are gratefully acknowledged for the use of facilities, various laboratories, Computer Centre and for the Graduate Fellowship awarded to the author.

The financial support of la Formation des Chercheurs et d'Action Concertee du Quebec (FCAC) (Equipe Fazio) and of the Natural Sciences and Engineering Research Council (NSERC) of the National Research Council of Canada, grant No. 4770, made the investigation possible. The materials required for the model were donated by the companies ALCAN and Dow Chemicals.

Sincere thanks are also expressed to the technical and secretarial staff of the Centre for the organization and execution of the experimental work and for the preparation of the manuscript. Of special note are: Denis Prud'homme, Joseph Zilka, Alfred Clarke, and Pamela O'Cain.

TABLE OF CONTENTS

LIST OF FIGURES

LIST OF TABLES

LIST OF APPENDICES

NOTATION

A	cross-section area
C	subgrade foundation (core) coefficient
E	Young's modulus
F	transverse force
G	shear modulus
H	sandwich panel height
I	moment of inertia
M	bending moment
N	axial force
P	compression load
R	stapled joints stiffness
S	section modulus
V	shear force
X	global X-axis
Y	global Y-axis
Z	global Z-axis
INC	increment
a	plastic zone
b	width
c	sandwich core thickness
d	sandwich skin inter-axes distance (d=c+t)
f	shear shape factor
h	sandwich panel depth
i	node number
j	node number
k	variable for spring

Notation - continued

l	beam span
p	uniformly distributed line load
q	uniformly distributed surface load
s	shear span
t	sandwich facing (or skin) thickness
w	wide-column beam rigid arm
x	local X-axis
y	local Y-axis
z	local Z-axis

MATRICES

{F}	vector of local member forces
{δ}	vector of local member displacement
[S]	local stiffness matrix of member
[K]	global stiffness matrix of member
[T]	transfomration matrix for parallel axes
[W]	transformation matrix for wide rigid arms
[R]	rotation matrix
[K]	stiffness matrix of global structure
{Δ}	vector of global structure displacement
{P}	vector of external nodal loads.

GREEK SYMBOLS

α	coefficient of limit load increment
β	coefficient of limit load increment
δ	wrinkling wave amplitude

Notation - continued

δ_o	initial δ_o
ϵ	normal strain
μ	Poisson's ratio
σ	normal stress
Δ	stapled joint shear slippage
Φ	coefficient of shear effect on beam deflection
ϕ	angle
γ	tangential strain
τ	tangential stress
Ω	accumulated γ

SUBSCRIPTS

c	core
cr	critical, post wrinkling
f	stiffening wood frame
p	composite sandwich panel
pr	proportional limit
s	sandwich panel skin or facing
sp	spring
sh	shrinkage
u	ultimate
y	yielding
wr	wrinkling
k	spring variable

Notation - continued

X	global X-axis
Y	global Y-axis
Z	global Z-axis
x	local X-axis
y	local Y-axis
z	local Z-axis

SUPERSCRIPTS

t	transpose of matrix
k	spring variable

CONCORDIA UNIVERSITY

CURRICULUM VITAE

NAME: SANTI RIZZO

ADDRESS: 228 Darwin, #403, Verdun, Quebec

DATE OF BIRTH: October 10, 1944

PLACE OF BIRTH: Agrigento FIRST LANGUAGE: Italian

THESIS TITLE: A STUDY OF PREFABRICATED SANDWICH-PANEL BUILDING STRUCTURES

DEPARTMENT: Centre for Building Studies THESIS SUPERVISOR: Dr. P. Fazio

MAJOR AREA(S) OF STUDY: Building Structures

UNIVERSITY EDUCATION:

Degree	Major Subject	University	Year
Civil Engineering	Structures	Palermo, Italy	1969

EXPERIENCE (RESEARCH OR RELATED EXPERIENCE):

Dates	Institution	Subject
8/69-10/71	Professional Engineer	Structures
1971-1976	Faculty of Engineering, University of Palermo, Italy	Structures

PUBLICATIONS: (see attached list)

SCHOLARSHIPS AND AWARDS (DURING UNIVERSITY CAREER):

Award	Period Held	Where Held
Concordia One Year Fellowship	1977-1978	Centre for Building Studies, Concordia University
Concordia One Year Fellowship	1978-to date	Centre for Building Studies, Concordia University

DATE: June, 1979 SIGNATURE: _____

LIST OF PUBLICATIONS

1. Rizzo, S., "Modal Analysis of Rigid Body with Elastic Any-Directional Constraints", Giornale del Genio Civile, Vol. 21, Feb., 1972, (in Italian).

2. Fazio, P. and Rizzo, S., "Wrinkling of Framed Aluminum Panels", 4th Symposium on Engineering Applications of Solid Mechanics, Ont. Res. Foundation, Mississauga, Ont., Sept. 25-26, 1978.

3. Rizzo, S. and Fazio, P., "Lateral Deflection of a Sandwich-Panel Building Model under Lateral Combined Loading", Experimental Mechanics, Journal of Society of Exp. Stress Analysis, June, 1979.

4. Fazio, P. and Rizzo, S. "Nonlinear Elastic Analysis of Panelized Shear Sandwich Walls", Journal of Structural Division, ASCE, Vol. 105 No. ST6, June, 1979.

5. Rizzo, S. and Fazio, P., "2-D Incremental Analysis of Sandwich Box Building Structure", Can. Congr. of Appl. Mech., CANCAM'79, May 29-June 1, 1979, Sherbrooke, Que., Canada.

6. Fazio, P. and Rizzo, S., "Comprehensive Strength Analysis of Sandwich Panels", Canadian Journal of Civil Engineering, December, 1979.

7. Fazio, P. and Rizzo, S., "Ultimate Strength of a Sandwich Panel Building Model", invited and accepted for presentation at ASCE Convention, Oct. 22-26, 1979, Alabama, and being submitted for publication in ASCE, Journal of Structural Division.

8. Rizzo, S. and Fazio P., "New Developments in Non-linear Elastic Analysis of Panelized Building", to be submitted for publication.

CHAPTER I

INTRODUCTION

1.1 Prefabricated Panelized Buildings

A prefabricated panelized building is made up of prefabricated wall and floor panels. These panels form the main load-carrying elements. The wall assemblies provide the building strength and stiffness against the lateral loads. The type of structural system is usually referred to as "shear-wall" structure.

1.2 Aims of the Research Programme

To improve the understanding of the behaviour of sandwich construction in the building industry, a research programme was begun in 1970, Fazio [1], to theoretically and experimentally study the structural performance of prefabricated rectangular framed aluminum sandwich panels when used as main load-carrying elements. The aim of the project was to assess the main parameters affecting:

i) the system's overall structural behaviour under static service loads;

ii) the resistance and stiffness of the system when subjected to simulated severe wind and earthquake loadings;

Separate studies were also undertaken to determine the behaviour of the framed aluminum sandwich panels and of the connection system. The objectives of these studies were to:

iii) investigate the stiffness and strength of edge reinforced sandwich panels;

iv) establish the structural reliability of the stapled joints for panel assemblies.

1.3 Structural Sandwich Panels

A sandwich beam or plate under flexure behaves much like an I-beam, with the flanges (the faces or skins of the sandwich) carrying the bending action and the web (the core of the sandwich) providing the bending lever arm and the shear strength.

The core also stabilizes the usually thin face plates, which may experience local instability phenomena such as wrinkling, dimpling or crimpling, especially in the case of low-density core materials.

1.4 Applications and Materials for Sandwiches

Sandwich technology has been traditionally used in the aircraft industry, where it was first introduced for the construction of the de Havilland "Mosquito" airplanes, during the second world war.

The structural sandwiches usually possess high and advantageous strength-weight and stiffness-weight ratios, which explain their diversified civil applications for buildings (walls, floors, doors, stressed-skin components), for the industry of naval constructions (plastic sandwich boat hulls) and mechanical constructions (containers, truck bodies, self-supporting car bodies, sub-way and railroad car bodies).

The growing number of applications in the building industry shows the great potentials of the structural sandwich for use as main-load carrying elements, in large space shells (Parton [2], Anonymous [3]), large-span folded-plate roofs (Fazio [4],[5]), panelized building assemblies (Fazio [1],[6], Nathan [7]) and as building structural components of various kinds (Teitsman [8], McLelland [9], Mateja [10], Abdel-Malek [11], Anonymous [12], Ha and Fazio [57], [58]).

The versatility of the sandwich elements is also shown by the wide range of component materials used in building constructions, both

for the faces:

a) aluminum (for example, Fazio, [1],[4],[5],[6],[8], Minford [13]);

b) steel (McCavour [14]);

c) plywood (Biblis [15]);

d) concrete (Nathan [7]);

e) glass-fibre reinforced plastics;

and the core;

f) expanded or foamed plastics [Gad [16], Fazio,[1],[4],[5],[6],[8]);

g) paper honeycomb (Reichard [17], Brentjes [18]).

1.5 Organization of the Thesis

The presentation of the research object of this thesis is organized as follows:

i) Chapter II describes, in detail, the half-scale panelized building model (Fig. 1.1), made up of framed sandwich panels and assembled by stapled connections. In the same chapter, the test set-up for the experimental study of the structural behaviour of the model is described in detail.

ii) Chapter III presents the results of tests during which the model was subjected to simulated vertical and lateral loads of various intensities, Rizzo and Fazio [19].

iii) The research on the stapled connections formed the object of Kaloskakis [20] Master of Engineering thesis; the part related to the overall structural behaviour of the system is briefly reported in Chapter IV.

iv) Chapter V reports on a comprehensive analysis of framed panels and the comparison with experimental results of a series of 8 sets of tests on 26 panels with various edge conditions, and subjected to

edgewise compression or bending, Fazio and Rizzo [21].

v) A two-dimensional non-linear analysis of the overall structural behaviour of the building is then presented in Chapter VI.

vi) Chapter VII presents the comparison of theoretical and experimental results of deflections and stresses obtained from a set of four tests, on the building model.

vii) Finally, the results of the failure test are reported in Chapter VIII. The failure modes of the lowest compressed sandwich panels and their sequence of failures are described. The early stages of the failure tests were compared with theoretical results obtained from the elastic theory.

CHAPTER II

THE HALF-SCALE BUILDING MODEL TEST SET-UP

2.1 The Characteristics of the Building Model

2.1.1 General

A general view of the sandwich panel building model is given in Fig. 1.1. The final model has a two-room base 12 ft-6 in. x 6 ft- 4 in. (3.81 x 1.93 m) and a height of six floor, 25 ft. (7.62 m).

The floor plan of the model, Fig. 2.1, is made up of square room units with internal and external side dimension (wall to wall) of 6 ft (183 cm) and 6 ft-4 in. (193 cm), respectively. A typical floor unit results; Fig. 2.1, from the assembly of 3 equal sandwich panels, placed with span perpendicular to the direction of the horizontal loads: the panel assembly will act as diaphragm and transmit the lateral loads to the shear sandwich walls.

A typical room side wall (Fig. 2.2) is made up of two 4 ft (122 cm) high panels, placed at the room corners, with an open space gap of 2 ft x 4 ft (61 x 122 cm), left between them to represent (in the prototype) the window, balcony or door openings. The height of one complete floor assembly (wall height and floor thickness) is 4 ft-2 in. (1.27 m).

The wall panels act as main load-carrying elements: as column supporting the vertical shear coming from the floors, and as coupled sandwich shear-walls against the lateral loads.

Aluminum extrusions were used to assemble the panels and high-strength steel staples to secure the panels to these extrusions. Panels and connecting extrusions are further described in the following sections, 2.1.2 and 2.1.3, respectively.

2.1.2 Panels

Panels are made up of two 0.025 in. (0.635 mm) thick aluminum skins and 1.875 in. (4.76 cm) thick styrofoam core, which has a density of 2 lb/cu.ft. (32 kg/m^3). The overall panel thickness is then 1.925 in. (4.9 cm), Fig. 2.3 (b and c). The panels have constant width 1 ft - 11 11/16 in. (23.69 cm) and length of: 1 ft (30.5 cm) for lintel beams, 4 ft (122 cm) and 5 ft 11 9/16 in (181.8 cm) for wall and floor panels respectively, Fig. 2.3.a.

The four edges of the panel are reinforced by clear white pine wood members, of 2 in. x 1.875 in. (5.08 cm x 4.76 cm) constant cross-section, assembled as rectangular closed frame by mitred corners (45 degree angle stud ends), Fig. 2.3.b, and by 1 in. x 3/8 in. (2.54 x 9.5 mm) metallic corrugated fasteners.

The assembly of the panel was done first by priming the aluminum faces with Bostick #1007 adhesive, air-dried for a minimum of 12 hours, then by priming the faces with an epoxy adhesive. The faces and the core system (frame and styrofoam) were then mated and stacked into clamp presses, subjected to a pressure of about 15 psi (102.5 kN/m^2) and left in the press to cure overnight.

2.1.3 Connections

Two types of connections, Fig. 2.4, are used in the model:

i) aluminum extrusion No. 1 (Fig. 2.4.a) is # shaped, and is used to connect panels oriented in orthogonal planes, namely floor to wall

panels (Fig. 2.5.b) (horizontal 5 ft-6 in. = 167.64 cm joint) or wall to wall panels (vertical 3 ft-6 in. = 106.68 cm joint) (Fig. 2.5.a.);

ii) aluminum extrusion No. 2 (Fig. 2.4.b), wide flange I shaped, is used to connect panels in the same plane or floor to floor panels (5 ft.-8 in. = 172.72 cm horizontal joint) (Fig. 2.5.b). The same extrusion, No. 2, with its web rotated by a 90 degree angle, is also used to connect the first-floor wall panels to the top of the base or foundation steel frame, Fig. 2.6.

The aluminum alloy used to extrude the connections was type 60-63-T5.

The longitudinal grooves provided in all the flanges of the extrusions (Fig. 2.4) were made to reduce the flange thickness to the minimum which allowed to drive the high-strength carbon steel staples through the connection flange, the panel skin and into the timber frame studs. The groove's profile was designed to accommodate the head of SENCO's air pressure staple gun.

The staples (see detail in Fig. 2.4) had 11/16 in. (17.4 mm) length, 13/32 in. (10.3 mm) crown and $\emptyset$ = 0.0057 in. (1.5 mm) wire diameter and were spaced at 3/4 in. (19 mm) along the connection.

2.2 Loading System

As already mentioned, the model was subjected to loading tests at its different stages of assembly. The loads were applied as follows:

2.2.1 Horizontal Loads

2.2.1.a Concentrated Loads

Lateral concentrated loads were applied at the floor levels with a two-ton (17.8 kN) ram and manually operated hydraulic pump. The

ram was connected to a stud load cell having a 4.5 lbf (20 kN) capacity. A chain connected the other end of the ram to a 4I7.7 steel beam fixed to two heavy steel columns of an adjacent test frame structure (details in Ref. [22]).

2.2.1.b Distributed Loads

To simulate horizontal loading conditions, uniformly distributed lateral loads were applied by the use of air pressure plastic bags which were made up of .006 in. (.15 mm) thick Tuftex plastic sheets, type No. 1010, and had final standard dimensions of 5 ft. x 7 ft (152.4 x 213.4 cm). Seams of the bags were sealed with polytape, Fig. 2.7.d. The volume of the bags was made larger than that provided by the gap between the model and the wall so as to allow the bag to expand without damage, when the model deflects under the bag pressure, Fig. 2.7.d. The air pressure was supplied by a 100 psi (690 kN/m^2) 3/4 in. (1.9 cm) diameter air pressure line. The input and output bag pressures were monitored with a tubemanometer panel, Fig. 2.8.

Each bag is inserted within the external protruding 1.86 in. (4.7 cm) flanges of aluminum extrusion No. 2 (Fig. 2.7.a.1) and a retaining platform (Fig. 2.7.a.3) made up of special tongue and groove sandwich panel removable assemblies (Fig. 2.7.b). A wooden support frame (Fig. 2.7.a.) was designed to transfer the air pressure from the retaining platform into the rigid wall of the laboratory (Fig. 2.7.a.5).

A bag is provided for each 6 ft x 4 ft (183 x 122 cm) wall unit. The system may then accommodate uniform and stepped loading conditions. The latter may have increasing or decreasing intensities from the bottom to the top, to simulate quasi-triangular or quasi-trapezoidal loads.

2.2.2 Vertical Loads

The gravity and live loads are simulated on the model by room-temperature water, supplied within water basins placed on each room module floor.

Two 1 ft x 2 ft (30.5 x 61 cm) non stapled lintel panels were temporarily placed at the bottom of the wall opening (Fig. 2.9) to retain the water. A plastic sheet 10 ft x 10 ft x 0.006 in (3.05 x 3.05 m x .15 mm) is thereafter spread on the floor and taped to the walls of each room module, forming a 6 ft x 6 ft (183 x 183 m) leak-proof open basin with 1 ft - 10 in. (56 cm) maximum water depth, which corresponds to a maximum uniform vertical load of intensity 114,500 psf (5500 kN/m^2).

A system of valves provides regulation of the water depth, according to the loading programme (see details in Ref. [22]). A pump is installed to remove the water.

2.3 Data Acquisition System

The data to be acquired consisted of strain and displacement measurements. Electrical resistance gages measured the strains at selected skin positions and electrical displacement transducers measured the building deflections.

2.3.1 Strain Measurements

Linear and rosette metal foil gages manufactured by Micro-Measurements were used. The linear gages are designated as EA-13-125BT-120, option E, and the rosettes as EA-13-125RA-120, option E. The nominal gage factor of the gages was 2.09 ± 20% (75°F), the gage length was 1/8 in. (3.175 mm), grid width 0.062 in. (1.575 mm), 120.0 ±

4% Ω resistance. They are all encapsulated. Figures 2.10 and 2.11 show the position of all the gages used during the test of assembly No. 1-7, namely the final building stage with two room modules and six-floors.

2.3.2 Displacement Measurements

Displacement transducers had been developed by Fazio to measure deflections automatically. These are made up of a steel cantilever strip with a strain gage close to the fixed end (Fig. 2.12.a). One end of the rigid aluminum support is fixed to a heavy magnetic base (Fig. 2.12.b). The movement of the pin (Fig. 2.12.c) due to the building displacement gives rise to strain changes.

2.3.3 Computerized Data Acquisition System

Strains sensed by the gages are monitored by a computerized data acquisition system (DAS) with 120 active channels. Wires from strain gages are connected to junction boxes. Voltage signals travel from these boxes to a signal conditioner and a multiplexer switcher, are amplified, converted to digital and received by the PDP-8/L computer. The computer records and converts the voltage readings into strain units at a rate of over 100 gages per second. The records can also be read onto magnatic tape and the data can be processed in a CYBER 172 (CDC 7200) computer by a program PDPRS developed by Sen [23]. A program called PANBLD has been written by the writer in Fortran IV language and included as Appendix A. This program transforms the strains into stresses and displacements.

CHAPTER III

PRESENTATION OF EXPERIMENTAL DEFLECTION AND STRESSES OF THE BUILDING MODEL

3.1 General

This chapter presents the experimental deflections and stresses obtained from a set of several loading tests on the building model.

The structural behaviour of the model was investigated at different stages of assembly. The assembly and tests are designated by a code number (see Figs. 3.1 and 3.2). In the convention code no. 05-11-L, the first digit describes the number of floor panels (0 for 1 floor panel assembly); the second digit, the number of floors (5 for a four storey assembly); the following two digits, the test number for that assembly. The letter at the end describes the load type (L for lateral load; TR for triangular load;CL for collapse test).

The results reported herein will treat, in particular, the deflections and stresses obtained from tests carried out on assemblies 05, 06, 07, (Rizzo and Fazio [19]) and 17. The results regarding the failure tests 17-06-CL1 and 17-07-CL2 will be treated in detail in Chapter VIII.

3.2 Presentation of Experimental Deflections

The various lateral or combined vertical-lateral loading conditions are represented in Fig. 3.1 for assemblies 05, 06, 07 and in Fig. 3.2 for assembly 17.

The experimental deflections of the model at respective maximum loading intensities are presented in Fig. 3.3 for assemblies 05, 06 and 07.

The deflections for assembly 17 were monitored by 18 cantilever gages and the deflected shapes for the different tests are presented in Figs. 3.4, 3.5, 3.6 and 3.7. The three readings at each storey

level were averaged and plotted in Figs. 3.8 and 3.9.

3.3 Presentation of Experimental Stresses

The numbering and positioning of rosette gages are reported in Fig. 3.10, which summarizes the more detailed description of Figs. 2.10 to 2.11. The strains from these rosettes were converted to stresses using the generalized Hooke's law and plotted in Figs. 2.11 to 2.14. The computer program written for this conversion is given in Appendix A. It should be noted that the stresses for assembly 17 only are reported in this thesis.

3.4 Discussion of Experimental Deflections

The deflected shapes of the model resembles the typical deflect-on shape of the shear-wall equivalent frame.

The drift coefficients (ratio of the top deflection to the building height) are reported in column (6) of Tables 3.1 and 3.2.

The National Building Code of Canada 1977 [24] requires the drift of the building not to exceed 1/500 at a lateral uniform pressure of 300 psf (1,400 kN/m^2). Column (7) of Tables 3.1 and 3.2 shows the approximate drift of the model under various test conditions. For simplicity a linear load-deflection relationship was assumed to hold for the model. The results show:

i) the reduced drift coefficient is between 1/300 and 1/400 for most of the scaled loading conditions;

ii) the model behaviour is very sensitive to upper triangular loading shapes (1/246 drift for Test 17-03-T1) and to tip (or concentrated at the top) loads (1/136 and 1/243 drift for Tests 06-01-L and 05-11-L respectively);

iii) the shapes of deflection diagrams of assemblies 05,06,07 and of the average deflections of assembly 17 (Figs. 3.3, 3.8, 3.9)

show the building behaves much like other shear wall buildings.

The relatively large deflections have led to a closer investigation of the behaviour of the stapled connections. The analysis is presented in Chapter IV.

3.5 Discussion of Experimental Stresses

Since the structure is symmetric, the stress distribution in each of the coupled shear walls should be similar. The discrepancy between stress levels of leeward (compression) and windward (tension) side flange panels, in Figs. 3.11 to 3.14, is mainly due to the direct application of bag pressures on the windward panels, which resulted in localized bending stresses.

All gages on the building were replaced for the test on assembly 17. Panels on the leeward side had previously failed and were replaced. The new panels were gaged before replacement and proper application could easily be carried out. Gages on panels in the windward side were applied in situ with some difficulty, which may have resulted in some poor installations and which would account for inconsistent results in Figs. 3.11 to 3.14.

The following observations can be made from the distribution of stresses at the leeward side:

a) Stresses in both facings of the panels in the leeward side generally show uniform distribution across the width of the panels. Variations exist at the corners of the model. This may be due to stress concentrations and flexibility of vertical connections.

b) The stress gradients in the web panels on the leeward side vary from compression at the exterior edges to tension at the interior edges.

c) From observations (a) and (b), it may be concluded that the panel assemblies act as integral ⌜ or T sections.

TABLE 3.1

ASSEMBLIES 05, 06 AND 07
LOADING AND MEASURED MODEL DEFLECTION

(see load schemes in Fig. 3.1)

ASSEMBLY	TEST NUMBER	LOAD TYPE	MAXIMUM INTENSITY OF LATERAL LOADS	DEFLECTION AT 4th FLOOR LEVEL	DRIFT COEFFICIENT†	REDUCED DRIFT*
(1)	(2)	(3)	(4)	(5)	(6)	(7)
05	10	C	2.0 kips (8.9 kN)	1.2 in. (3.05 cm)	1/167	1/391
05	11	L	3.0 kips (13.35 kN)	0.74 in. (1.88 cm)	1/270	1/243
06	01	L	2.5 kips (11.125 kN)	0.88 in. (2.23 cm)	1/227	1/136
06	02	L	104.17 psf (5 kN/m^2)	0.04 in. (0.1 cm)	-	-
06	03	L	104.17 psf (5 kN/m^2)	0.26 in. (0.66 cm)	1/769	1/923
06	04	L	104.17 psf (5 kN/m^2)	0.56 in. (1.42 cm)	1/357	1/643
06	05	L	83.33 psf (4 kN/m^2)	0.80 in. (2.03 cm)	1/250	1/480
06	06	L	62.50 psf (3 kN/m^2)	0.88 in. (2.23 cm)	1/227	1/409
07	01	L	46.88 psf (2.25 kN/m)	0.915 in. (2.32 cm)	1/219	1/296
07	02	C	46.86 psf (2.25 kN/m)	0.735 in. (1.87 cm)	1/272	1/367
07	03	C	46.86 psf (2.25 kN/m)	0.605 in. (1.54 cm)	1/330	1/446

(†) height of the building: 200 in. (508 cm); 250 in. (635 cm); 300 in. (762 cm) for assemblies 05, 06 and 07 respectively.

(*) obtained from column (6) / (column (4) in Table 3.3).

TABLE 3.2

ASSEMBLY 17. LOADING AND MEASURED MODEL TOP DEFLECTIONS

(see load schemes in Fig. 3.2)

ASSEMBLY	TEST NUMBER	LOAD TYPE	MAXIMUM INTENSITY OF LATERAL LOADS	TOP DEFLECTION	DRIFT† COEFFICIENT	REDUCED DRIFT*
(1)	(2)	(3)	(4)	(5)	(6)	(7)
17	01	P1	15.625 psf (.75 kN/m²)	.285 in. (.72 cm)	1/1052	1/473
17	02	P2	26.04 psf (1.25 kN/m²)	.670 in. (1.70 cm)	1/448	1/338
17	03	T1	41.67 psf (2.00 kN/m²)	.916 in. (2.32 cm)	1/328	1/246
17	04	SL	do	.835 in. (2.12 cm)	1/359	1/269
17	05	T3	do	.353 in. (.90 cm)	1/850	1/638
17	06	CL1	83.33 psf (4.00 kN/m²)	2.03 in. (5.16 cm)	1/148	1/355
17	07	CL2	177.08 psf (8.48 kN/m²)	>4.00 in. (10.16 cm)	1/75	1/383

(†) height of building: 300 in. (762 cm) for assembly 17.

(*) obtained from column (6) / (column (4) in Table 3.5)

TABLE 3.3

COMPARISON OF DESIGN WIND LOADS
AND APPLIED TEST HORIZONTAL LOADS

TEST	TEST LOAD	DESIGN* WIND LOAD	RATIO (2)/(3)
(1)	(2)	(3)	(4)
05-10-C	8000 lbs (35.6 kN)	3334 lbs (14.9 kN)	2.34
05-11-L	3000 lbs (13.4 kN)	3334 lbs (14.9 kN)	0.9
06-01-L	2500 lbs (11.13 kN)	4166 lbs (18.6 kN)	0.6
06-03-L	5000 lbs (22.3 kN)	4166 lbs (18.6 kN)	1.2
06-04-L	7500 lbs (33.4 kN)	do	1.8
06-05-L	8000 lbs (35.6 kN)	do	1.92
06-06-L	7500 lbs (33.4 kN)	do	1.8
07-03-C 07-01-L 07-02-C	6750 lbs (30 kN)	5000 lbs (22.3 kN)	1.35
17-01-P1	4500 lbs (20.0 kN)	10000 lbs (44.5 kN)	0.45
12-02-P1	7500 lbs (33.4 kN)	10000 lbs (44.5 kN)	0.75
17-03-T1	7500 lbs (33.4 kN)	10000 lbs (44.5 kN)	0.75
17-04-T3	7500 lbs (33.4 kN)	10000 lbs (44.5 kN)	0.75
17-06-CL1	24000 lbs (107.0 kN)	10000 lbs (44.5 kN)	2.4
17-07-CL2	51000 lbs (227.0 kN)	10000 lbs (44.5 kN)	5.1

* Assumed average uniform wind pressure q_w = 30 psf (1.437 kN) on the lateral surface of the building model.

CHAPTER IV

THE BEHAVIOUR OF STAPLED CONNECTIONS

4.1 Discussion of Experimental Deflections

The straight curves in Fig. 4.1 would seem to indicate the deflection of the model to be of the shear type. This deflection, in fact, is due to a combination of shear and bending displacements of panels and shear slippage of the stapled joints (Chapter III). This slippage is reduced by vertical forces which substantially increase friction forces between the connections and the panel. The reduction in slippage, due to increasing friction forces, is demonstrated in Fig. 4.1.a where it is shown that deflections decrease with increase in vertical loads, namely in those tests where vertical loads were actually applied before the lateral loads. Typical displacement vs. loading-unloading curves are plotted in Fig. 4.2.a for lateral loading and in Fig. 4.2.b for combined loading.

The effect of friction forces is also demonstrated in this figure where it is shown that because of the presence of vertical load the initial portion of the curve in Fig. 4.2.b has a greater slope than the corresponding portion of the curve in Fig. 4.2.a. Because of the joint slippage and the influence of varying vertical loads on this slippage, the behaviour of the model in non-linear, (Fig. 4.1) and a closer examination of the joint behaviour is required for better interpretation of the model deflections.

4.2 Results from Experimental Study on Stapled Joints

An experimental investigation was carried out on a series of typical stapled joined sections [20]. Figure 4.3 shows a typical family

of curves resulting from a series of tests carried out on a two-foot (61 cm) stapled joint subjected to combined shear forces along the joint axis and variable uniformly-distributed normal forces, perpendicular to the joint axis. They clearly show the friction variable stiffness as the normal force N varies from 0 to 6 kips (0 to 26.70 kN). It can be noted that:

(i) the curves are non-linear and the stiffness coefficients of the joint must be evaluated from the tangent values to the curves;

(ii) the stiffness of the joint increases with increasing shear forces, V;

(iii) the stiffness of the joint increases with normal forces, N;

(iv) despite the non-linearity of the curves, the test showed that the behaviour of the joints is elastic within the range of forces shown.

These curves confirm the interpretation of the model deflections discussed above. Such curves can be used to model the joint behaviour in a theoretical analysis to predict the behaviour of such panelized structures (see Section 6.3.3).

CHAPTER V

BEHAVIOUR OF FRAMED SANDWICH PANELS

5.1 Introduction

A theoretical and experimental investigation was carried out on the type of sandwich panels used in the building model to determine:

1. The behaviour of the panels in their elastic range.
2. The stresses at which wrinkling of the skins would occur.
3. The ultimate capacity of the panels.
4. The influence of the wood frames on the load-carrying capacity of the panels.

Panels with various edge conditions (Figs.5.1 and 5.2) were tested. These panels had a styrofoam core 1.875 in. (4.76 cm) thick, aluminum facings of 0.025 in. (.635 mm) thick and a 2-in. (5.08 cm) wide wood frame. The properties of the various materials of the panels are presented in Table 5.6. Close agreement exists between the experimental results and those obtained from a strength analysis developed to take into account the contribution of the edge frames. A design formula is revised to yield closer agreement with experimental results. The reduction in strength leading to early wrinkling of the aluminum facings and lower ultimate load has been recognized to be due to the residual stresses due to shrinkage of the wood framing of the panel, and corner detailing of this framing, (Fazio and Rizzo [21]).

5.2 Behaviour of Frameless Panels

5.2.1 Review of Existing Wrinkling Stress Formulae for Thin Metalic Skins

In developing these formulae, Williams [25], and Allen [26]

assumed the sandwich skin as an infinitely long plate bearing on elastic foundation (the core) and subjected to uniform compression. These formulae are given by Allen [26];

$$\sigma_{wr} = B_1 E_s^{1/3} E_c^{2/3} \tag{5.1}$$

where

$$B_1 = 3[12(3-\mu_c)^2(1+\mu_c)^2]^{-1/3};$$

and by Williams [25]:

$$\sigma_{wr} = 0.76\ (G_c E_c E_s)^{1/3} \tag{5.2}$$

Norris [27] suggested, for the purpose of design, to reduce the coefficient 0.76 in Eq. (5.2) to 0.5. Thus,

$$\sigma_{wr} = 0.5\ (G_c E_c E_s)^{1/3} \tag{5.3}$$

The Equations (5.1) to (5.3) may also be used to predict the wrinkling stress of the compressed face of panels under out-of-plane bending, provided the panel falls within the range of thin facings type, Allen (1969). It is understood that the occurrence of the wrinkling of the facings represents the ultimate limit state of the panels: after wrinkling any load is no longer supported by the skins.

By substituting the data given in Table 5.6 into Eqs. (5.1), (5.2) and (5.3), σ_{wr} = 16100 psi (111200 kN/m^2); σ_{wr} = 16800 psi (116100 kN/m^2) and σ_{wr} = 10600 psi (73100 kN/m^2) respectively.

Two sets of four panels each were tested under edgewise compression (Fig. 5.2.a) and two sets of three panels each were subjected to the four-point load-bending test (Figs. 5.3.a and 5.3.b) to check the validity of the existing wrinkling formulae (Eqs. (5.1) to (5.3)).

5.2.2 Edgewise Compression Tests

The first set of panels had a width b_c^I = 7-7/8 in. (20 cm) and the second set b_c^{II} = 12 in. (30.5 cm) where Roman superscripts refer to panel sets. Both sets had a length H = 23-5/8 in. (60 cm). Wrinkling occurred at an average ultimate load of P_u^I = 3900 lb. (17300N) and P_u^{II} = 5300 lb. (23600 N) respectively. The scatter of the individual ultimate loads was ±3%. The corresponding wrinkling stresses

$$\sigma_{wr} = P_u/2\ t\ b_c \tag{5.4}$$

are reported in column (3) of Table 5.1.

5.2.3 Four-Point Load Bending Tests

Two sets of panels had a width of b_c^{III} = 8-7/8 in. (22.5 cm) and b_c^{IV} = 18-11/16 in. (47.5 cm) respectively. Both sets had a bearing span ℓ = 45 in. (114.3 cm) and symmetric shear spans s = 18 in. (45.7 cm). The test set-up is shown in Fig. 5.3.a. The load was applied with a Tinius-Olsen testing machine and transferred to the beam through rollers and bearing plates. Wrinkling occurred at the loading points in the central span of the beam at an average load of F_u^{III} = 520 lb. (2300 kN), with scatter ±1%, and F^{IV} = 1120 lb. (4500 kN), with scatter ±1%. Thus, the corresponding wrinkling stresses, also reported in Table 5.1, column (3),

$$\sigma_{wr} = \frac{M_u}{tb_c(\frac{h+c}{2})} = \frac{F_u s}{tb_c(h+c)} \tag{5.5}$$

since, referring to Fig. 5.3.a,

$$M = \frac{F_u . s}{2} \tag{5.6}$$

5.2.4 Comparison of Experimental and Theoretical Results

From Table 5.1 it can be seen that Equations (5.1) and (5.2) overestimate the wrinkling stresses of the frameless panels by 40 to 80% whereas Eq. (5.3) predicts them within ±10%. Therefore, it is suggested that only Eq. (5.3) be used to predict wrinkling stresses of frameless sandwich panels of the type presented herein. It should also be noted that (column (9) of Table 5.1) this equation overestimates and underestimates by 10% the experimental σ_{wr} obtained from the edgewise compression tests and the four-point load bending test respectively. The 20% scatter between the two different tests is analogous to scatter reported by Norris [27]. It is recommended that in practice the edgewise compression test be carried out to obtain the more conservative wrinkling stress value and, for design, the coefficient of Eq. (5.3) be further reduced to 0.45. Thus,

$$\sigma_{wr} = 0.45\ (G_c E_c E_s)^{1/3} \qquad (5.7)$$

5.3 Behaviour of Framed Panels with Reinforced Longitudinal Edges Only

Edgewise compression tests and four-point load bending tests were carried out on two sets of three panels each (Fig. 5.2.b) and one set of three panels (Fig. 5.3.c), respectively, in order to determine the influence of longitudinal edge reinforcement on the wrinkling stresses of the facings. The results of the tests are given in Tables 5.2 and 5.3.

5.3.1 Characteristics of Limit States

The behaviour of the panels having reinforced longitudinal edges (see Fig. 5.2.b, edgewise compression case, and Fig. 5.3.c,

out-of-plane bending case) may be theoretically described by tne following limit states:

i) wrinkling of the facings (along width of core);

ii) post-wrinkling (extension of wrinkling of face along width of frame);

iii) ultimate (rupture of the panel)..

The corresponding load carrying capacity of the panels are given below, for edgewise compression and out-of-plane bending respectively.

5.3.1.1 Wrinkling Limit State

The edge strut and facings behave as a true composite section up to the point where wrinkling stress in the facings is reached. At this point, a wrinkle forms on the skin and extends over the width of the core b_c, Fig. 5.4, and stops short of the edge struts. These wrinkles occurred at approximately mid-height in the compression specimens, and beside the load bearing plates in the central portion of the beam specimens.

For the edgewise compression cases, the wrinkling load

$$P_{wr} = 2b_p\, t\sigma_{wr} + 2b_f c\sigma_{f1} \tag{5.8}$$

where geometric symbols are identified in Fig. 5.4.

The σ_{wr} is assumed not to exceed the value given by Eq. (5.3) and the normal stress on the cross section of the strut σ_{f1} is obtained from strain compatibility as

$$\sigma_{f1} = \varepsilon_{wr} E_f = E_f\, \sigma_{wr}/E \tag{5.9}$$

For the bending case, the moments of inertia

$$I_f = 2\,(b_f c^3/12) \tag{5.10}$$

$$I_s = [b_p t(\frac{h+c}{4})^2].2$$

$$I_p = I_s + I_f\,(E_f/E_s) \tag{5.11}$$

and the section modulus

$$S_p = \frac{I_p}{h/2} \tag{5.12}$$

The bending moment at which wrinkling occurs

$$M_{wr} = \sigma_{wr}.S_p \tag{5.13}$$

where σ_{wr} does not exceed the value given by Eq. (5.3).

5.3.1.2 Post-Wrinkling Limit State

As the load is increased beyond the wrinkling limit state, the half-wave length, λ, of the wrinkle (Fig. 5.5) is reduced and its amplitude increased, producing compression at A and tension at B on the core, up to the point where either the core or the adhesive C fails. This failure is shown in Figs. 5.6.b and 5.8.a and the corresponding critical stress in the skin σ_{cr} can be predicted by the following expression developed by Marsh [28] and briefly presented in Appendix B.

$$\sigma_{cr} = \varepsilon_{cr}E_s = \sigma_{wr} + 0.25 \times 10^{-4}.E_s \tag{5.14}$$

Thus, for the edgewise compression case

$$P_{cr} = 2b_f c\sigma_{f1} + 4b_f t\sigma_{cr} + 2b_c t\sigma_{wr} \tag{5.15}$$

where σ_{f1} is obtained from Eq. (5.9).

The critical moment M_{cr} for the bending case can be derived from Eq. (5.13) by substituting σ_{wr} with σ_{cr} or Eq. (5.14).

$$M_{cr} = \sigma_{cr} S_p \tag{5.16}$$

When the limit states described by Eqs. (5.15) and (5.16) are reached, the wrinkling wave propagates over the edge frames and all compression stresses are transferred completely onto the edge-frames (Fig. 5.8.a).

5.3.1.3 Ultimate Limit State

For the edgewise compression case, the ultimate load at this state can be expressed as

$$P_u = \sigma_{uf} 2b_f c \tag{5.17}$$

where $(2b_f c)$ is the cross area of the strut. It should be noted that edge-frames are generally required to achieve effective connections in sandwich panel assemblies.

The dimension b_f of these frames can be varied so as to yield a value for P_u not less than P_{cr} in Eq. (5.15) and thus provide a secondary load-carrying mechanism in case of wrinkling failure.

For the bending case, the ultimate moment M_u is carried by the composite section made up of the facing under tension and the edge-frames (Fig. 5.7.a). The corresponding normal stress distribution on the cross-section is shown in Fig. 5.7.b. It is assumed that at failure the stress developed in the aluminum is $1.5(\sigma_{ys})$. From equilibrium and Fig. 5.7.b,

$$2ab_f\sigma_{uf} = b_p t(1.5\sigma_{ys}) \tag{5.18}$$

$$a = \frac{3b_p t\sigma_{ys}}{4b_f\sigma_{uf}} \tag{5.19}$$

Taking moments of forces in Fig. 5.7.b, the ultimate moment

$$M_u = 2\sigma_{uf} b_f \left[a\left(c + \frac{t}{2} - \frac{a}{2}\right) + \frac{(c-a)^2}{3}\right], \tag{5.20}$$

5.3.1.4 Comparison of Experimental and Theoretical Results

Results given by the above formulae compared favourably to corresponding experimental results (Table 5.4) with differences varying between 1% and 11%.

5.4 Panels with Closed Edge-Frames

Panels with closed edge-frames (see Fig. 5.1) were used in the panelized building model. Skin stresses were monitored during tests with rosette strain gages (Fig. 5.9) and an automatic PDP-8/L Data Acquisition System. The stress values recorded prior to wrinkling ranged from 5531 psi (38164 kN/m^2) to 5560 psi (38985 kN/m^2) (see Section 8.3.1), approximately half the values for wrinkling stresses yielded by Eq. (5.3) and obtained from comparable panels with longitudinal edge reinforcement only (see Section 5.2.4).

Edgewise compression tests carried out on a three panel set having closed edge-frames confirms the lower stresses which occurred in the model for this type of panel. The average wrinkling P_{wr}^{VIII} and ultimate loads P_u^{VIII} reported in Table 5.5 are also approximately half of those obtained from panels with longitudinal edge reinforcement only (see Table 5.1, Series V).

5.4.1 Effect of Edge Wood Frame Shrinkage on Wrinkling Load Reduction

The shrinkage which had developed in the previous 8 years in these panels was shown by the inward bowing along the wood thickness around the edge of the panels and by small, yet visible wave deformations of the plate along the core contour. The edge longitudinal shrinkage reduces the overall dimensions of the wood frames and consequently introduces orthogonal compressive strains in the facings.

The values of the shrinkage strains of wood in the direction parallel (or longitudinal ε) and orthogonal (radial ε) to the fibers were reported by Milbradt in 1968 [29] and range as follows:

$$\varepsilon_{long} = 0.1 \text{ to } 0.3\%, \quad \varepsilon_{rad} = 4 \text{ to } 6\%$$

These strains due to shrinkage would induce initial stresses in the facings which would account for the reduction of wrinkling stresses in these panels. Further reduction may be attributed to the plate bowing which causes secondary face bending moments when subjected to face compression (Fig. 5.10.b).

5.4.2 Effect of Corner Frame Details in Ultimate Panel Capacity

The reduction of the ultimate load P_u can be mainly attributed to the 45° corner connection of the frames (Fig. 5.1.b). Under edgewise compression, a lateral force component results at the edges of the longitudinal edge studs causing a combined compression-bending strut failure at mid-height (Fig. 5.11). The wood frame is assumed to be pin-connected at its corners and does not contribute to the shear stiffness of the panels. This assumption is adopted in the analysis in Chapter VI.

5.5 Conclusions

A test programme on aluminum sandwich panels with no reinforcement showed that wrinkling stresses due to edgewise compression are 20% lower than wrinkling stresses obtained from the four-point loading bending test.

Existing formulae by Allen [26] (Eq. (5.1)) and Williams [23] (Eq. (5.2)) overestimate these stresses by 40% and 70% for bending and edgewise compression, respectively (Table 5.1). The formula by Norris [27] (Eq. (5.3)) overestimates the wrinkling stresses due to edgewise

compression by 10% but it can be used safely by reducing its coefficient according to Eq. (5.7).

Expressions have been developed to predict wrinkling P_{wr} and ultimate load carrying capacity P_u of panels with longitudinal edge reinforcement subjected to edgewise compressions or bending. The expressions derived from Eqs. (5.8), (5.16), (5.17) and (5.20) yield results which compare favourably with experimental results (Table 5.4).

Wrinkling stresses in panels with close edge-frames were found to be approximately 50% lower than those of corresponding panels with longitudinal edge reinforcement only. The ultimate load carrying capacity P_u of these panels was found to be approximately 40% of panels with longitudinal edge reinforcement. The combined effects described in Sections 5.4.1 and 5.4.2 may have contributed to these observed reductions.

TABLE 5.1 - FRAMELESS PANELS - COMPARISON OF THEORETICAL AND EXPERIMENTAL WRINKLING STRESSES (*)

PANEL SERIES	TEST TYPE	EXP.	THEORY EQ.(5.1)	% DIFF. (4)-(3)	THEORY EQ.(5.2)	% DIFF. (6)-(3)	THEORY EQ.(5.3)	% DIFF. (8)-(3)
(1)	(2)	(3)	(4)	(5)	(6)	(7)	(8)	(9)
I	COMPR.	9854[a]	16109	+63	16823	+70	10598	+7
II	COMPR.	9400[a]		+71		+79		+13
III	BEND.	11500[b]		+39		+46		-8
IV	BEND.	11700[b]		+37		+43		-10

(*) Unit for stresses is psi (1 psi = 6.9 kN/m^2)

(a) The experimental σ_{wr} is given by Eq. (5.4)

(b) The experimental σ_{wr} is given by Eq. (5.5)

TABLE 5.2 - EDGEWISE COMPRESSION TESTS ON FRAMED PANELS (*)

PANEL SERIES	DIMENSIONS (in.), see Fig. 5.2.b				LOADS (lb.)	
	b_p	b_c	b_f	H	P_{wr}	P_u
(1)	(2)	(3)	(4)	(5)	(6)	(7)
V	12	8.06	1.97	19.5	11600	41000
	12	8.06	1.97	19.5	20000	44700
	12	8.06	1.97	19.5	17500	44000
	AVERAGE VALUES				16376	43233
VI	23.69	19.75	1.97	17.88	18400	50000
	23.69	19.75	1.97	17.88	24000	48000
	23.69	19.75	1.97	17.88	19400	47000
	AVERAGE VALUES				20600	48333

(*) (1 in. = 2.54 cm; 1000 lbs = 4,45 kN)

TABLE 5.3 - BENDING TESTS ON FRAMED PANELS (*)

PANEL SERIES	DIMENSIONS (in.), see Fig. 5.4				LOADS (lb)			
	b_p	b_a	b_f	h	F_{wr}	$M_{wr}^{(a)}$	F_u	$M_u^{(a)}$
(1)	(2)	(3)	(4)	(5)	(6)	(7)	(8)	(9)
VII	23.69	19.75	1.97	1.87	1860	16740	4050	36540
	23.69	19.75	1.97	1.87	2000	18000	4100	36900
	23.69	19.75	1.97	1.87	2100	18900	4400	39600
	AVERAGE VALUES				1987	17880	4183	37650

(*) (1 in. = 2.54 cm; 1000 lb = 4.45 kN; 1000 lb x in = 11,298 kN x cm)

(a) The bending moment (in lb x in.) is calculated from the corresponding load by Eq.(5.6) with s = 18 in. (45.7 cm).

TABLE 5.4 - COMPARISON OF EXPERIMENTAL AND THEORETICAL LOADS (*)

PANEL SERIES	WRINKLING				ULTIMATE			
	TEST	THEORY	EQ.#	% DIFF.	TEST	THEORY	EQ.#	% DIFF.
(1)	(2)	(3)	(4)	(5)	(6)	(7)	(8)	(9)
V	16367	16060	(5.8)	-1.9%	43233	45675	(5.17)	+6%
VI	20600	21254	(5.8)	+3.2%	48333	45675	(5.17)	-5%
VII[a]	1987	1779	(5.16)	-10.5%	4183	4127	(5.20)	-1%

(*) Unit for loads is lb (1000 lbs. = 4.45 kN).

(a) The wrinkling and ultimate theoretical beam transversal loads are calculated from P = 2M/s (Eq.(5.6)), M being given from Eqs. (5.16) and (5.20) respectively.

TABLE 5.5 - EDGEWISE COMPRESSION TESTS ON PANELS WITH CLOSE EDGE-FRAMES (*)

PANEL SERIES	DIMENSIONS (in.), see Fig. 5.1				LOADS (lb)	
	b_p	b_c	b_f	H	P_{wr}	P_u
(1)	(2)	(3)	(4)	(5)	(6)	(7)
VIII	12	8.06	1.97	23.63	10750	18375
	12	8.06	1.97	23.63	8500	18750
	12	8.06	1.97	23.63	8900	19375
	AVERAGE VALUES				9383	18958

(*) (1 in. = 2.54 cm; 1000 lbs. = 4.45 kN)

TABLE 5.6 - PROPERTIES OF MATERIALS OF FRAMED SANDWICH PANELS (*)

ALUMINUM (skin)	ELASTIC MODULUS	E_s = 10,000,000 psi
	YIELDING STRESS	σ_{ys} = 22,000 psi
	ULTIMATE STRESS	σ_{us} = 36,000 psi
WOOD (frame)	ELASTIC MODULUS	E_f = 1,150,000 psi
	ULTIMATE STRESS (COMPR.)	σ_{uf} = 6,400 psi
	PROP. LIMIT STRESS	$0.7 \cdot \sigma_{uf} \approx \sigma_{pr}$ = 4,500 psi
	STRAIN AT σ_{uf} ATTAINMENT	$\varepsilon(\sigma_{uf})$ = 9.55×10^{-3}
STYROFOAM (core)	ELASTIC MODULUS	E_c = 1,380 psi
	SHEAR MODULUS	G_c = 690 psi
	POISSON'S RATIO	μ_c = 0

(*) Unit is psi (1 psi = 6.9 kN/m^2)

CHAPTER VI

THE ELASTIC NONLINEAR ANALYSIS OF THE SANDWICH BUILDING SYSTEM

6.1 General

The sandwich panel building system studied in this programme falls within the class of shear wall type structures. The available methods of linearly elastic analysis for these structures can be grouped into the following:

(i) the Continuum of Lamina Method

(ii) the Equivalent Frame Method

(iii) the Finite Element Method

The structures can also be analysed experimentally through models.

The basic concept of the "Lamina Method", developed by Albiges and Goulet [30], Beck [31], Rosman [32] and Coull [33], [34], is to replace the discontinuous lintel beam connecting the solid shear wall cantilevers by an equivalent laminal or continuous medium (Fig. 6.1.b), and thus solve the differential equation governing the behaviour of the cantilever wall subjected to the load actions and the reactions of the equivalent continuum. The contributions of bending and shear deformation in the connection lintel beams and of the deformation due to bending and axial loads in the walls are incorporated within this model. Design aids, Rosman [35] and Schwaighofer and Tai [36], cover the most usual shear-wall configurations.

The "Finite Element Method" has been widely and successfully applied to analyse shear-wall structures. It has also been sucessfully applied to sandwich panel structures by Ha [37]. However, this method still remains prohibitive in terms of cost for large shear wall structures.

The "Equivalent Frame Method" remains the most powerful and versatile method at the disposal of today's structural analyst and designer. The basic concept, Jenkins and Harrison [38], (Fig. 6.7.c) is the replacement of the shear-wall by a frame which behaves identically to the given shear wall. This analogous behaviour is achieved by carefully selecting the cross-sectional properties of the frame members, Stafford - Smith [39]. It requires medium-large computers, but it is simple and efficient to use for any shear wall configuration and any lateral or combined loading condition, Schwaighofer [40].

Structural model analysis is employed in the solution of unusual structures and to confirm accuracy of analytical assumptions.

A wide spectrum of aspects have been treated in the above studies: elastic approach, elastoplastic behaviour, dynamic response, stability, variable geometric configurations of the walls, foundation settlement. However, little has been done on lightweight multistory shear-walls made up of sandwich panels.

The "Equivalent Frame Method" was adopted for reasons mentioned above, and extended to predict the behaviour of the sandwich panel structure investigated in this program. The non-linear behaviour of the stapled joints was taken into account in this analysis (Section 6.3.3). The results compared favourably with those obtained from experimental programs as presented in Chapter VII.

6.2 Review of Past Research on Non-Linear Frame Analysis

Many researchers have shown that joints between prefabricated elements seldom give full structural restraint to the elements they join. For instance, bolted, welded or riveted connections in steel frame systems have a rotational capacity within the joints, and more

accurate analyses have been developed in order to take into account this additional variable by Lightfoot and Le Mesurier [41], Lionberger and Weaver [42], Montforton and Wu [43], Romstad and Subramanian [44], Suko and Adams [45].

Slippage in connections of prefabricated panelized concrete structures has been studied by Burnett and Rejendra [46] and Cholewicki [47], [48]. Theories have been developed by Pollner, Tso and Heidebrecht [49] and Robinson [50] to predict the behaviour of such structures taking into account joint slippage.

Joint force-displacement curves in the above studies are generally non-linear, piece-wise linearized: bi-linear [42], [44], three-linear [45], multi-linear [50], and linear in an early paper in 1963 [43] and more recently in 1974 [41].

Because of the non-linear behaviour of the joint, the analysis had to be performed by a piece-wise procedure, the final output being a sum of a series of small incremental linear analyses, [42], [50], [44], [45]. Almost all quoted papers [41], [42], [43], [44], [45], introduce the joint variable within the bar local stiffness matrix, through "correction matrices" or "modified member stiffness matrices". These modified member stiffness matrices contain appropriate coefficients which account for the variable joint stiffness. This approach is complex because these coefficients must be modified at different stages corresponding to different segments of the assumed force-displacement curve. Therefore, it is necessary to rebuild the global general stiffness matrix at each stage.

Recently, Tso, Pollner and Heidebrecht [49], approached the problem differently, by separating the joints from the panels and setting

up a stiffness matrix for each vertical joint. This matrix takes into account the varying stiffness of the joint. Each joint is thus simulated as a spring with variable stiffness. It should be noted that the authors assumed full friction to develop along the horizontal joints, thus making the connections fully rigid. This assumption was justified in the case of panelized concrete structures where such friction is developed by the weight of the components.

The main advantage of this approach lies in the separation of elements whose local matrices have constant terms from those whose local matrices have variable terms. Therefore, only the latter matrices need to be modified at the different stages of the piece-wise analysis. Moreover, different joint behaviour can be easily accommodated within the analysis.

6.3 Assumptions

6.3.1 Shear Walls

- Web and flange panels act together as composite T or ⌐ sections.
- Compression and out-of-plane bending stresses in the flange panels (Fig. 6.2) are carried by facings and wood frames acting as composite sections.
- The in-plane shear and bending stresses in the web panels are carried by the facings only, since the wood frames are considered pinned at the corners.

6.3.2 Floor Assemblies

- Floor assemblies are infinitely rigid in their own plane, but flexible normal to the plane.
- The effective width of the floor contributing to the bending stiffness of the lintel between the coupled shear walls is cal-

culated in accordance with the design aids presented by Schwaighofer [40].

The ratio ℓ_e/ℓ, where ℓ_e is the effective width and ℓ the wall spacing is governed by the aspect ratios $\frac{d}{L}$ and $\frac{\ell}{L}$. The actual values of these ratios for the model (d/L = .438 with ℓ/L = 1.10 and d/L = .378 with ℓ/L = .956) would yield a ratio ℓ_e/ℓ = .76, (Fig. 6.3). This ratio was reduced to 0.65 for this study so that the effective flange width would not exceed the width of the flanges of the wall panel assemblies (Fig. 6.2), i.e. 48 in. (122 cm) and 24 in. (61 cm) for mid and side shear walls, respectively.

6.3.3 Stapled Joint

To take into account the joint behaviour shown in Fig. 4.3 in the structural analysis, the following assumptions are made:

(a) Shear displacement Δ along the joint axis is elastic and can be represented by the displacement of a spring with stiffness R_{sp} (Fig. 6.4.a)

(b) The shear displacement curves in Fig. 4.3 were obtained from joint specimens of two ft (61 cm) in length. Since this length corresponds to the width of each of the coupled shear walls, direct use of the R_{sp} values obtained from the curves in Fig. 4.3 can be made for horizontal joints of the shear walls. Since the joint has two shear planes, R_{sp} is reduced to $R_{sp}/2$. (Fig. 6.4.b)

(c) The incremental stiffness coefficient R_{sp} of the spring is evaluated as the slope of the tangent to the curve at the shear

value V. For negative values of N (tension) the curve N = 0 is used, since tensile normal force creates no friction. Table 6.1 reports the values of the stiffnesses R_{sp} /2.

6.4 Equivalent Frame Method

The "Equivalent Frame Method" is adopted for the idealization of the structural behaviour of the sandwich shear wall system. A typical beam or slender column member with 6-degrees of freedom is shown in Fig. 6.6.a. The matrix stiffness or displacement method is adopted. The sign and numbering convections for end member forces and corresponding displacements are given in Fig. 6.6.a. The member stiffness matrices are developed below.

6.4.1 Stiffness Matrix of Sandwich Members

The stiffness matrix of a 6-degrees of freedom member, may be generally expressed, following Przemieniecki [51], with reference to the member local axes (x,y,z) system, (Figs. 6.6.b and 6.6.c), as

$$[S] = \begin{array}{c} \begin{matrix} 1 & 2 & 3 & 4 & 5 & 6 \end{matrix} \\ \begin{vmatrix} \frac{EA_p}{\ell} & & & & & \\ 0 & \frac{12EI_z}{\ell^3(1+\phi_y)} & & & \text{Symmetric} & \\ 0 & \frac{6EI_z}{\ell^2(1+\phi_y)} & \frac{(4+\phi_y)EI_z}{\ell(1+\phi_y)} & & & \\ \frac{-EA_p}{\ell} & 0 & 0 & \frac{EA_p}{\ell} & & \\ 0 & \frac{-12EI_z}{(1+\phi_y)\ell^3} & \frac{-6EI_z}{\ell^2(1+\phi_y)} & 0 & \frac{12EI_z}{\ell^3(1+\phi_y)} & \\ 0 & \frac{6EI_z}{\ell^2(1+\phi_y)} & \frac{(2-\phi_y)EI_z}{\ell(1+\phi_y)} & 0 & \frac{-6EI_z}{\ell^2(1+\phi_y)} & \frac{(4+\phi_y)EI_z}{\ell(1+\phi_y)} \end{vmatrix} \begin{matrix} 1 \\ 2 \\ 3 \\ 4 \\ 5 \\ 6 \end{matrix} \end{array} \qquad (6.1)$$

where A_p Cross-sectional area of the member

E Young's modulus

I_z Moment of inertia

ℓ Span

The beam shear deformations are accounted for by the coefficient

$$\phi_y = \frac{12EI_z}{\ell^2 GA_{sy}} \tag{6.2}$$

where G Shear modulus

A_{sy} effective shear area

According to Feodosiev [52], the shear shape factor is expressed, in general terms, by

$$f = \frac{A}{A_{sy}} = \frac{A}{I_z^2} \int_{A^*} \frac{S_z^{*2}\, dA}{b^2} \tag{6.3}$$

where b cross-area width

S_z^* static moment of the area A^* included between width b and upper section contour (Fig. 6.6.c); and

$$A_{sy} = \frac{I_z^2}{\int_{A^*} \frac{S_z^{*2}\, dA}{b^2}} \tag{6.4}$$

For thin webbed cross-sections such as the flanged sandwich shear-walls, Eqs. (6.3) and (6.4) simplify into, Gere and Weaver [53],

$$f \simeq \frac{A}{A_{web}} \tag{6.5}$$

$$A_{sy} \simeq A_{web} \tag{6.6}$$

The composite cross sectional area, A_p, and moment inertia, I_z, are calculated according to the assumptions made in Sections 6.3 and 6.3.2.

6.4.2 Stiffness Matrix of Spring

In accordance with the assumptions made in Section 6.3.3, the stiffness matrix S_{sp} of the springs, in terms of its local axes, may be expressed as

$$[S_{sp}] = \begin{array}{c|cccccc|c} & 1 & 2 & 3 & 4 & 5 & 6 & \\ \hline & R_{sp}/2 & 0 & 0 & -R_{sp}/2 & 0 & 0 & 1 \\ & 0 & 0 & 0 & 0 & 0 & 0 & 2 \\ & 0 & 0 & 0 & 0 & 0 & 0 & 3 \\ & -R_{sp}/2 & 0 & 0 & R_{sp}/2 & 0 & 0 & 4 \\ & 0 & 0 & 0 & 0 & 0 & 0 & 5 \\ & 0 & 0 & 0 & 0 & 0 & 0 & 6 \end{array} \qquad (6.7)$$

This stiffness matrix changes with R_{sp} in the stepwise manner described by Fig. 6.5, and Table 6.1, during the incremental procedure of analysis, which is closely described in Section 6.8.

6.4.3 Transformations of Member Stiffness Matrices

The stiffness matrices (Eqs. (6.1) and (6.7)) are expressed in terms of local member axes. The system of general axes for the structure is chosen together with a reference structure layout, Fig. 6.7. Figure 6.7 summarizes the structural idealization which is adopted for the analysis of the sandwich panelized shear walls, and displays the nonlinear springs at floor levels. The member local stiffnesses are assembled in this reference structure layout.

Before the assemblage, the local member axes are translated and rotated as required. Three types of matrix transformations are

required:

i) transformation of forces and displacements of a member with its longitudinal x-axis parallel to a reference layout axis, Fig. 6.8.a;

ii) transformation of forces and displacements of a member with wide rigid arms at its ends, Fig. 6.8.b, also called "gussets";

iii) rotation of forces and displacements of a member into general axes, Fig. 6.8.c.

A member may undergo none or any combination of the above transformations.

6.4.3.1 Parallel Axes Transformation - (Fig. 6.9.a)

The displacements of the member CD can be expressed in terms of its local coordinate system as

$$\{\delta\} = \begin{vmatrix} \delta_1 \\ \delta_2 \\ \delta_3 \\ \delta_4 \\ \delta_5 \\ \delta_6 \end{vmatrix} \qquad (6.8)$$

and, in terms of the structural layout axes, as

$$\{\Delta\} = \begin{vmatrix} \Delta_1 \\ \Delta_2 \\ \Delta_3 \\ \Delta_4 \\ \Delta_5 \\ \Delta_6 \end{vmatrix} \qquad (6.9)$$

Provided that these displacements are relatively small, from geometric compatibility, it can be stated that

$$\begin{aligned} \delta_1 &= \Delta_1 + \Delta_3 y_p \\ \delta_2 &= \Delta_2 \\ \delta_3 &= \Delta_3 \\ \delta_4 &= \Delta_4 + \Delta_6 y_p \\ \delta_5 &= \Delta_5 \\ \delta_6 &= \Delta_6 \end{aligned} \tag{6.10}$$

or, in matrix form,

$$[T]\{\Delta\} = \{\delta\} \tag{6.11}$$

where

$$[T] = \begin{array}{c} \begin{array}{cccccc} 1 & 2 & 3 & 4 & 5 & 6 \end{array} \\ \left|\begin{array}{cccccc} 1 & 0 & y_p & & & \\ 0 & 1 & 0 & & [0] & \\ 0 & 0 & 1 & & & \\ & & & 1 & 0 & y_p \\ & [0] & & 0 & 1 & 0 \\ & & & 0 & 0 & 1 \end{array}\right| \end{array} \begin{array}{c} 1 \\ 2 \\ 3 \\ 4 \\ 5 \\ 6 \end{array} \tag{6.12}$$

The forces of member CD in terms of its local coordinate system can be expressed as

$$\{f\} = \begin{Vmatrix} f_1 \\ f_2 \\ f_3 \\ f_4 \\ f_5 \\ f_6 \end{Vmatrix} \tag{6.13}$$

and in terms of the structural layout axes, as

$$\{F\} = \begin{Vmatrix} F_1 \\ F_2 \\ F_3 \\ F_4 \\ F_5 \\ F_6 \end{Vmatrix} \tag{6.14}$$

Equilibrium requires that

$$\begin{aligned} F_1 &= f_1 \\ F_2 &= f_2 \\ F_3 &= f_1 y_p + f_3 \\ F_4 &= f_4 \\ F_5 &= f_5 \\ F_6 &= f_4 y_p + f_6 \end{aligned} \tag{6.15}$$

or, in matrix form

$$\{F\} = [T]^t \{f\} \tag{6.16}$$

where superscript t indicates matrix transposition.

The sign of y_p is taken in accordance with the true local member coordinate system, with origin at C shown in Fig. 6.8.a. In this particular case, (Fig. 6.9.a), y_p is negative.

The member governing equation is, in member axes

$$\{f\} = [S]\{\delta\} \tag{6.17}$$

By substituting Eq. (6.11) into Eq. (6.17) and the latter into Eq. (6.16)

$$\{F\} = [K]\{\Delta\} \tag{6.18}$$

where, for controgradient law,

$$\{K\} = [T]^t[S][T] \tag{6.19}$$

6.4.3.2 Wide Rigid Arms Transformation - (Fig. 6.9.b)

The displacements of member CD are expressed by Eqs. (6.8) and (6.9). From geometric compatibility and for small displacements

$$\begin{aligned} \delta_1 &= \Delta_1 \\ \delta_2 &= \Delta_2 + w_1\Delta_3 \\ \delta_3 &= \Delta_3 \\ \delta_4 &= \Delta_4 \\ \delta_5 &= \Delta_5 - w_2\Delta_6 \\ \delta_6 &= \Delta_6 \end{aligned} \tag{6.20}$$

or, in matrix form

$$[W]\{\Delta\} = \{\delta\} \tag{6.21}$$

where

$$[W] = \begin{array}{c} \begin{array}{cccccc} 1 & 2 & 3 & 4 & 5 & 6 \end{array} \\ \left|\begin{array}{cccccc} 1 & 0 & 0 & & & \\ 0 & 1 & w_1 & & [0] & \\ 0 & 0 & 1 & & & \\ & & & 1 & 0 & 0 \\ & [0] & & 0 & 1 & -w_2 \\ & & & 0 & 0 & 1 \end{array}\right| \begin{array}{c} 1 \\ 2 \\ 3 \\ 4 \\ 5 \\ 6 \end{array} \end{array} \qquad (6.22)$$

The forces of member CD, Fig. 6.9.b, are expressed by Eqs. (6.13) and (6.14). Equilibrium of forces applied to each gusset requires

$$\begin{aligned} F_1 &= f_1 \\ F_2 &= f_2 \\ F_3 &= f_2 w_1 + f_3 \\ F_4 &= f_4 \\ F_5 &= f_5 \\ F_6 &= -w_2 f_5 + f_6 \end{aligned} \qquad (6.23)$$

where w_1 and w_2 are absolute values. In matrix form

$$\{F\} = [W]^t\{f\} \qquad (6.24)$$

Using Eqs. (6.17), (6.21) and (6.24), the stiffness matrix [S] of the member is transformed as follows

$$[K] = [W]^t[S][W] \qquad (6.25)$$

6.4.3.3 Rotation of Axes

For members whose local axes are rotated by an angle α (Fig. 6.8.c), with respect to the global axes, a rotation transfor-

mation is required. The rotation matrix is expressed by

$$[R] = \begin{array}{c} \begin{matrix} 1 & 2 & 3 & 4 & 5 & 6 \end{matrix} \\ \left|\begin{matrix} \cos\alpha & \sin\alpha & 0 & & & \\ -\sin\alpha & \cos\alpha & 0 & & [0] & \\ 0 & 0 & 1 & & & \\ & & & \cos\alpha & \sin\alpha & 0 \\ & [0] & & -\sin\alpha & \cos\alpha & 0 \\ & & & 0 & 0 & 1 \end{matrix}\right| \begin{matrix} 1 \\ 2 \\ 3 \\ 4 \\ 5 \\ 6 \end{matrix} \end{array} \qquad (6.26)$$

where, from Fig. 6.8.c,

$$\cos\alpha = \frac{x_j - x_i}{L} \qquad (6.27)$$

and

$$\sin\alpha = \frac{y_j - y_i}{L} \qquad (6.28)$$

where α is the angle of rotation (anticlockwise positive), between the local positive x-axis and the general positive X-axis.

Following similar procedure as in the previous two transformations, the local stiffness matrix for rotation [S] is transformed as

$$[K] = [R]^t[S][R] \qquad (6.29)$$

6.4.4 Assemblage of General Stiffness Matrix

In the most general case, any member may undergo all the three above contrograd ient transformations. In such cases, Eqs. (6.19), (6.25) and 6.29) can be combined into Equ. (6.30) as follows

$$[K_1] = [T]^t[S][T] \qquad (6.19)$$

$$[K_2] = [W]^t[K_1][W] \qquad (6.25)$$

$$[K_3] = [K] = [R]^t[K_2][R] \qquad (6.29)$$

$$[K] = [R]^t[W]^t[T]^t[S][T][W][R] \tag{6.30}$$

The global structure stiffness matrix is then assembled from the transformed stiffness matrices [K], (Eq. (6.30)), by use of addressing {L} vectors, and according to the assumed number of degrees of freedom of the entire structure (Fig. 6.10). This figure shows the selected degrees of freedom are: i) displacements to axial forces and bending moments in sandwich members; ii) floor horizontal displacements; iii) spring displacements.

Since the structure is symmetric (Fig. 6.11), only half of it is analysed in order to reduce computer storage and running time. The two couple shear-walls on one side of the axis of symmetry (Fig. 6.11) will be both lumped on an assumed structural frame lay-out, Fig. 6.7; the distances between each member local axes and frame lay-out accounted for. The assemblage procedure may be expressed as

$$[K] = \sum_{I=1}^{NB} [K_I] \tag{6.31}$$

where $[K_I]$ are the transformed member matrices and NB is the total number of members. The equation governing the entire structural behaviour is then

$$[K]\{\Delta\} = \{P\} \tag{6.32}$$

where $[\Delta]$ is a displacement vector, unknown, and $\{P\}$ is the vector of external loads applied to the nodes of the structure. The well established matrix displacement method is used to solve Eq. (6.32) in terms of $\{\Delta\}$. Back substitution yields internal forces and displacements.

6.5 The Nonlinear Analysis

In a linear elastic analysis, the global stiffness matrix [K] in Eq. (6.32) is a constant. In a nonlinear elastic structure, such as the model under investigation, the matrix [K] becomes a variable to reflect the nonlinear load-displacement relationship of the joints shown in Fig. 6.5. Equation (6.33) can then be rewritten as

$$\{P\} = [K(F,\Delta)]\{\Delta\} \qquad (6.33)$$

To solve this equation, a step-by-step approach is required. An updated summary of available methods for this approach is given by Sahlin [54]. These methods are grouped as follows:

i) Methods of initial constraints:

At each step, the governing matrix [K] is updated to account for variations of stiffnesses produced by the incremented forces and displacements. To avoid this matrix updating, and the consequent new inversion or solution of the system of linear equations, fictitious elementary external forces (initial constraints) are introduced which can account for the difference between the forces linearly obtained at the end of the step, and the real forces, which may be calculated from the deformations at the end of the step. These fictitious forces are unknown and to be obtained, numerous iterations are needed to complete each incremental step.

ii) Methods of initial deformations:

These methods are dual to the methods described above; they operate through the deformations to correct the values of the forces. They present the same inconvenient number of iterations to be performed at each step of increment.

iii) Methods of variable stiffness (or arbitrary incrementals):

This method replaces the nonlinear member characteristics by stepwise linearized characteristics. Thus, an incremental step-by-step linearized procedure may be performed which avoids the step iterations necessary in the two previous approaches. The increments needed to obtain the structural response may vary according to the required accuracy.

The stapled joints characteristics, Reference [20], have not yet received a complete mathematical formulation which would allow their functions to be incorporated within stiffness matrices. Therefore, for the present structure, it is more suitable to operate geometrically on the curves of Fig. 4.3, as assumed in Section 6.3.3, to obtain step-by-step polygonals as close as possible to the true ones, Fig. 6.5. Accordingly, a method of variable stiffness is adopted and is described below. (See flow chart in Fig. 6.12)

1. *Carry out analysis to determine initial shear forces V and normal forces N acting on the springs.*

1.1 Generate the member stiffness matrices with constant coefficients, Eq. (6.1), transform them if necessary (Eq. (6.30), assemble them into Eq. (6.31) and store them.

1.2 Select initial values of spring stiffnesses $R_{sp}/2$ from Table 6.1 for N=0, V=0 and store first limit values of V^k_{lim} and N^k_{lim}, where k indicates the spring number. (e.g., points 1,2,3...5 in Fig. 6.13 are true values of shear force V^k_{lim} at which the spring k changes stiffness values for a given value of N).

1.3 Generate the *spring* stiffness matrices, Eq. (6.7), transform them

if necessary (Eq. (6.30)), and complete the global stiffness matrix assembly, Eq. (6.31).

1.4 Compute forces and displacements due to the actual values of *vertical loads*, if any, Eq. (6.32), and store them.

2. *Update spring constants and iterate.*

2.1 Update with new spring stiffnesses, the spring stiffness matrices in Step 1.3, and substitute, if necessary, the next values of *limit* shear V^k_{lim} and axial force N^k_{lim} (Fig. 6.5) and complete the global stiffness matrix assembly.

2.2 Compute *incremental* forces and displacements due to a set of unit lateral loads and store them.

2.3 Evaluate for each spring k the ratios (Fig. 6.13 and 6.14):

$$\alpha_k(INC) = \frac{V^k_{lim} - V^k_{acc}(INC-1)}{\Delta V^k_{unit}(INC)}$$

$$\beta_k(INC) = \frac{N^k_{lim} - N^k_{acc}(INC-1)}{\Delta N^k_{unit}(INC)} \qquad (6.34)$$

where α_k is the ratio between maximum allowable increment of shear force V without exceeding the limit value assumed for this increment and shear force due to the set of unit loads;

β_k is the same as α_k, but for the axial force N acting perpendicular to the joint axis (Fig. 6.4.b);

V^k_{acc} (or N^k_{acc}) is the force accumulated in all previous steps;

ΔV^k_{unit} (or ΔN^k_{unit}) is the force due to the set of unit lateral loads;

INC is the number of current step and denotes the incremental external load required for the next spring to reach one of its true limits V^k_{lim} of N^k_{lim}.

The geometric presentation of factors α_k and β_k (Eq.(6.34) are given in Fig. 6.13. and 6.14., respectively.

2.4 Select the minimum value of all α_k and β_k determined in Step 2.3 and take it as the load factor $\gamma_{min}(INC)$. It may happen that more than one spring yields α_k and/or β_k equal γ_{min}.

2.5 Calculate the coefficient Ω of accumulated external loads, as

$$\Omega = \sum_{j=1}^{INC} \gamma_{min}(j) = \tag{6.35}$$

$$= \gamma_{min}(INC) + \sum_{j=1}^{(INC-1)} \gamma_{min}(j) \tag{6.36}$$

and check if

$$\Omega \leq \Gamma \tag{6.37}$$

where

$$\Gamma = \frac{\text{DESIGN LATERAL LOADS}}{\text{UNIT LATERAL LOADS}} \tag{6.38}$$

2.5.1 If $\Omega \leq \Gamma$ use $\gamma_{min}(INC)$ from Step 2.4.

2.5.2 If $\Omega > \Gamma$ use

$$\gamma_{min}(INC) = \gamma_{min,abs.} = \Gamma - \sum_{j=1}^{(INC-1)} \gamma_{min}(j) \tag{6.39}$$

2.6 Multiply the incremental forces and displacements of all members (Step 2.2) by the load factor selected in Step 2.5, accumulate to forces and displacements (Step 1.4), and store.

2.7 If from Step 2.5,

2.7.1 - the load factor was given by Step 2.5.1, iterate from Step 2.

2.7.2 - the load factor was given by Step 2.5.2, Eq. (6.39), terminate the incremental procedure.

The above analysis is slightly modified when used for lateral loads only. The corresponding flow chart is given in Fig. 6.12. The above nonlinear procedure can be found within the computer program NOLI which is shown in Appendix C.

6.6 Conclusions

From the use of this analysis, the following observations can be made:

i) the Frame Equivalent Method for the analysis of shear-wall structures has been extended to cope with the case of lightweight sandwich panel structures.

ii) the effect of wide rigid arms has been incorporated within the analysis.

iii) simplified assumption has been made for the bending contribution of floor assemblies.

iv) two-dimensional (N,V) stapled joint characteristics are dealt with within the analysis by setting up joint-spring matrix stiffnesses, and using an incremental approach of analysis.

v) a computer program for the nonlinear analysis of an Equivalent Frame (NOLI) has been developed. The programme (Appendix C) can be modified to treat other structural typologies (i.e., nonlinear infill frames or concrete frames).

vi) the accuracy of the method depends on the number of curves representing the spring stiffnesses (Table 6.1). From Fig. 6.14 it may be noted that the average joint stiffness during each step is underestimated because the axial force on the joint is assumed constant during the step. Then the analysis should predict deflections higher than the actual ones.

TABLE 6.1

STIFFNESS $R_{sp}/2$ OF STAPLED-JOINT EQUIVALENT SPRINGS (*)

AXIAL FORCE N		0 ÷ 1000	1000 ÷ 2000	2000 ÷ 4000	4000 ÷ 6000	6000 ÷ up
SHEAR FORCE V		(1)	(2)	(3)	(4)	(5)
0÷250	(1)	16,800	42,000	78,400	102,400	136,600
250÷500	(2)	31,000	34,000	52,500	64,000	71,700
500÷1000	(3)	47,000	47,800	55,200	72,600	75,000
1000÷1500	(4)	76,000	69,500	84,400	99,000	112,500
1500÷up	(5)	109,000	112,000	141,300	185,000	197,800

(*) Units are: force lbf (1 lb = 4.45 N), stiffness lbf/in. (1 lbf/in. = 1.75 N/cm)

CHAPTER VII

COMPARISON AND DISCUSSION OF THEORETICAL AND EXPERIMENTAL RESULTS OF THE SANDWICH BUILDING MODEL

7.1 Introduction

The theory presented in Chapter VI was used to predict the theoretical stresses and deflections for loads corresponding to the tests on assembly 17. The data used in the theory are given in Table 7.5, and they were calculated according to the assumptions in Chapter VI. Theoretical calues were compared with the experimental ones, which were already presented in Chapter III.

7.2 Comparison of Deflections

Deflections are compared in Figs. 7.1 to 7.3 and in Table 7.1. The following observations can be made from Figs. 7.1 and 7.2.

a) In these figures, curve II represents the results obtained directly from the analysis. The horizontal segments of the curves represent the localized displacement of the springs which simulate the stapled joints (Fig. 6.4.b).

b) Curve III is obtained by averaging the results in curve II. Curve III closely represents the deformed shape of the model under the various load distributions adopted for the tests.

c) Curve III slightly underestimates the model deflections (Curve I) at the bottom of the model and overestimates them towards the top.

The average theoretical deflections and the experimental ones for test 17-03-T1 were also compared on a 3-dimensional plot, as shown in Fig. 7.3. From this figure, we observe the following:

d) The theoretical deformed shape is in very good agreement with the experimental one.

e) In the analysis, it was assumed that floors are infinitely rigid. For uniform lateral loads, this analysis yields equal deflections at different levels of the building. This behaviour is confirmed by uniform experimental deflections shown in the model.

The comparison of the values of the deflections at the top level is reported in Table 7.1. It can be seen (column (4)) that the percentage differences between experimental and theoretical results range between +4 and +18%, which are acceptable differences on the safe side. Column (5) reports the number of increments needed to perform the analysis.

A study was carried out to evaluate the influence of the two "secondary" effects on the deflections due to:

a) columns shear deformations;

b) beam effective width (see Sect. 6.3.2).

Results are reported in Table 7.2. It can be observed in this table that shear deformation in columns slightly increase the building deflections, say 6 + 7% (column 2). If the beam effective width is accounted for, a consistent reduction of approximately 11 to 13% (column (3)) will result. Combination of both effects will reduce the deflections (column (4)) by approximately 5 to 7%. Close agreement were observed (column 5, table 7.2) between the experimental and theoretical results after secondary effects were taken into account.

7.3 Comparison of Normal Stresses

From the end forces of the members obtained by means of the incremental analysis, the distribution of theoretical normal stresses at foundation level were calculated and plotted in Figs. 7.4, 7.6, 7.8

and 7.10 for the different tests. These figures show the flange panels of shear-wall AB to have higher normal stress levels than the flange panels of the internal shear-wall EF.

In order to compare theoretical and experimental stresses, the procedure indicated below was followed.

Section (a) of Figs. 7.5, 7.7, 7.9 and 7.11 present the theoretical envelopes of bending moments of the columns (or shear-walls) EE' and AA'. The value of the bending moment at the level of the rosette gages, 4 in. (10.2 cm) above the foundation level, was obtained from the moment envelopes. Normal stresses were calculated from these moment envelopes and plotted in sections (b) and (c) of Figs. 7.5, 7.7, 7.9 and 7.11 for shear-walls EF and AB respectively.

The experimental stresses at gage location were indicated on the latter diagrams and a dotted linear distribution of experimental stress was traced. The comparison of stresses is also reported in Table 7.4. The theory yields symmetric stress envelopes (Figs. 7.4, 7.6, 7.8 & 7.10) when springs at floor level are lumped. However, if the difference in spring stiffnesses is taken into account, these stresses shift by approximately 4%.

The figures (sections (b) and (c) of Figs. 7.5, 7.7, 7.9 and 7.11) generally show quite good agreement on the shape of the stress blocks, as well as good agreement on the values of stresses for most of the points of gage location.

Column (5) of Table 7.4 reports the percentage differences between experimental and theoretical stresses, which vary by 4 ± 15% for over 75% of the strain gages. Experimental normal stresses in

the vertical direction were calculated from the data obtained from the rosettes and plotted in the above figures. The extreme points were used to plot the stress envelopes. These curves compare favourably with the theoretical ones.

For a number of gages shown, the percentage difference varied up to 45%. This may be attributed to localized stress conditions which are difficult to avoid in sandwich construction.

In Fig. 7.7, the lines ----- represent the theoretical stress distribution. In this the effective width of beams has been accounted for in these results. Analogous shapes can be obtained for the other stress distributions Figs. 7.5, 7.9 and 7.11.

7.4 Influence of Stiffer Lintel Beams

A theoretical study was also conducted to determine the extent by which the building deflections could be reduced by increasing stiffness of the lintel beam. In fact if a lintel beam, made up of a sandwich panel 1 ft. deep, is assumed to be stapled to the column webs and horizontal joint, the theory predicts a reduction of approximately -12% for the deflections and of approximately -21 to 28% for the stresses.

7.5 Conclusions

The comparison shows that the proposed theory may be used to predict the deflection and stress distributions of framed sandwich shear-wall systems.

Any arrangement of sandwich shear-wall may be analyzed by the proposed theory. The analytical results will generally exceed the actual values by some 15%. It will be shown in Chapter VIII that localized stresses which may exceed analytical values do not affect the over-

all strength of the building, as predicted by the theory (see Section 8.3).

The use of stiffer lintel beams is highly recommended for this kind of panel assembly to control deflections and reduce stress.

The secondary effects of column shear deformations and beam effective width tend to cancel each other with a net reduction of deflections and stresses.

This theory can also be used to predict the stress levels at which wrinkling will occur in the flange panels. These stress levels are treated in Chapter VIII.

TABLE 7.1

ASSEMBLY 17 - COMPARISON OF EXPERIMENTAL AND THEORETICAL MAXIMUM DEFLECTIONS(1)

TEST	TOP DEFLECTIONS		% DIFFERENCE (3)-(2)	INCREMENTS(*)
	EXPERIMENTAL	THEORETICAL		
(1)	(2)	(3)	(4)	(5)
17-01-P1	.285 in. (.72 cm)	.336 in. (.85 cm)	+17.9	8
17-02-P2	.670 in. (1.7 cm)	.7607 in. (1.93 cm)	+11.45	14
17-03-T1	.913 in. (2.32 cm)	.9484 in. (2.41 cm)	+ 3.9	23
17-04-T3	.353 in. (.90 cm)	.394 in. (1.0 cm)	+11.16	8

(1) column shear deformation and beam effective width have not been taken into account.

(*) number of Steps in the Nonlinear Analysis

TABLE 7.2

ASSEMBLY 17 - INFLUENCE OF COLUMN SHEAR DEFORMATION AND EFFECTIVE WIDTH ON THEORETICAL DEFLECTIONS

(Percentage Increments With Respect to Deflections in Column (3) of Table 7.1)

TEST	COLUMN SHEAR DEFORMATION	BEAM (*) EFFECTIVE WIDTH	COMBINED EFFECT (2) + (3)	COMPARISON WITH EXPERIMENTS AFTER COMBINED EFFECT (*)
(1)	(2)	(3)	(4)	(5)
17-01-P1	+5.9%	-11.2%	-5.3%	+12.6%
17-01-P2	+6.5%	-12.3%	-5.8%	+ 5.6%
17-03-T1	+6.4%	-13.0%	-6.6%	- 2.7%
17-04-T3	+6.7%	-11.8%	-5.1%	+ 6.1%

(*) Effective width calculated according to Sect. 6.3.2.

(*) Percentages in column (5) are the differences of percentages in column (4) of the above Table and percentages of column (4) of Table (7.1)

TABLE 7.3

COMPUTATION OF THEORETICAL NORMAL STRESSES, IN PSI, AT GAGE LEVEL, ASSEMBLY T7

TEST	SHEAR WALL	BENDING MOMENT (lbf x in.)*			STRESSES AT GAGE LEV. DUE TO BENDING		AXIAL FORCE (lbf)	COMPR. STR. DUE TO AX.FOR.(PSI)	RESULTANT STRESSES (PSI)	
		FOUND.	1st FLOOR	GAGE LEVEL	COMPR.	TENSILE			COMPR.	TENSILE
(1)	(2)	(3)	(4)	(5)	(6)	(7)	(8)	(9)	(10)	(11)
T7-01-P1	AB	28130	1235	25683	-1082.75	2012.77	2000	-991.08	-2074	1022
	EF	34530	5732	31175	- 663.86	2722.69	3413	-991.14	-1655	1732
T7-02-P2	AB	46890	2059	42811	-1827.97	3355.09	3333	-1651.64	-3480	1703
	EF	57550	9553	51948	-1106.43	4537.82	5688	-1651.81	-2758	2886
T7-03-TT	AB	53400	-1787	49099	-2069.94	3847.88	4385	-2172.79	-4243	1675
	EF	64930	5835	59033	-1255.09	5155.72	7482	-2172.94	-3428	2983
T7-04-T3	AB	40370	5906	36514	-1539.36	2861.57	2281	-1130.33	-2670	1731
	EF	50180	13270	44893	- 955.97	3920.74	3893	-1130.54	-2087	2790

Units are: force, lbf (1 lbf = 4.45 N), moment, lbf x in. (1 lbf x in = 11.3 N x cm), stress, psi (1 psi = 6.9 kN/m^2)

(*) See also Section a) of Figs. 7.5, 7.7, 7. 9, 7.11

TABLE 7.4

COMPARISON OF THEORETICAL AND EXPERIMENTAL NORMAL STRESSES IN PSI AT GAGE LOCATIONS ASSEMBLY 17

(see Figs. 7.5, 7.7, 7.9 and 7.11)

TEST NUMBER	GAGE NUMBER	EXPERIMENTAL	THEORETICAL	% DIFFERENCE (4) - (3)
(1)	(2)	(3)	(4)	(5)
17-01-P1	38	1245	1400	+11
	8	1714	1601	- 7
	27	1931	2077	+ 7
	3	923	903	- 2
17-02-P2	38	2417	2758	+12
	10	1127	1465	+23
	27	3869	3480	-10
	3	1542	1504	- 2
17-03-T1	10	1361	1948	+30
	9	1678	1750	+ 4
	15	3032	2877	- 5
	3	1714	1447	-16
17-04-T3	10	530	961	+45
	9	1918	1477	-13
	15	1867	1655	+11
	14	1174	885	-25

(1 psi = 6.9 kN/m^2)

TABLE 7.5

GEOMETRIC PROPERTIES OF EQUIVALENT FRAME MEMBERS

MEMBER*	A(in^2)	I(in^4)	$\bar{z}$(in)
(1)	(2)	(3)	(4)
AB	3.20	178.4	50
EF	5.22	207.4	50
BC	4.37	7.32	24
FG	5.80	8.53	24

(*) See Fig. 7.4 for member identification

(1 in = 2.54 cm)

CHAPTER VIII

SEQUENCE OF FAILURES IN PANELIZED SANDWICH SHEAR-WALL STRUCTURES

8.1 Introduction

The analysis developed in Chapter VI was used to predict the structural behaviour during the failure test. Uniform lateral pressures were applied and progressively increased. The objectives of the test were to:

i) record the actual sequence of panel failures and compare it with the one predicted by theory.

ii) investigate the different modes of panel failures

iii) determine the ultimate load-carrying capacity of the structural system.

8.2 Experimental Set-Up

To record the occurence of skin deformation at the bottom of the compressed flange panels and the corresponding load distribution, two reflex cameras were set up (Fig. 8.1) and connected to a single remote-control air-shutter-release.

Failures were preceded by crackling noises and accompanied by a loud bang. The operator would inspect the panels where the noises occurred and take pictures of the wrinkling failures. At the same time, a set of readings of strains and displacements was taken with the PDP-8/L data acquisition system (DAS). The crew required to carry out this test consisted of four persons.

The theory predicted lateral top deflections large enough to exhaust the maximum travel (1 in. = 2.54 cm) of the pin of the canti-

lever transducers (Fig. 2.12). To record larger deflections, a set of three other cantilevers were placed beside the first ones and offset from the building by a distance somewhat less than 1 in. (2.54 cm). The second set of transducers thus started to record deflections just before the travel of the first set was exhausted. The readings of the second set were taken by a set of strain-indicator and switch-balance units, to avoid new balance and calibration of the DAS during the test.

After all main panel failures were recorded by camera #1, Fig. 8.1, the same camera was used to measure the approximate deflections of the building (see Fig. 8.5.a), as the building approached ultimate failure.

The increments of loadings were applied by very small and progressive openings of the air pressure valves which regulated the pressure within the plastic bags at different floor levels. The step-by-step opening of the valves produced small displacement of the building model, which in turn reduced the pressure in all the other bags. This variation in pressure produced, at several stages, non-symmetric loading components. Air leakages which occurred in several bags also contributed to this variation. Figure 8.2 shows the pictures taken by camera #2 (Fig. 8.1) of the panel of manometers monitoring the pressures of the air bags, at different load intensities. In section (i) and (e) of this figure, the level of pressure of three bags may be observed to have dropped towards zero which indicates the heavy leaking of these bags, due to the unexpected large pressures required to fail the building.

8.3 Presentation of the Experimental Results

The actual loading condition was recorded at the time of failures by photographing the panel of manometers (camera #2, Fig. 8.2).

In the following presentation:

- the panel code number refers to the panels shown in Figs. 8.1 and 8.6.a.
- the Load Index (L.I.) number indicates, in inches of water, the pressures in the 12 plastic bags (2 for each floor).

8.3.1 Sequence of Panel Failures and Corresponding Facing Stresses

Failures started at the flange panels 0616 and 0611 (Fig. 8.6.a) of corner shear-walls which failed very close to and at L.I.12 (Figs. 8.2.e and 8.2.f) or at uniform lateral pressure of 62.4 psf (3.0 kN/m^2) respectively.

Flange panel 0614 failed next at a load intensity close to 78 psf (3.74 kN/m^2) (Fig. 8.2.g). Experimental flange skin stresses close to failure ranged between 5531 psi (38164 kN/m^2) and 5560 psi (38985 kN/m^2). After flange failure, the experimental strain outputs from rosettes following on the wrinkles gave erratic results, because of the large curvature of the delaminated facing.

Next, the web panels of the corner shear walls failed: panel 0314 at L.I.16, Fig. 8.2.h, which corresponds to a uniform pressure of 83.2 psf (4.0 kN/m^2); panel 0114 at L.I.20, Fig. 8.2.i, which is equivalent to a uniform pressure of 104 psf (5.0 kN/m^2).

Flange panel 0613 failed later at L.I.24, or pressure equal to 125 psf (6 kN/m^2). The sequence ended with web panel 0214 at load distribution close to the ultimate load of 177 psf (8.5 kN/m^2)

8.3.2 Modes of Panel Failures

The modes of failure of all flange panels were similar, with large delamination of both faces, Figs. 8.3.a, c, e and f, show typical

flange delamination extending over the entire panel width. Figs. 8.3.b, and d) show similar skin delaminations on both sides of the panels, which indicates the same level of skin compression stresses on both facings.

Figures 8.3.g and h show the typical mode of failures of web panels 0114 and 0314, with facing delamination limited to approximately half the web depth, and starting from the web-flange junction. In the same figures, the length and amplitude of the wrinkle may be observed to progressively decrease and to disappear as it approaches the tension zone of the panel. The gradient of normal compressive stresses across the depth of the web is confirmed by this mode of web failure.

8.3.3 Deflections

Figure 8.4 presents the experimental deflected shapes of the model at the first stages of the failure test. The portions of the deflection curves at L.I.12 and L.I.16 with dotted lines, were traced from the outputs of the second set of transducers (see Section 8.2).

The full line in curve 8.6.b also shows the shape of the experimental load-deflection curve during the test. In particular, from this curve, it may be observed that the occurrence of the first flange panel failure ① corresponds to the development of large building deflections, to the reduction of the stiffness or loss of integrity of the panel, and, consequently, to the end of the elastic behaviour of the structure.

At L.I.24 (q=125psf=6.0 kN/m^2) the top deflection was recorded by camera #1 and it can be evaluated as close to 4 in. (10.2 cm) if the hand in Fig. 8.5.a is used as a reference. Figs. 8.5.b and c show the deflection at top and the deflected shape at same L.I.24.

8.3.4 Ultimate Load

The load intensity at ultimate was close to L.I.34, namely, a lateral uniform pressure of 177 psf (8.5 kN/m). As already mentioned in Section 8.2, at higher load intensities, three bags were leaking. After unloading, the structure recovered about three-quarters of its displacement.

8.4 Comparison of Experimental and Theoretical Results

8.4.1 Sequence of Failures

Comparison of predicted and actual sequence of failures is presented in Fig. 8.6.a. The theoretical one may be explained (numbers in squares [ ]) with reference to the distribution of theoretical normal stresses (Figs. 7.5, 7.7, 7.9 and 7.11). From these figures, the flange panels of side shear-walls were predicted as the most stressed in compression. The structural and loading symmetry also led to the predicted symmetric pattern of failures shown in Fig. 8.6.a. The comparison shows that:

i) A very good qualitative agreement exists between the two patterns. Flange panels 0616 (1) and 0611 (2) failed almost simultaneously, as predicted. Subsequently, flange panels always failed before web panels, as predicted.

ii) The late failure of panel 0613 (6) is the only discrepancy in the series. This failure was predicted to occur at the same time as failure (3) in panel 0614. This discepancy may be mainly attributed to:

a) difficulties arising during the test, on the regulation of the pressures of the bags, as described in Section 8.2.

b) unavoidable variations in strength and stiffness of panels.

8.4.2 Normal Stresses at Failure

The compressive normal stresses, at gage level, were theoretically calculated for the load distribution described in Fig. 8.2.e, just before the first flange panel failure (panel 0616). The corresponding stresses for flange panels of the side walls were predicted by the theory to be 6346 psi (43787 kN/m^2), an overestimate by 11 to 13% as compared to the experimental stress (see Section 8.3.1).

It may be noted that the experimental normal stresses at wrinkling had values which match the corresponding values obtained from the investigation on single panels (see Section 5.4 and Table 5.5).

8.4.3 Load-Deflection History

Figure 8.6.b presents the load-deflection history. Table 8.1 also summarizes the deflection comparison. Two phases may be observed by inspection of Fig. 8.6.b, i.e.,

i) elastic range - up to the first flange-panel failure, where the analysis is shown to predict deflection values larger than the experimental ones, by 8 to 10% (column (5) of Table 8.1).

ii) post-elastic range - the analysis in this zone was continued using the same elastic properties for the member, i.e., without accounting for the delaminations which had occurred. The theoretical deflections in this zone were, therefore, expected to be lower than the true ones, as shown in Fig. 8.6.b and column (5) of Table 8.1 (between L.I.12 and L.I.16).

The analysis was discontinued after the first web-panel failure (④, panel 0314), in the absence of reliable information on the true stiffness of assembled shear sandwich walls with buckled flanges.

8.5 Conclusions

The following conclusions may be drawn from this failure test:

i) The analysis presented herein may be used to predict the level of stresses at which the first failure of flange panels will occur.

ii) The analysis may be used to predict the lateral deflections for the elastic range, and for the early stage of post-elastic behaviour.

iii) The sequence of failures may be established from the wrinkling stresses predicted by the theory.

iv) The different modes of failure in the flange and web panels have been described and related to the overall behaviour of the structure.

v) The ultimate lateral load carried by the structure was 177 psf (8.5 kN/m^2) which corresponds to six times the design wind load stipulated by the code [24]. Because of the large scale used in designing the model, no problems of model distortion [59] will arise. Thus the model can be considered as prototype and comparison is directly made to analytical results. However a check of the behaviour of the stapled joints of the full-scale prototype should be carried out.

TABLE 8.1

COMPARISON OF THEORETICAL AND EXPERIMENTAL TOP DEFLECTIONS AT EARLY STAGES OF FAILURE TEST

LOAD INDEX	LOAD INTENSITY	DEFLECTIONS		% DIFFERENCE (4)-(3)
		EXPERIMENTAL	THEORETICAL	
(1)	(2)	(3)	(4)	(5)
5	26 psf (1.25 kN/m^2)	.566 in. (1.44 cm)	.620 in. (1.575 cm)	+9.6
8	41.6 psf (2 kN/m^2)	1.012 in. (2.57 cm)	1.09 in. (2.77 cm)	+7.7
close to 12	59.3 psf (2.84 kN/m^2)	1.348 in. (3.42 cm)	1.453 in. (3.69 cm)	+7.8
12	62.4 psf (3 kN/m^2)	1.616 in. (4.10 cm)	1.535 in. (3.9 cm)	-5.0
16	83.2 psf (4 kN/m^2)	2.03 in. (5.16 cm)	1.9625 in. (4.98 cm)	-3.0
20	104 psf (5 kN/m^2)	2.58 in (6.55 cm)	discontinued	-
24	125 psf (6 kN/m)	4. in. (10.2 cm)	discontinued	-

CHAPTER IX

CONCLUSIONS AND RECOMMENDATIONS

9.1 Conclusions

From the theoretical and experimental studies carried out on the structural aspects of the model, the following observations can be made:

i) The experimental investigation on the model (Chapter III), carried out with various loading conditions and at its different stages of assembly, has shown:

   a) the similarity of the model behaviour to the behaviour of shear-wall structures, for both deflections and stresses;

   b) a composite web-flange behaviour of the wall panel assemblies;

   c) non-dimensional drift coefficients which, for lateral loads, equivalent to code stipulated wind loads, ranged between 1/300 and 1/400 (Section 3.4).

ii) A computer program (PANBLDG, Appendix A) was developed to process the experimental data acquired by a 120 channel data acquisition system.

iii) A comprehensive analysis has been developed to predict the behaviour of sandwich panels with various edge conditions (Chapter V). The comparison of this analysis with the results of 8 sets of tests on 26 panels, subjected to edgewise compression or bending loads, has shown that:

   a) design formulae for wrinkling stresses of unreinforced edge panels need to be revised according to Eq. (5.7);

b) the expressions developed to predict loads at wrinkling, post-wrinkling and ultimate stages compared favourably with the experimental results.

c) mitred corner details and transverse shrinkage of the wood frames reduce the level of ultimate and wrinkling load carrying capacity of the panels, respectively.

iv) A theory has been developed for the overall behaviour of the system (Chapter VI). It accounts for the panel behaviour (Chapter V) and for the non-linear behaviour of stapled joints (Chapter IV). In the analysis, stapled joints were replaced by springs, whose stiffnesses varied according to piece-wise linearized joint characteristics.

a) from this incremental analysis a computer program was derived in Fortran IV (Program NOLI, Appendix C). This program performs non-linear elastic analysis which is included within the category of Equivalent Frame Method for shear-walls, and it can deal simply and efficiently with any sandwich wall assembly.

b) this theory was applied to predict the stresses and deflections obtained from 4 tests. The comparison shows that (Chapter VII) the analysis closely predicts shape and value of the lateral building deflections and stresses. The predicted values will usually exceed the true ones by an average of 15%.

c) Substantial reduction in the deflection and stresses is theoretically achieved by increasing the stiffness of the lintels.

v) A failure test of the model (Chapter VIII) has shown that:

a) the above analysis may be used to predict the level of wrinklink stress at which failure of the first panel occurs under increasing lateral loads.

b) the sequence of failures may be established from the stress distribution predicted by the theory.

c) the different modes of failure of panels under out-of-plane bending (flange panels) and in-plane bending (web panels) have been described and related to the overall behaviour of the structure.

d) The structure resisted lateral loads close to 180 psf (8.6 kN/m^2) an equivalent wind pressure approximately six times larger than design load.

9.2 Recommendation for Future Research

This study has been limited to the structural behaviour of panelized assemblies made up of lightweight sandwich panels. Other effects may be investigated:

i) the connection system could be improved to reduce slippage and designed to resist climate conditions.

ii) the strength of the panel can be increased by using better corner details for the wood frame.

iii) a dynamic investigation would help to determine the behaviour of this type of structure under earthquake forces.

iv) effects of concentrated loads on the panels due to appliances and furniture.

v) fire rating.

vi) construction procedure and related costs

vii) architectural aspects

REFERENCES

[1] Fazio, P., "Study of Modular Panelized Buildings", ASCE, National Structural Engineering Meeting, Baltimore, Maryland, April 19-26, 1971, ASCE Preprint #1419.

[2] Parton, G.M., "Polyhedral Sandwich Domes: Construction and Analysis", IASS WCOSE-76, Montreal, Quebec, July 4-9, 1976, Vol. 1, pp. 241-247.

[3] Anonymous, "Cupola made of Sandwich Construction with Plastic Foam Core", (Belg. Plast), No. 7, May 1970, pp. 28-29.

[4] Fazio, P., "Ultimate Strength of Folded Sandwich Panel Roofs", ASCE Nat. Struct. Eng. Meeting, Baltimore, Apr. 19-23, 1971, Reprint #1382, 29 pages.

[5] Fazio, P., "Failure Modes of Folded Sandwich Panel Roofs", ASCE J. Struct Div., Vol. 97, ST5, May 1972, Paper 8913, pp. 1085-1104.

[6] Fazio, P., "Investigation of Sandwich Panel Assemblies for Industrialized Buildings", Symposium on Ind. Spat. and Shell Struct., IASS, Ed. Kielce, Pol. June 18-23, 1973, pp. 201-214.

[7] Nathan, J., Lugex, J., et al, "Design and Manufacture of Large Pre-Cast Concrete Panels", Ann. Inst. Tech. Bat. Trav. Publics, N. 339, May 1976, pp. 69-119.

[8] Teitsma, G.J., "Structural Sandwich Panel System for Agricultural Buildings", Am. Soc. Agr. Eng. Winter Meet., Chicago, Ill., Dec., 1969, Paper #69903, 24 pages.

[9] McLelland, W., "Use of Structural R.P. Sandwich Panels in Housing and Building Construction", Proc. 24th Ann. Tech. Conf., Compes. Inst., Feb. 8-11, 1972, Sect. 20-A, 4 pages.

[10] Mateja, Krzysztof, "Investigation of Bearing Lightweight Panels for External Walls", Inz. Budowinctwo N32, N. 10, Oct. 1975, pp. 422-424.

[11] Abdel-Malek, R.A., Dean, D.L., "New Idea in Sandwich Panel Construction", Int. J. Mech. Sci., Vol. 10, N. 3, 1977, pp. 177-191.

[12] Anonymous, "Prototype of a Service Station made of Prefabricated Sandwich Panels", Plast. Mod. Elastomeres, Vol. 24, N. 3, April 1972, pp. 92-93.

[13] Minford, J.D., Vader, B.M., "Aluminum-Faced Sandwich Panels and Laminates", Adhes. Age., V. 18, N. 2, Feb. 1975, pp. 30-35.

[14] McCavour, T.C., "Criteria for the Design of Steel Sandwich Panels", ASCE, Nat. Str. Eng. Meeting, Baltimore, Md., Apr. 19-23, 1971, Reprint #1407, 29 pages.

[15] Biblis, E.J.. Chiu, W., "Preliminary Evaluation of Two Tongue and Groove Joints for Five Ply Structural Sandwich Wood Panels for Floors", For. Prod. J., V. 26, N. 7, July 1976, pp. 55-57

[16] Gad, Waldemar, "Foamed Plastics as Core Material in Light-Weight Sandwich Panels", Kunstst Bau, V. 12, N. 2, 1977, pp. 26-29.

[17] Reichard, T.W., "Paper Honeycomb Sandwich Panels as Light-Weight Structural Components", Nat. Bur. Stand. of U.S.A., Build. Sci. Serv., N. 43, April 1972, 8 pages.

[18] Brentjes, Jay, "Use of Honeycomb Sandwich Construction in Recreational Vehicles", S.A.E., Preprint #770425 for Meet., Feb. 24-March 4, 1977, 9 pages.

[19] Rizzo, S. and Fazio, P., "Lateral Deflection of a Sandwich-Panel Building Model under Combined Loading", Report No. CBS-50, March 1978; accepted for publication in "Experimental Mechanics", J. of the Soc. of Experimental Stress Analysis.

[20] Kalosinakis, M., "Theoretical and Experimental Investigation of Stapled Connections", M.Eng. Thesis, Centre for Building Studies, Concordia Univ., June 1978.

[21] Fazio, P. and Rizzo, S., "Wrinkling of Framed Aluminum Sandwich Panels", Proc. of 4th Symp. on Engineering Applications of Solid Mechanics, Ont. Res. Found., Mississauga, Ont., Sept. 25-26, 1978.

[22] Fazio, P. and Mikler, J., "Modular Panelized Buildings, Final Design of the Experimental Set-up of a Half Scale Four-story Panelized Building Model", Rep. No. SBC-09, Dept. of Civi. Eng., Concordia Univ., Montreal, July 1970.

[23] Sen, A., "Program Listing to Process Raw Data from PDP-8/L by CDC CYBER 172/7 Computer Data Acquisition System", Report No. CBS-57, August, 1978, Centre for Bldg. Studies, Concordia Univ., Montreal.

[24] National Building Code of Canada, 1977, National Research Council of Canada, Publ. No. 75555, 1977.

[25] Williams, D., "Sandwich Construction, A Practical Approach for the use of Designers", Royal Aircraft Establishment Report No. Structures 2, 1947.

[26] Allen, H.G., "Analysis and Design of Structural Sandwich Panels", Pergamon Press, 1969.

[27] Norris, C.B., et al., "Wrinkling of the Facings of Sandwich Construction Subjected to Edgewise Compression", FPL Report 1810, 1949.

[28] Marsh, C., private communication, unpublished.

[29] Milbradt, K.P., "Timber Structures", Sect. 16 of the Structural Engineering Handbook, Gaylord, F.H. and Gyalord, C.N., editors, McGraw Hill, 1968.

[30] Albiges, M. and Goulet, J., "Contreventement des Batiments", Annales de l'Institut Technique du Batiment et des Travaux Publiques, Vol. 13, No. 149, May 1960, pp. 473-500.

[31] Beck, H., "Contribution to the Analysis of Coupled Shear Walls", ACI Journal, Title No. 59-39, Aug. 1962, pp. 1055-1069.

[32] Rosman, R., "Approximate Analysis of Shear Walls Subject to Lateral Loads", ACI Journal, Title No. 64-41, June 1964, pp. 717-733.

[33] Coull, A., Choudhury, J.R., "Stresses and Deflections in Coupled Shear Walls", ACI Journal, Title No. 64-6, Feb. 1967, pp. 65-72.

[34] Coull, A., Choudhury, J.R., "Analysis of Coupled Shear Walls", ACI Journal, Sept. 1967, pp. 587-593.

[35] Rosman, R., "Tables for the Internal Forces of Pierced Shear Walls subjected to Lateral Loads", Bauingenier, Praxis #66, W.Ernst and Sohn, Berlin, 1966, 76 pages.

[36] Schwaighofer, J. and Tai, C., "Tables for the Analysis of Shear Walls with Two Vertical Rows of Openings", Rep. No. 71-27, Dept. of Civ. Engr., Univ. of Toronto, Ont., Canada, Nov. 1971, 64 pages.

[37] Ha, H.K., "Analysis of Three-Dimensionsl Orthotropic Sandwich Plate Structures F.E.M.", D.Eng. Thesis, Sir George Williams Univ., Montreal, Que., August 1972, 134 pages.

[38] Jenkins, W.M. and Harrison, T., "Proc. of a Symp. on Tall Buildings"., Univ. of Southampton, England, April 1966, pp. 413-444.

[39] Stafford Smith, B., "Modified Beam Method for Analyzing Symmetrical Interconnected Shear Walls", ACI Journal, Title No. 67-68, Dec. 1970, pp. 977-980.

[40] Schwaighofer, J., "Shear Wall Structures", Structural Concrete Symposium, Toronto, May 13-14, 1971, pp. 139-145.

[41] Lightfoot, E. and Le Mesurier, A.P., "Elastic Analysis of Frameworks with Elastic Connections", Journ. of Struc. Div., ASCE, Proc. Paper No. 10632, Vol. 100, No.ST6, June 1974, pp. 1297-1309.

[42] Lionberger, S.R. and Weaver, W., "Dynamic Response of Frames with Non-rigid Connections", Journ. of Eng. Mech. Div., ASCE Proc. Paper No. 6393, Vol. 95, No. E1, Feb. 1969, pp. 95-114.

[43] Monforton, G.R. and Wu, T.S., "Matrix Analysis of Semi-rigidly Connected Frames", Journ. Struc. Div., ASCE Proc. Paper No. 3713, Vol. 89, No. ST6, Dec. 1963, pp. 13-42.

[44] Romstad, K.M. and Subramanian, C.V., "Analysis of Frames with Partial Connection Rigidity", Journ. of Struc. Div., ASCE Proc., Paper No. 7664, Vo.. 96, No. St11, Nov., 1970, pp. 2283-2300.

[45] Suko, M. and Adams, P.F., "Dyanmic Analysis of Multibay Multistory Frames", Journ. of Struc. Div., ASCE, Proc. Paper No. 8443, Vol. 97, No. ST10, Oct. 1971, pp. 2519-2533.

[46] Burnett, E.F.P. and Rejendra, R.C.A., "Influence of Joints in Panelized Structure Systems", Journ. Struc. Div., ASCE Proc., Vol. 98, No. ST8, Sept. 1972, pp. 1943-1955.

[47] Cholewicki, A., "Behaviour of Prefabricated Stiffening Walls subjected to Action of Horizontal Forces", Symposium on Tall Buildings, CIB Report No. 21, Moscow, October 1971, pp. 179-192.

[48] Cholewicki, A., "Loadbearing Capacity and Deformability of Vertical Joints in Structural Walls of large Panel Buildings", Building Science, Vol. 6, Dec. 1971, 4 pages.

[49] Pollner E., Tso, W.K. and Heidbrecht, A.C., "Analysis of Shear Walls in Large-Panel Construction", Can. J. Civ. Eng., Vol. 2, 1975, pp. 357-367.

[50] Robinson, J., "Recommendations internationales unifiees pour le calcul et l'execution des structures en panneaux assembles de grand format", C.E.B., C.I.B., U.E.A., etc., AITEC, Rome, 1969.

[51] Przemieniecki, J.S., "Theory of Matrix Structural Analysis", McGraw-Hill, New York, 1968.

[52] Feodosyev, V., "Strength of Materials", MIR Publishers, Moscow, 1973.

[53] Gere, J.M. and Weaver, W., "Analysis of Framed Structures", D. VAnNostrand, 1965.

[54] Sahlin, S., "Methodes d'analyse non-lineaire de proche en proche - Programmes sur ordinateurs - Effects structuraux d'attenuation des deformationes", ASCE-IABSE Joint Committee, Tall Buildings International Conference, University of Letigh, Aug. 21-26, 1972, Vol. III - 22, Report No. 2. (in French).

[55] Perry, C.C., Lissner, H.R., "The Strain Gage Primer", McGraw-Hill, 1962.

[56] Fazio, P., Palusamy, S., "Panelized Building Model - Acquisition and Coding of Experimental Data", Report No. SBC-19, Dept. of Civil Eng., Concordia Univ., Montreal, March, 1972.

[57] Fazio, P., Ha, K.H., "Sandwich Plate Structure Analysis by Finite Element", J. of the Structural Division, A.S.C.E., Vol. 100, No. ST6 June, 1974, pp. 1243-1262.

[58] Ha, H.K., Fazio, P.P., "Flexural Behaviour of Sandwich Floor Assembly", Build. and Env., Vol. 13, No. 1, pp. 61-67, 1978.

[59] Murphy, C., "Similitude in Engineering", Ronald Press Co., New York, 1950.

APPENDIX A

COMPUTER PROGRAM PANBLDG TO TRANSFORM STRAINS INTO STRESSES

The computer program, PANBLDG, was developed to process the experimental data obtained from the building model; it transforms the strains of the gages on the model into stresses in psi in selected directions and the strains from the deflection transducers into deflections in inches. The theory of elasticity is used to describe the two-dimensional plane state stress condition on the facing and in the cantilevered element of the deflection transducer. The main steps in the program are traced in Fig. A.1.

A.2 Governing Equations

A.2.1 Transformation of Measured Strains to Strains in Any Direction

The positive conventions of strains and stresses are derived from Perry and Lissner [55], with reference to Fig. A.2;

$$\varepsilon_n = \frac{\varepsilon_x + \varepsilon_y}{2} + \frac{\varepsilon_x - \varepsilon_y}{2} \cos 2\phi + \frac{\gamma_{xy}}{2} \sin 2\phi \qquad (A.1)$$

To determine the three unknowns, ε_x, ε_y, γ_{xy} three measured strains ε_1, ε_2, ε_3, in different directions ϕ_1, ϕ_2, ϕ_3, respectively, are required to form a linear system of equations:

$$\varepsilon_1 = \frac{\varepsilon_x + \varepsilon_y}{2} + \frac{\varepsilon_x - \varepsilon_y}{2} \cos 2\phi_1 + \frac{\gamma_{xy}}{2} \sin 2\phi_1$$

$$\varepsilon_2 = \frac{\varepsilon_x + \varepsilon_y}{2} + \frac{\varepsilon_x - \varepsilon_y}{2} \cos 2\phi_2 + \frac{\gamma_{xy}}{2} \sin 2\phi_2 \qquad (A.2)$$

$$\varepsilon_3 = \frac{\varepsilon_x + \varepsilon_y}{2} + \frac{\varepsilon_x - \varepsilon_y}{2} \cos 2\phi_3 + \frac{\gamma_{xy}}{2} \sin 2\phi_3$$

Solution of Eq. (A.2) gives ε_x, ε_y, γ_{xy}

A.2.2 Principal Strains

Differentiating Eq. (A.1) with respect to the angle ϕ, after simplification, is:

$$\frac{\sin 2\phi_p}{\cos 2\phi_p} = \tan 2\phi_p = \frac{\gamma_{xy}}{\varepsilon_x - \varepsilon_y} \tag{A.3}$$

where

$$\sin 2\phi_p = \pm \frac{\gamma_{xy}}{\sqrt{(\varepsilon_x - \varepsilon_y)^2 + \gamma_{xy}^2}}$$

$$\cos 2\phi_p = \pm \frac{\varepsilon_x - \varepsilon_y}{\sqrt{(\varepsilon_x - \varepsilon_y)^2 + \gamma_{xy}^2}} \tag{A.4}$$

Use of the positive and negative value of Eq. (A.4) into Eq. (A.1) yields, respectively,

$$\varepsilon_{max} = \frac{\varepsilon_x + \varepsilon_y}{2} + \frac{\sqrt{(\varepsilon_x - \varepsilon_y)^2 + \gamma_{xy}^2}}{2}$$

$$\varepsilon_{min} = \frac{\varepsilon_x + \varepsilon_y}{2} - \frac{\sqrt{(\varepsilon_x - \varepsilon_y)^2 + \gamma_{xy}^2}}{2} \tag{A.5}$$

$$\gamma_{max} = \sqrt{(\varepsilon_x - \varepsilon_y)^2 + \gamma_{xy}^2}$$

which represent the principal strain values.

A.2.3 Principal Stresses

From the generalized Hooke's law,

$$\sigma_{max} = \frac{E}{(1-\mu^2)} (\varepsilon_{max} + \mu\, \varepsilon_{min})$$

$$\sigma_{min} = \frac{E}{(1-\mu^2)} (\varepsilon_{min} + \mu\, \varepsilon_{max}) \tag{A.6}$$

$$\tau_{max} = \frac{E}{2(1+\mu)} \gamma_{max} \qquad (A.6)$$

A.2.4 Rectangular Rosettes

Strains were recorded with rectangular rosette gages, Fig. A.3. After substitution of the values of $\phi_1 \phi_2$ and ϕ_3 into Eq. (A.2) and solving for $\varepsilon_x \varepsilon_y$ and γ_{xy}, the following expressions are obtained:

$$\varepsilon_x = \varepsilon_1 \qquad \varepsilon_y = \varepsilon_3$$
$$\gamma_{xy} = 2\varepsilon_2 - (\varepsilon_1 + \varepsilon_3) \qquad (A.7)$$

Substituting Eq. (A.7) into Eq. (A.5) and simplifying,

$$\varepsilon_{max} = \frac{\varepsilon_1+\varepsilon_3}{2} + \frac{\sqrt{(\varepsilon_1-\varepsilon_3)^2 + [2\varepsilon_2 - (\varepsilon_1+\varepsilon_3)]^2}}{2}$$

$$\varepsilon_{min} = \frac{\varepsilon_1+\varepsilon_3}{2} - \frac{\gamma_{max}}{2}$$

$$\gamma_{max} = \sqrt{(\varepsilon_1-\varepsilon_3)^2 + [2\varepsilon_2 - (\varepsilon_1+\varepsilon_3)]^2}$$

$$\phi_p = \frac{1}{2} \text{arctg} \frac{2\varepsilon_2 - (\varepsilon_1+\varepsilon_3)}{\varepsilon_1-\varepsilon_3}$$

These values are substituted in Eqs. (A.6) to obtain the principal stresses.

A.3 Details of the PANBLDG Program

Data from strain gages are processed and stored on tape. Each strain gage is read 50 times consecutively, then the average value of the voltages is read and stored. For every load increment, three sets of such readings are recorded. A calibration reading is also taken. The

tape is then processed by the CYBER 172 (CDC 7200). The voltage readings are converted to strains with the Sen program [23]. The results are stored in a tabular form. Each line contains, from left to right, the load index ALOAD, channel No. NCH, calibration reacing CAL, average reading AVGRD. Erroneous readings are eliminated by inspection, replaced by 0 and the respective channels identified.

The program PANBLDG operates on the above data, which are called vai TAPE 5. Calibrated average readings are calculated according to Fazio and Palusamy [56]:

$$AVGC = AVGRD \times CF \qquad (A.9)$$

where

$$CF = \frac{2000}{CAL - AVGRD} \quad \text{is the calibration factor} \qquad (A.10)$$

The program distinguishes the rosettes on the model from the linear gages and the deflection transducers and makes appropriate transformations into deflections or stresses. The array INDEX is used to identify the rosettes and deflection transducers and stored in a file which is retrieved via TAPE 4. The complete content of this data file is given below.

Card No.		NR	NCT	NLG	HCHA	
1						
	ARRAY INDEX	1	2	3		← typical row for rosettes
		4	5	6		
		.	.	.		
		12	0	13		← typical row for rosettes with 2 orthogonal gages only
		.	.	.		
NR+NCT+NLG+1		0	31	0		← typical row for linear gage
		915.24	918.4	1018.24	*	

* a calibration coefficient for each transducer EPSL is stored and used to transform strains to displacements.

The final stresses and deflections are printed in tabular form.

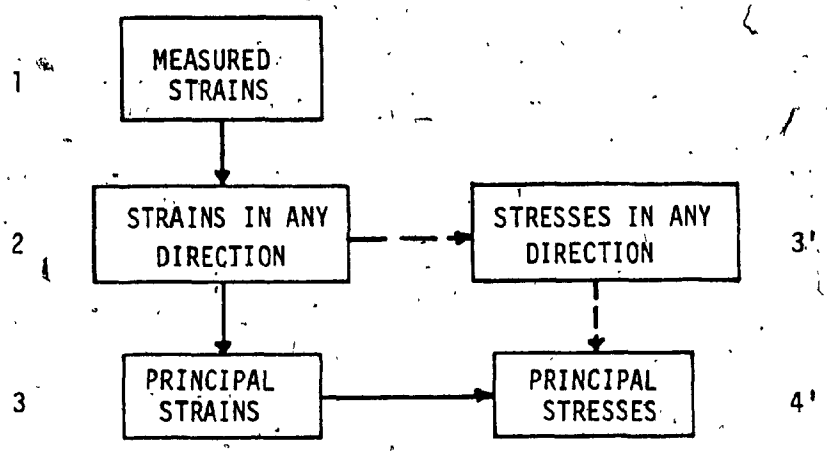

FIG. A.1 - TRANSLATION OF MEASURED STRAINS INTO STRESSES IN ANY DIRECTION

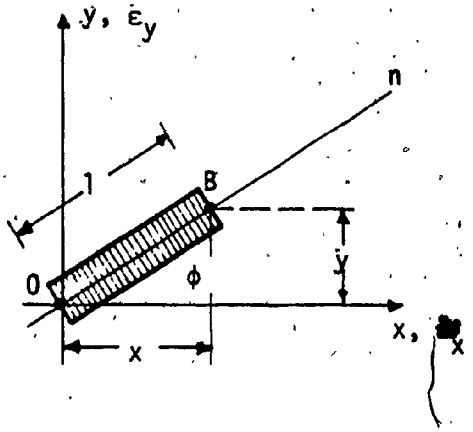

FIG. A.2 - REPRESENTATION OF LINEAR STRAIN GAGE $\overline{OB}$

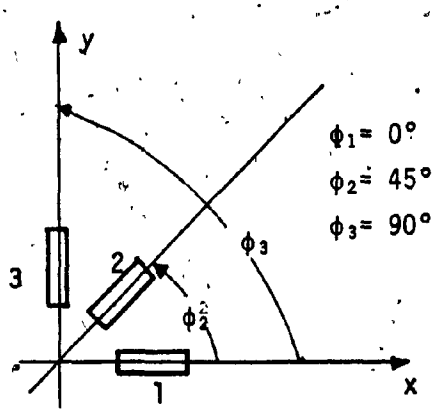

FIG. A.3 - NUMBERING CONVENTION OF RECTANGULAR ROSETTES

PROGRAM PANBLDG LISTING

```
      PROGRAM PANBLDG    73/172  OPT=1          PAGE 1.              FTN 4.7+470
 1              PROGRAM PANBLDG(INPUT,OUTPUT,TAPE4,TAPE5)
                DIMENSION ALOAD(1200),NCH(1200),CAL(1200),AVGRD(1200)
                DIMENSION EPS(100,3),INDEX(100,3),EPSL(100,2),INDEM(50)
                DIMENSION AVGC(200),AVGDISP(100),SXY(100,3),EPSS(100)
 5              DIMENSION EXY(100,3),EMAX(100),EMIN(100),GMAX(100),IMOD(100,3)
                DIMENSION PRANG(100),CR(100),STRESS(100),DISPL(100),PSTR(100,3)

                READ(4,*)NR,NCT,NLG,NCHA
                ND=NR+NCT+NLG
10              PRINT 444
                PRINT 445,ND,NR,NCT,NLG,NCHA

           CCC READING AND PRINTING ARRAY INDEX.
                READ(4,*)((INDEX(I,J),J=1,3),I=1,ND)
15              PRINT 7
                DO 85 I=1,ND
                PRINT 6,I,(INDEX(I,J),J=1,3)
             85 CONTINUE

20         CCC READING MATERIAL ELASTIC MODULUS (PSI) AND POISSON RATIO.
           CC  (PRESENT VALUES ARE FOR ALUMINIUM)
                TE=10000000
                E=TE/1000000
                POIS=1./3
25
           CCC READING CANTILEVER FACTORS EPSL(I,2) AND THEIR AVG CONST.
                IF(NCT.EQ.0)25,26
             26 READ(4,*)(EPSL(L,2),L=1,NCT)
                PAS=0.
30              DO 30 L=1,NCT
                PAS=PAS+EPSL(L,2)
             30 CONTINUE
                CONST=PAS/NCT

35         C*C*C*C*C*C*C*C*C*C*C*      OUTPUT PROCESSING FOR DISPLACEMENTS
           C.                          (INCH) AND STRESSES (PSI).
                PRINT 909
                READ *,NREC
             25 DO 900 KK=1,NREC
40              KL=KK-1
                PRINT 2000,KK

           CCC READ DATA FROM TAPE5.
                DO 1 J=1,NCHA
45              KJ=J+(NCHA*KL)
                READ(5,555)ALOAD(KJ),NCH(KJ),CAL(KJ),AVGRD(KJ)
                IF(AVGRD(KJ).EQ.CAL(KJ))620,630
            620 AVGC(J)=AVGRD(KJ)
                GO TO 1
50          630 AVGC(J)=AVGRD(KJ)*(2000/(CAL(KJ)-AVGRD(KJ)))
              1 CONTINUE
                LI=ALOAD(KJ)
                PRINT 3000,LI

55         CCC PRINTING STRAINS DATA FROM TAPE5.
                PRINT 18
                PRINT 19
```

```
PROGRAM PANBLDG    73/172  OPT=1          PAGE 2.          FTN 4.7+470
                KN=NCHA/5
                DO 90 I=1,KN
 60             J=I+KN
                L=J+KN
                M=L+KN
                N=M+KN
                PRINT 2,I,AVGC(I),J,AVGC(J),L,AVGC(L),M,AVGC(M),N,AVGC(N)
 65           90 CONTINUE

          CCC INDEX ARRAY MODIFICATION FOR NOT RELYABLE READINGS.
                PRINT 700
                READ *,NRR
 70             PRINT 707,NRR
                READ *,(INDEM(IM),IM=1,NRR)
                DO 111 I=1,ND
                DO 111 J=1,3
                IMOD(I,J)=INDEX(I,J)
 75           111 CONTINUE
                JL=1
                KM=1
                LM=1
                DO 888 K=KM,ND
 80             DO 888 L=LM,3
                IF(IMOD(K,L).EQ.INDEM(JL))666,888
              666 IMOD(K,L)=150
                IF(JL.EQ.NRR)777,776
              776 JL=JL+1
 85             GO TO 888
              777 KM=ND
                KL=3
              888 CONTINUE

 90       CCC ADRESSING STRAINS OUTPUT
                PRINT 336
                IC=0
                IR=0
                IL=0
 95             DO 20 K=1,ND
                IF(IMOD(K,3).EQ.0)220,230
              220 IF(IMOD(K,2).EQ.0)240,255
              240 IC=IC+1
                LL=IMOD(K,1)
100             IF(LL.LE.120)242,244
              242 EPSL(IC,1)=AVGC(LL)
                GO TO 20
              244 EPSL(IC,1)=0.
                PRINT 337,K,LL
105             GO TO 20
              255 IL=IL+1
                LL=IMOD(K,2)
                IF(LL.LE.120)257,259
              257 EPSS(IL)=AVGC(LL)
110             GO TO 20
              259 EPSS(IL)=0.
                PRINT 337,K,LL
                GO TO 20
              230 IR
```

```
      PROGRAM PANBLDG    73/172  OPT=1          PAGE 3.          FTN 4.7+470

115               LL=IMOD(K,1)
                  IF(LL.LE.120)231,232
              231 EPS(IR,1)=AVGC(LL)
                  GO TO 233
              232 EPS(IR,1)=0.
120               PRINT 337,K,LL
              233 MK=IMOD(K,3)
                  IF(MK.LE.120)234,235
              234 EPS(IR,3)=AVGC(MK)
                  GO TO 236
125           235 EPS(IR,3)=0.
                  PRINT 337,K,MK
              236 JJ=IMOD(K,2)
                  IF(JJ.EQ.0)260,270
              270 IF(JJ.LE.120)280,290
130           260 EPS(IR,2)=0.
                  GO TO 20
              280 EPS(IR,2)=AVGC(JJ)
                  GO TO 20
              290 EPS(IR,2)=0.
135               PRINT 337,K,JJ
               20 CONTINUE

            CCC CALCULATING CANTILEVER DISPLACEMENTS.
                  IF(NCT.EQ.0)125,124
140           124 DO 850 L=1,NCT
                  DISPL(L)=(EPSL(L,1)*EPSL(L,2))/1000000
                  AVGDISP(L)=(EPSL(L,1)*CONST)/1000000
              850 CONTINUE

145         CCC PRINTING CANTILEVER STRAINS FACTORS AND DISPLACEMENTS.
                  PRINT 14
                  PRINT 15,CONST
                  DO 880 II=1,21
                  PRINT 460,II,EPSL(II,1),EPSL(II,2),II,DISPL(II),AVGDISP(II)
150           880 CONTINUE

            CCC PRINTING ROSETTES AND ROS.2 OUTPUT STRAINS.
              125 IF(NR.EQ.0)160,99
               99 PRINT 12
155               PRINT 13
                  DO 80 I=1,NR
                  PRINT 8,I,EPS(I,1),EPS(I,2),EPS(I,3)
               80 CONTINUE

160         CCC CALCULATING AND PRINTING ROSETTES AND ROS./2 PRINC.STRESSES AND STR
                  PRINT 1000
                  PRINT 1001
                  PRINT 550
                  DO 100 I=1,NR
165               IF(EPS(I,1).EQ.0)95,91
               95 IF(EPS(I,3).EQ.0)94,97
               94 IF(EPS(I,2).EQ.0)92,97
               92 PRINT 193,I
                  GO TO 100
170            91 IF(EPS(I,1).EQ.EPS(I,2))191,97
              191 IF(EPS(I,1).EQ.EPS(I,3))96,97
```

```
      PROGRAM PANBLDG    73/172  OPT=1              PAGE 4.          FTN 4.7+470

               96 A8=E/(1.-(POIS*POIS))
                  SXY(I,1)=(EPS(I,1)+(POIS)*EPS(I,3))*AS
                  PRINT 196,I
      175         PRINT 195,EPS(I,2),SXY(I,2)
                  GO TO 100
               97 A1=.5*(EPS(I,1)+EPS(I,3))
                  A2=EPS(I,1)-EPS(I,3)
                  EXY(I,1)=EPS(I,1)
      180         EXY(I,2)=EPS(I,3)
                  EXY(I,3)=EPS(I,2)-A1
                  A3=2*EXY(I,3)
                  GMAX(I)=SQRT(A2**2+A3**2)
                  AP=.5*ATAN2(A3,A2)
      185         PRANG(I)=57.3*AP
                  CR(I)=GMAX(I)*.5
                  EMAX(I)=A1+CR(I)
                  EMIN(I)=A1-CR(I)
                  PSTR(I,3)=CR(I)*(E/(1.+POIS))
      190         PS=A1*E/(1.-POIS)
                  PSTR(I,1)=PS+PSTR(I,3)
                  PSTR(I,2)=PS-PSTR(I,3)
                  AS=E/(1.-(POIS*POIS))
                  SXY(I,1)=(EXY(I,1)+(POIS*EXY(I,2)))*AS
      195         SXY(I,2)=(EXY(I,2)+(POIS*EXY(I,1)))*AS
                  SXY(I,3)=E*EXY(I,3)/(1.+POIS)
                  PRINT 400,I,EMAX(I),EMIN(I),GMAX(I),PRANG(I),CR(I),EXY(I,1),
                 *EXY(I,3),EXY(I,2),I
                  PRINT 600,PSTR(I,1),PSTR(I,2),PSTR(I,3),PSTR(I,3),
      200        *SXY(I,1),SXY(I,3),SXY(I,2)
              100 CONTINUE

            CCC CALCULATING AND PRINTING LINEAR GAGES STRESSES.
              160 IF(NLG.EQ.0)900,170
      205     170 PRINT 333
                  DO 180 L=1,NLG
                  STRESS(L)=EPSS(L)*E
                  PRINT 334,L,EPSS(L),STRESS(L)
              180 CONTINUE
      210
              900 CONTINUE

                2 FORMAT(5(3X,I4,3X,E10.4))
                6 FORMAT(5X,I3,3(4X,I3))
      215       7 FORMAT(/,4X,*ARRAY INDEX*,/,2X,*DEVICE*,4X,*(1)*,4X,*(2)*,4X,
                 *'(3)',/)
                8 FORMAT(3X,I3,3(6X,E10.4))
               12 FORMAT(/,*ROSETTES AND ROS./2 OUTPUT(MICROINCH/INCH)*,/)
               13 FORMAT(4X,*NO*,8X,*EPS(I,1)*,8X,*EPS(I,2)*,8X,*EPS(I,3)*)
      220      14 FORMAT(/,*CANTILEVER TRANSDUCERS OUTPUT(MICROINCH/INCH)*,4X,*DISPL
                *ACEMENTS(INCH)*,/)
               15 FORMAT(4X,*NO*,7X,*EPSL*,8X,*FACTOR*,8X,*NO*,5X,
                **DISPL.*,7X,*AVGDISP*,3X,*(CONST.FACTOR=*,F7.2,*)*)
               18 FORMAT(/,*DATA ACQUISITION SYSTEM OUTPUT(MICROINCH/INCH)*,/)
      225      19 FORMAT(5(2X,*CHANNEL*,3X,*STRAIN*))
               23 FORMAT(5(2X,I3))
              192 FORMAT(1X,I3,10X,*NO STRAINS EXISISTING (EPS1=EPS2=EPS3=0.)*,/)
              195 FORMAT(14X,*(EPS1=EPS2=EPS3=*,E10.4,*)*,2X,*SIGMAX=SIGMAY= *,
```

```
      PROGRAM PANBLDG    73/172  OPT=1            PAGE 5.        FTN 4.7+470
         *E10.4,/)
  230   196 FORMAT(1X,I3,10X,*GAMMAXY=TAUXY=0.(MOHR'S CIRCLES ARE POINTS)*)
        200 FORMAT(2(I3))
        250 FORMAT(I8,F5.3)
        333 FORMAT(/,2X,*1-D LINEAR GAGES*,/,3X,*NO*,6X,*STRAIN*,
         *4X,*STRESS*)
  235   334 FORMAT(2X,I3,2(2X,E10.4))
        336 FORMAT(/,2X,*NO CALIBRATED CHANNELS*,/,2X,*DEV.*,5X,*CHAN*)
        337 FORMAT(3X,I3,6X,I3)
        350 FORMAT(F9.6,F5.3)
        400 FORMAT (1X,I3,' STRAIN',1X,3(E10.4,1X),F7.2,4(1X,E10.4),* STRAIN*,
  240    *1X,I3)
        444 FORMAT(/,2X,*NO. OF MEASURING DEVICES USED*,/,2X,*1)TOTAL*,2X,
         *'2)ROSETTES',2X,*3)CANT.TRANSD.*,2X,*4)LIN.GAGES*,2X,*5)D.A.S. CHA
         *NNELS*)
        445 FORMAT(4X,I3,8X,I3,10X,I3,14X,I3,12X,I3)
  245   460 FORMAT(3X,I3,2(3X,E10.4),6X,I3,2(3X,E10.4))
        550 FORMAT(/,'ROSETTE',10X,'MAX.',7X,'MIN.',6X,'TANG.',
         *3X,'ALFAPR',4X,*RADIUS*,8X,*X*,9X,*XY*,10X,*Y*,8X,*ROSETTE*,/)
        555 FORMAT(F2.0,I3,2(F8.2))
        600 FORMAT(5X,'STRESS',3(1X,E10.4),9X,E10.4,3(1X,E10.4),* STRESS*,/)
  250   700 FORMAT(//,2X,*ENTER NUMBER OF NOT RELYABLE READINGS*)
        707 FORMAT(//,2X,*ENTER*,3X,I3,3X,*CHANNEL NUMBERS*)
        909 FORMAT(//,2X,*ENTER NUMBER OF TAPE RECORDS=LOAD INDEXES*)
       1000 FORMAT(//,12X,'-PRINCIPAL STRAINS AND STRESSES-',10X,'-MOHR'S CIRC
         *LE A)STRAIN WITH (EPS,GAMMA/2) AXES-')
  255  1001 FORMAT(18X,*(MICROINCH/INCH)*,3X,*(PSI)*,24X,*B)STRESS WITH (SIGMA
         *,TAU) AXES-*)
       2000 FORMAT(///,55X,*TAPE RECORD NO. =*,I3)
       3000 FORMAT(55X,*LOAD INDEX    =*,I3,///)

  260       STOP
            END
```

APPENDIX B

POST-WRINKLING CORE TENSION FAILURE ANALYSIS BY C. MARSH

An initial plate imperfection may be expressed as

$$\delta_o = \lambda/1000 \qquad (a)$$

The wave displacement function is assumed as, Fig. 5.5,

$$w = \delta . e^{-Cz} \sin \frac{\pi}{\lambda} x \qquad (b)$$

with C the subgrade (core) foundation coefficient.

$$C = (\pi/\lambda) \sqrt{G_c/E_c} \qquad (c)$$

The effective strain in the waved skin will be incremented to a value equal to

$$\varepsilon_{cr} = \frac{\sigma_{wr}}{E_s} + \frac{\pi^2}{4} \left(\frac{\delta}{\lambda}\right)^2 \qquad (d)$$

If

$$\delta = \delta_o/(1 - \frac{\sigma}{\sigma_{wr}}); \quad \sigma = 0,9\ \sigma_{wr} \qquad (e)$$

the strain increment value in Eq. (d), and Eq. (5.14),

$$\frac{\pi^2}{4} \left(\frac{\delta}{\lambda}\right)^2 = 0.25 \times 10^{-4} \qquad (f)$$

APPENDIX C

COMPUTER PROGRAM NOL1

The program, NOL1, whose listing follows, performs the analysis of sandwich shear-walls with two-dimensional (N,V) horizontal joint characteristics.

It incorporates the effects of rigid arms parallel and orthogonal to the longitudinal member axis. It includes 22 subroutines which perform the various matrix algebra operations needed for the analysis.

The data needed to operate the programe are: (notation is given at the beginning of the program listing)

1. via TAPE 4

CARD	NO	
1		NT
2	I=1	A(1), FL(1), FI(1), E(1), V(1)
NT + 1	I=NT	A(NT), ... , V(NT) (*)
NT + 2		SPG(1,) . . . . . , SPG(1,K)
NT+ 2 + J		SPG(J,1) . . . . . , SPG(J,K)
NT + J + 3		VL1M(1) . . . . . , VL1M(L)
NT + J + 4		AXL1M(1) . . . . . , AXL1M(L)

* The program organization requires that for I = NT, or for the last set of member properties, the spring properties must be input as follows: A(NT) = 1.0 FL(NT) = 1.0 FI(NT) = 0.0 E(NT) = 1.0 V(NT) = 0.0

2. via TAPE 5

CARD NO.		
1		NB, LDF
2		ICON(1) . . . . . , ICON(NB)
3	I=1	LBL(1,1)..,(LBL(1,6),MTY(1),CX(1),W1(1),W2(1),DY(1)
NB + 2	I=NB	LBL(NB,1). . ,LBL(NB,6),MTY(NB),CX(NB), W1(NB), W2(NB),DY(NB)

2. via TAPE 6

CARD NO.		
1		NDF, NLV
2	I=1	ALD(1,1), ... , ALD(1,NLV)
NDF + 1	I=NDF	ALD(NDF,1) . . . . . , ALD(NDF,NLV)

The input data are organized to give flexibility to the use of the program. Thus, different combinations of data files may be made.

```
LEVEL 2.2.1 (DEC 77)                    05/360  FORTRAN H EXTENDED          DA

REQUESTED OPTIONS: NODECK,NOOBJECT

OPTIONS IN EFFECT: NAME(MAIN) NOOPTIMIZE LINECOUNT(60) SIZE(MAX) AUTODBL(NONE)
                   SOURCE EBCDIC NOLIST NODECK NOOBJECT NOMAP NOFORMAT NOGOSTMT NOXREF

                      CCCC
                      CCCCC PROGRAM NOLI (INPUT,OUTPUT)
                      CCCC
                      CCC NOTATION :
                      C    NT  = INTEGER NO. OF SETS OF MEMBER PROPERTIES
                      C          (MEMBERS WITH EQUAL PROPERTIES ARE INPUT ONCE ONLY)
                      C    NB = INTEGER NO. OF MEMBERS OF THE STRUCTURE
                      C    LDF = MEMBER LOCAL DEGREES OF FREEDOM
                      C    NDF = STRUCTURE' DEGREES OF FREEDOM
                      C    NLV = INTEGER NO. OF LOAD VECTORS
                      C    NJB = INTEGER NO. OF BARS SUBJECT TO STRESS CHECK
                      C    KINC= MAXIMUM NO. OF LOAD INCREMENTS
                      C    AMIN= THE INCREMENT' LOAD FACTOR
                      C    SUMAMIN= ACCUMULATED AMIN IN PREVIOUS AND CURRENT STEP
                      C    SCALOAD= FACTOR OF LOAD REDUCTION
                      CCC  DUEMAX = INVERSE OF SCALOAD
                      CCCC
                      CCC ARRAYS HAVING MINIMUM DIMENSION =NT :
                      C    A(NT), CROSS AREA OF MEMBER
                      C    FL(NT), LENGTH OF MEMBER
                      C    FI(NT), MOMENT OF INERTIA OF MEMBER
                      C    E(NT), YOUNG' MODULUS OF MEMBER
                      C    V(NT), FACTOR FOR MEMBER SHEAR DEFORMATION
                      CCCC
ISN 0002                    DIMENSION A(5),FL(5),FI(5),E(5),V(5)
                      CCCC
                      CCC ARRAYS HAVING FIRST DIMENSION = NB :
                      C    LBL(NB,LDF), INTEGER ARRAY OF ADRESSING LABELS
                      C    INDE(NB,2), INTEGER ARRAY TO SELECT SPRING STIFFNESS
                      C    CX(NB), COSINE OF ANGLE OF LOCAL AND GLOBAL X-AXES
                      C    W1(NB), LEFT-HAND SIDE RIGID ARM OF MEMBER
                      C    W2(NB),RIGTH-HAND SIDE RIGID ARM OF MEMBER
                      C    DY(NB), DISTANCE OF LAYOUT AXIS TO MEMBER X-AXIS
                      C    MTY(NB), MEMBER TYPE (REFERS TO ARRAYSO A,FL,FI,E,V)
                      C    BV (NB),SPRING LO. FACTOR FOR SHEAR
                      C    BAX(NB),SPRING LO. FACTOR FOR AXIAL FORCE
                      C    ICON(NB), INDEX TO CONNECT SPRING TO COLUMN
                      C    FACC(NB,LDF), ACCUMULATED LOCAL MEMBER FORCES
                      C    DACC(NB,LDF), ACCUMULATED LOCAL MEMBER DISPLACEMENTS
                      C    FINC(NB,LDF), INCREMENTAL LOCAL MEMBER FORCES
                      C    DINC(NB,LDF), INCREMENTAL LOCAL MEMBER DISPLACEMENTS
                      C    CHA(NB), ARRAY FOR CHANGE OF SPRING STIFFNESS
                      CCCC
ISN 0003                    DIMENSION CX(56),W1(56),W2(56),DY(56),MTY(56),BV(56),BAX(56)
ISN 0004                    DIMENSION FINC(56,6),LBL(56,6),INDE(56,2),DACC(56,6),FACC(56,6)
ISN 0005                    DIMENSION DINC(56,6),ICON(56),CHA(56)
                      CCCC
                      CCC ARRAYS HAVING FIRST DIMENSION = LDF
                      C    S(LDF,LDF), MEMBER LOCAL STIFFNESS MATRIX
                      C    SG(LDF,LDF), MEMBER GLOBAL STIFFNESS MATRIX
                      C    R (LDF,LDF), ROTATION MATRIX
                      C    TR(LDF,LDF), TRANSFORMATION MATRIX
                      C    SR(LDF,LDF)
```

```
LEVEL 2.2.1 (DEC 77)          MAIN          OS/360  FORTRAN H EXTENDED          CA

                C   TS(LDF,LDF)
                C   FLC(LDF), LOCAL MEMBER FORCES
                C   DILL(LDF), LAYOUT MEMBER DISPLACEMENTS
                C   DIL(LDF), LOCAL MEMBER DISPLACEMENTS
                C   DIP(LDF), DIPLACEMENTS // TO LAYOUT
                C   DIW(LDF), DIPLACEMENTS AT RIGID ARMS ENDS
                C   DIR(LDF), DIPLACEMENTS AFTER ROTATION
                CCCC
ISN 0006              DIMENSION S(6,6),R(6,6),TR(6,6),SG(6,6),SR(6,6),TS(6,6),FLC(6)
ISN 0007              DIMENSION DILL(6),DIL(6),DIP(6),DIW(6),DIR(6)
                CCCC
                CCC ARRAYS HAVING FIRST-DIMENSION = NDF )
                C   STG(NDF,NDF), STRUCTURE' GENERAL STIFFNESS MATRIX
                C   DST(NDF,NDF), STG DUPLICATED
                C   STI(NDF,NDF), STG INVERTED
                C   ALD(NDF,NLV), MATRIX OF EXTERNAL NODAL LOADS
                C   ALDV(NDF), A LOAD VECTOR EXTRACTED FROM ALD
                C   DIV(NDF), STRUCTURE' GENERAL DISPLACEMENTS (DIV=STI*ALDV)
                C   ALAV(NDF),ARGUMENT OF LIBRARY SUBROUTINE MINV
                C   BLAV(NDF),ARGUMENT OF LIBRARY SUBROUTINE MINV
                C   ACCLD(NDF), ACCUMULATED LOADS
                C   ACCDI(NDF), ACCUMULATED DISPLACEMENTS
                CCCC
ISN 0008              DIMENSION STG(40,40),DST(40,40),STI(40,40),ALD(40,6),ALDV(40)
ISN 0009              DIMENSION DIV(40),ALAV(40) ,BLAV(40),CLAV(40,40)
ISN 0010                 DIMENSION ACCLD(40),ACCDI(40)
                CCCC
                CCC FURTHER ARRAYS
                C   NLC(LL), ARGUMENT OF PRINTING SUBROUTINES
                C   SPG, ARRAY OF SPRING STIFFNESSES
                C   VLIM, ARRAY OF SPRING LIMIT SHEARS
                C   AXLIM, ARRAY OF SPRING LIMIT AXIAL FORCES
                CCCC
ISN 0011              DIMENSION NLC(10),SPG(5,6),VLIM(5),AXLIM(6)
                CCCC
                CCC ARRAYS HAVING DIMENSION =NJB (
                C   JBAR(NJB),  VECTOR OF BAR NO. SUBJECT TO STRESS CHECK
                C   WSX(NJB), SECTION MODULUS(LEFT)
                C   WDX(NJB), SECTION MODULUS(RIGTH)
                CCCC
ISN 0012              DIMENSION JBAR(4),WSX(4),WDX(4)
                CCCC
ISN 0013              CALL ERRSET(207,300,-1,1,1,207)
                CCC
                CCCCC DATA READING
                CCC
ISN 0014              READ (5,71) NT
ISN 0015              WRITE (6,56)
ISN 0016              DO 11 I=1,NT
ISN 0017              READ (5,72) A(I),FL(I),FI(I),E(I),V(I)
ISN 0018              WRITE (6,110) I,A(I),FL(I),FI(I),E(I),V(I)
ISN 0019           11 CONTINUE
ISN 0020              READ(5,71)NAX
ISN 0021              READ(5,71)NSH
ISN 0022              READ (5,73) ((SPG(I,J),J=1,NAX),I=1,NSH)
ISN 0023              WRITE(6,666)NSH,NAX
ISN 0024              CALL PRINT (SPG,NSH,NAX,NLC)
ISN 0025              READ (5,72) (VLIM(I),I=1,NSH)
```

```
LEVEL 2.2.1 (DEC 77)          MAIN          OS/360  FORTRAN H EXTENDED          DATE

  ISN 0026            READ (5,73)(AXLIM(I),I=1,NAX)
  ISN 0027            WRITE (6,75) (VLIM(I),I=1,NSH)
  ISN 0028            WRITE (6,74)(AXLIM(I),I=1,NAX)
  ISN 0029            READ (5,71) NB
  ISN 0030            READ (5,71) LDF
  ISN 0031            CALL ZERO (LBL,NB,LDF)
  ISN 0032            WRITE (6,115)
  ISN 0033            DO 1111 K= 1,NB
  ISN 0034            READ (5,76) (LBL(K,J),J=1,LDF),MTY(K),CX(K),W1(K),W2(K),DY(K),
                     1ICON(K)
  ISN 0035            WRITE (6,12 )K,(LBL(K,J),J=1,LDF),MTY(K),CX(K),W1(K),W2(K),DY(K),
                     =ICON(K)
  ISN 0036       1111 CONTINUE
  ISN 0037            READ (5,71) NDF
  ISN 0038            READ (5,71) NLV
  ISN 0039            READ (5,73)((ALD(I,J),J=1,NLV),I=1,NDF)
  ISN 0040            WRITE(6,669J) NDF,NLV
  ISN 0041            CALL PRINT(ALD,NDF,NLV,NLC)
  ISN 0042            READ(5,71) NJB
  ISN 0043            WRITE(6,44 0 )
  ISN 0044            DO 1515 KK=1,NJB
  ISN 0045            READ(5,450 ) JBAR(KK),WSX(KK),WDX(KK)
  ISN 0046            WRITE(6,46 ) KK,JBAR(KK),WSX(KK),WDX(KK)
  ISN 0047       1515 CONTINUE
  ISN 0048      44 00 FORMAT (/,3X,'NO.',3X,'BAR',8X,'WSX', 9X,'WDX')
  ISN 0049      45 00 FORMAT (I3,2(F12.2))
  ISN 0050      46 00 FORMAT (/,3X,I3,3X,I3,2(2X,F10.3))
                CCC
                CCCCC LOAD VECTOR SELECTION
                CCC
  ISN 0051      45454 DO 43 L=1,NLV
  ISN 0052            DO 222 J=1,NB
  ISN 0053            INDE(J,1)=1
  ISN 0054            INDE(J,2)=1
  ISN 0055        222 CONTINUE
  ISN 0056            CALL ZERO (STG,NDF,NDF)
  ISN 0057            CALL ZERO (FACC,NB,LDF)
  ISN 0058            CALL ZERO (DACC,NB,LDF)
  ISN 0059            CALL ZEROV(CHA,NB)
  ISN 0060            CALL ZEROV(ACCLC,NDF)
  ISN 0061            CALL ZEROV(ACCDI,NDF)
  ISN 0062            SUMANI =0.)
  ISN 0063            KINC=1.0
  ISN 0064            WRITE(6,6681)L
                CCC
                CCCCC BEGINNING OF INCREMENTAL ANALYSIS
                CCC
  ISN 0065      33338 DO 333 INC=1,KINC
  ISN 0066            WRITE(6,3300C)INC
  ISN 0067            CALL IPRNT   (INDE,NB,2,NLC)
                CCC
                CCCCC GENERATION OF MEMBER STIFFNESS MATRICES
                CCC
  ISN 0068            CALL ZERO (DST,NDF,NDF)
  ISN 0069            CALL ZERO (STI,NDF,NDF)
  ISN 0070            DO 10 I=1,NB
  ISN 0071            KKI=MTY(I)
  ISN 0072            IF(KKI.EQ.NT) GO TO 2)
```

```
LEVEL 2.2.1 (DEC 77)          MAIN          OS/360  FORTRAN-H EXTENDED          DA

 ISN 0074           IF (INC.GT.1) GO TO 10
 ISN 0076           GO TO 40
 ISN 0077        20 IV=INDE(I,1)
 ISN 0078           IAX=INDE(I,2)
 ISN 0079           A(KKI)=SPG(IV,IAX)
 ISN 0080           WRITE(6,676)IV,IAX
 ISN 0081           WRITE(6,677) I,KKI,SPG(IV,IAX)
 ISN 0082        40 CALL MESTI (S,LDF,A,E,FI,FL,V,NT,KKI)
 ISN 0083           IF(IL.GT.1).OR.(INC.GT.1)) GO TO 5540
 ISN 0085           WRITE(6,50) I
 ISN 0086           CALL PRINT (S,LDF,LDF,NLC)
 ISN 0087      5540 CONTINUE
 ISN 0088           CCX=CX(I)
 ISN 0089           WI=W1(I)
 ISN 0090           WJ=W2(I)
 ISN 0091           DP=DY(I)
 ISN 0092           CALL GESTI(S,SG,LDF,R,TR,TS,SR,CCX,WI,WJ,DP)
 ISN 0093           IF((L.GT.1).OR.(INC.GT.1)) GO TO 5540
 ISN 0095           WRITE(6,60) I
 ISN 0096           CALL PRINT(SG,LDF,LDF,NLC)
 ISN 0097      5540 CONTINUE
 ISN 0098           IF (KKI.EQ.NT) GO TO 240
 ISN 0100           IF (INC.GT.1) GO TO 1
 ISN 0102           CALL ACCUST  (SG,STG,LBL,I,NDF,LDF,NB)
 ISN 0103           GO TO 10
 ISN 0104       240 CALL ACCUST  (SG,DST,LBL,I,NDF,LDF,NB)
 ISN 0105         1 CONTINUE
                CCC
                CCCCC SOLUTION OF THE GLOBAL STRUCTURE MATRIX
                CCC
 ISN 0106           CALL ADD (STG,DST,STI,NDF,NDF)
 ISN 0107           CALL DUPL (STI,DST,NDF,NDF)
 ISN 0108           CALL DUPL(STI,CLAV,NDF,NDF)
 ISN 0109           WRITE(6,70)NDF,NDF
 ISN 0111           CALL MINV (DST,NDF,D,ALAV,WLAV)
 ISN 0111           CALL DUPL(DST,STI,NDF,NDF)
 ISN 0112           WRITE(6,30)NDF,NDF
 ISN 0113           CALL MULT(CLAV,STI,DST,NDF,NDF,NDF)
 ISN 0114           CALL EXTVH (ALDV,ALD,NDF,NLV,L,1)
 ISN 0115           SCALDA =1./1000.
 ISN 0116           CALL SCALEV (ALDV,SCALDA ,ALDV,NDF)
 ISN 0117           CALL MULTV (STI,ALDV,DIV,NDF,NDF)
 ISN 0118           WRITE(6,90)L,INC
 ISN 0119           DO 42 M=1,NDF
 ISN 0120           WRITE(6,97)M,DIV(M),ALDV(M)
 ISN 0121        42 CONTINUE
                CCC
                CCCCC INCREMENTAL  FORCES AND DISPLACEMENTS
                CCC
 ISN 0122           CALL ZEROV (BAX,NB)
 ISN 0123           CALL ZEROV (BV ,NB)
 ISN 0124           CALL ZERO (DINC,NB,LDF)
 ISN 0125           CALL ZERO (FINC,NB,LDF)
 ISN 0126     56666 DO 46 N=1,NB
 ISN 0127           CALL EXTV (DILC,DIV,LBL,N,LDF,NDF,NB)
 ISN 0128           CCX=CX(N)
 ISN 0129           WI=W1(N)
 ISN 0130           WJ=W2(N)
```

```
LEVEL 2.2.1 (DEC 77)          MAIN          OS/360  FORTRAN H EXTENDED          DA

 ISN 0131            DP=DY(N)
 ISN 0132            CALL LOCOIS (CILL,CIL,LDF,N,TR,DIR,DIP,DIN,CCX,NI,NJ,DP)
 ISN 0133            KKI=MTY(N)
 ISN 0134            CALL MESTI (S,LDF,A,E,FI,FL,V,NT,KKI)
 ISN 0135            CALL MULTV (S,DIL,FLC,LDF,LDF)
 ISN 0136            FLM=FL(KKI)
 ISN 0137            CALL EQUCHK (FLC,LDF,FLM)
 ISN 0138            CALL ACCUVM (FLC,FINC,NB,LDF,N,2)
 ISN 0139            CALL ACCUVM (CIL,CINC,NB,LDF,N,2)
 ISN 0140         48 CONTINUE
 ISN 0141            WRITE(6,10000)INC
 ISN 0142            CALL PRINT (FINC,NB,LDF,NLC)
                  CCC
                  CCCCC ANALYSIS OF RESULTING INCREMENTAL FORCES
                  CCC
 ISN 0143            WRITE(6,3500)
 ISN 0144            DO 666 IB=1,NB
 ISN 0145            KKI=MTY(IB)
 ISN 0146            IF (KKI.NE.NT) GO TO 666
 ISN 0148            IF(FINC(IB,1).EQ.0.0) STOP
 ISN 0150            KV=INDE(IB,1)
 ISN 0151            VLINC=VLIM(KV)
 ISN 0152            BV(IB)=(VLINC-ABS(FACC(IB,1)))/ABS(FINC(IB,1))
 ISN 0153            RATIO=FACC(IB,1)/FINC(IB,1)
 ISN 0154            IF(RATIO.GE.0.0) GO TO 4343
 ISN 0156            BV(IB)=-BV(IB)
 ISN 0157         4240 JK=ICON(IB)
 ISN 0158            IF(FINC(JK,1).EQ.0.0) STOP
 ISN 0160            IF(FACC(JK,1).GE.0.0) GOTO 4242
 ISN 0162         4141 BAX(IB)=10000000000.**2
 ISN 0163              GO TO 6611
 ISN 0164         4242 RATIO=FACC(JK,1)/FINC(JK,1)
 ISN 0165            IF(RATIO.GE.0.0) GO TO 4343
 ISN 0167            GO TO 622
 ISN 0168         4343 KAX=INDE(IB,2)
 ISN 0169            AXLINC=AXLIN(KAX)
 ISN 0170            BAX(IB)=(AXLINC-FACC(JK,1))/FINC(JK,1)
 ISN 0171            GO TO 6611
 ISN 0172          622 IF(KAX.EQ.1) GO TO 4141
 ISN 0174              KAX=KAX-1
 ISN 0175              AXLINC=AXLIN(KAX)
 ISN 0176              BAX(IB)=(FACC(JK,1)-AXLINC)/FINC(JK,1)
 ISN 0177         6611 WRITE(6,3000) IB,ICON(IB),BAX(IB),BV(IB)
 ISN 0178          666 CONTINUE
                  CCC
                  CCCCC MINIMUM LOAD FACTOR SELECTION
                  CCC
 ISN 0179            AMIN=10000000000.**2
                  CCC
                  CCCCC POSSIBLE LIMIT LOAD FACTORS FOR SPRINGS
                  CCC
 ISN 0180            DO 777 LB=1,NB
 ISN 0181            IF (MTY(LB).EQ.NT) GO TO 722
 ISN 0183            GO TO 777
 ISN 0184          722 IF (BV(LB).GE.AMIN) GO TO 744
 ISN 0186            AMIN=BV(LB)
 ISN 0187            IBAR=LB
 ISN 0188          744 IF(BAX(LB).LT.0.0) GO TO 777
```

```
LEVEL 2.2.1 (DEC 77)          MAIN          OS/360  FORTRAN H EXTENDED          DAT
   ISN 0190            IF (BAX(LB)*GE*AMIN) GO TO 777
   ISN 0192            AMIN=BAX(LB)
   ISN 0193            IBAR=LB
   ISN 0194          777 CONTINUE
   ISN 0195            WRITE(6,6677)AMIN,IBAR,L,INC
                     CCC
                     CCCCC CHECK FOR TERMINATION OF INCREMENTAL ANALYSIS
                     CCC
   ISN 0196            COEMAX=1./SCALOA
   ISN 0197            IF (AMIN.GE.COEMAX) GO TO 7777
   ISN 0199            GO TO 78
   ISN 0200         7777 AMIN=COEMAX
   ISN 0201            SUMAMI =SUMAMI +AMIN
   ISN 0202            WRITE(6,2277)AMIN,AMAX,COEMAX,SUMAMI
   ISN 0203            GO TO 89222
   ISN 0204           78 AMAX=COEMAX-SUMAMI
   ISN 0205            IF (AMAX.LE.AMIN) GO TO 87
   ISN 0207            SUMAMI =SUMAMI +AMIN
   ISN 0208            WRITE(6,2277)AMIN,AMAX,COEMAX,SUMAMI
   ISN 0209            GO TO 88
   ISN 0210           87 AMIN =AMAX
   ISN 0211            SUMAMI =SUMAMI +AMIN
   ISN 0212            WRITE(6,2277)AMIN,AMAX,COEMAX,SUMAMI
   ISN 0213            GO TO 89111
                     CCC
                     CCCCC MODIFICATION OF ARRAY INDE
                     CCC
   ISN 0214           38 DO 8989 KB=1,NB
   ISN 0215            IF (MTY(KB),NE,MT) GO TO 8989
   ISN 0217            IF (AMIN.EQ.BV(KB)) GO TO  888
   ISN 0219            GO TO 1818
   ISN 0220          888 INDE(KB,1)=INDE(KB,1)+1
   ISN 0221            CHA(KB)=1.)
   ISN 0222         1818 IF(AMIN.EQ.BAX(KB)) GO TO 999
   ISN 0224            GO TO 8989
   ISN 0225          999 INDE(KB,2)=INDE(KB,2)+1
   ISN 0226            CHA(KB)=1.
   ISN 0227         3949 CONTINUE
                     CCC
                     CCCCC FORCES AND DISPLACEMENTS TO BE ACCUMULATED
                     CCC
   ISN 0228            INCP=INC-1
   ISN 0229            WRITE(6,4000)INCP
   ISN 0231            CALL PRINT (FACC,NB,LDF,NLC)
   ISN 0231            WRITE(6,1177)AMIN
   ISN 0232            GO TO 99
   ISN 0233        89222 WRITE(6,4477)AMIN
   ISN 0234            GO TO 89
   ISN 0235        89111 WRITE(6,3377)AMIN
   ISN 0236           89 CALL SCALE (FINC,AMIN,FINC,NB,LDF)
   ISN 0237            WRITE(6,1000)INC
   ISN 0238            CALL PRINT (FINC,NB,LDF,NLC)
   ISN 0239            CALL ADD (FACC,FINC,FACC,NB,LDF)
   ISN 0240            WRITE(6,4000)INC
   ISN 0241            CALL PRINT (FACC,NB,LDF,NLC)
   ISN 0242            CALL SCALEV(ALDV,AMIN,ALDV,NDF)
   ISN 0243            CALL ADDV(ALDV,ACCLD,ACCLD,NDF)
   ISN 0244            CALL SCALEV( DIV,AMIN, DIV,NDF)
```

```
LEVEL 2.2.1 (DEC 77)          MAIN          OS/360  FORTRAN H EXTENDED          DATE

  ISN 0245          CALL ADDV( DIV*ACCDI,ACCDI,NDF)
  ISN 0246          WRITE(6,909)L,INC,SUMAMI
  ISN 0247          DO 707 J=1,NDF
  ISN 0248          WRITE(6,97) J,ACCDI(J),ACCLD(J)
  ISN 0249      707 CONTINUE
  ISN 0250          IFIN=INC
  ISN 0251          IF (AMIN.EQ.AMAX)   GO TO 454
  ISN 0253      333 CONTINUE
                CCC
                CCCCC END OF INCREMENTAL ANALYSIS
                CCC
  ISN 0254      454 CONTINUE
  ISN 0255          CALL STRESS (UBAR,WSX,WDX,NJB,FACC,NB,LDF,NTY,A,NT)
  ISN 0256          WRITE(6,6679)L,IFIN
  ISN 0257       45 CONTINUE
                CCC
                CCCCC FORMATS
                CCC
  ISN 0258        5 FORMAT(/,1X,'LOCAL STIFMAT  SL',I3)
  ISN 0259       56 FORMAT(/,2X,'TYPE',11X,'A',16X,'L',16X,'I',16X,'E',14X,'PHI')
  ISN 0260       60 FORMAT(/,1X,'GLOBAL STIFMAT SG',I3)
  ISN 0261       71 FORMAT(/,1X,'GLOBAL   STIFFNESS MATRIX STG(',I3,',',I3,')')
  ISN 0262       71 FORMAT (I3)
  ISN 0263       72 FORMAT (5(F12.2))
  ISN 0264       73 FORMAT (6(F12.2))
  ISN 0265       74 FORMAT (5(2X,F12.2))
  ISN 0266       75 FORMAT (5(2X,F12.2))
  ISN 0267       76 FORMAT (7(I3),4(F8.2),I3)
  ISN 0268       77 FORMAT (6(F8.4))
  ISN 0269       80 FORMAT(/,1X,'INVERTED STIFFNESS MATRIX STI(',I3,',',I3,')')
  ISN 0270       90 FORMAT(///,8X,'DISPL.VECT.RED.LD.VET.NO.',I3,2X,'(INC=',I3,')')
  ISN 0271      909 FORMAT(///,8X,'ACC.DIS. AND ACC.LD.VECT.',I3,2X,'(INC=',I3,')',
                    12X,'SUMAMI=',F9.3)
  ISN 0272       97 FORMAT(1H ,2X,I3,3X,E10.4,3X,E9.3)
  ISN 0273      111 FORMAT(/,2X,I3,5(2X,F15.3))
  ISN 0274      115 FORMAT(/,4X,'BAR',12X,'CODE NUMBERS',9X,'TYPE',4X,'COSX',8X,'W1',
                    18X,'W2',8X,'DY',6X,'ICON',/)
  ISN 0275      120 FORMAT(1H ,2X,I3,1X,6(2X,I3),3X,I3,1X,4(2X,F8.3),2X,I3)
  ISN 0276      676 FORMAT(/,2X,'BAR',2X,'TYPE',2X,'SPG(',I3,',',I3,')')
  ISN 0277      677 FORMAT(1H ,2X,2(I3,2X),F12.4)
  ISN 0278     1177 FORMAT(//,3X,'MINIMUM OF AMIN=',E12.4)
  ISN 0279     2277 FORMAT(/,3X,'AMIN=',E12.4,2X,'AMAX=',E12.4,2X,'COEMAX=',E12.4,2X,
                    1'SUMAMI=',E12.4)
  ISN 0280     3377 FORMAT(/,3X,'AMIN=  AMAX=',E12.4)
  ISN 0281     4477 FORMAT(/,3X,'AMIN=COEMAX=',E12.4)
  ISN 0282     5000 FORMAT(1H ,2(2X,I3),2(2X,E12.4))
  ISN 0283     5500 FORMAT(/,3X,'BAR',2X,'ICON',6X,'BAX',12X,'BV')
  ISN 0284     6677 FORMAT(//,3X,'AMIN=',E12.4,3X,'AT BAR NO.',I3,4GX,'**LD.VECT.NO.',
                    I3,'(INC=',I3,')**')
  ISN 0285     6679 FORMAT(////,2X,'*** END OF INCREMENTAL ANALYSIS FOR LOAD VECTOR NO
                    1.=',I3,2X,'AT INC=',I3,2X,'***')
  ISN 0286     6680 FORMAT(/,2X,'MATRIX SPG(',I3,',',I3,')','OF SPRING STIFFNESSES')
  ISN 0287     6690 FORMAT(/,2X,'MATRIX ALD(',I3,',',I3,')','OF LOAD VECTORS')
  ISN 0288     6681 FORMAT(1H1,2X,////,'****** INCREMENTAL ANALYSIS FOR LOAD VECTOR NO
                    1.=',I3,2X,'******',/////)
  ISN 0289    10000 FORMAT(/,2X,'FINC OF INC=',I3)
  ISN 0290    20000 FORMAT(/,2X,'DINC OF INC=',I3)
  ISN 0291    30000 FORMAT(/,2X,'INDE OF INC=',I3)
  ISN 0292    40000 FORMAT(/,2X,'FACC OF INC=',I3)
  ISN 0293          STOP
  ISN 0294          END
```

```
 LEVEL 2.2.1 (DEC 77)                    OS/360  FORTRAN H EXTENDED          DATE

REQUESTED OPTIONS: NODECK,NOOBJECT

OPTIONS IN EFFECT: NAME(MAIN) NOOPTIMIZE LINECOUNT(60) SIZE(MAX) AUTODBL(NONE)
                   SOURCE EBCDIC NOLIST NODECK NOOBJECT NOMAP NOFORMAT NOGOSTMT NOXREF N

   ISN 0002           SUBROUTINE STRESS(JBAR,WSX,WDX,NJB,FACC,NB,LOF,MTY,A,NT)
   ISN 0003           DIMENSION JBAR(NJB),WSX(NJB),WDX(NJB),FACC(NB,LOF),A(NT),MTY(NB)
   ISN 0004           DO 100 I=1,NJB
   ISN 0005           IIB=JBAR(I)
   ISN 0006           KKI=MTY(IIB)
   ISN 0007           SAX=-(FACC(IIB,1)/A(KKI))
   ISN 0008           SSX=  FACC(IIB,3)/WSX(I)
   ISN 0009           SDX=-(FACC(IIB,3)/WDX(I))
   ISN 0010           STSX=SAX+SSX
   ISN 0011           STDX=SAX+SDX
   ISN 0012           WRITE (6,1) IIB
   ISN 0013           WRITE (6,2)(FACC(IIB,1),A(KKI),FACC(IIB,3),WSX(I),WDX(I)
   ISN 0014           WRITE (6,2)SAX,SSX,SDX,STSX,STDX
   ISN 0015           WRITE (6,3 )
   ISN 0016       100 CONTINUE
   ISN 0017         1 FORMAT(/,9X,'FACC(1)',11X,'A',11X,'FACC(3)',9X,'WSX',12X,'WDX',5X,
                     *' ** BAR NO. ',I3,' **')
   ISN 0018         2 FORMAT (1H ,2X,5(E13.4,2X))
   ISN 0019         3 FORMAT (1H , 9X,'SAX',12X,'SSX',12X,'SDX',11X,'STSX',11X,'STDX')
   ISN 0020           RETURN
   ISN 0021           END
```

```
 LEVEL 2.2.1 (DEC 77)                    OS/360  FORTRAN H EXTENDED          DATE 79

REQUESTED OPTIONS: NODECK,NOOBJECT

OPTIONS IN EFFECT  NAME(MAIN) NOOPTIMIZE LINECOUNT(60) SIZE(MAX) AUTODBL(NONE)
                   SOURCE EBCDIC NOLIST NODECK NOOBJECT NOMAP NOFORMAT NOOSTPT NOXREF NOAL

   ISN 0002            SUBROUTINE GESTI (S,SG,LDF,R,TR,TS,SR,CCX,NI,NJ,DP)
                 CCCC  THIS ROUTINE TRANSFORMS STIFFNESS MATRICES FROM LOCAL TO GLOBAL AXES
   ISN 0003            DIMENSION TR(LDF,LDF),S(LDF,LDF),R(LDF,LDF),SR(LDF,LDF)
   ISN 0004            DIMENSION TS(LDF,LDF),SG(LDF,LDF)
   ISN 0005            CALL ZERO (SG,LDF,LDF)
   ISN 0006            IF((NI.EQ.1.)).AND.(NJ.EQ.0.0)) GO TO 48
   ISN 0008            CALL TRANSF (TR,1,NI,NJ,DP,LDF)
   ISN 0009            CALL TRIMU (S,LDF,TR,SR,LDF,TS)
   ISN 0010            CALL DUPL (TS,S,LDF,LDF)
   ISN 0011         48 IF (DP.EQ..0) GO TO 50
   ISN 0013            CALL TRANSF (TR,2,NI,NJ,DP,LDF)
   ISN 0014            CALL TRIMU (S,LDF,TR,SR,LDF,TS)
   ISN 0015            CALL DUPL (TS,S,LDF,LDF)
   ISN 0016         50 IF (CCX.EQ.1.)  GO TO 52
   ISN 0018            CALL ROTA (R,CCX,LDF)
   ISN 0019            CALL TRIMU (S,LDF, R,SR,LDF,TS)
   ISN 0020            CALL DUPL (TS,S,LDF,LDF)
   ISN 0021         52 CALL DUPL (S,SG,LDF,LDF)
   ISN 0022            RETURN
   ISN 0023            END
```

```
LEVEL 2.2.1 (DEC 77)                    OS/360  FORTRAN H EXTENDED          DA

REQUESTED OPTIONS: NODECK,NOOBJECT

OPTIONS IN EFFECT: NAME(MAIN),NOOPTIMIZE,LINECOUNT(60),SIZE(MAX),AUTODBL(NONE),
                   SOURCE,EBCDIC,NOLIST,NODECK,NOOBJECT,NOMAP,NOFORMAT,NOGOSTMT,NOXREF

ISN 0002            SUBROUTINE MULT (G,F,GF,L,M,N)
                    C     MATRIX MULTIPLICATION ROUTINE
ISN 0003            DIMENSION G(L,M),F(M,N),GF(L,N)
ISN 0004            DO 10 I=1,L
ISN 0005            DO 10 J=1,N
ISN 0006            GF(I,J)=0.
ISN 0007            DO 10 K=1,M
ISN 0008            GF(I,J)=GF(I,J)+G(I,K)*F(K,J)
ISN 0009         10 CONTINUE
ISN 0010            RETURN
ISN 0011            END
```

```
LEVEL 2.2.1 (DEC 77)                    OS/360  FORTRAN H EXTENDED              D

REQUESTED OPTIONS: NODECK,NOOBJECT

OPTIONS IN EFFECT: NAME(MAIN) NOOPTIMIZE LINECOUNT(60) SIZE(MAX) AUTODBL(NONE)
                   SOURCE EBCDIC NOLIST NODECK NOOBJECT NOMAP NOFORMAT NOGOSTMT NOXREF

ISN 0002            SUBROUTINE TRANSP (G,F,L,M)
                  CCCCC MATRIX TRANSPOSITION ROUTINE
ISN 0003            DIMENSION G(L,M),F(M,L)
ISN 0004            DO 201 J=1,M
ISN 0005            DO 2010 I=1,L
ISN 0006            F(J,I)=0.0
ISN 0007            F(J,I)=G(I,J)
ISN 0008          2 10 CONTINUE
ISN 0009            RETURN
ISN 0010            END
```

```
LEVEL 2.2.1 (DEC 77)                    OS/360  FORTRAN H EXTENDED          DA

REQUESTED OPTIONS: NODECK,NOOBJECT

OPTIONS IN EFFECT: NAME(MAIN) NOOPTIMIZE LINECOUNT(60) SIZE(MAX) AUTODBL(NONE)
                   SOURCE EBCDIC NOLIST NODECK NOOBJECT NOMAP NOFORMAT NOGOSTMT NOXREF

   ISN 0002         SUBROUTINE ZERO (G,L,M)
   ISN 0003         DIMENSION G(L,M)
   ISN 0004         DO 20 KM=1,L
   ISN 0005         DO 20 LM=1,M
   ISN 0006         G(KM,LM)=0.
   ISN 0007      20 CONTINUE
   ISN 0008         RETURN
   ISN 0009         END
```

```
LEVEL 2.2.1 (DEC 77)                    OS/360  FORTRAN H EXTENDED                C

REQUESTED OPTIONS: NODECK,NOOBJECT

OPTIONS IN EFFECT: NAME(MAIN) NOOPTIMIZE LINECOUNT(60) SIZE(MAX) AUTODBL(NONE)
                   SOURCE EBCDIC NOLIST NODECK NOOBJECT NOMAP NOFORMAT NOGOSTMT NOXRE

ISN 0002            SUBROUTINE DUPL (F,G,L,M)
ISN 0003            DIMENSION F(L,M),G(L,M)
ISN 0004            DO 53 LT=1,L
ISN 0005            DO 53 KT=1,M
ISN 0006            G(LT,KT)=0.0
ISN 0007            G(LT,KT)=F(LT,KT)
ISN 0008         53 CONTINUE
ISN 0009            RETURN
ISN 0010            END
```

```
LEVEL 2.2.1 (DEC 77)                    OS/360  FORTRAN H EXTENDED

REQUESTED OPTIONS: NODECK,NOOBJECT

OPTIONS IN EFFECT: NAME(MAIN) NOOPTIMIZE LINECOUNT(60) SIZE(MAX) AUTODBL(NONE)
                   SOURCE EBCDIC NOLIST NODECK NOOBJECT NOMAP NOFORMAT NOGOSTMT NOX

ISN 0002            SUBROUTINE PRINT (A,NR,NC,NA)
                CCCCC PRINT ROUTINE OF REAL ARRAYS
ISN 0003            DIMENSION A(NR,NC),NA(10)
ISN 0004            IF (NC.LE.10) GO TO  6
ISN 0006            GO TO 7
ISN 0007          6 IA=1
ISN 0008            NST=10
ISN 0009            GO TO 14
ISN 0010          7 NP=0
ISN 0011         11 NP=NP+1
ISN 0012            NST=NP*10
ISN 0013            IA=NST-9
ISN 0014         14 NA(1)=IA
ISN 0015            DO 30 LA=2,10
ISN 0016            KA=LA-1
ISN 0017            NA(LA)=NA(KA)+1
ISN 0018         30 CONTINUE
ISN 0019            IF (NC.LE.NST) GO TO 9
ISN 0021            IB=NST
ISN 0022            WRITE (6,110) (NA(JA),JA=1,10)
ISN 0023            GO TO 12
ISN 0024          9 IB=NC
ISN 0025            KKK=10-NST+NC
ISN 0026            WRITE (6,110) (NA(JA),JA=1,KKK)
ISN 0027         12 DO 20 I=1,NR
ISN 0028            WRITE (6,100) I,(A(I,J),J=IA,IB)
ISN 0029         20 CONTINUE
ISN 0030            IF (IB.EQ.NC) GO TO 15
ISN 0032            GO TO 11
ISN 0033         15 CONTINUE
ISN 0034        100 FORMAT (I3,1X,(2X,E11.4))
ISN 0035        110 FORMAT (1H0,8X,10(I3,9X))
ISN 0036            RETURN
ISN 0037            END
```

```
LEVEL 2.2.1 (DEC 77)                    OS/360 FORTRAN H EXTENDED

REQUESTED OPTIONS: NODECK,NOOBJECT

OPTIONS IN EFFECT: NAME(MAIN) NOOPTIMIZE LINECOUNT(60) SIZE(MAX) AUTODBL(NONE)
                   SOURCE EBCDIC NOLIST NODECK NOOBJECT NOMAP NOFORMAT NOGOSTPT NOXR

ISN 0002            SUBROUTINE IPRNT(IR,NR,NC,NA)
ISN 0003          CCCCC PRINT ROUTINE OF INTEGER ARRAYS
ISN 0004            DIMENSION IR(NR,NC),NA(10)
ISN 0005            IF (NC.LE.10) GO TO  6
ISN 0006            GO TO 7
ISN 0007          6 IA=1
ISN 0008            NST=10
ISN 0009            GO TO 14
ISN 0010          7 NP=0.
ISN 0011         11 NP=NP+1
ISN 0012            NST=NP*10
ISN 0013            IA=NST-9
ISN 0014         14 NA(1)=IA
ISN 0015            DO 30 LA=2,10
ISN 0016            KA=LA-1
ISN 0017            NA(LA)=NA(KA)+1
ISN 0018         30 CONTINUE
ISN 0019            IF (NC.LE.NST) GO TO 9
ISN 0021            IB=NST
ISN 0022            WRITE (6,110) (NA(JA),JA=1,10)
ISN 0023            GO TO 12
ISN 0024          9 IB=NC
ISN 0025            KKK=10-NST+NC
ISN 0026            WRITE (6,110) (NA(JA),JA=1,KKK)
ISN 0027         12 DO 20 I=1,NR
ISN 0028            WRITE (6,100)I,(IR(I,J),J=IA,IB)
ISN 0029         20 CONTINUE
ISN 0030            IF (IB.EQ.NC) GO TO 15
ISN 0032            GO TO 11
ISN 0033         15 CONTINUE
ISN 0034        100 FORMAT (I3,10(2X,I10))
ISN 0035        110 FORMAT (1H ,8X,10(I3,9X))
ISN 0036            RETURN
ISN 0037            END
```

```
 LEVEL 2.2.1 (DEC 77)                    OS/360  FORTRAN H EXTENDED

 REQUESTED OPTIONS: NODECK,NOOBJECT

 OPTIONS IN EFFECT: NAME(MAIN) NOOPTIMIZE LINECOUNT(60) SIZE(MAX) AUTODBL(NONE)
                    SOURCE EBCDIC NOLIST NODECK NOOBJECT NOMAP NOFORMAT NOGOSTMT NOX

   ISN 0002            SUBROUTINE MESTI (AB,LOF,AM,EM,FIM,FLM,VM,NT,KK)
                 CCCC  ROUTINE  TO CREATE LOCAL MEMBER STIFFNESS MATRICES
   ISN 0003            DIMENSION AB(LOF,LOF),AM(NT),EM(NT),FIM(NT),FLM(NT),VM(NT)
   ISN 0004            CALL ZERO (AB,LOF,LOF)
   ISN 0005            C=EM(KK)/FLM(KK)
   ISN 0006            ST1=AM(KK)*C
   ISN 0007            AB(1,1)=ST1
   ISN 0008            AB(4,4)=AB(1,1)
   ISN 0009            AB(4,1)=-AB(1,1)
   ISN 0010            AB(1,4)=AB(4,1)
   ISN 0011            IF (FIM(KK).EQ.0.0) GO TO 10
   ISN 0013            D=(C*FIM(KK))/(1.+VM(KK))
   ISN 0014            ST2=(4+VM(KK))*D
   ISN 0015            ST3=(2-VM(KK))*D
   ISN 0016            ST4=(6*D)/FLM(KK)
   ISN 0017            ST5=(2*ST4)/FLM(KK)
   ISN 0018            AB(2,2)=ST5
   ISN 0019            AB(5,5)=AB(2,2)
   ISN 0020            AB(5,2)=-AB(5,5)
   ISN 0021            AB(5,3)=-ST4
   ISN 0022            AB(2,3)=ST4
   ISN 0023            AB(2,5)=AB(5,2)
   ISN 0024            AB(2,6)=AB(2,3)
   ISN 0025            AB(5,6)=AB(5,3)
   ISN 0026            AB(3,2)=AB(2,3)
   ISN 0027            AB(3,3)=ST2
   ISN 0028            AB(3,5)=AB(5,3)
   ISN 0029            AB(3,6)=ST3
   ISN 0030            AB(6,2)=AB(2,6)
   ISN 0031            AB(6,3)=AB(3,6)
   ISN 0032            AB(6,5)=AB(5,6)
   ISN 0033            AB(6,6)=AB(3,3)
   ISN 0034         10 CONTINUE
   ISN 0035            RETURN
   ISN 0036            END
```

```
LEVEL 2.2.1 (DEC 77)                    OS/360  FORTRAN H EXTENDED

REQUESTED OPTIONS: NODECK,NOOBJECT

OPTIONS IN EFFECT: NAME(MAIN) NOOPTIMIZE LINECOUNT(60) SIZE(MAX) AUTODBL(NONE)
                   SOURCE EBCDIC NOLIST NODECK NOOBJECT NOMAP NOFORMAT NOGOSTMT NOX

ISN 0002            SUBROUTINE ROTA (R,CCX,LDF)
ISN 0003            DIMENSION R(LDF,LDF)
ISN 0004            CALL ZERO (R,LDF,LDF)
ISN 0005            CCY=SQRT(1.-(CCX*CCX))
ISN 0006            R(3,3)=1.
ISN 0007            R(1,1)=CCX
ISN 0008            R(2,2)=CCX
ISN 0009            R(4,4)=CCX
ISN 0010            R(5,5)=CCX
ISN 0011            R(6,6)=1.
ISN 0012            R(1,2)=CCY
ISN 0013            R(2,1)=-CCY
ISN 0014            R(4,5)=CCY
ISN 0015            R(5,4)=-CCY
ISN 0016            RETURN
ISN 0017            END
```

```
LEVEL 2.2.1 (DEC 77)                    OS/360 FORTRAN H EXTENDED            DATE 79.

REQUESTED OPTIONS: NODECK,NOOBJECT

OPTIONS IN EFFECT: NAME(MAIN) NOOPTIMIZE LINECOUNT(60) SIZE(MAX) AUTODBL(NONE)
                   SOURCE EBCDIC NOLIST NODECK NOOBJECT NOMAP NOFORMAT NOOPTSTAT NOXREF NOAL

ISN 0002            SUBROUTINE EXTV (DIL,DIV,LAB,N,LDF,NDF,NB)
                  CCCCC ROUTINE TO EXTRACT LOCAL FROM GLOBAL DISPLACEMENTS, USING LBL VECTOR
ISN 0003            DIMENSION DIL(LDF),DIV(NDF),LAB(NB,LDF)
ISN 0004            DO 30 K=1,LDF
ISN 0005            LR=LAB(N,K)
ISN 0006            IF (LAB(N,K).EQ.0) GO TO 32
ISN 0008            DIL(K)=DIV(LR)
ISN 0009            GO TO 30
ISN 0010          32 DIL(K)=0.
ISN 0011          30 CONTINUE
ISN 0012            RETURN
ISN 0013            END
```

```
LEVEL 2.2.1 (DEC 77)                    OS/360  FORTRAN H EXTENDED

REQUESTED OPTIONS: NODECK,NOOBJECT

OPTIONS IN EFFECT: NAME(MAIN) NOOPTIMIZE LINECOUNT(60) SIZE(MAX) AUTODBL(NONE)
                   SOURCE EBCDIC NOLIST NODECK NOOBJECT NOMAP NOFORMAT NOXREF

ISN 0002            SUBROUTINE MULTV (G,F,GF,L,M)
ISN 0003            DIMENSION G(L,M),F(M),GF(L)
ISN 0004            DO 1010 I=1,L
ISN 0005            GF(I)= .
ISN 0006            DO 1010 K=1,M
ISN 0007            GF(I)=GF(I)+G(I,K)*F(K)
ISN 0008        1010 CONTINUE
ISN 0009            RETURN
ISN 0010            END
```

LEVEL 2.2.1 (DEC 77) OS/360 FORTRAN H EXTENDED

REQUESTED OPTIONS: NODECK,NOOBJECT

OPTIONS IN EFFECT: NAME(MAIN) NOOPTIMIZE LINECOUNT(60) SIZE(MAX) AUTODBL(NONE)
SOURCE EBCDIC NOLIST NODECK NOOBJECT NOMAP NOFORMAT NOGOSTMT

```
ISN 0002            SUBROUTINE TRIMU (B,N,A,C,M,D)
                C     ROUTINE FOR CONTROGRADIENT TRANSFORMATION
ISN 0003            DIMENSION A(N,M),B(N,N),C(N,M),D(M,M)
ISN 0004            CALL ZERO (D,M,M)
ISN 0005            CALL ZERO (C,N,N)
ISN 0006            CALL MULT (B,A,C, A,N,M)
ISN 0007            CALL TRANSP(A,B,N,M)
ISN 0008            CALL MULT (B,C,C,P, N,M)
ISN 0009            RETURN
ISN 0010            END
```

```
LEVEL 2.2.1 (DEC 77)                    OS/360  FORTRAN H EXTENDED

REQUESTED OPTIONS: NODECK,NOOBJECT

OPTIONS IN EFFECT: NAME(MAIN) NOOPTIMIZE LINECOUNT(60) SIZE(MAX) AUTODBL(NONE)
                   SOURCE EBCDIC NOLIST NODECK NOOBJECT NOMAP NOFORMAT NOGOSTPT NO

   ISN 0002           SUBROUTINE TRANSF (WT,IND,A,B,C,LDF)
                  CCCCC ROUTINE FOR AXES TRANSFORMATION
                  CCCCC IND = 1, FOR WIDE RIGID ARMSS TRANSFORMATION.
                  CCCCC IND GT OR LT 1, FOR PARALLEL AXES TRANSFORMATION.
   ISN 0003           DIMENSION WT(LDF,LDF)
   ISN 0004           CALL ZERO (WT,LDF,LDF)
   ISN 0005           WT(1,1)=1.
   ISN 0006           WT(2,2)=1.
   ISN 0007           WT(3,3)=1.
   ISN 0008           WT(4,4)=1.
   ISN 0009           WT(5,5)=1.
   ISN 0010           WT(6,6)=1.
   ISN 0011           IF (IND.EQ.1)  GO TO 10
   ISN 0012           WT(1,3)=C
   ISN 0013           WT(4,6)=C
   ISN 0014           GO TO 30
   ISN 0015        10 WT(2,3)=-A
   ISN 0016           WT(5,6)=-B
   ISN 0017        30 CONTINUE
   ISN 0018           RETURN
   ISN 0019           END
```

```
 LEVEL 2.2.1 (DEC 77)                    OS/360  FORTRAN H EXTENDED

 REQUESTED OPTIONS0 NODECK,NCOBJECT

 OPTIONS IN EFFECT. NAME(MAIN) NOOPTIMIZE LINECOUNT(60) SIZE(MAX) AUTODBL(NONE)
                    SOURCE EBCDIC NOLIST NODECK NOOBJECT NOMAP NOFORMAT NOGOSTMT NC

   ISN 0002             SUBROUTINE ACCUST  (SG,BTG,LAB,I,NDF,LDF,NB)
                    CCCCC ROUTINE TO ACCUMULATE LOCAL INTO GLOBAL STIFNESS MATRIX
   ISN 0003             DIMENSION BTG(NDF,NDF),SG(LDF,LDF),LAB(NB,LDF)
   ISN 0004               DO 30 K=1,LDF
   ISN 0005             IF (LAB(I,K).EQ.0.) GO TO 30
   ISN 0007             LR=LAB(I,K)
   ISN 0008             DO 31 L=1,LDF
   ISN 0009             IF (LAB(I,L).EQ.0.)  GO TO 31
   ISN 0011             LS=LAB(I,L)
   ISN 0012             BTG(LR,LS)=BTG(LR,LS)+SG(K,L)
   ISN 0013          31 CONTINUE
   ISN 0014          30 CONTINUE
   ISN 0015             RETURN
   ISN 0016             END
```

```
LEVEL 2.2.1 (DEC 77)                    OS/360  FORTRAN H EXTENDED          DAT

REQUESTED OPTIONS. NODECK,NOOBJECT

OPTIONS IN EFFECT) NAME(MAIN) NOOPTIMIZE LINECOUNT(60) SIZE(MAX) AUTODBL(NONE)
                   SOURCE EBCDIC NOLIST NODECK NOOBJECT NOMAP NOFORMAT NOGOSTMT NOXREF

   ISN 0002           SUBROUTINE  LOCDIS (DILL,DIL,LDF,R,TR,DIR,DIP,DIW,CCX,WI,WJ,DP)
                  CCCCC ROUTINE TO TRANSFORM LOCAL INTO MEMBER DISPLACEMENTS
   ISN 0003           DIMENSION TR(LDF,LDF),DILL(LDF),R(LDF,LDF),DIL(LDF)
   ISN 0004           DIMENSION DIP(LDF),DIR(LDF),DIW(LDF)
   ISN 0005           CALL ZEROV (DIL,LDF)
   ISN 0006           CALL ZEROV (DIR,LDF)
   ISN 0007           CALL ZEROV (DIP,LDF)
   ISN 0008           CALL ZEROV (DIW,LDF)
   ISN 0009           IF (CCX.EQ.1.) GO TO 46
   ISN 0011           CALL ROTA (R,CCX,LDF)
   ISN 0012           CALL MULTV (R,DILL,DIR,LDF,LDF)
   ISN 0013           CALL DUPLV (DIR,DILL,LDF)
   ISN 0014        46 IF (DP.EQ.0.0) GO TO 48
   ISN 0016           CALL TRANSF (TR,2,WI,WJ,DP,LDF)
   ISN 0017           CALL MULTV (TR,DILL,DIP,LDF,LDF)
   ISN 0018           CALL DUPLV (DIP,DILL,LDF)
   ISN 0019        48 IF ((WI.EQ.0.0).AND.(WJ.EQ.0.0)) GO TO 50
   ISN 0021           CALL TRANSF (TR,1,WI,WJ,DP,LDF)
   ISN 0022           CALL MULTV (TR,DILL,DIW,LDF,LDF)
   ISN 0023           CALL DUPLV (DIW,DILL,LDF)
   ISN 0024        5  CALL DUPLV (DILL,DIL,LDF)
   ISN 0025           RETURN
   ISN 0026           END
```

```
 LEVEL 22.1 (DEC 77)                    OS/360  FORTRAN H EXTENDED          DATE

REQUESTED OPTIONS: NODECK,NOOBJECT

OPTIONS IN EFFECT: NAME(MAIN) NOOPTIMIZE LINECOUNT(60) SIZE(MAX) AUTODBL(NONE)
                   SOURCE EBCDIC NOLIST NODECK NOOBJECT NOMAP NOFORMAT NOGOSTMT NOXREF NO

   ISN 0002            SUBROUTINE EQUCHK(FLC,LDF,FLM)
                    CCCCC ROUTINE TO CHECK MEMBER FORCES EQUILIBRIUM
   ISN 0003            DIMENSION FLC(LDF)
   ISN 0004            DN=ABS(FLC(1)+FLC(4))
   ISN 0005            CNK=ABS(FLC(1)/1000.)
   ISN 0006            DT=ABS(FLC(2)+FLC(5))
   ISN 0007            CTK=ABS(FLC(2)/1000.)
   ISN 0008            CMK1=FLC(3)+FLC(6)
   ISN 0009            CMK2=FLC(2)+FLM
   ISN 0010            CMK=ABS(CMK1/1000.)
   ISN 0011            DM=ABS(CMK1-CMK2)
   ISN 0012            IF ((DN.GT.0.00000001).AND.(DN.GT.CNK)) GO TO 47
   ISN 0014            IF ((DT.GT.0.00000001).AND.(DT.GT.CTK)) GO TO 47
   ISN 0016            IF ((DM.GT.0.00000001).AND.(DM.GT.CMK)) GO TO 47
   ISN 0018            GO TO 48
   ISN 0019         47 WRITE (6,999)
   ISN 0020            WRITE (6,888) DN,DT,DM,CMK1,CMK
   ISN 0021         48 CONTINUE
   ISN 0022        888 FORMAT (5(6X,E10.4))
   ISN 0023        999 FORMAT(/,2X,'DN=ABS(F1+F4)',2X,'DT=ABS(F2+F5)',2X,'DM=ABS(CMK1-CMK-
                      12)',5X,'CMK1=F3+F6',5X,'CMK=CMK1/1000')
   ISN 0024            RETURN
   ISN 0025            END
```

```
LEVEL 2.2.1 (DEC 77)                    OS/360  FORTRAN H EXTENDED

REQUESTED OPTIONS: NODECK,NOOBJECT

OPTIONS IN EFFECT: NAME(MAIN) NOOPTIMIZE LINECOUNT(60) SIZE(MAX) AUTODBL(NONE)
                   SOURCE EBCDIC NOLIST NODECK NOOBJECT NOMAP NOFORMAT NOGOSTMT NO

ISN 0002            SUBROUTINE EXTVN (VEC,CMAT,N,M,L,IND)
                  CCCCC ROUTINE TO EXTRACT VECTOR FROM MATRIX
                  CCCCC IND = 1, COLUMNWISE
                  CCCCC IND = 2, ROWWISE
ISN 0003            DIMENSION VEC(N),CMAT(N,M)
ISN 0004            CALL ZEROV (VEC,N)
ISN 0005            IF (IND.EQ.1) GO TO 110
ISN 0007            JK=M
ISN 0008            GO TO 130
ISN 0009          11) JK=1
ISN 0011          13) DO 3) K=1,JK
ISN 0011            IF (IND.EQ.1) GO TO 1)
ISN 0013            VEC(K)=CMAT(L,K)
ISN 0014            GO TO 3)
ISN 0015          1) VEC(K)=CMAT(K,L)
ISN 0016          3) CONTINUE
ISN 0017            RETURN
ISN 0018            END
```

```
LEVEL 2.2.1 (DEC 77)                    OS/360  FORTRAN H EXTENDED

REQUESTED OPTIONS: NODECK,NOOBJECT

OPTIONS IN EFFECT: NAME(MAIN) NOOPTIMIZE LINECOUNT(60) SIZE(MAX) AUTODBL(NONE)
                   SOURCE EBCDIC NOLIST NODECK NOOBJECT NOMAP NOFORMAT NOGOSTMT NO

ISN 0002            SUBROUTINE ACCUVM(VEC,DMAT,N,M,L,IND)
                  CCCCC ROUTINE TO ACCUMU. VECTOR INTO MATRIX0
                  CCCCC IND = 1, COLUMNWISE
                  CCCCC IND = 2, ROWWISE
ISN 0003            DIMENSION VEC(N1),DMAT(N,M)
ISN 0004            IF (IND.EQ.1) GO TO 110
ISN 0005            JK=M
ISN 0006            GO TO 130
ISN 0007          110 JK=N
ISN 0008          130 DO 30 K=1,JK
ISN 0009            IF (IND.EQ.1) GO TO 10
ISN 0010            DMAT(L,K)=VEC(K)
ISN 0011            GO TO 30
ISN 0012           10 DMAT(K,L)=VEC(K)
ISN 0013           30 CONTINUE
ISN 0014            RETURN
ISN 0015            END
```

```
 LEVEL 2.2.1 (DEC 77)                    OS/360  FORTRAN H EXTENDED

 REQUESTED OPTIONS: NODECK,NOOBJECT

 OPTIONS IN EFFECT: NAME(MAIN) NOOPTIMIZE LINECOUNT(60) SIZE(MAX) AUTODBL(NONE)
                    SOURCE EBCDIC NOLIST NODECK NOOBJECT NOMAP NOFORMAT NOGOSTMT

   ISN 0002          SUBROUTINE ZEROV (G,L)
   ISN 0003           DIMENSION G(L)
   ISN 0004          DO 20 LM=1,L
   ISN 0005          G(LM)=0.0
   ISN 0006        2. CONTINUE
   ISN 0007          RETURN
   ISN 0008          END
```

```
LEVEL 2.2.1 (DEC 77)                    OS/360  FORTRAN H EXTENDED

REQUESTED OPTIONS: NODECK,NOOBJECT

OPTIONS IN EFFECT: NAME(MAIN),NOOPTIMIZE,LINECOUNT(60),SIZE(MAX),AUTODBL(NONE
                   SOURCE,EBCDIC,NOLIST,NODECK,NOOBJECT,NOMAP,NOFORMAT,NOGOST

   ISN 0002            SUBROUTINE CUPLV (F,G,L)
   ISN 0003            DIMENSION F(L),G(L)
   ISN 0004            DO 53 LT=1,L
   ISN 0005            G (LT)=0.
   ISN 0006            G(LT)=F(LT)
   ISN 0007         53 CONTINUE
   ISN 0008            RETURN
   ISN 0009            END
```

```
LEVEL 2.2.1 (DEC 77)                    05/365  FORTRAN H EXTENDED

REQUESTED OPTIONS: NODECK,NOOBJECT

OPTIONS IN EFFECT: NAME(MAIN) NOOPTIMIZE LINECOUNT(60) SIZE(MAX) AUTODBL(NONE)
                   SOURCE EBCDIC NOLIST NODECK NOOBJECT NOMAP NOFORMAT NOXREF NO

   ISN 0002            SUBROUTINE ADD (G,F,GF,L,M)
   ISN 0003            DIMENSION G(L,M),F(L,M),GF(L,M)
   ISN 0004            DO 1010 I=1,L
   ISN 0005            DO 1010 J=1,M
   ISN 0006            GF(I,J)=G(I,J)+F(I,J)
   ISN 0007       1010 CONTINUE
   ISN 0008            RETURN
   ISN 0009            END
```

```
LEVEL 2.2.1 (DEC 77)                    OS/360 FORTRAN H EXTENDED

REQUESTED OPTIONS: NODECK,NOOBJECT

OPTIONS IN EFFECT: NAME(MAIN) NOOPTIMIZE LINECOUNT(60) SIZE(MAX) AUTODBL(NONE)
                   SOURCE EBCDIC NOLIST NODECK NOOBJECT NOMAP NOFORMAT NOGOSTPT NOX

ISN 0002            SUBROUTINE ACCV(G,F,GF,L)
ISN 0003            DIMENSION G(L),F(L),GF(L)
ISN 0004            DO 10 I=1,L
ISN 0005            GF(I)=G(I)+F(I)
ISN 0006        10  CONTINUE
ISN 0007            RETURN
ISN 0008            END
```

```
LEVEL 2.2.1 (DEC 77)                    OS/360  FORTRAN H EXTENDED

REQUESTED OPTIONS.  NODECK,NOOBJECT

OPTIONS IN EFFECT   NAME(MAIN),OPTIMIZE,LINECOUNT(60),SIZE(MAX),AUTODBL(NONE)
                    SOURCE,EBCDIC,NOLIST,NODECK,NOOBJECT,NOMAP,NOFORMAT,NOOSTPT

ISN 0002            SUBROUTINE SCALE (G,COEFF,GF,L,M)
ISN 0003            DIMENSION G(L,M),GF(L,M)
ISN 0004            DO 1 I=1,L
ISN 0005            DO 1 J=1,M
ISN 0006            GF(I,J)=G(I,J)*COEFF
ISN 0007          1 CONTINUE
ISN 0008            RETURN
ISN 0009            END
```

```
LEVEL 2.2.1 (DEC 77)                    OS/360  FORTRAN H EXTENDED

REQUESTED OPTIONS:  NODECK,NOOBJECT

OPTIONS IN EFFECT:  NAME(MAIN),NOOPTIMIZE LINECOUNT(60) SIZE(MAX) AUTODBL(NONE)
                    SOURCE EBCDIC NOLIST NODECK NOOBJECT NOMAP NOFORMAT NOGOSTMT

ISN 0002            SUBROUTINE SCALEV (G,COEFF,GF,L)
ISN 0003            DIMENSION G(L),GF(L)
ISN 0004            DO 1 I=1,L
ISN 0005            GF(I)=G(I)*COEFF
ISN 0006          1 CONTINUE
ISN 0007            RETURN
ISN 0008            END
```

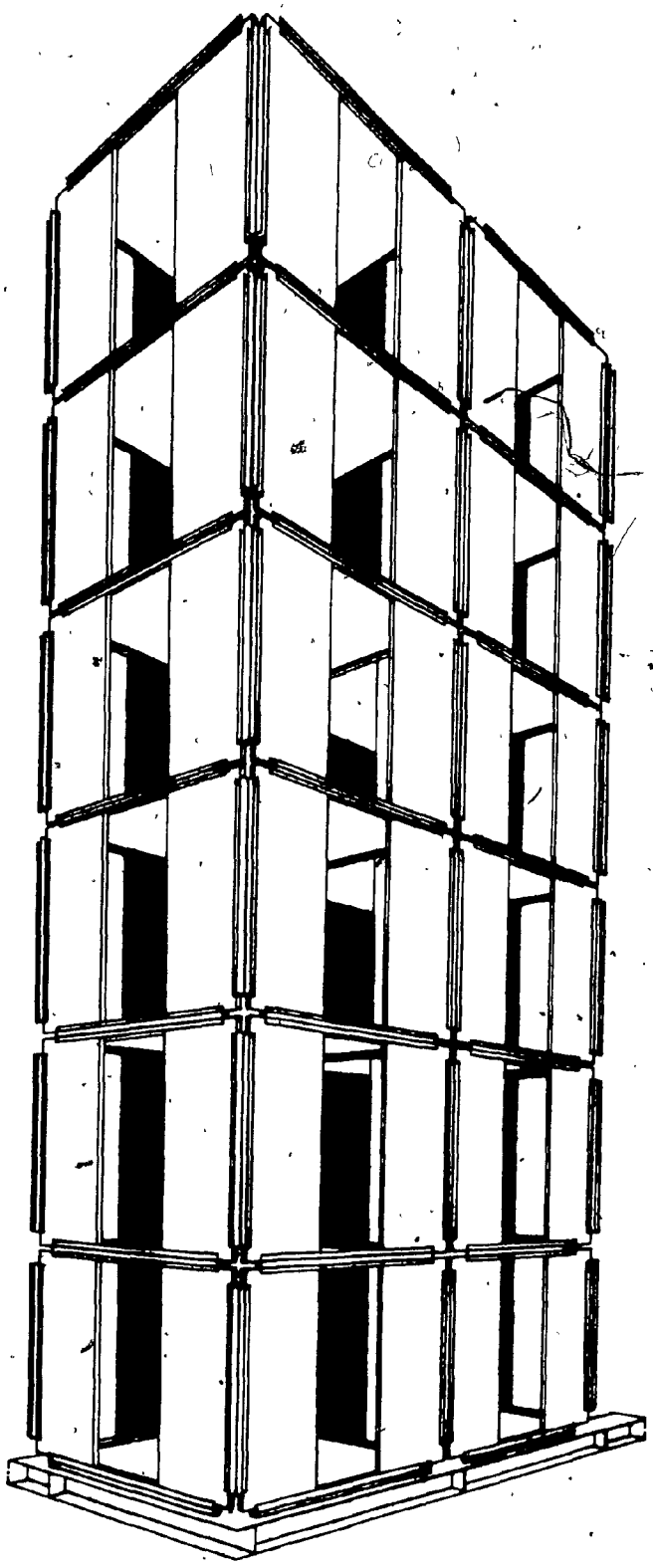

FIG. 1.1 - PERSPECTIVE VIEW OF PANELIZED BUILDING MODEL

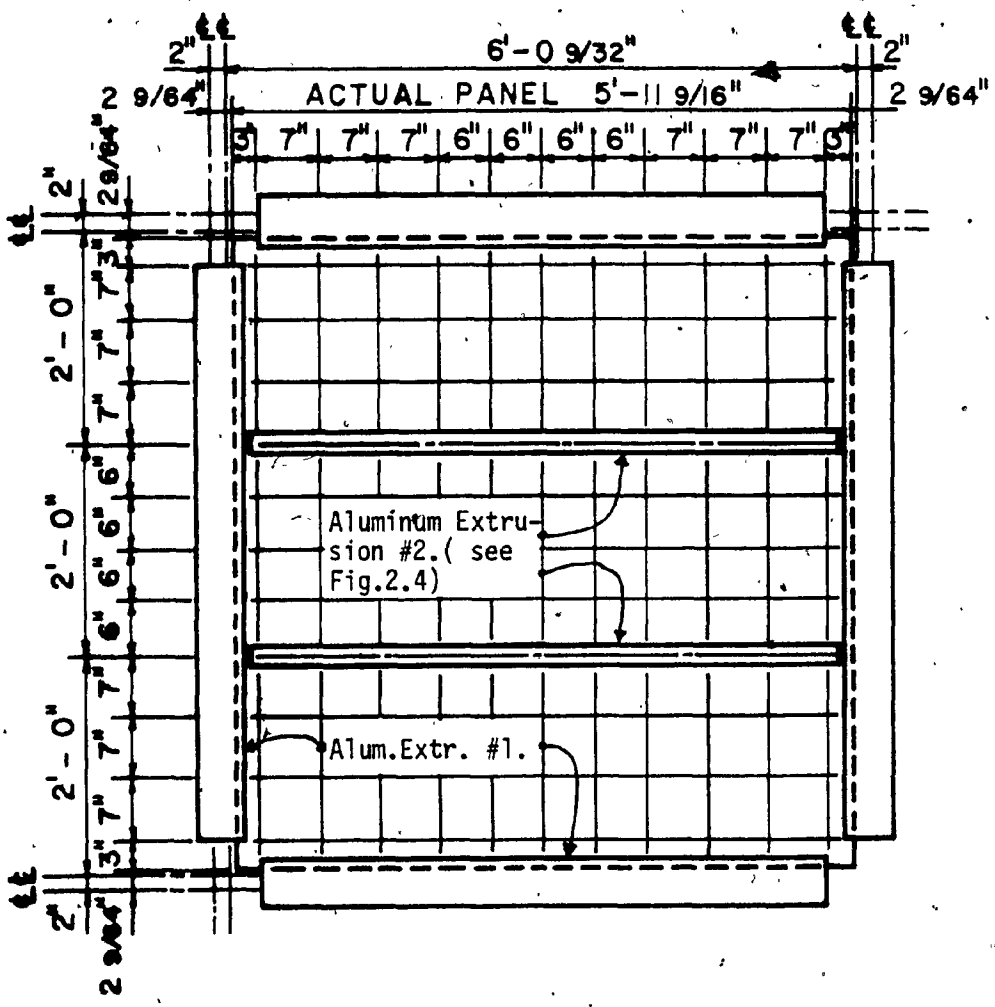

FIG. 2.1 - TYPICAL FLOOR ASSEMBLY

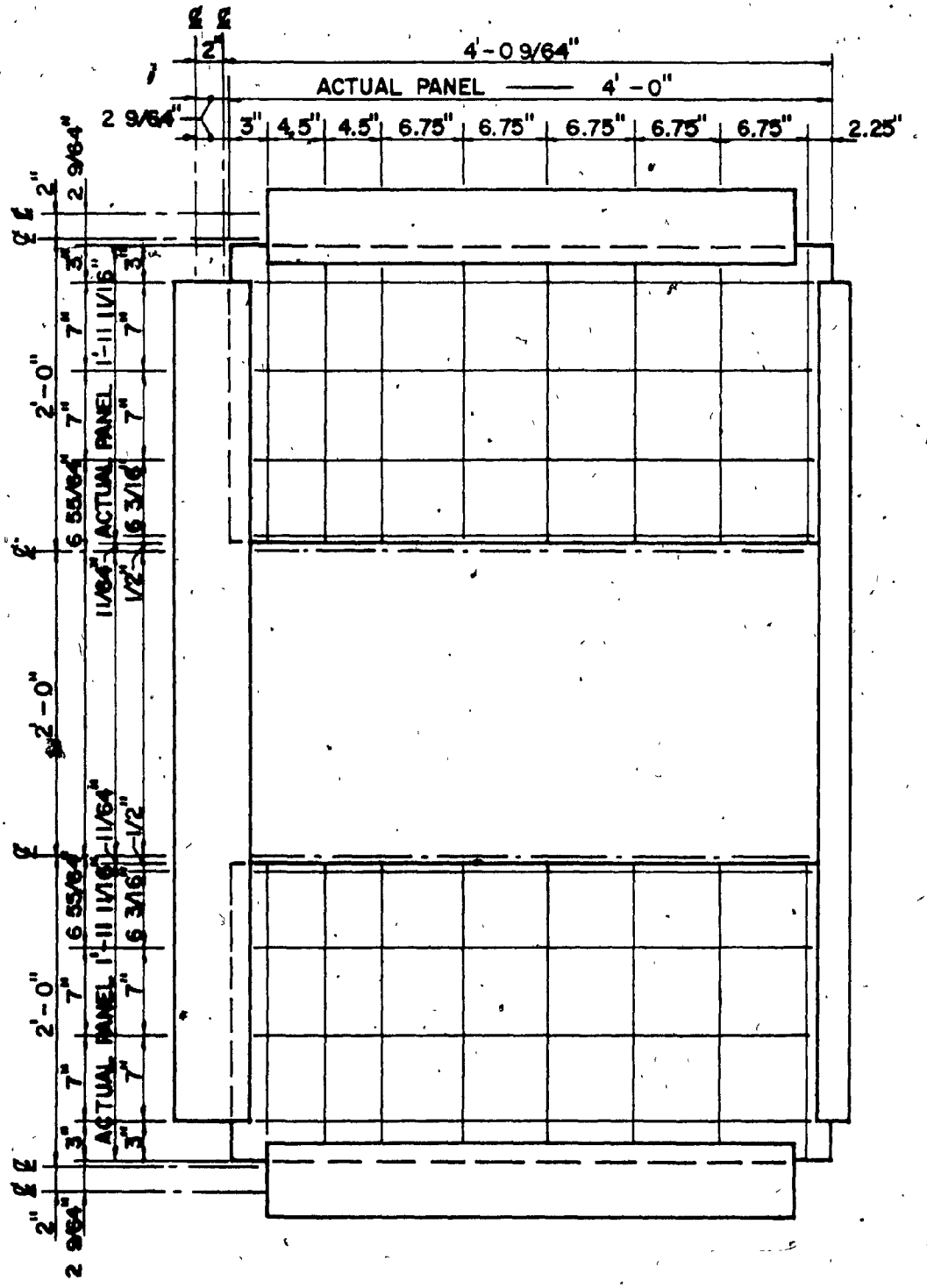

FIG. 2.2 - TYPICAL WALL ASSEMBLY

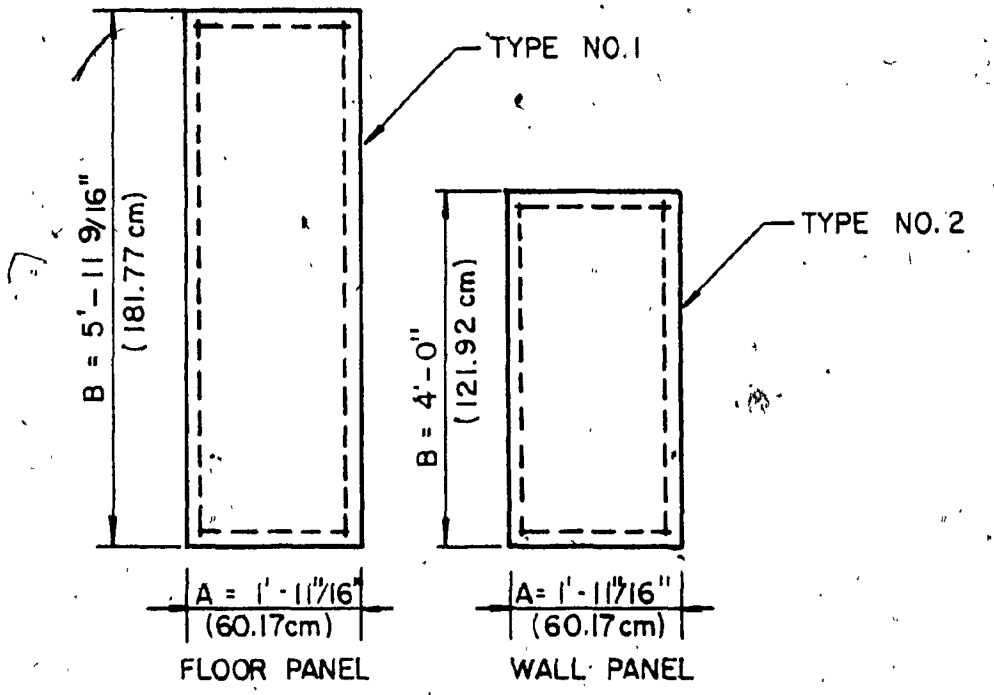

A) PANEL SIZES

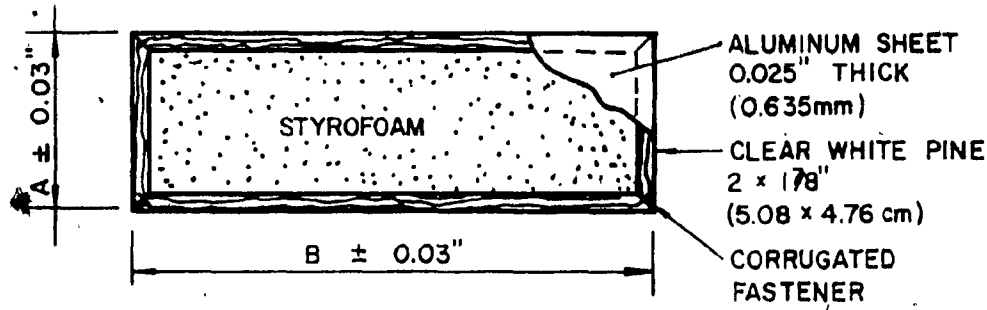

B) TYPICAL PANEL FRAME

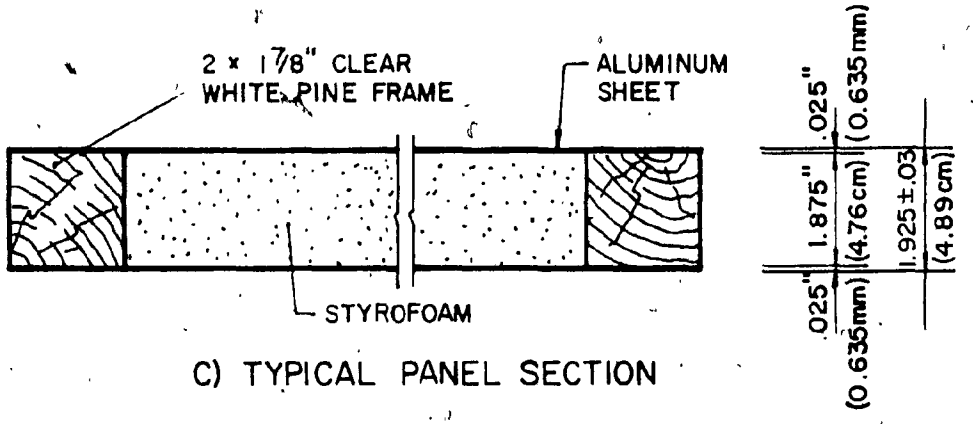

C) TYPICAL PANEL SECTION

FIG. 2.3 - DETAILS OF SANDWICH PANELS

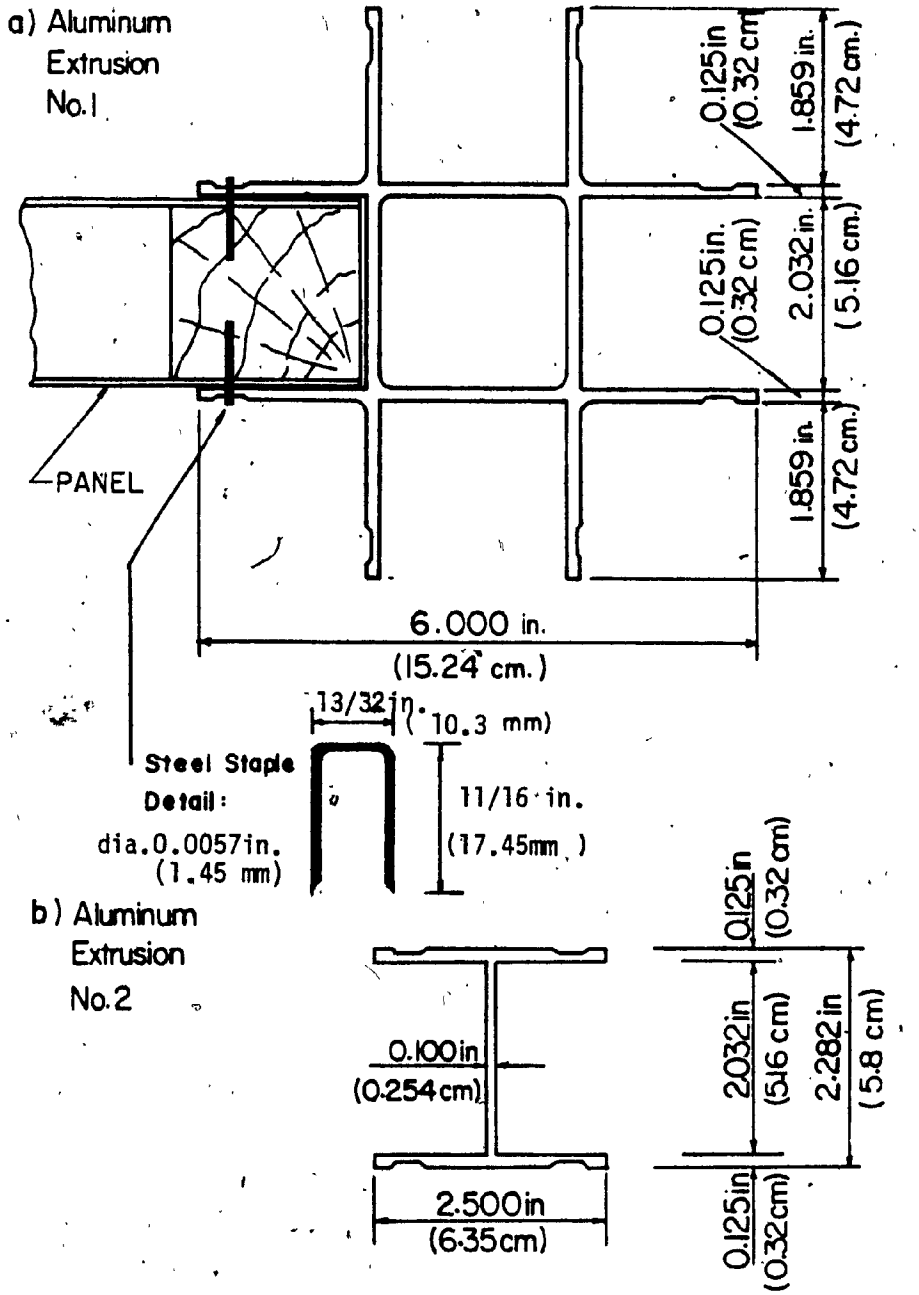

FIG. 2.4 - CROSS SECTION AT CONNECTING EXTRUSIONS

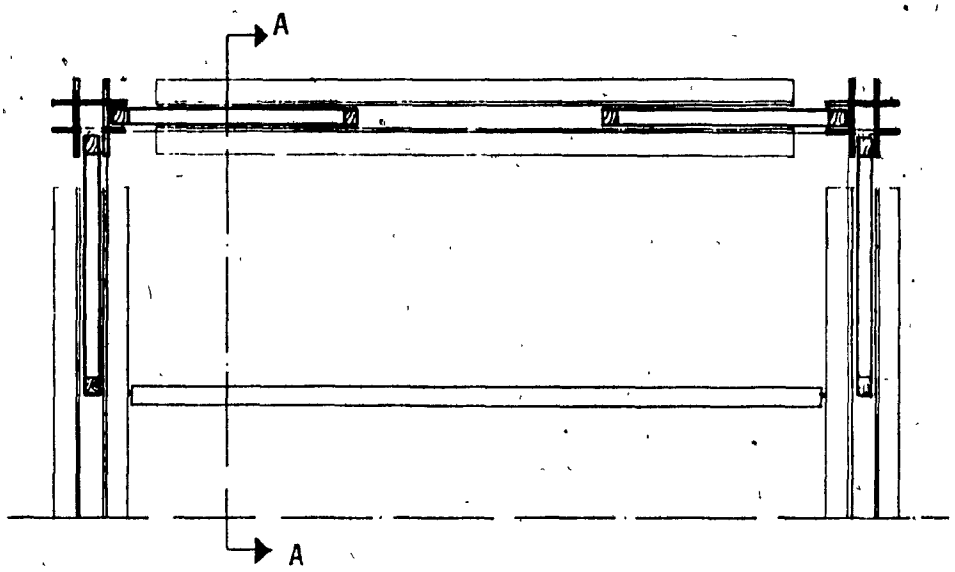

a) HORIZONTAL CROSS SECTION OF THE MODEL

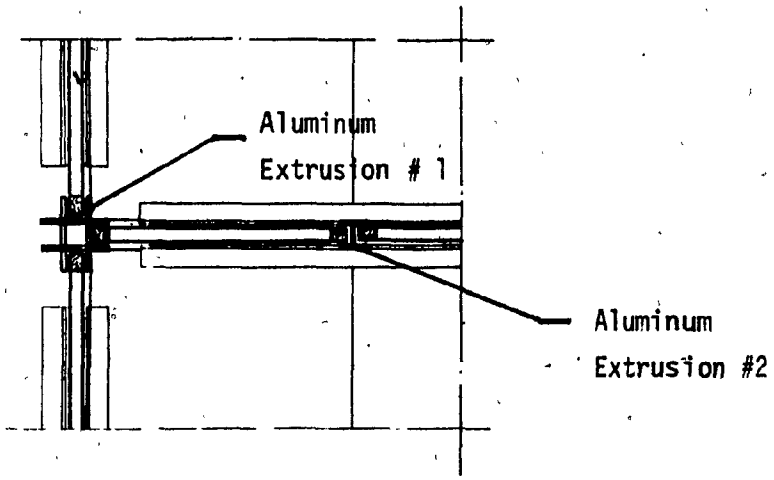

b) SEC. A-A OF TYPICAL FLOOR ASSEMBLY

FIG. 2.5 - CROSS SECTION ON WALL AND FLOOR ASSEMBLIES

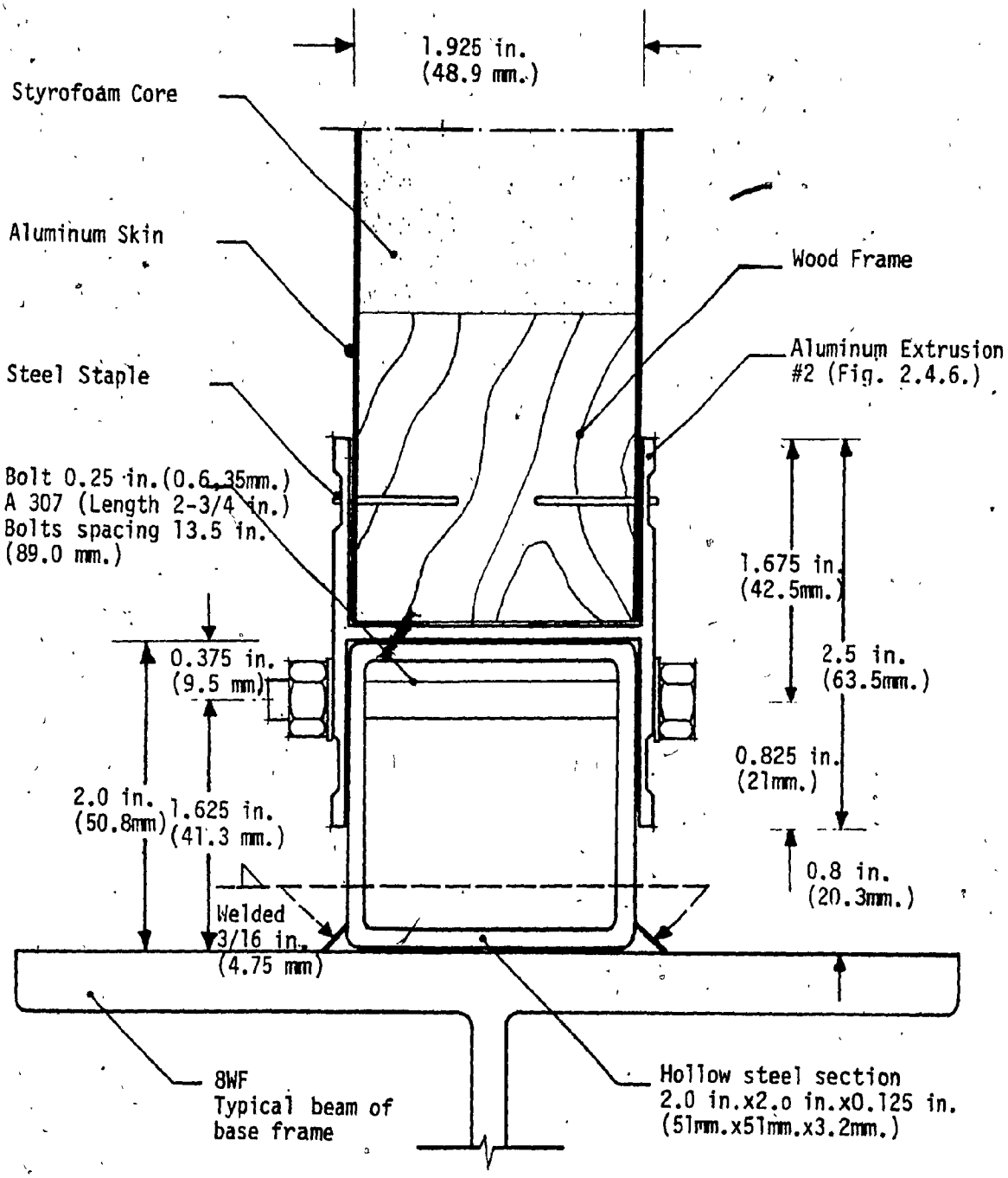

FIG. 2.6 - CROSS SECTION OF CONNECTION BETWEEN WALLS OF MODEL AND BASE FRAME

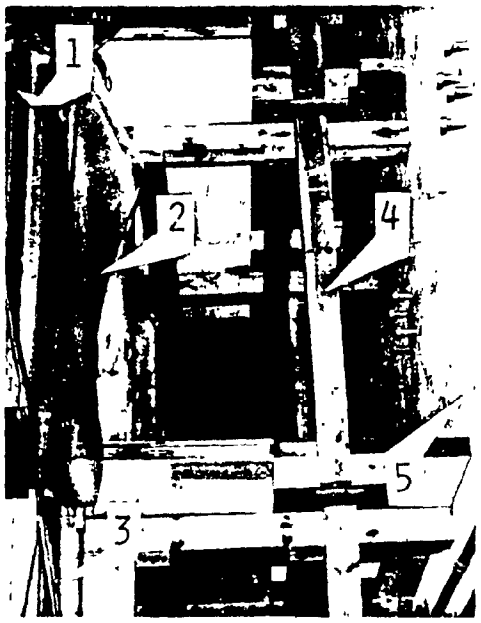

a) WOOD SUPPORT FRAME

1. side of model; 2. plastic sheet; 3. retaining platform; 4. wood support frame; 5. structural wall of laboratory.

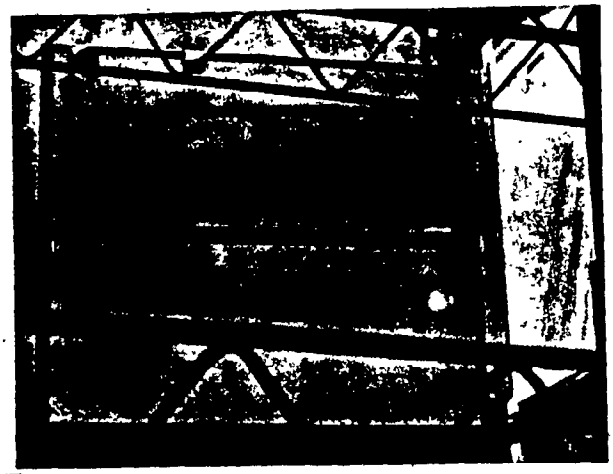

b) REMOVAL OF RETAINING PLATFORM TO CHECK AIR BAG LEAKAGES

c) INPUT PIPE OF THE BAGS

d) BLOWN AIR BAG

FIG. 2.7 - LATERAL LOADING SYSTEM

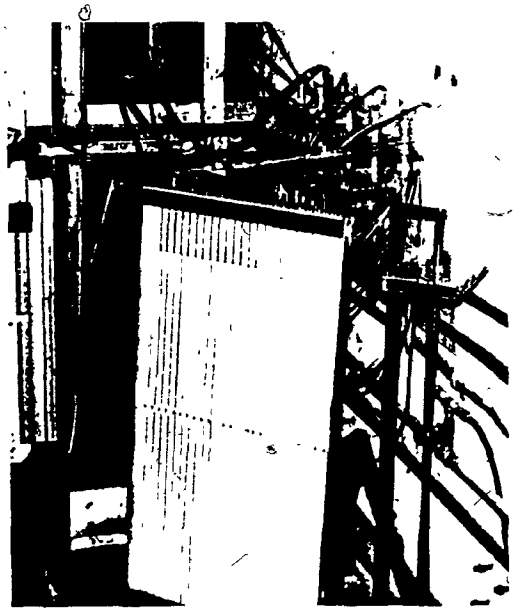

FIG. 2.8 - PANEL OF MANOMETERS MONITORING AIR BAG PRESSURES

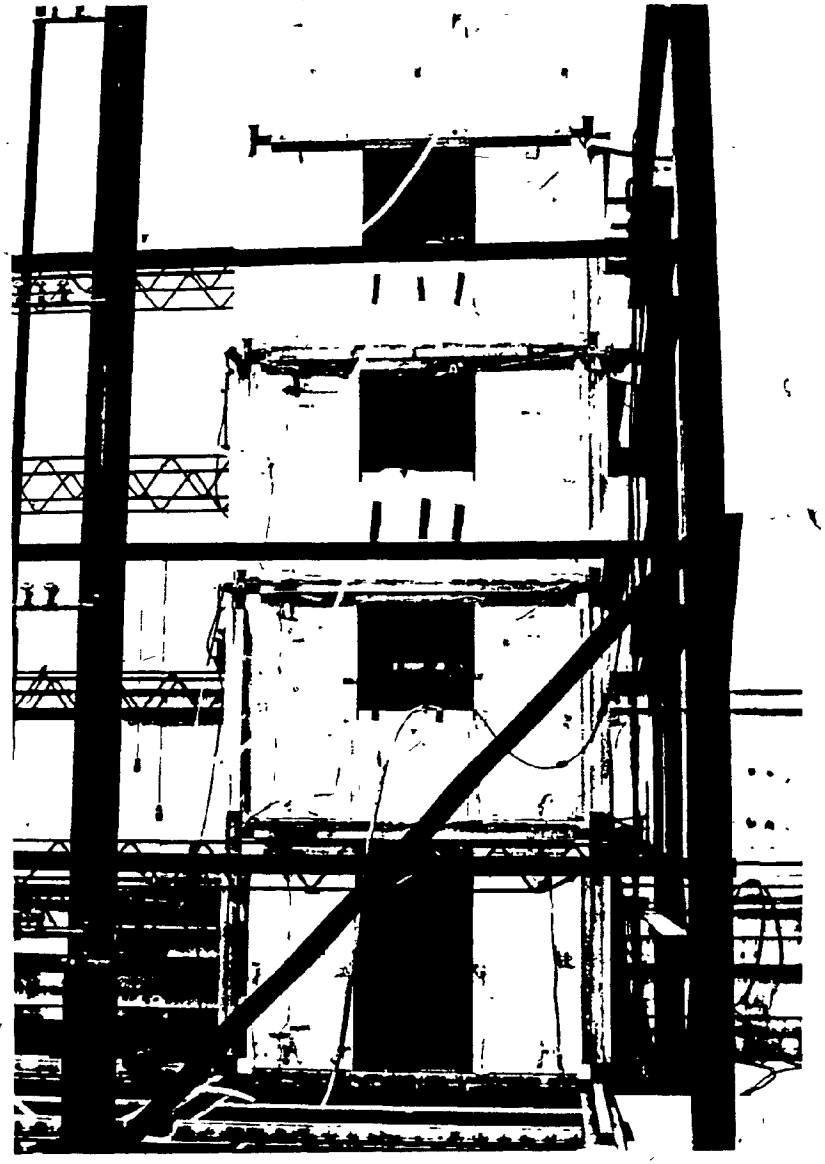

FIG. 2.9 - VERTICAL LOADS SIMULATED BY OPEN WATER BASINS

Note : In this Fig. 2.10,

- A, B identify the two sandwich skins of the panels, reported in Fig. 2.11;
- the numbers identify the panels (also Fig. 2.11).

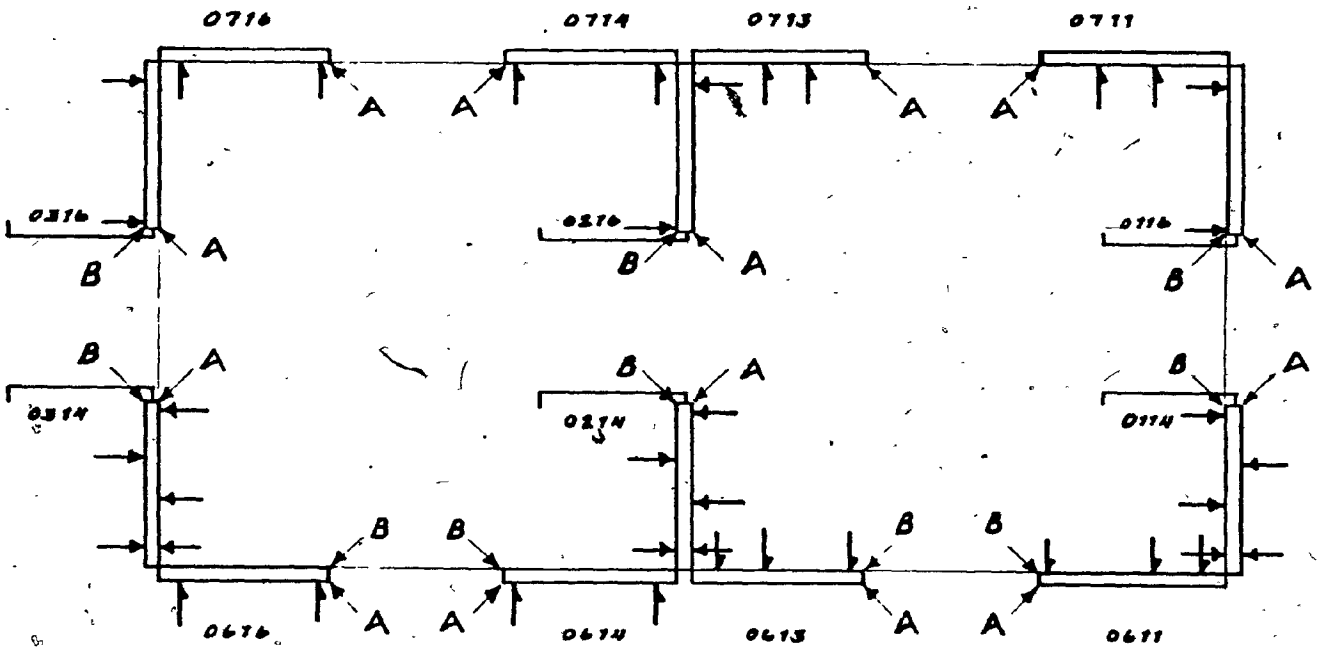

FIG. 2.10 - GENERAL PLAN OF ROSETTE POSITIONING, 4 in. (10 cm) ABOVE THE BOTTOM OF THE MODEL.

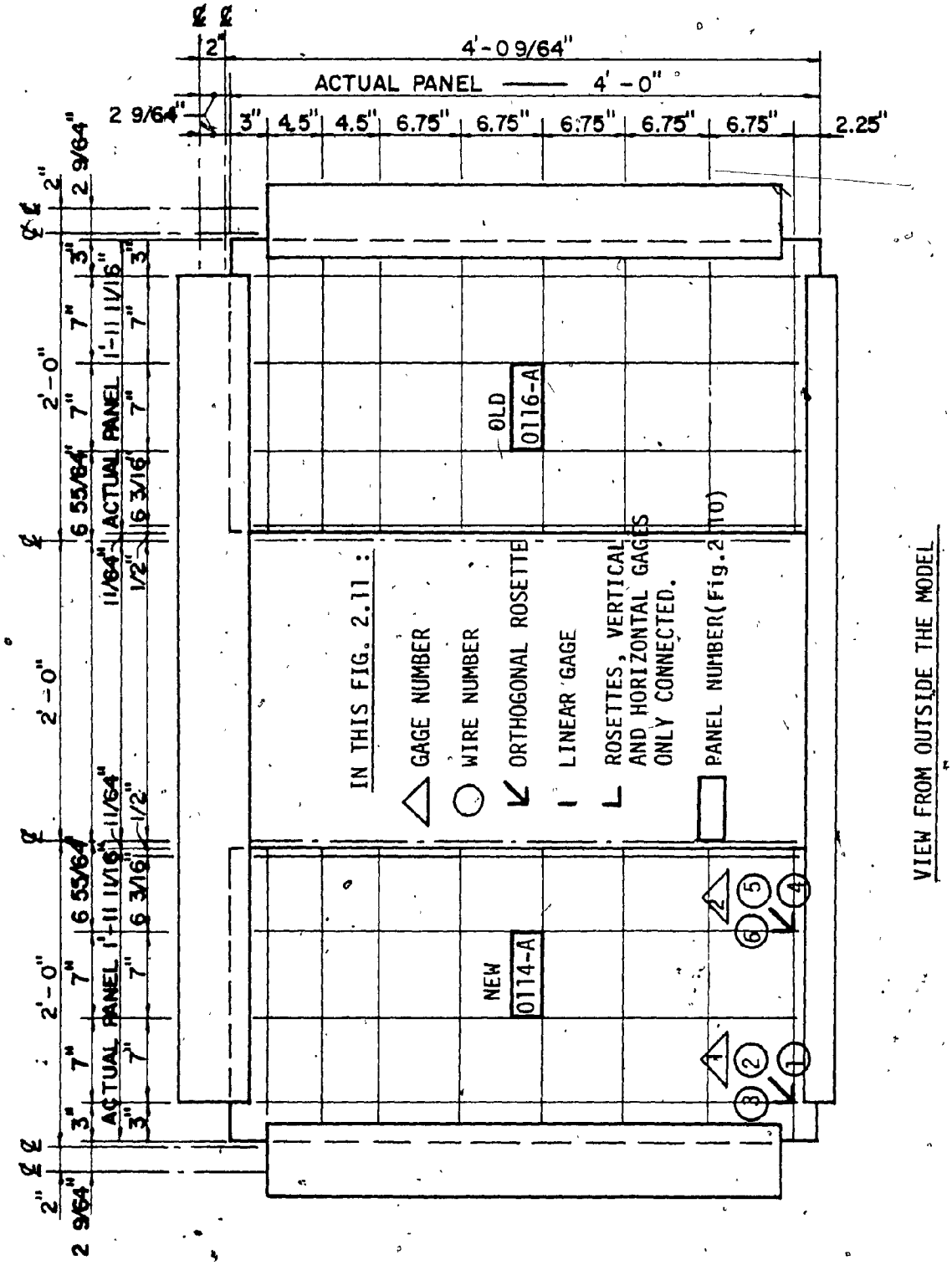

FIG. 2.11 - DETAILS OF STRAIN GAGES POSITIONING, AT THE BOTTOM OF THE MODEL.

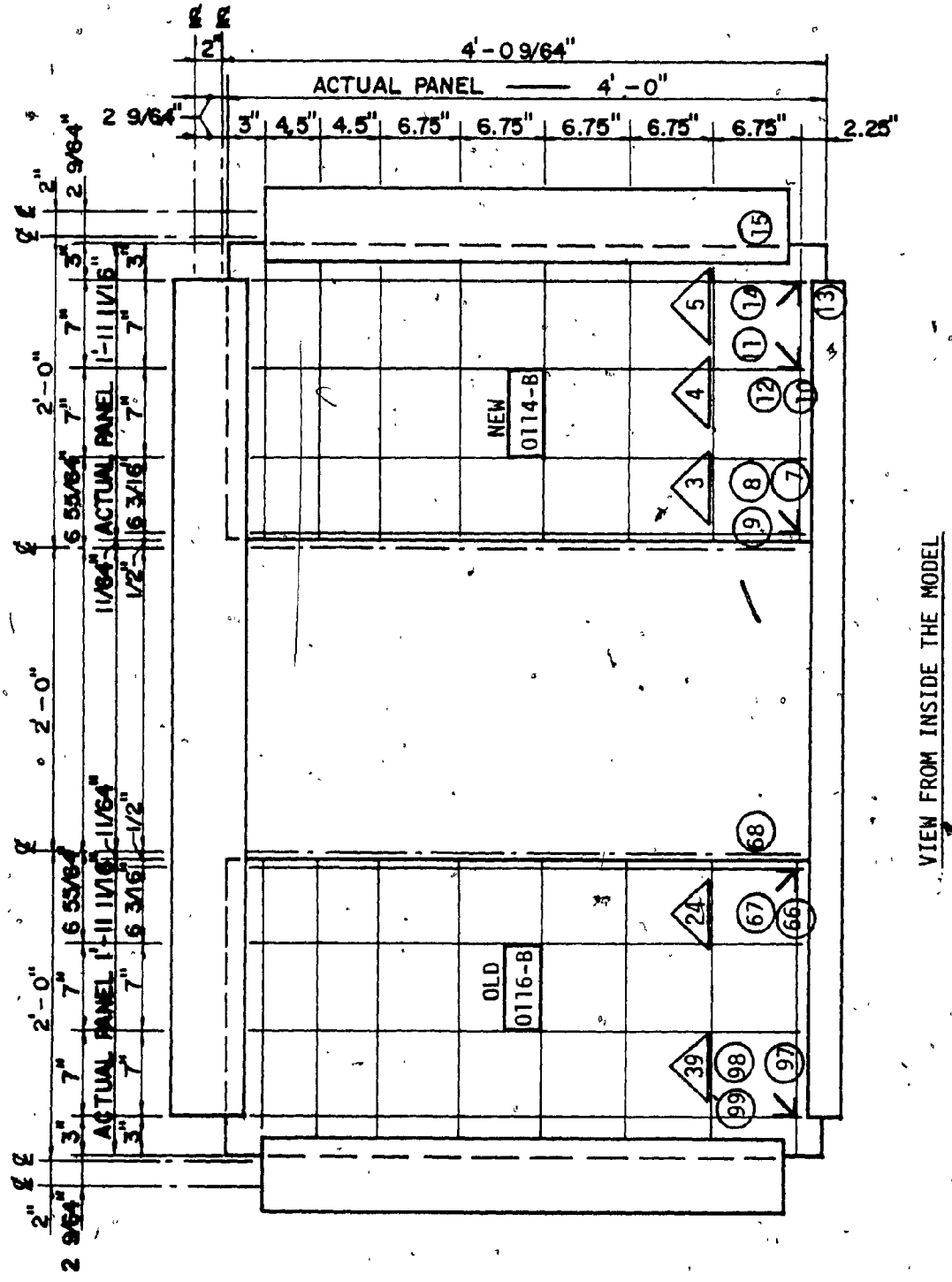

FIG. 2.11 - continued

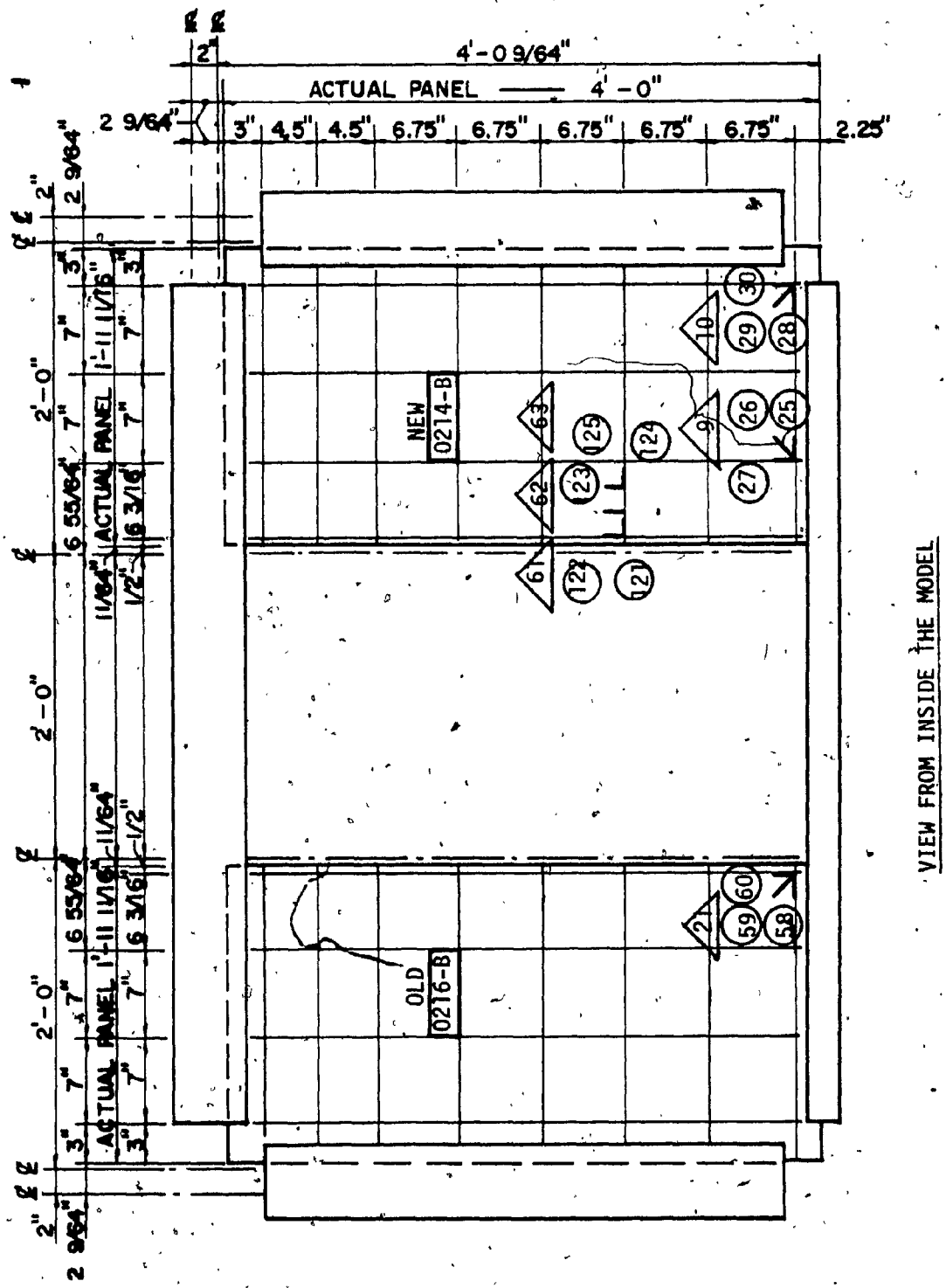

FIG. 2.11 - continued

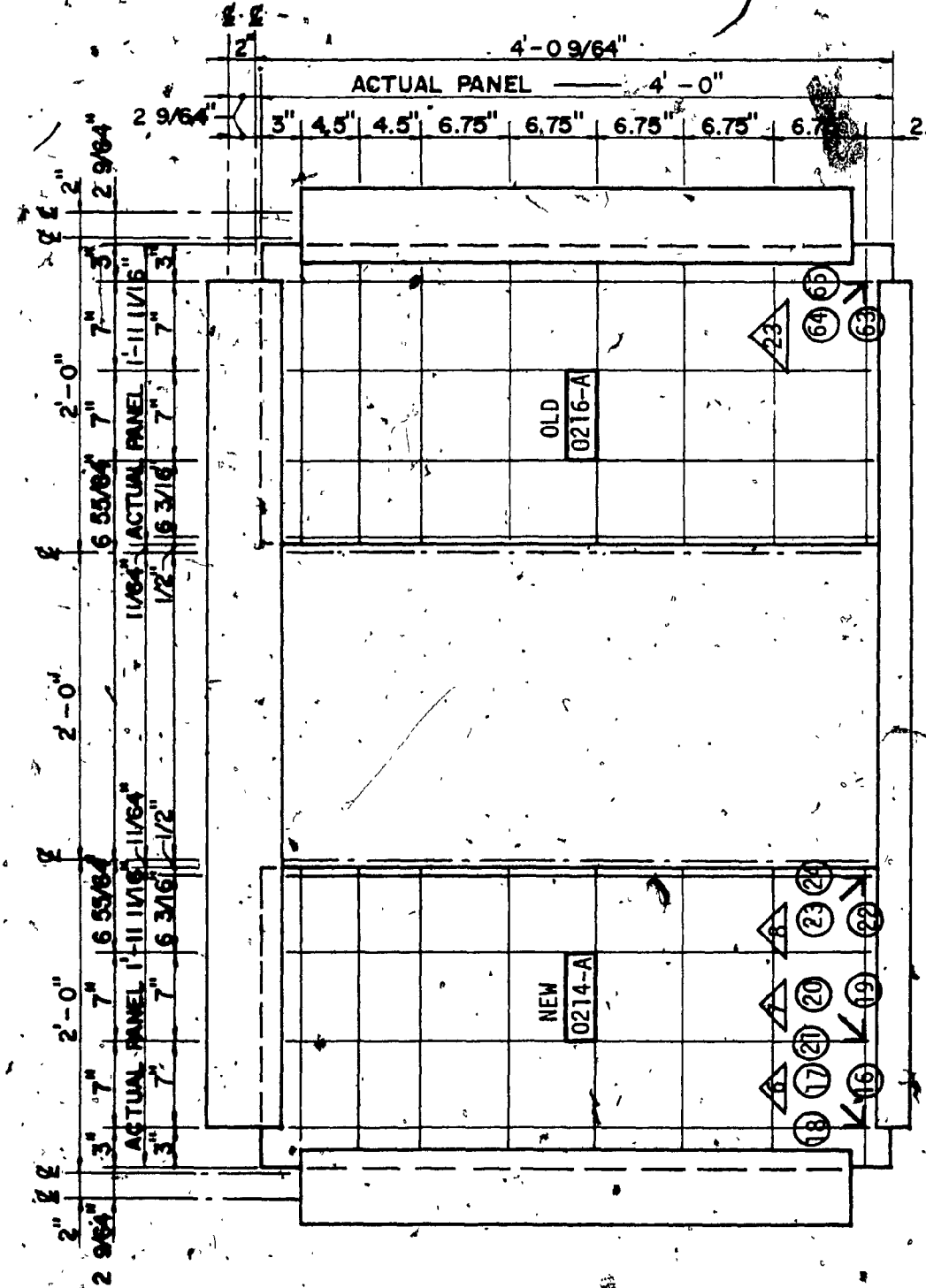

FIG. 2.11 - continued

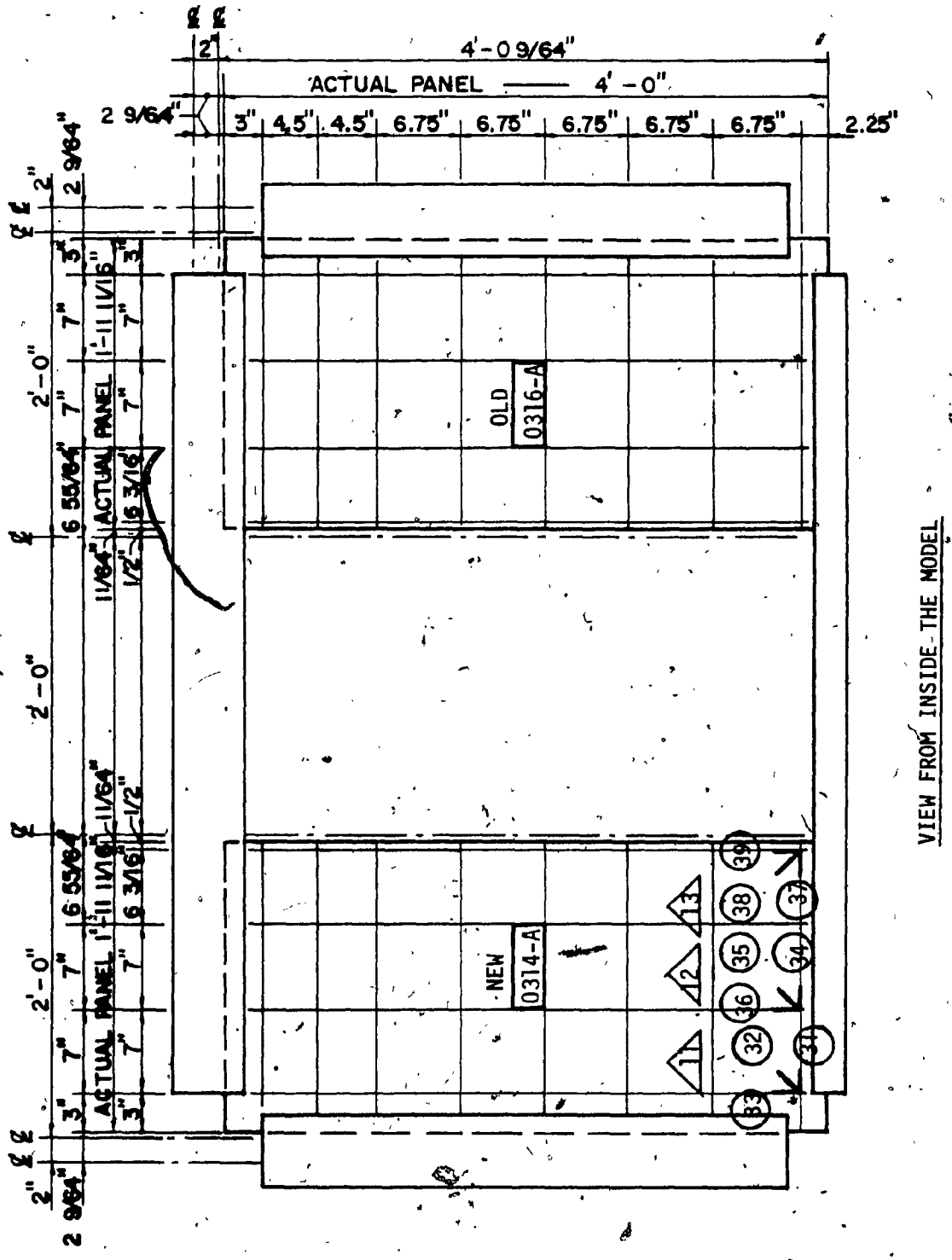

FIG. 2.11 - continued

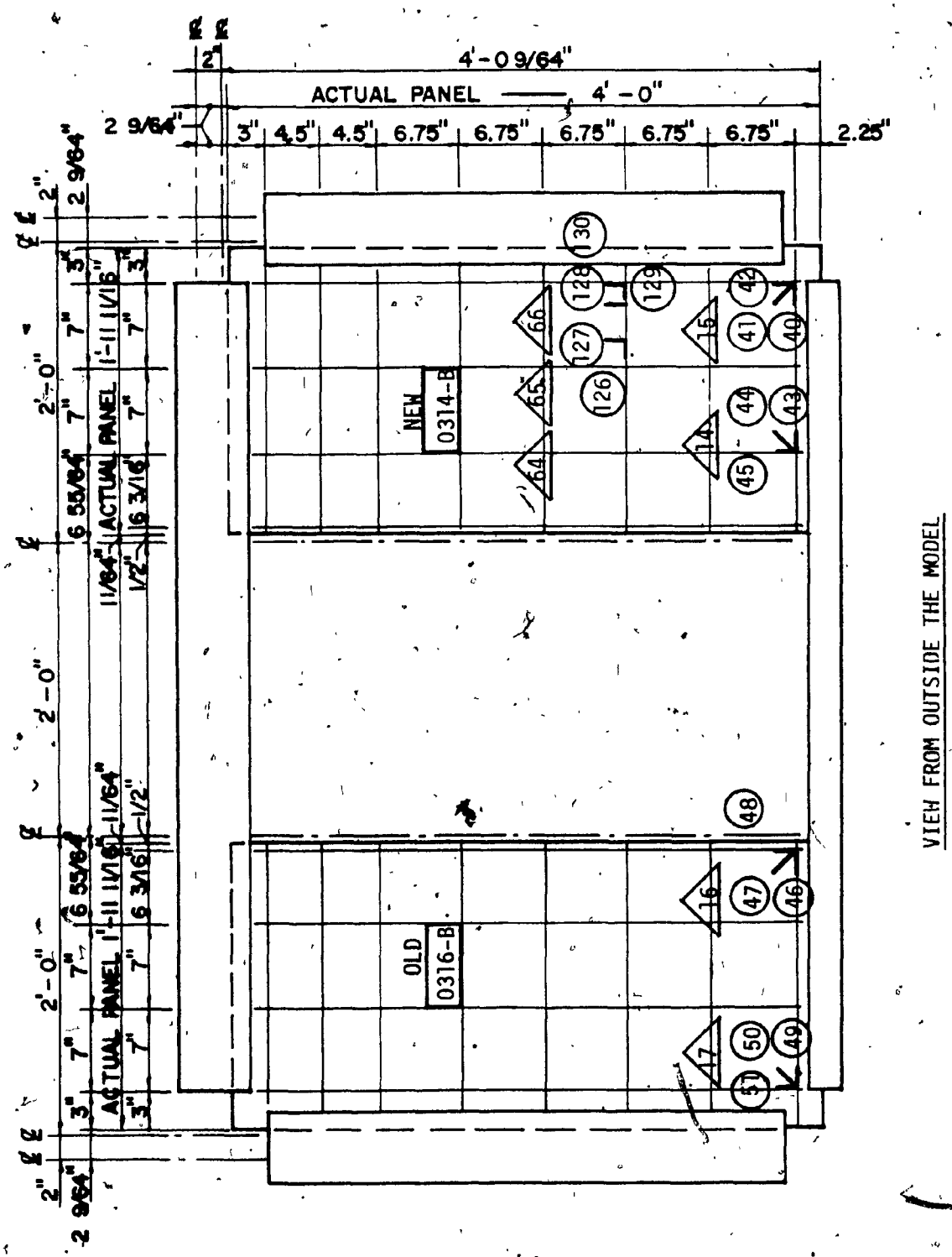

FIG. 2.11 - continued

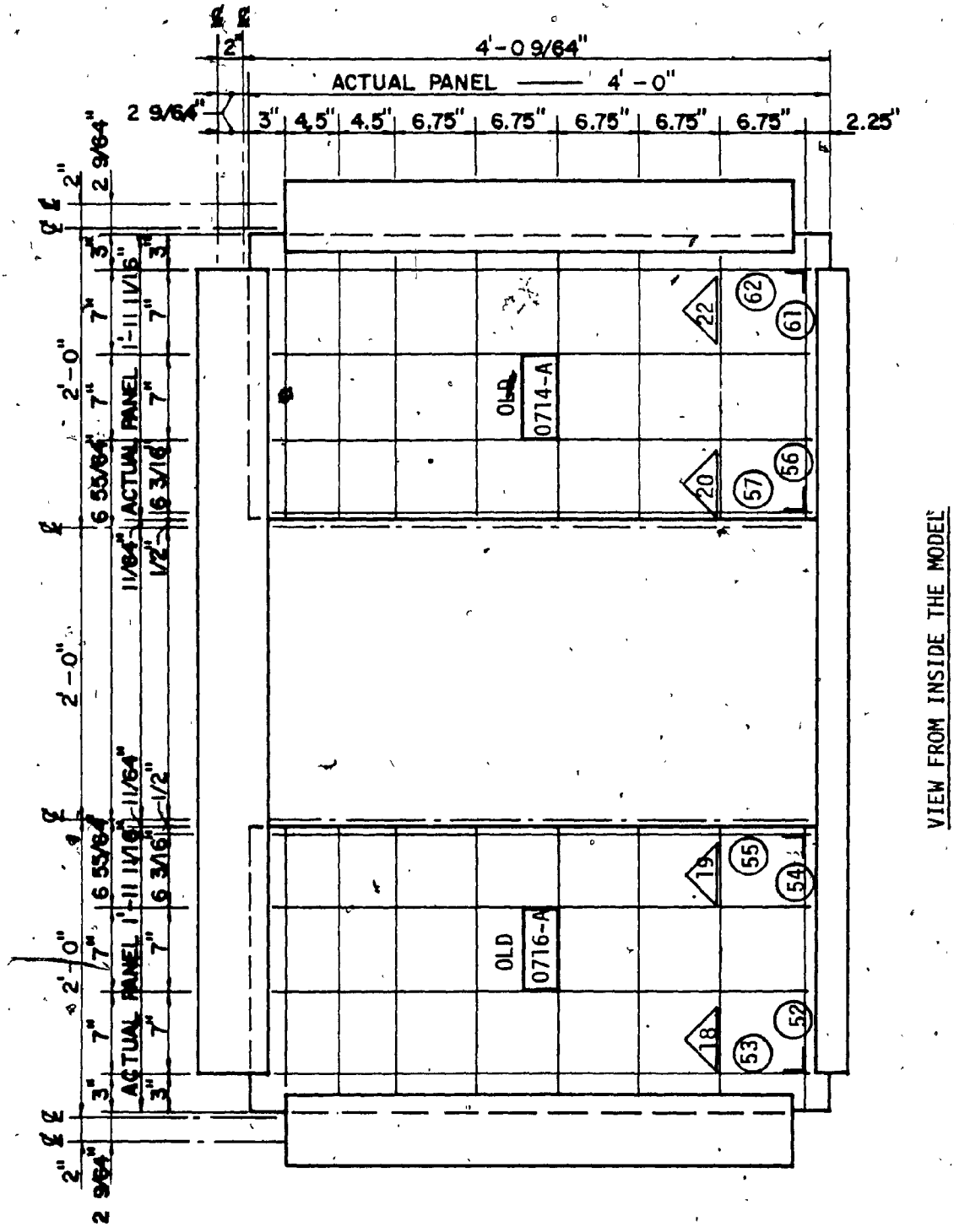

VIEW FROM INSIDE THE MODEL

FIG. 2.11 - continued

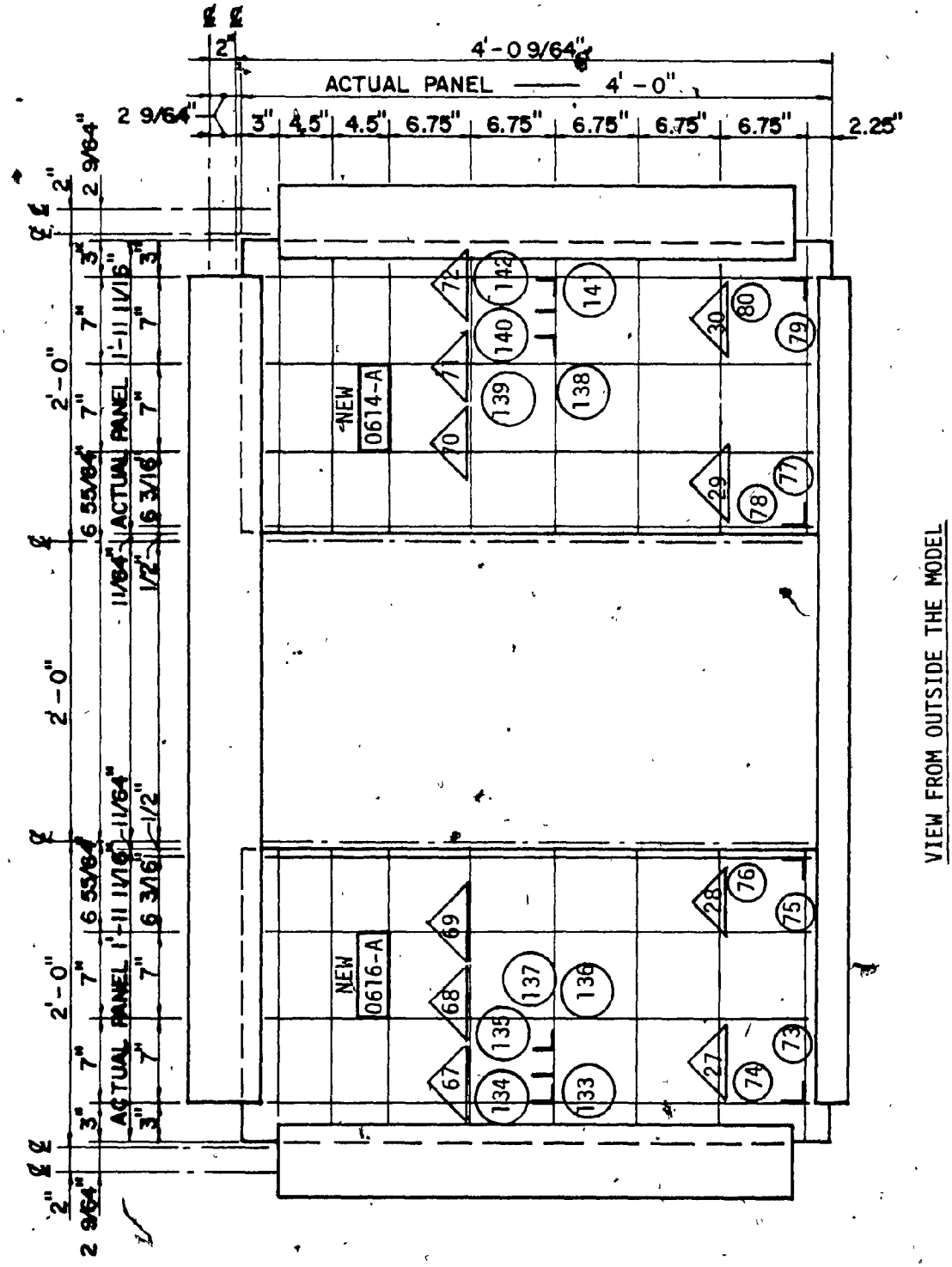

FIG. 2.11 - continued

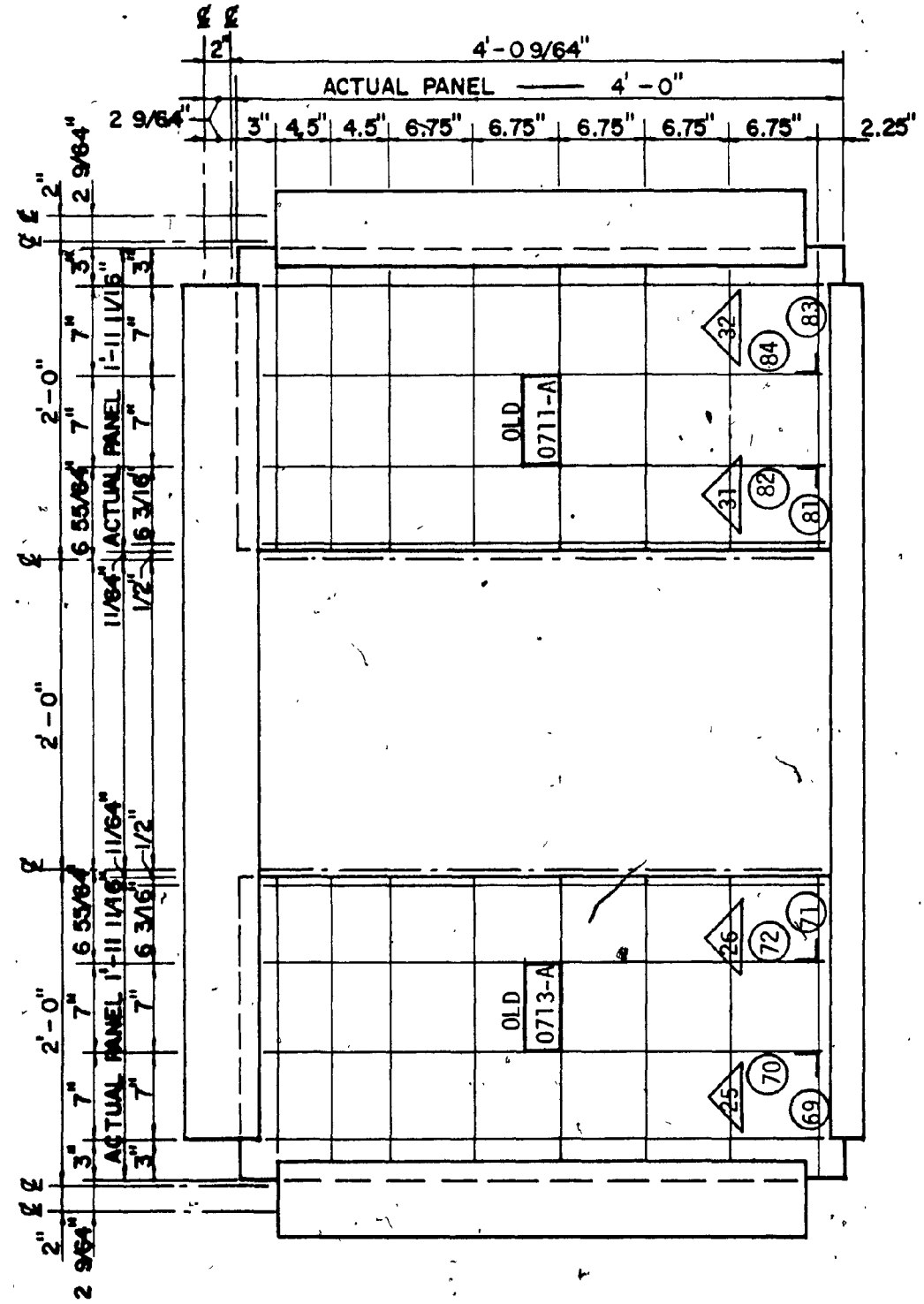

FIG. 2.11 - continued

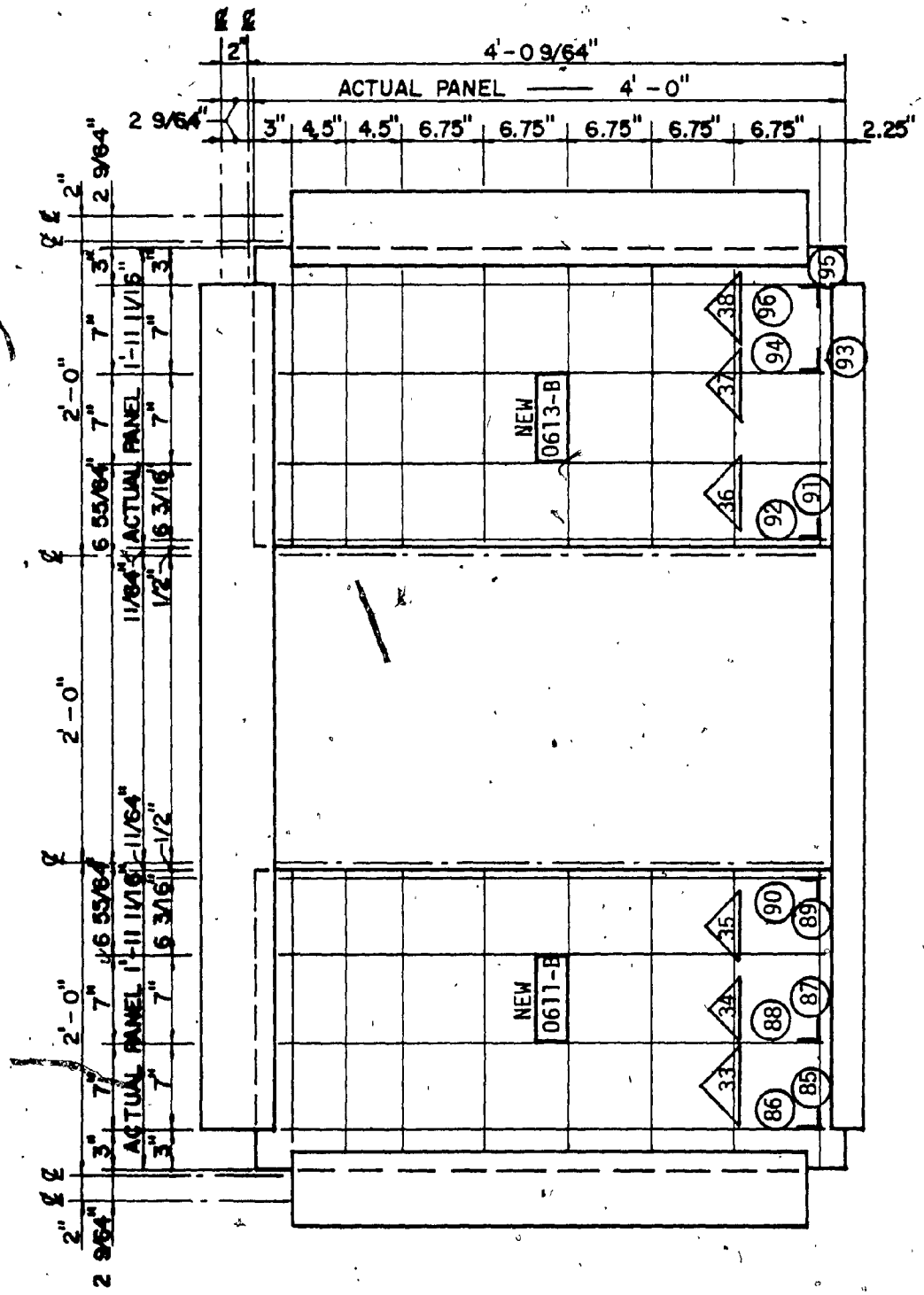

VIEW FROM INSIDE THE MODEL

FIG. 2.11 - continued

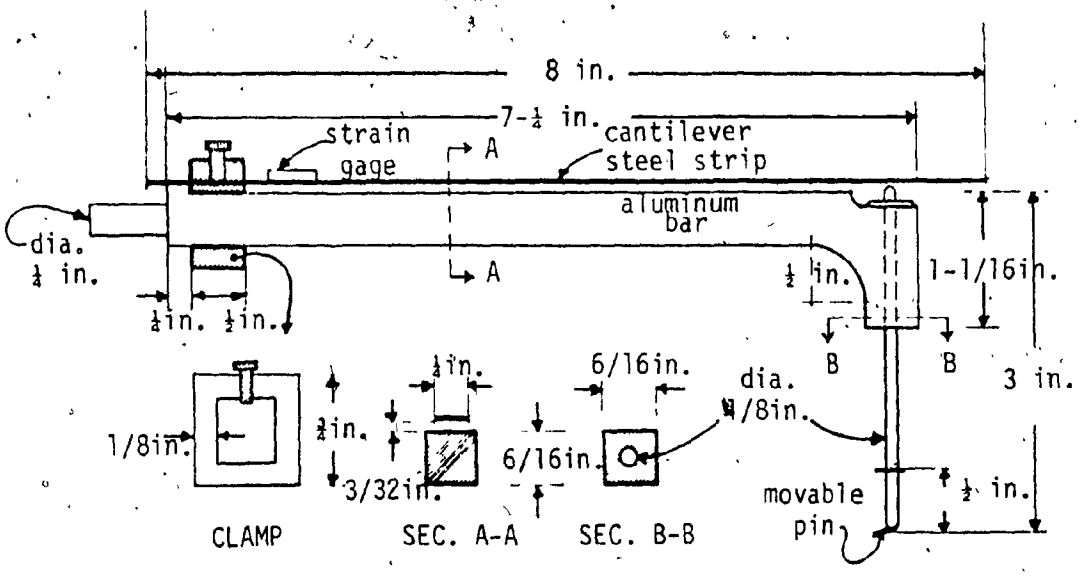

a) CANTILEVER DISPLACEMENT TRANSDUCER

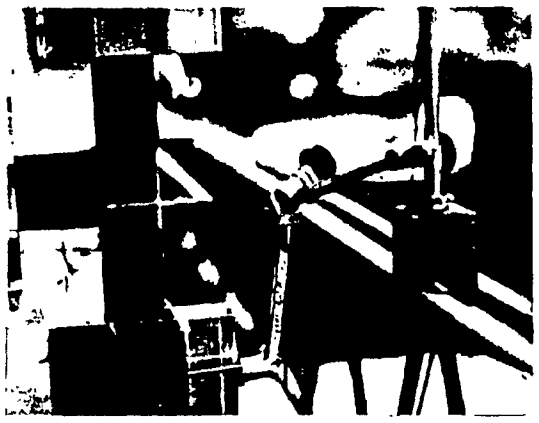

b) cantilever transducer and magnetic base

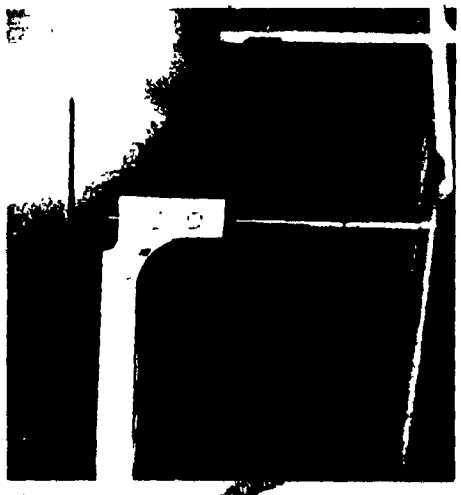

c) detail of movable pin

FIG. 2.12 - ELECTRICAL DISPLACEMENT TRANSDUCERS
(1 in. 2.54 cm.)

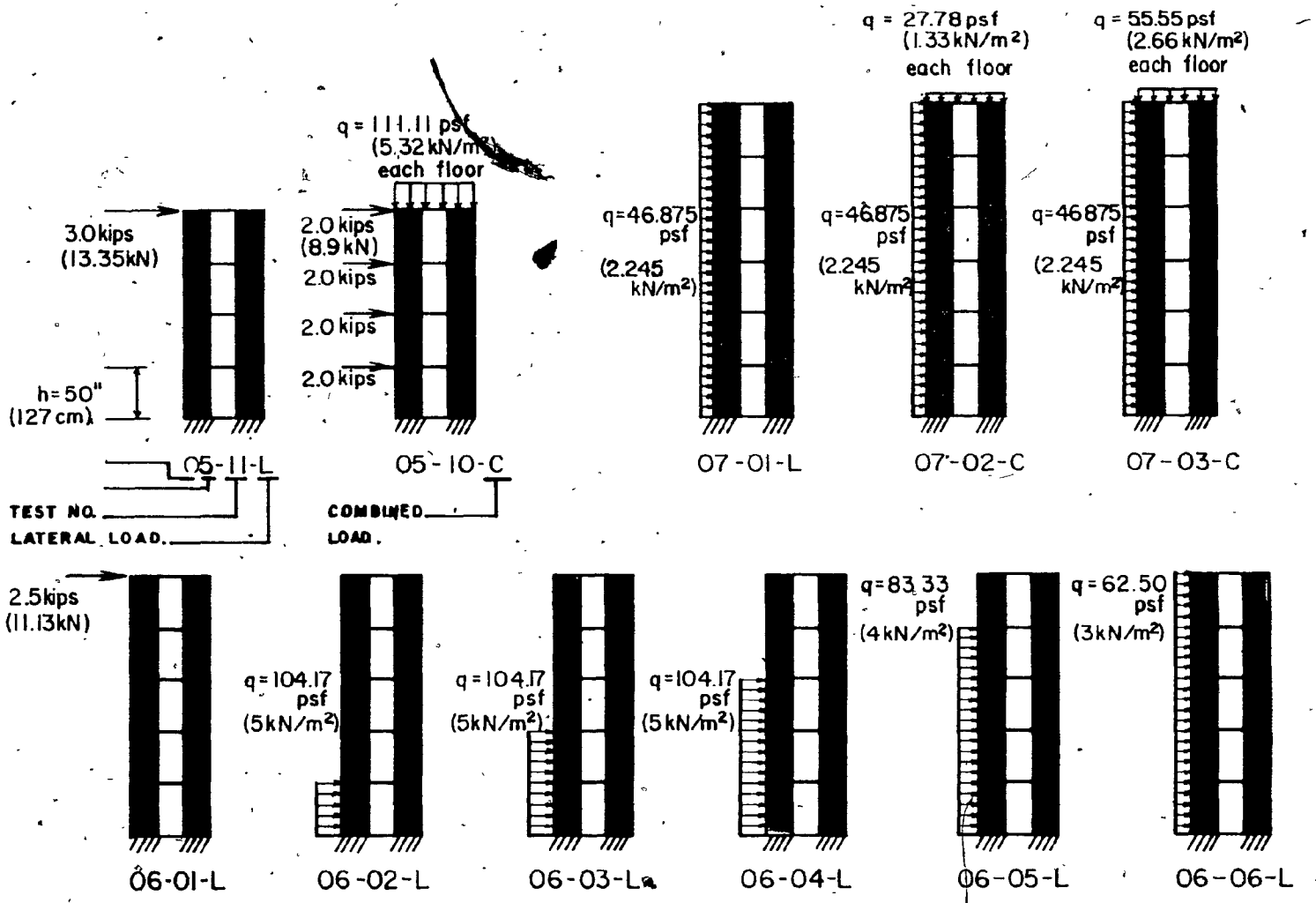

FIG. 3.1 - LATERAL AND COMBINED LOADING SCHEMES ON ASSEMBLIES 05, 06 AND 07.

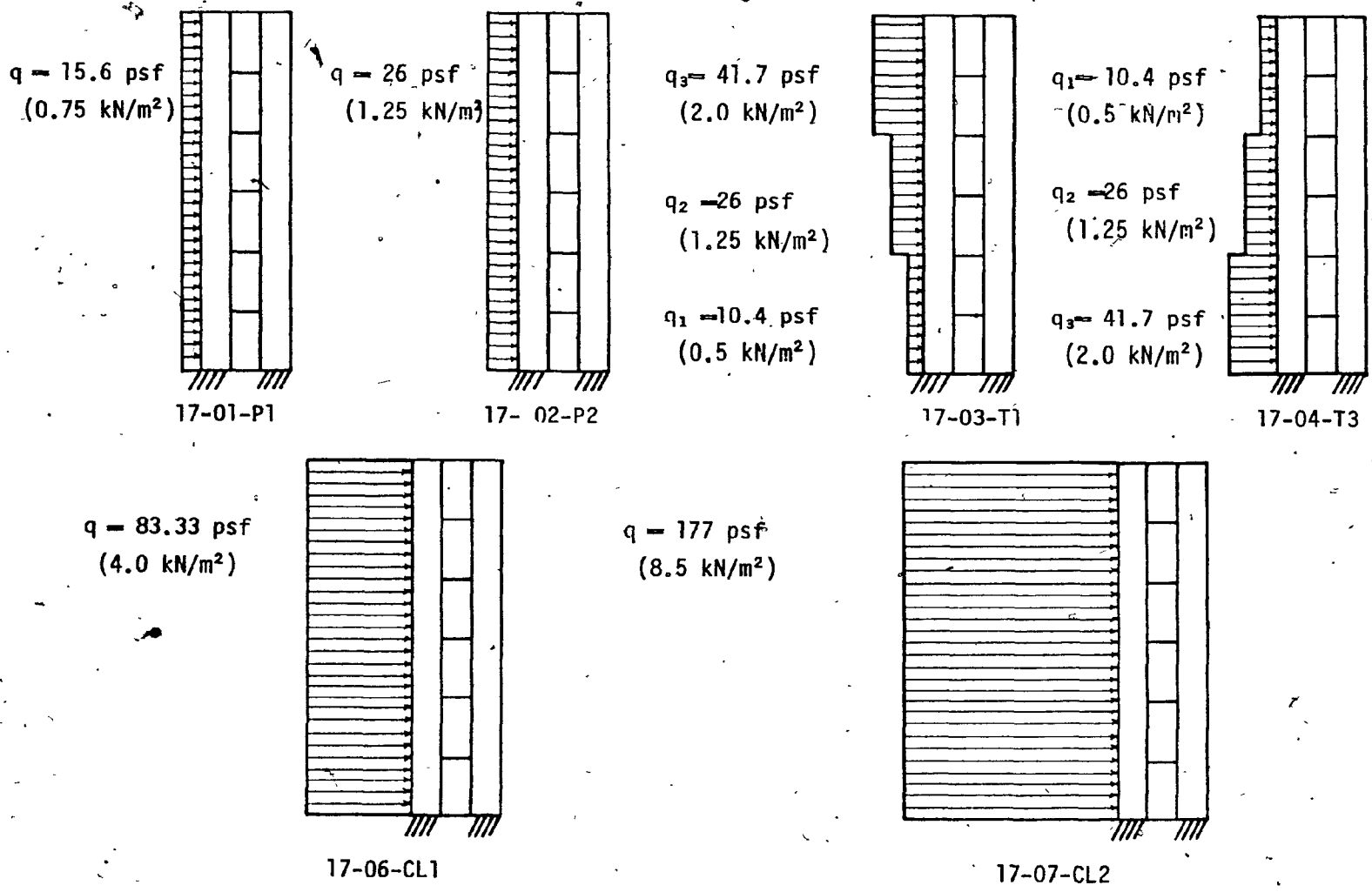

FIG. 3.2 - LATERAL LOADING SCHEMES ON ASSEMBLY 17

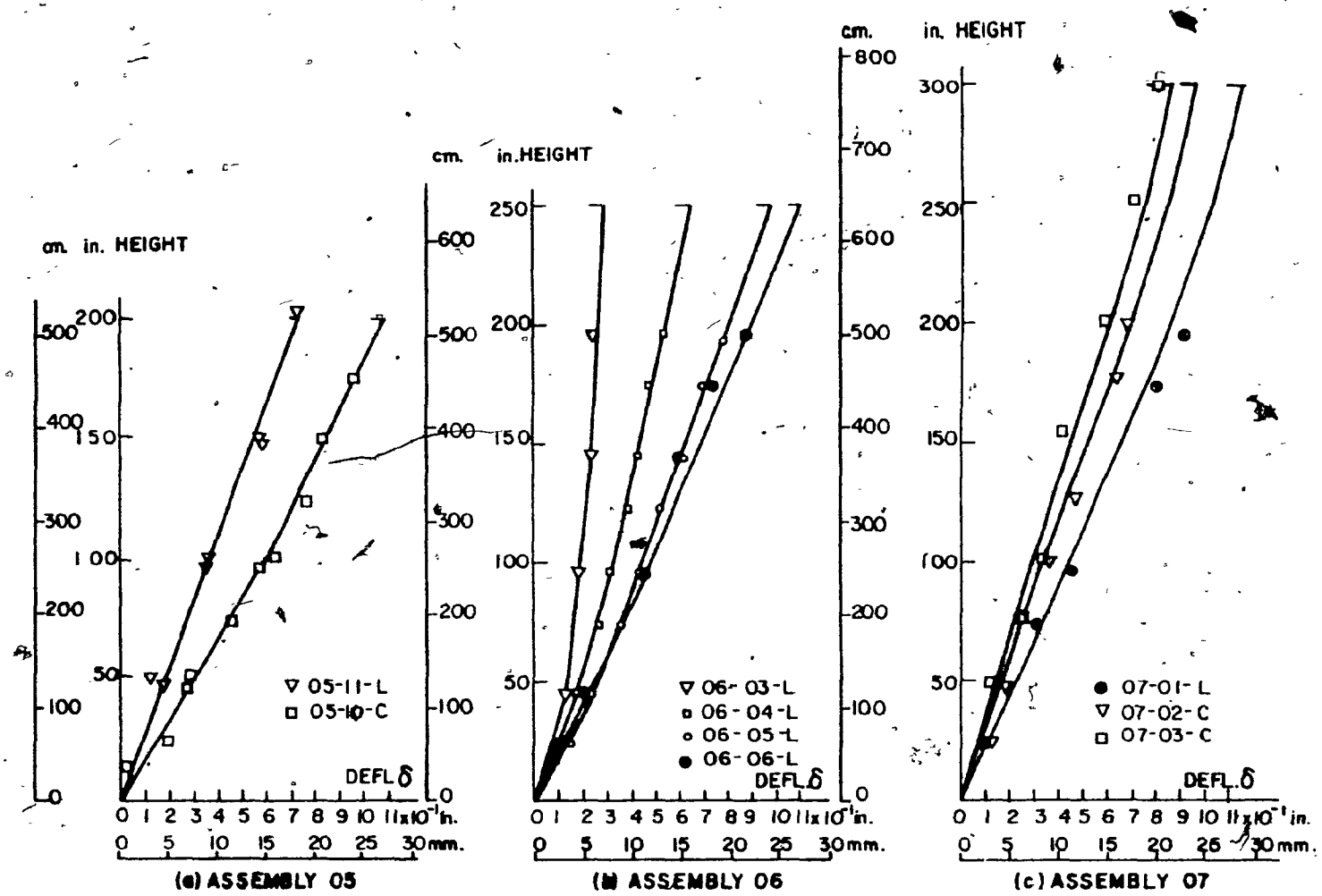

FIG. 3.3 - EXPERIMENTAL MODEL DEFLECTIONS

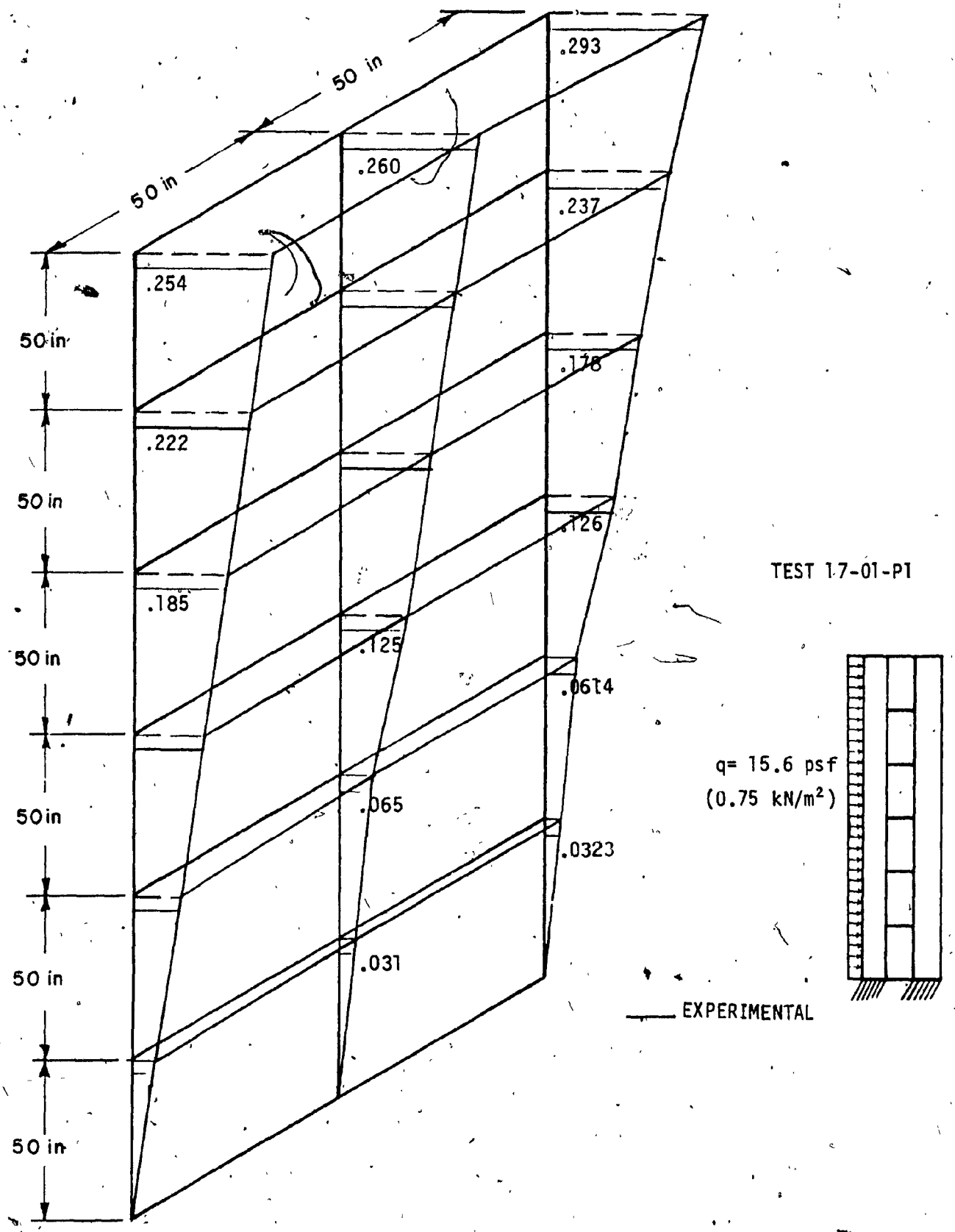

FIG. 3. 4 - 3-DIMENSIONAL PLOT OF EXPERIMENTAL DEFLECTIONS IN INCHES - TEST 17-01-P1 (1 in.=25.4 mm)

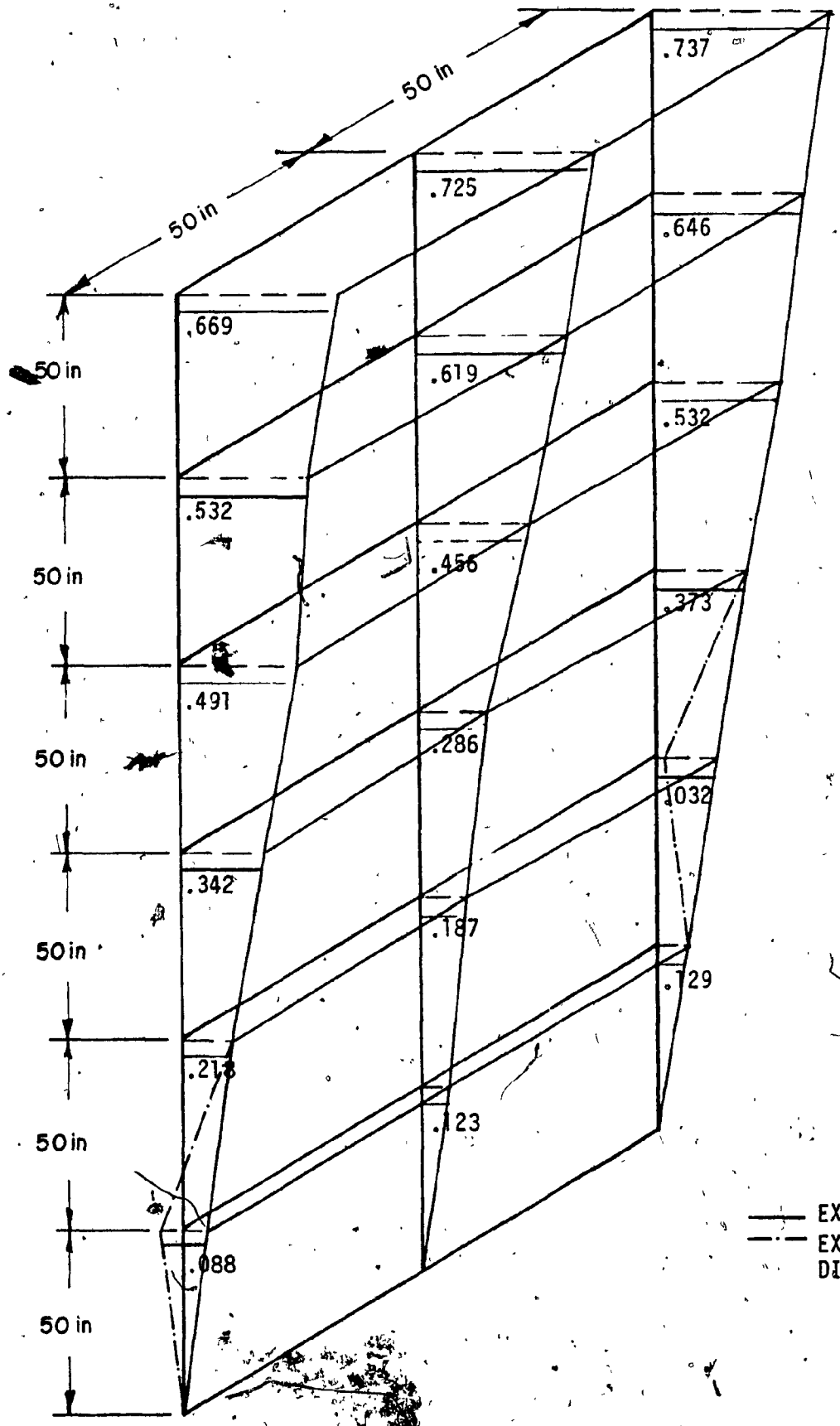

TEST 17-02-P2

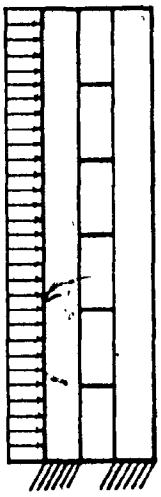

q= 25 psf
(1.25kN/m²)

—— EXPERIMENTAL
—·— EXP. TO BE DISCARDED

FIG. 3.5 - 3-DIMENSIONAL PLOT OF EXPERIMENTAL DEFLECTIONS IN INCHES - TEST 17-02-P2 (1in.=25.4 mm)

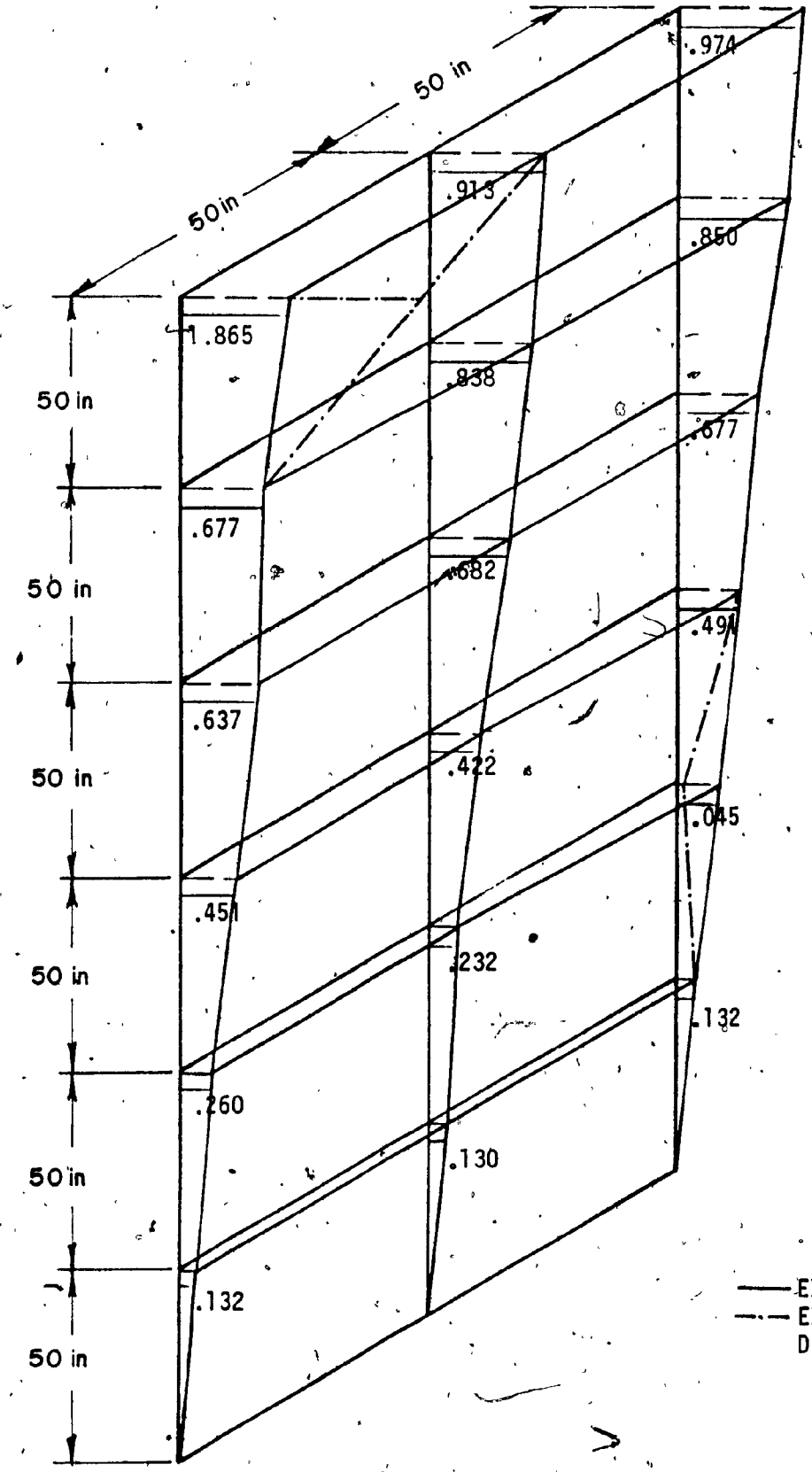

TEST 17-03-T1

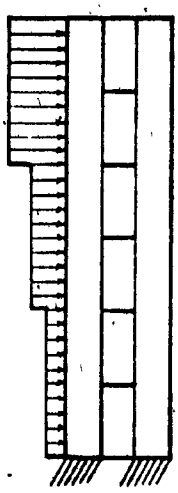

q_3= 41.7 psf
(2.0 kN/m²)

q_2= 26 psf
(1.25 kN/m²)

q_1= 10.4 psf
(0.5 kN/m²)

——EXPERIMENTAL
—·— EXP. TO BE DISCARDED

FIG. 3.6 - 3-DIMENSIONAL PLOT OF EXPERIMENTAL DEFLECTIONS IN INCHES - TEST 17-03-T1 (1 in.=25.4 mm)

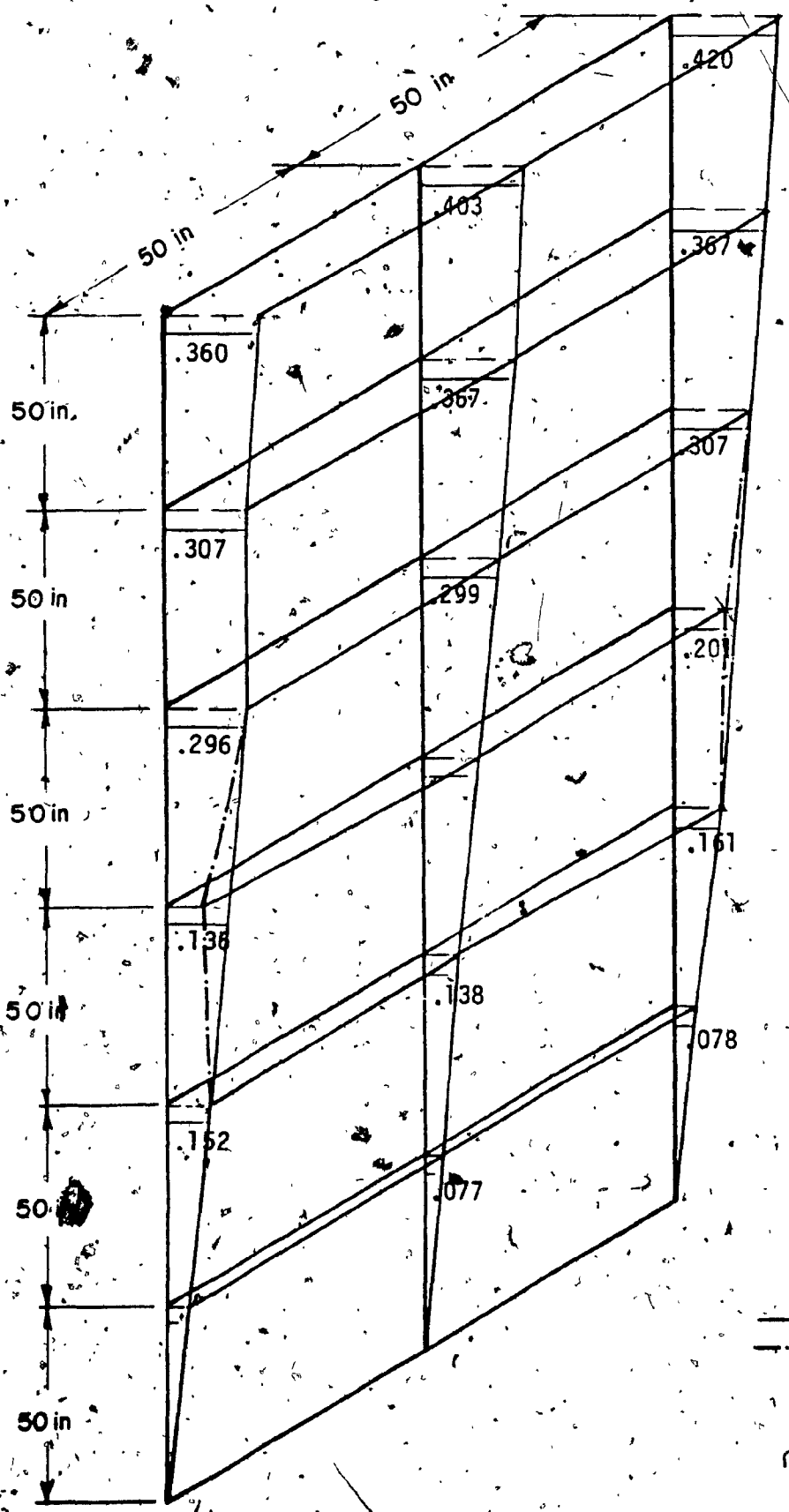

TEST 17-04-T3

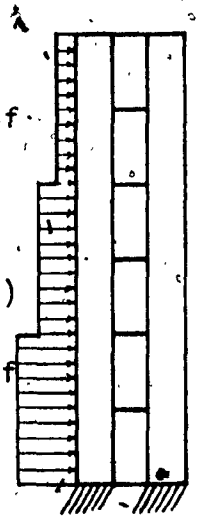

q_1 = 10.4 psf
(0.5 kN/m²)

q_2 = 26 psf
(1.25 kN/m²)

q_3 = 41.7 psf
(2.0 kN/m²)

——— EXPERIMENTAL
—·—·— EXP. TO BE DISCARDED

FIG. 3.7 - 3-DIMENSIONAL PLOT OF EXPERIMENTAL DEFLECTIONS IN INCHES - TEST 17-04-T3 (1 in.=25.4 mm)

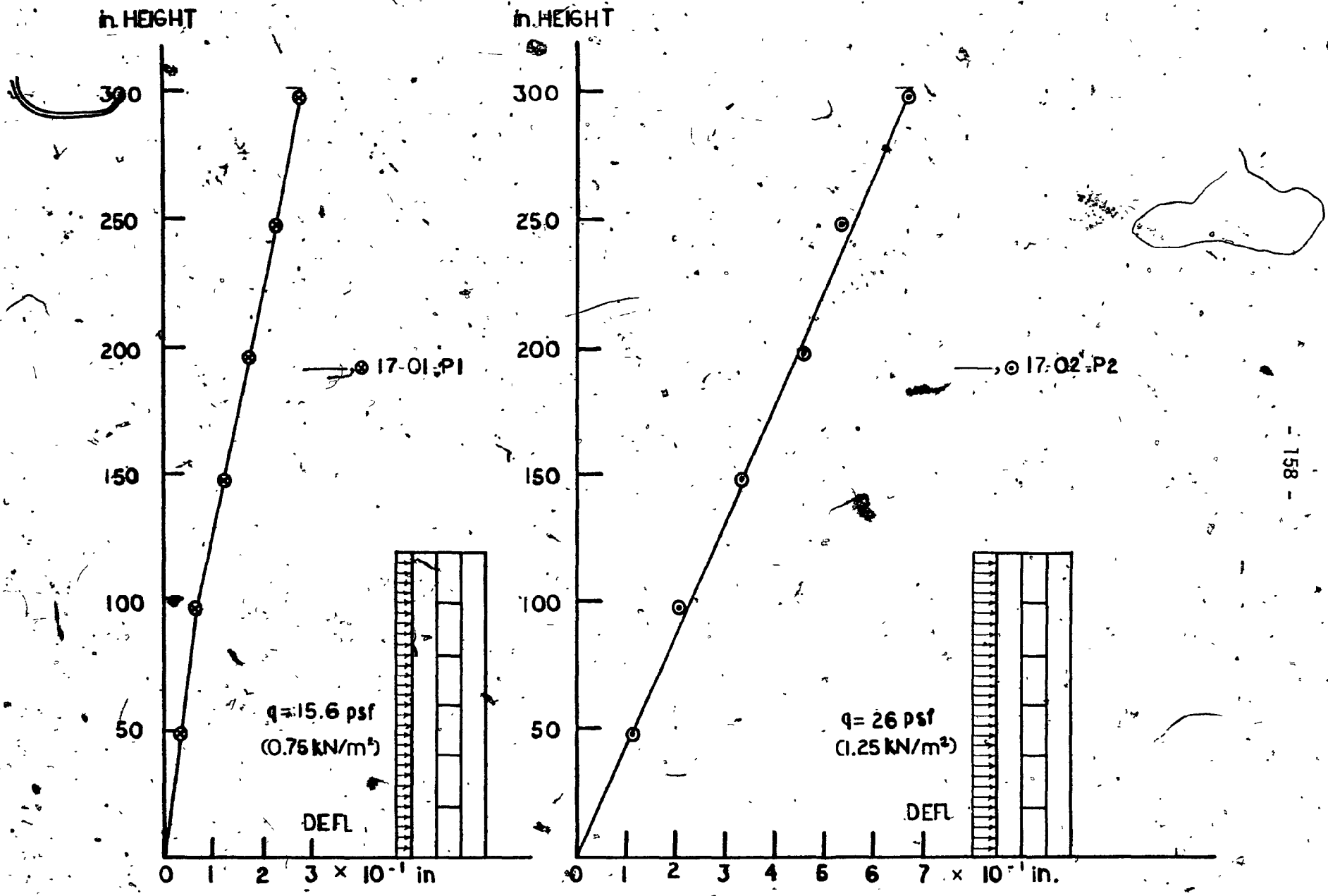

FIG. 3.8 - AVERAGE EXPERIMENTAL DEFLECTIONS IN INCHES
ASSEMBLY 17 (1 in.=25.4 mm)

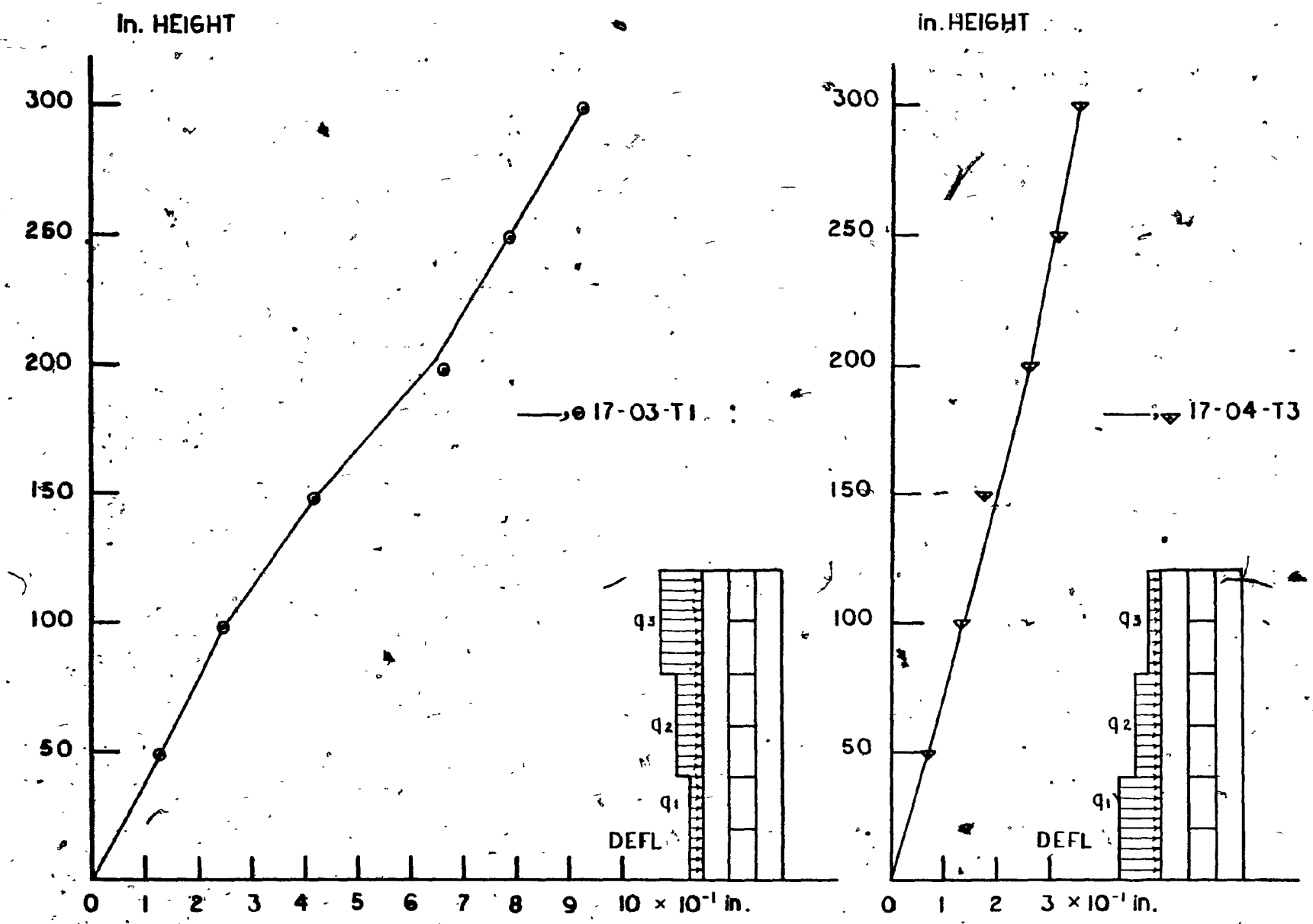

FIG. 3.9 - AVERAGE EXPERIMENTAL DEFLECTIONS IN INCHES
ASSEMBLY 17 (1in.=25.4 mm)

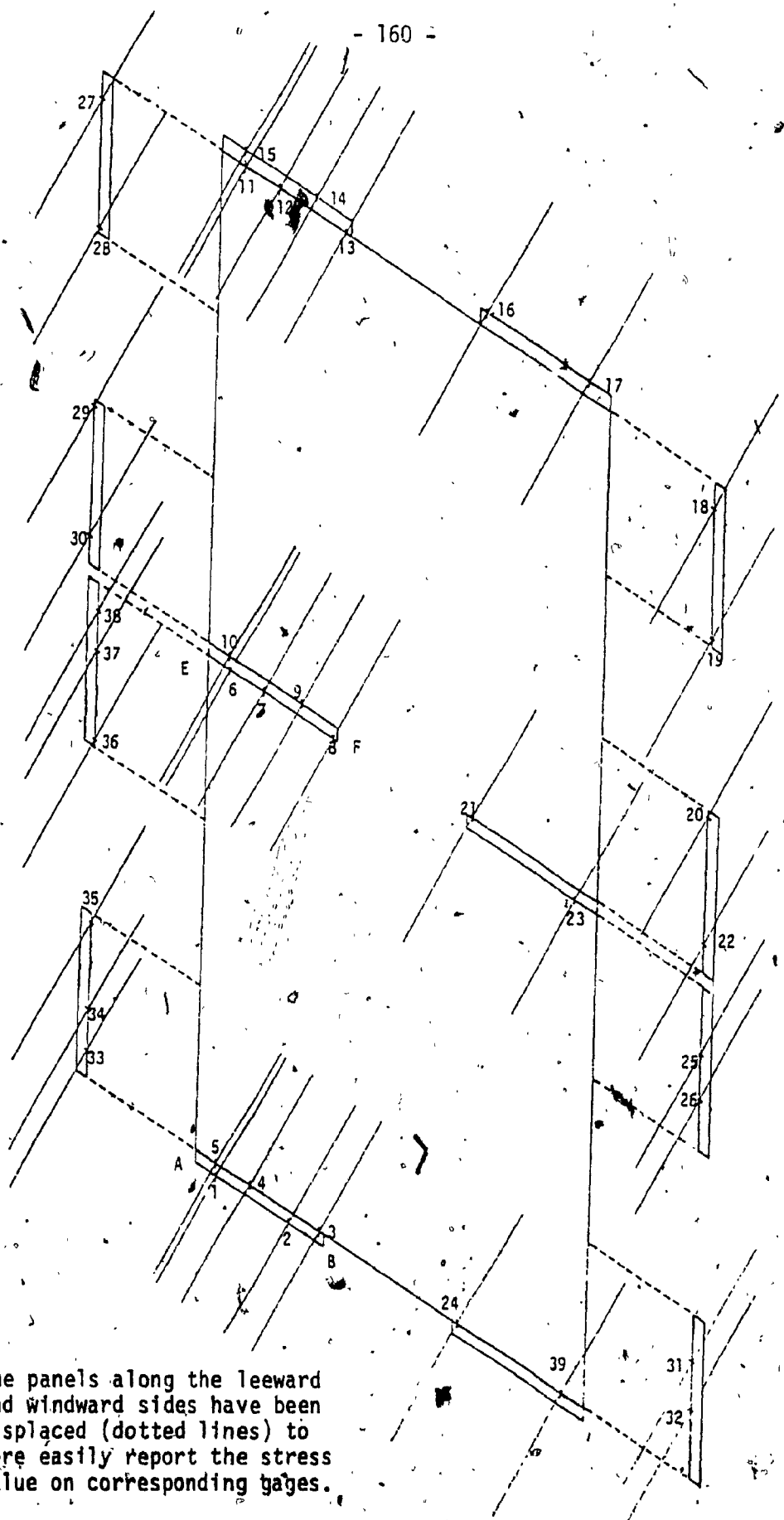

Note: The panels along the leeward and windward sides have been displaced (dotted lines) to more easily report the stress value on corresponding gages.

FIG. 3.10 - NUMBERING AND POSITION OF BASE ROSETTE GAGES (see also Figs. 2.10 and 2.11)

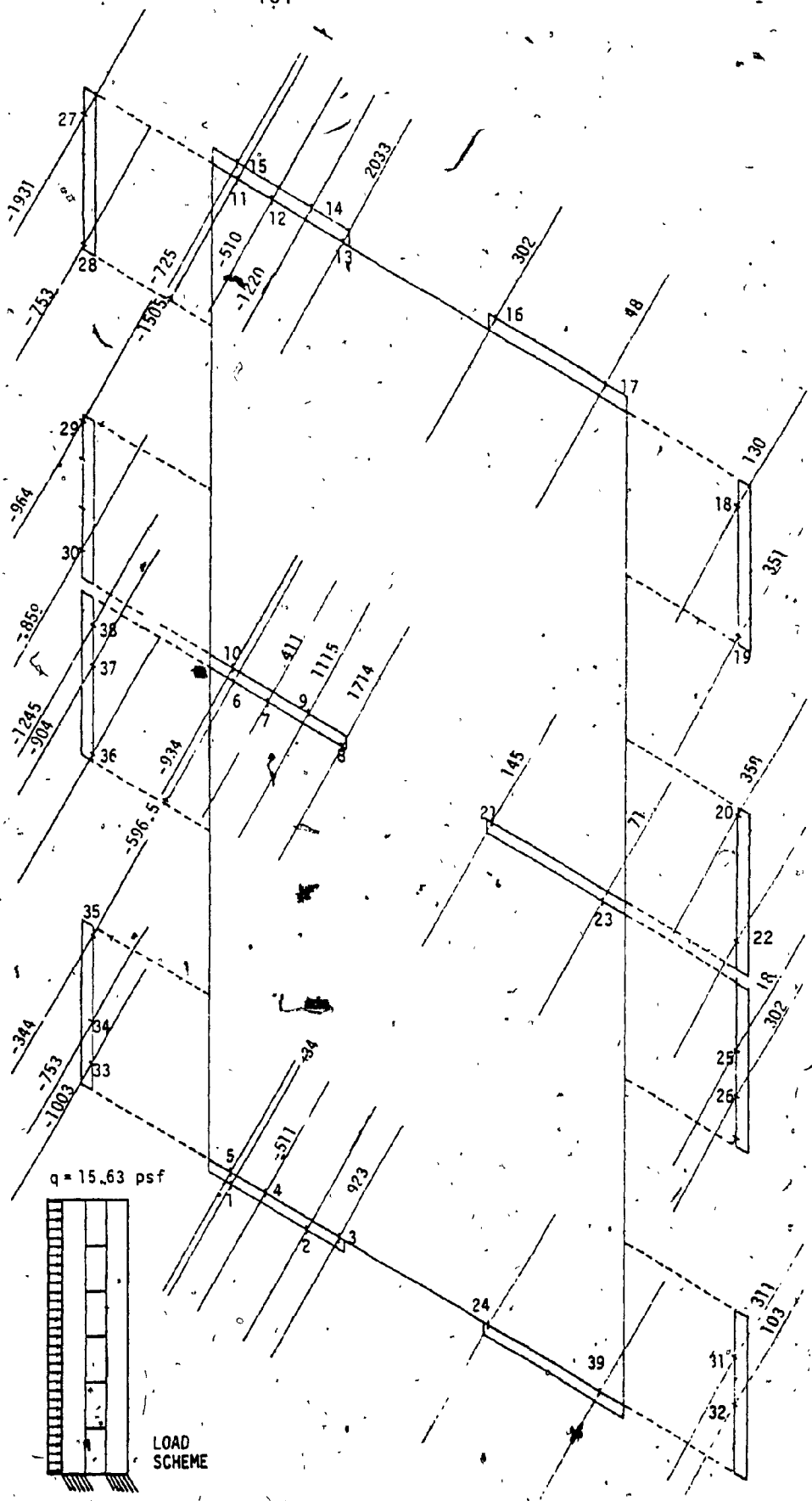

FIG. 3.11 - EXPERIMENTAL NORMAL STRESSES IN PSI
TEST 17-01-P1 (1 psi = 6.9 kN/m²)

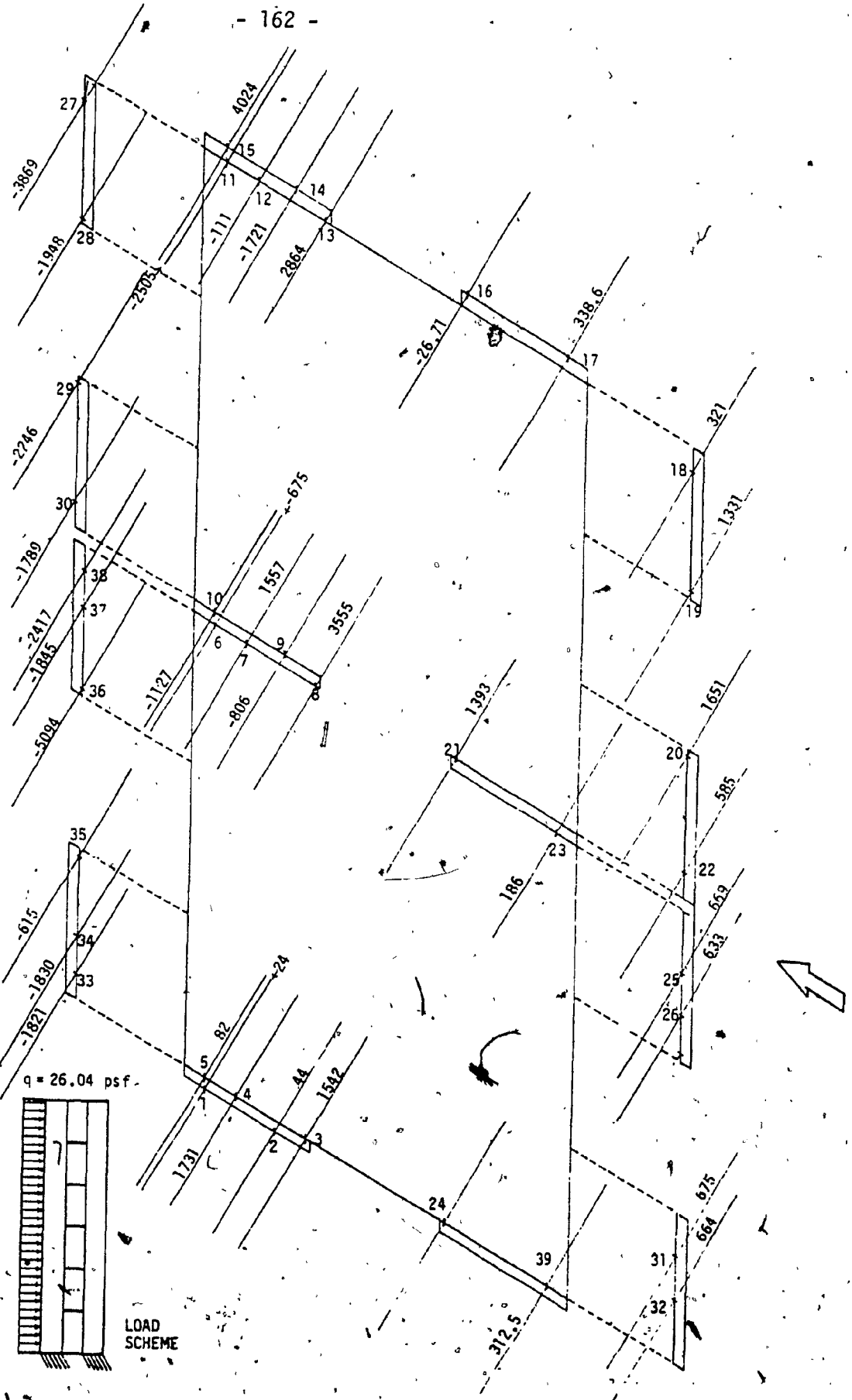

FIG. 3.12 - EXPERIMENTAL NORMAL STRESSES IN PSI
TEST 17-01-P2 (1 psi = 6.9 kN/m²)

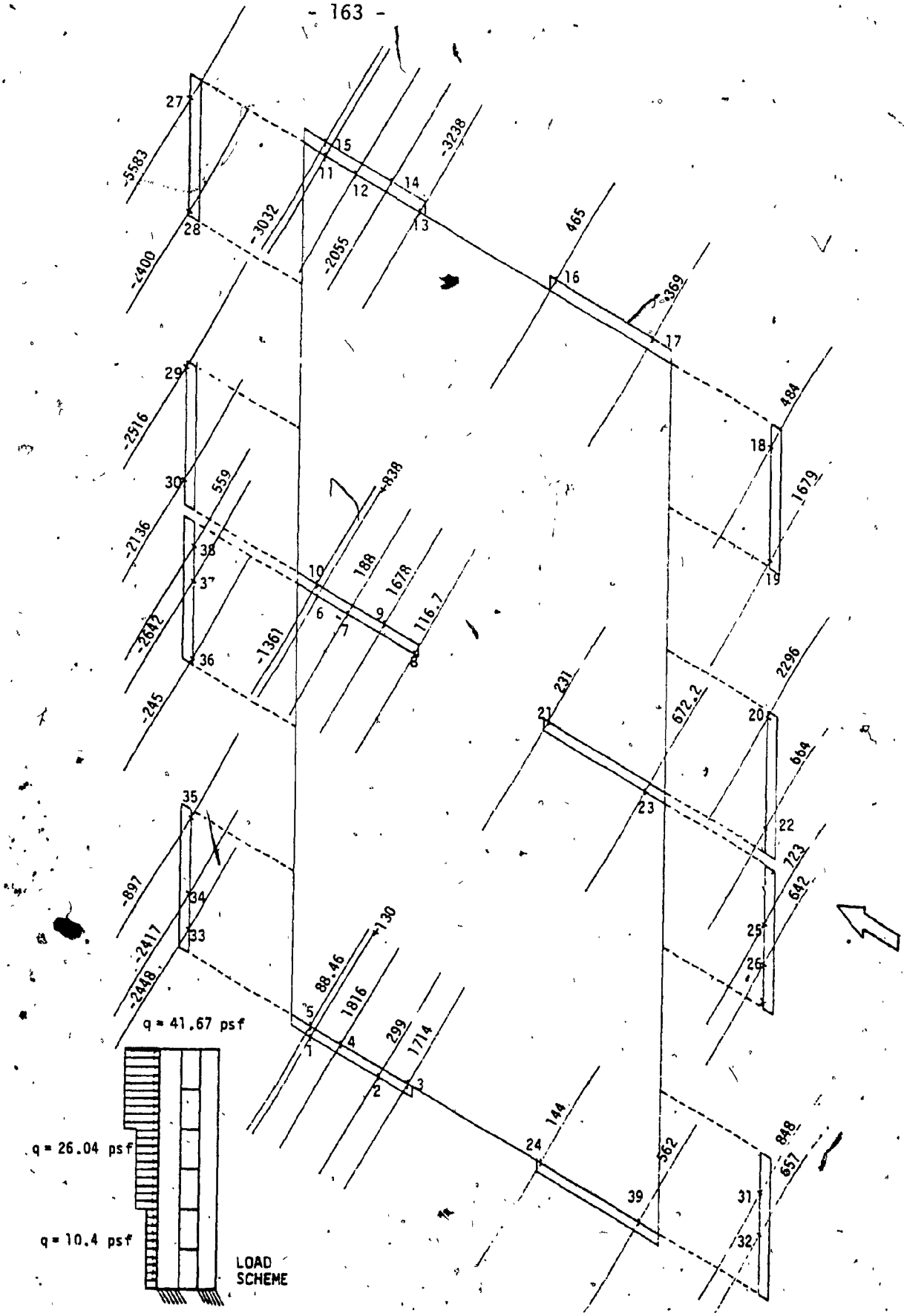

FIG. 3.13 - EXPERIMENTAL NORMAL STRESSES IN PSI
TEST 17-03-T1 (1 psi = 6.9 kN/m²)

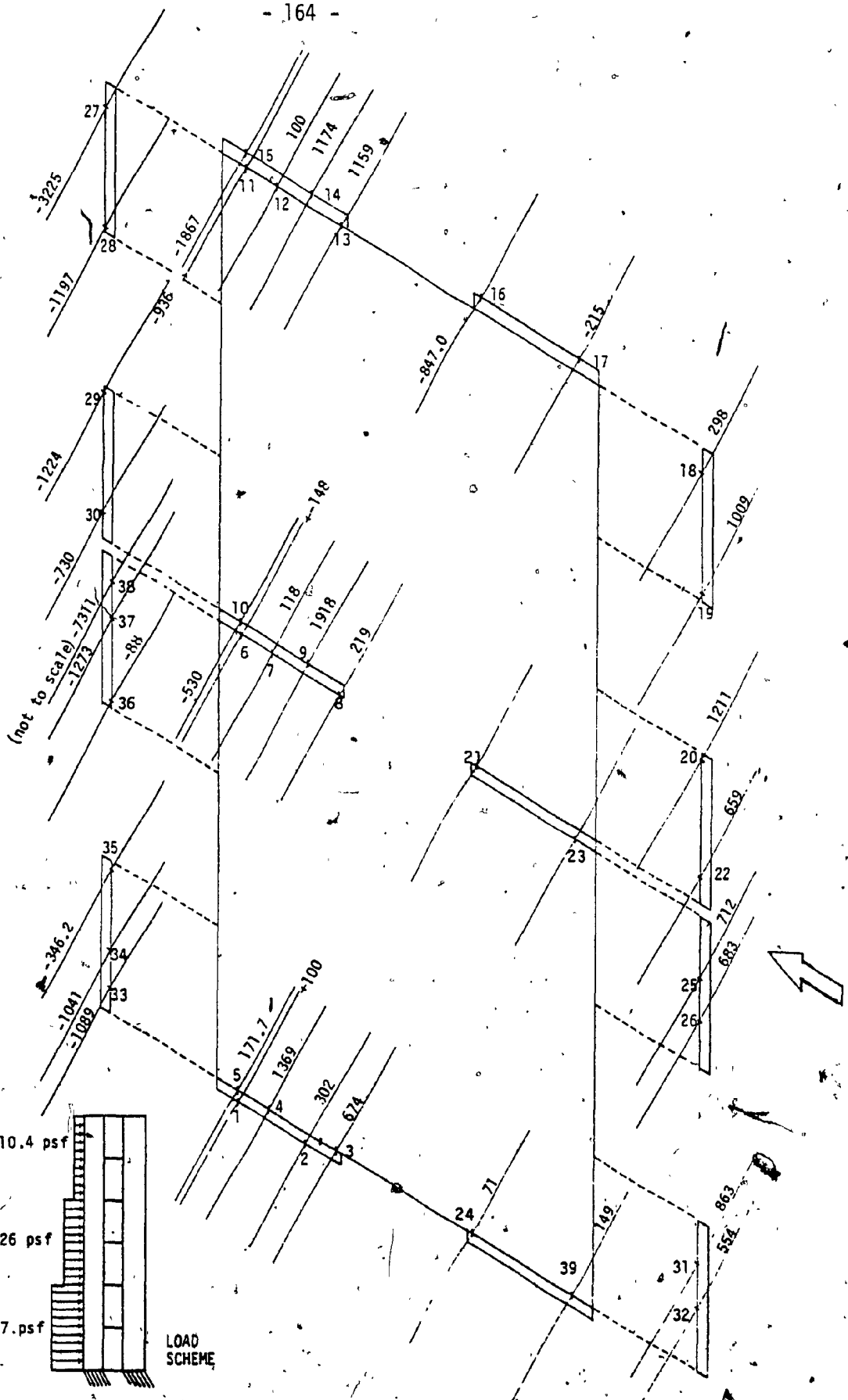

FIG.3.14 - EXPERIMENTAL LONGITUDINAL STRESSES IN PSI
TEST 17-04-T3 (1 psf = 6.9 kN/m²)

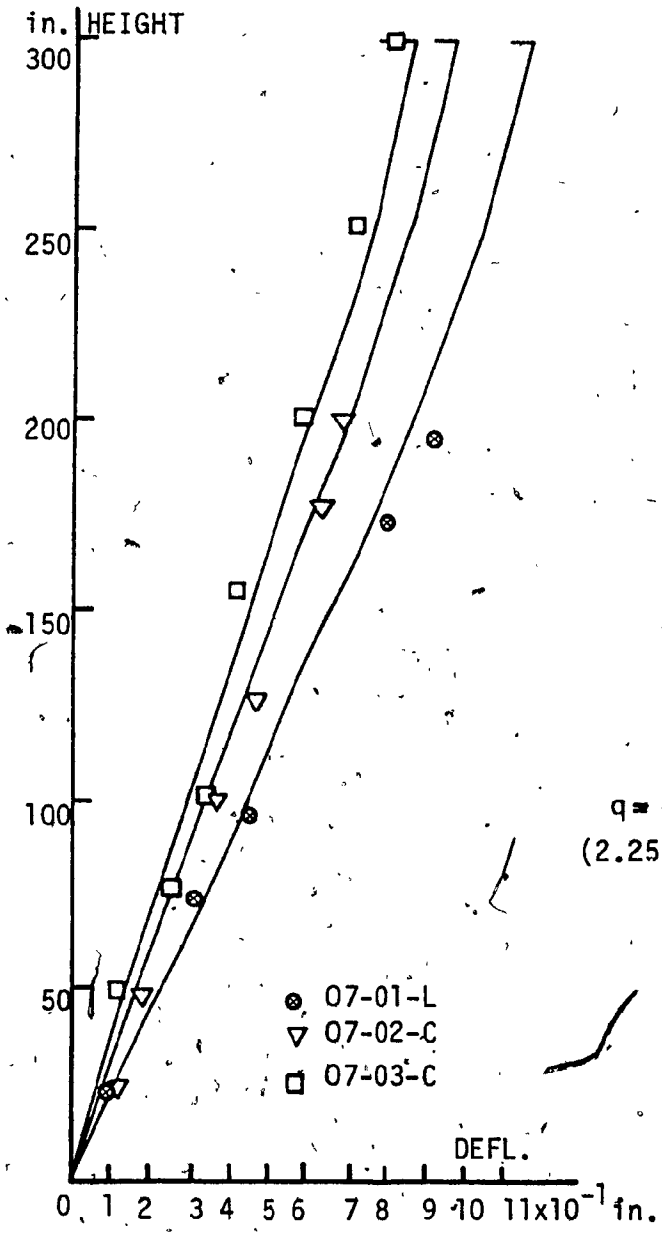

a) LATERAL DEFLECTIONS

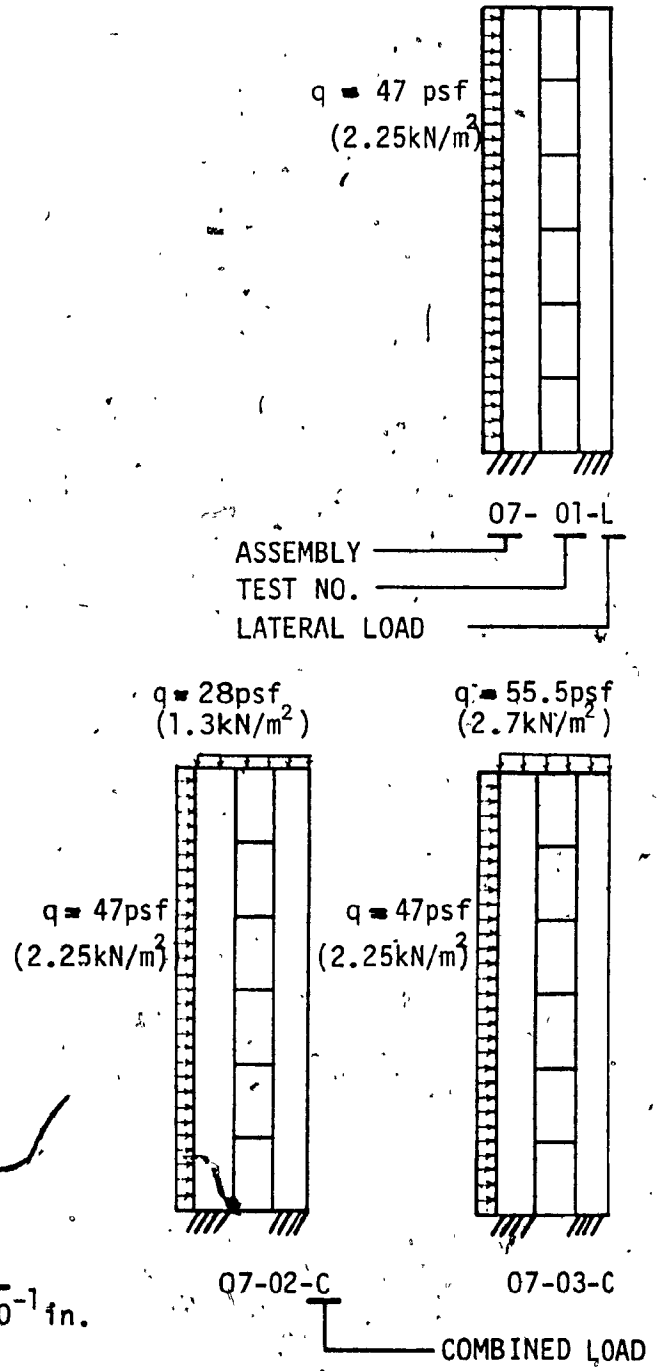

b) LOAD SCHEMES

FIG. 4.1 - REDUCTION OF MODEL LATERAL DEFLECTIONS DUE TO JOINT FRICTION FORCES (1in. 2.54 cm.; 1psf 47.9N/m²)

NOTE : The vertical loads of tests 07-02-C and 07-03-C were applied before the lateral loadings.

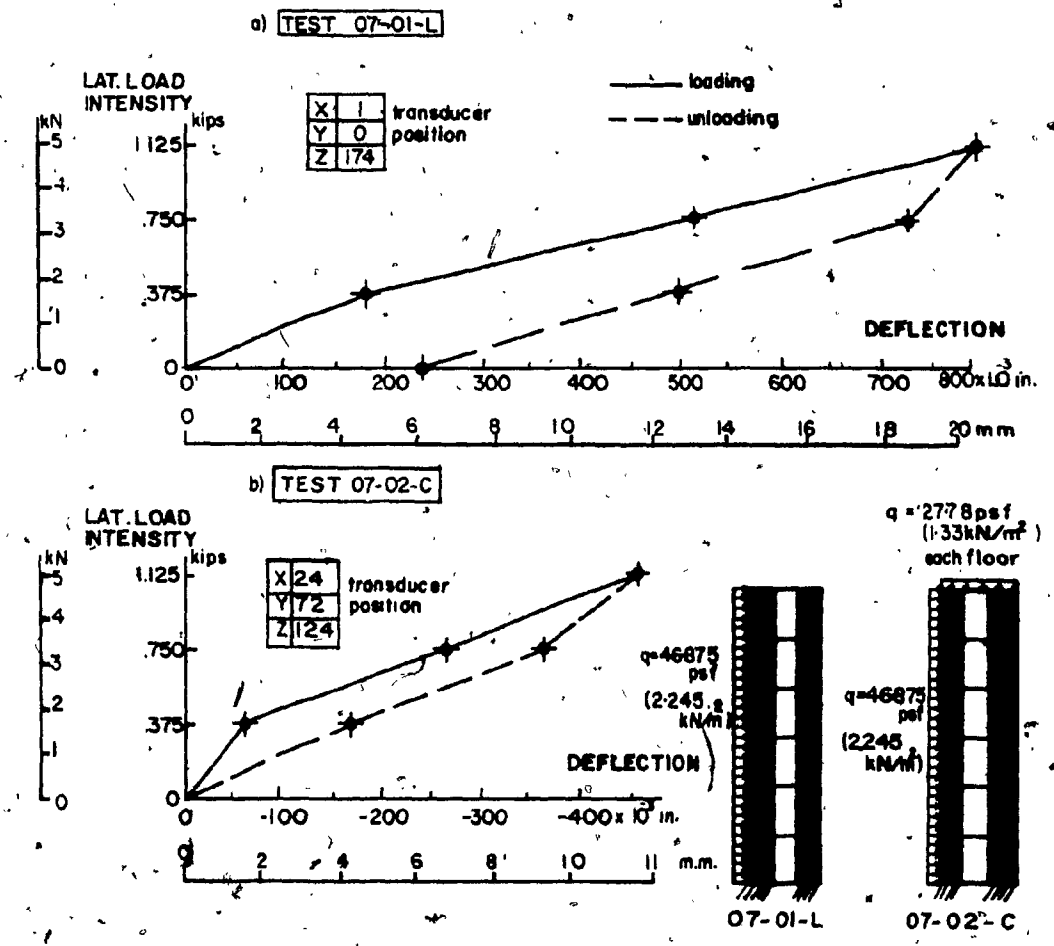

FIG. 4.2 - TYPICAL DEFLECTION HISTORIES

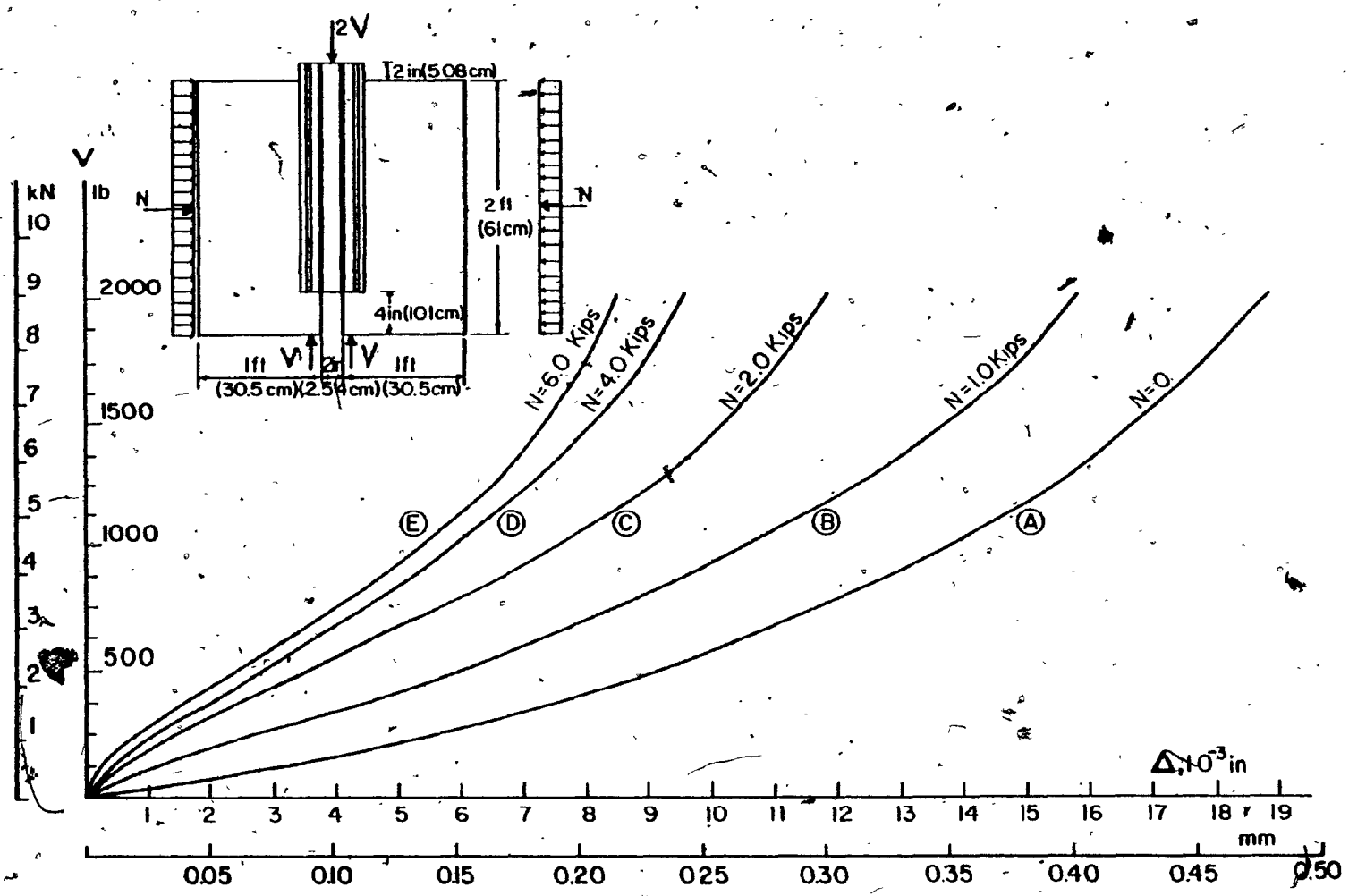

FIG. 4.3 - SHEAR-DISPLACEMENT CURVES OF STAPLED CONNECTION (REF. [20]).

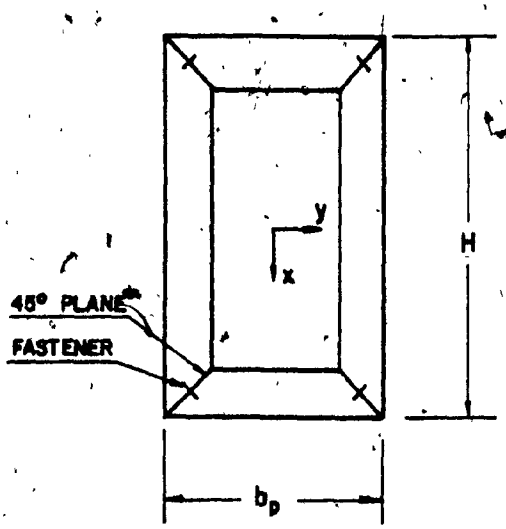

a) TYPICAL FRAMED PANEL.

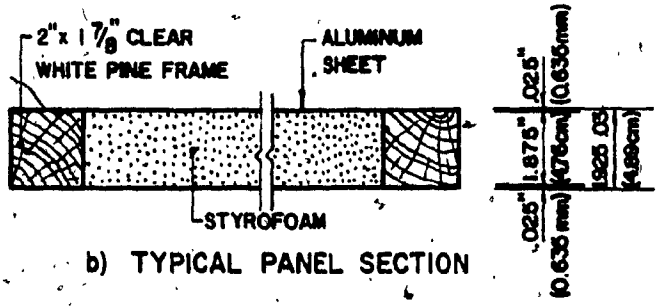

b) TYPICAL PANEL SECTION

FIG. 5.1 - DETAILS OF FRAMED SANDWICH PANELS

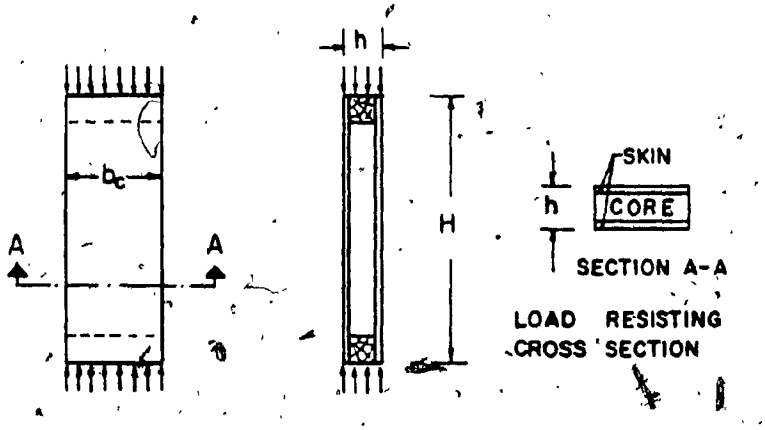

a) FRAMELESS SANDWICH PANELS

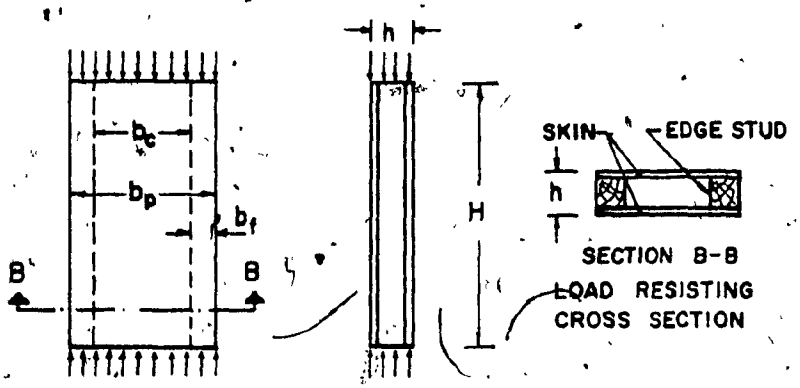

b) EDGE REINFORCED PANELS

FIG. 5.2 - EDGEWISE COMPRESSION TESTS ON PANELS WITH VARIOUS EDGES

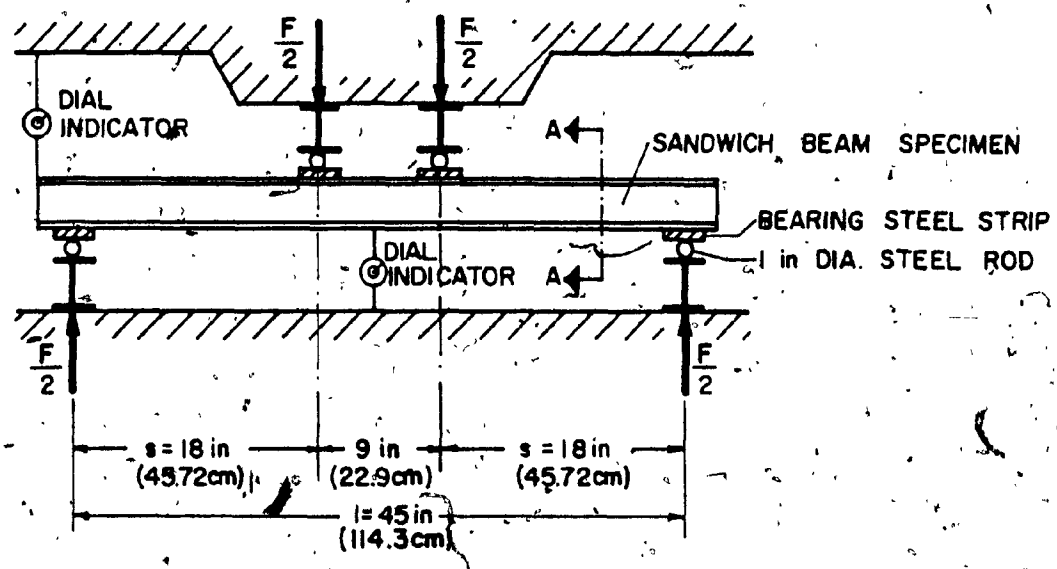

a) FOUR POINTS BENDING TEST SET-UP.

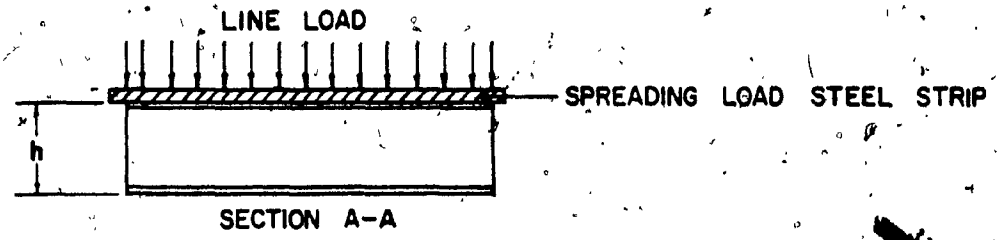

b) FRAMELESS PANEL CROSS SECTION

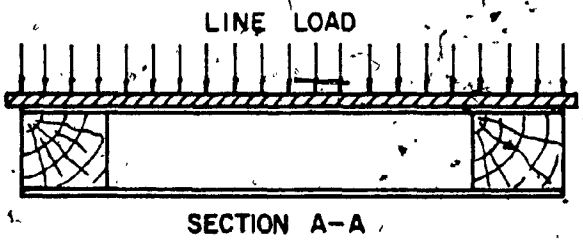

c) REINFORCED EDGE PANEL CROSS SECTION

FIG. 5.3 - BENDING TEST SET-UP

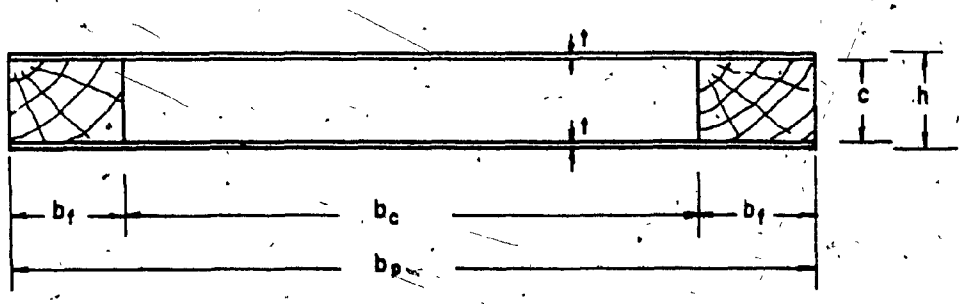

FIG. 5.4 - SANDWICH CROSS SECTION GEOMETRY

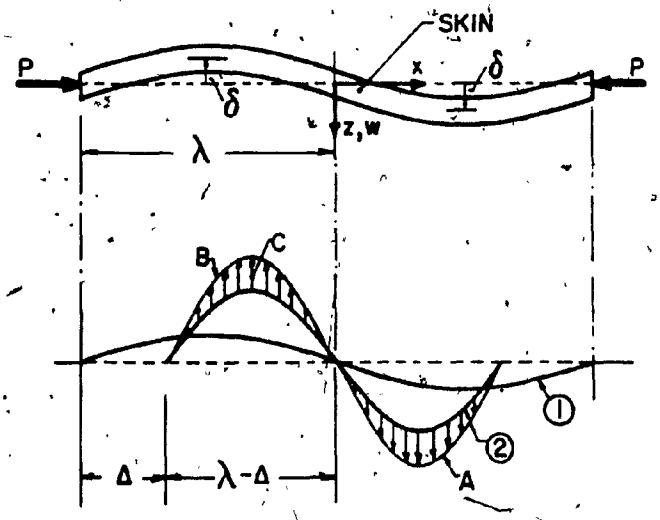

① CORE SURFACE AT WRINKLING
② CORE SURFACE AT POST WRINKLING

FIG. 5.5 - POST-WRINKLING LIMIT STATE. CORE TENSION OR CORE-SKIN BOND FAILURE

a)

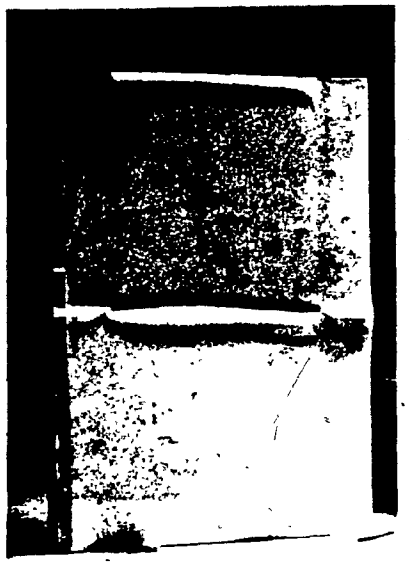

b)

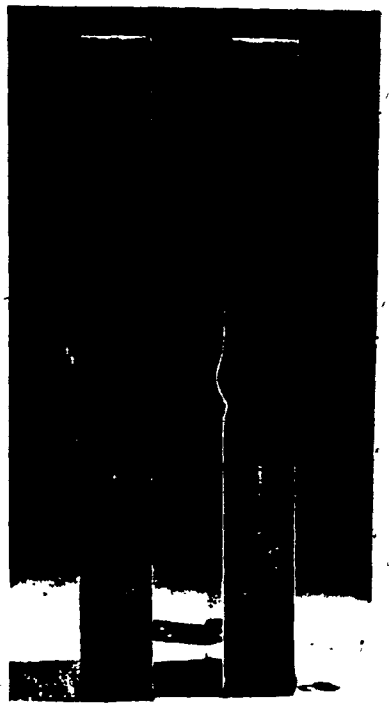

a) PANEL VIEW AFTER TEST

b) SAME PANEL, CUT ALONG MID-WIDTH, SHOWING POST-WRINKLING CORE-SKIN BOND FAILURE

FIG. 5.6 - EDGEWISE COMPRESSION ON EDGE-REINFORCED SANDWICH PANELS

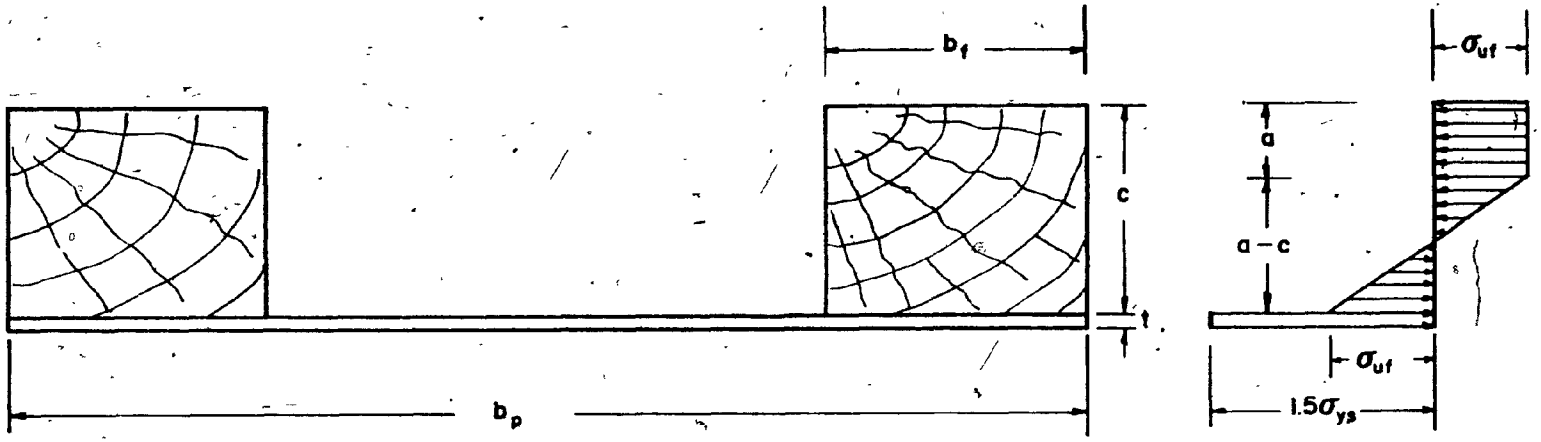

a) LOAD CARRYING CROSS SECTION

b) ULTIMATE BENDING STRESS BLOCK

FIG. 5.7 - EDGE-REINFORCED BEAM PANEL AT ULTIMATE BENDING MOMENT

a) Compression face at post-wrinkling stage

b) Tension face at ultimate stage

FIG. 5.8 - BENDING OF REINFORCED EDGE PANELS

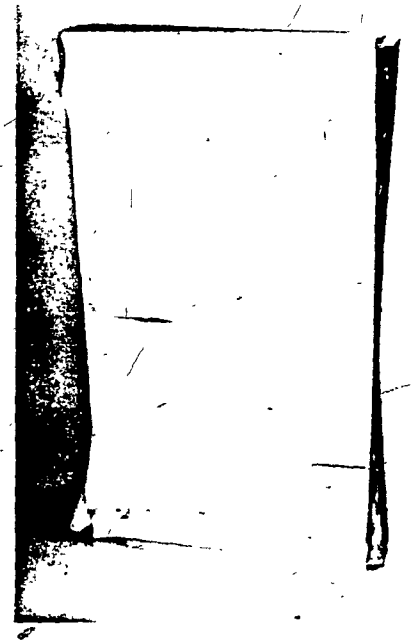

FIG. 5.9 - FAILURE MODE OF A PANEL WITH CLOSED EDGE FRAME, UNDER EDGEWISE COMPRESSION. STUD COMPRESSION-BENDING FAILURE.

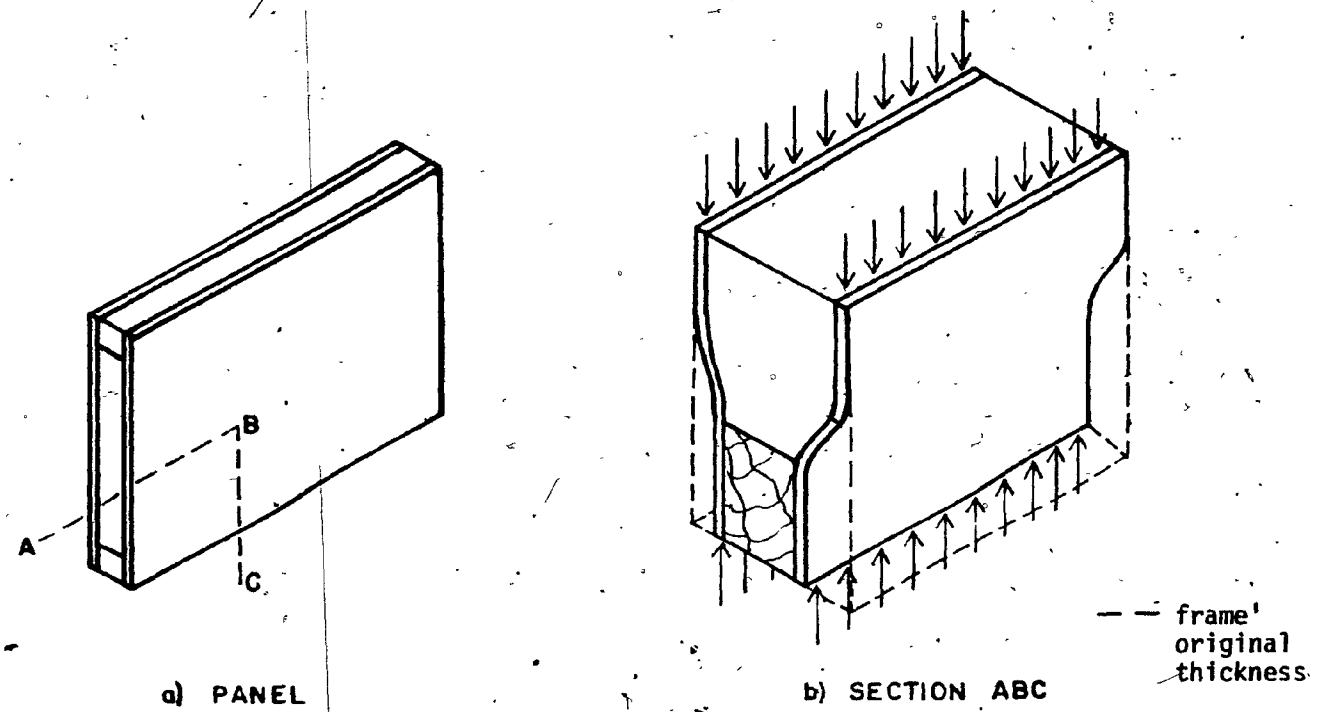

FIG. 5.10 - TRANSVERSE SHRINKAGE OF WOOD EDGE FRAME

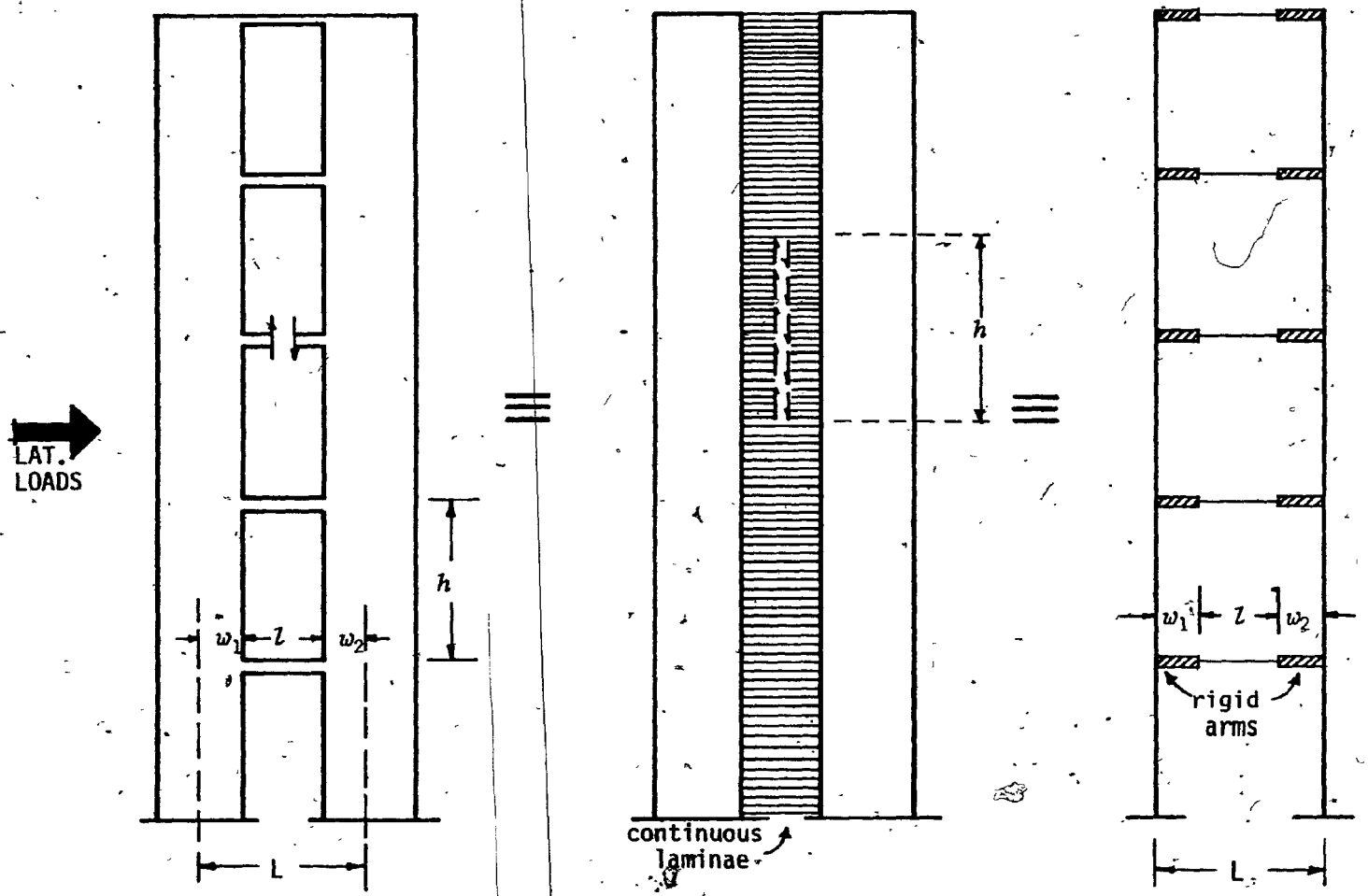

a) TRUE STRUCTURE

b) EQUIVALENT CONTINUOUS METHOD

c) EQUIVALENT FRAME METHOD

FIG. 6.1 - METHODS OF ANALYSIS OF SHEAR-WALL STRUCTURES

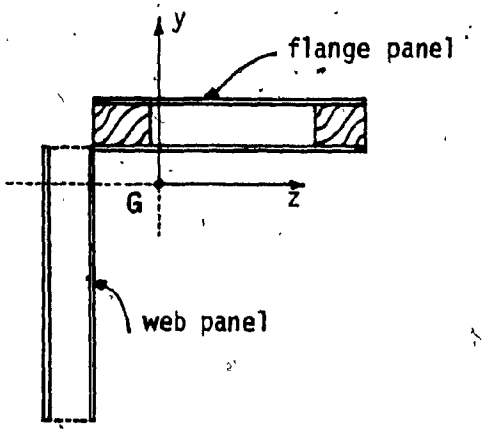

a) CORNER FLANGED SHEAR WALLS

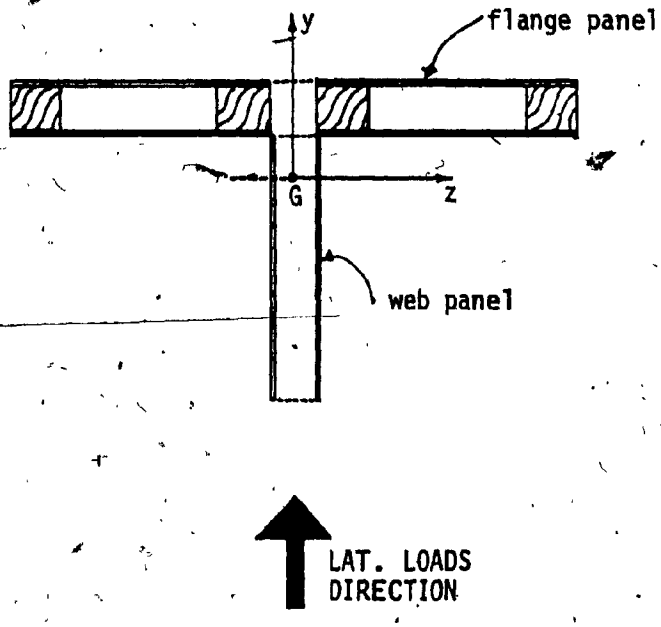

b) CENTRAL FLANGED SHEAR WALL

FIG. 6.2 - COMPOSITE SHEAR SANDWICH WALLS

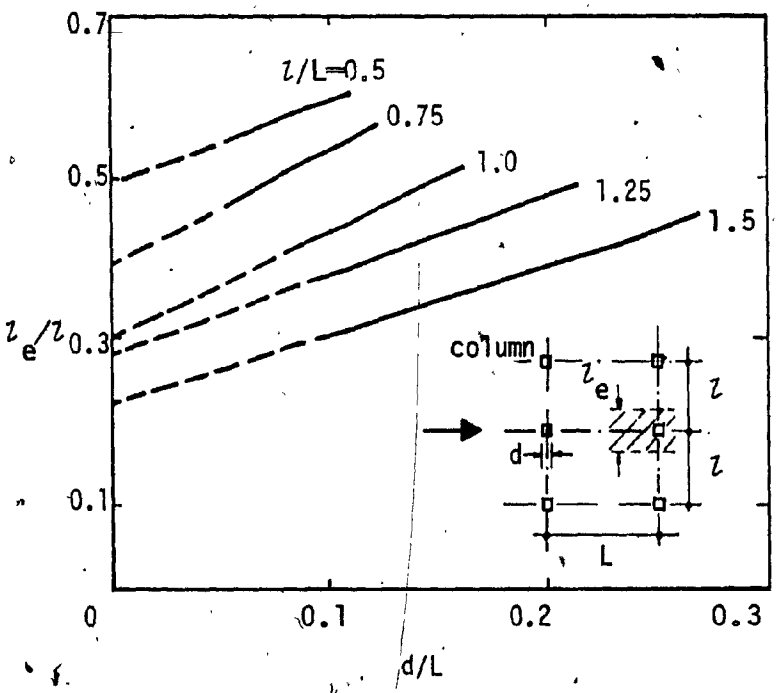

FIG. 6.3 - EFFECTIVE WIDTH OF SLAB IN FLAT-SLAB STRUCTURES (FROM REF.[40])

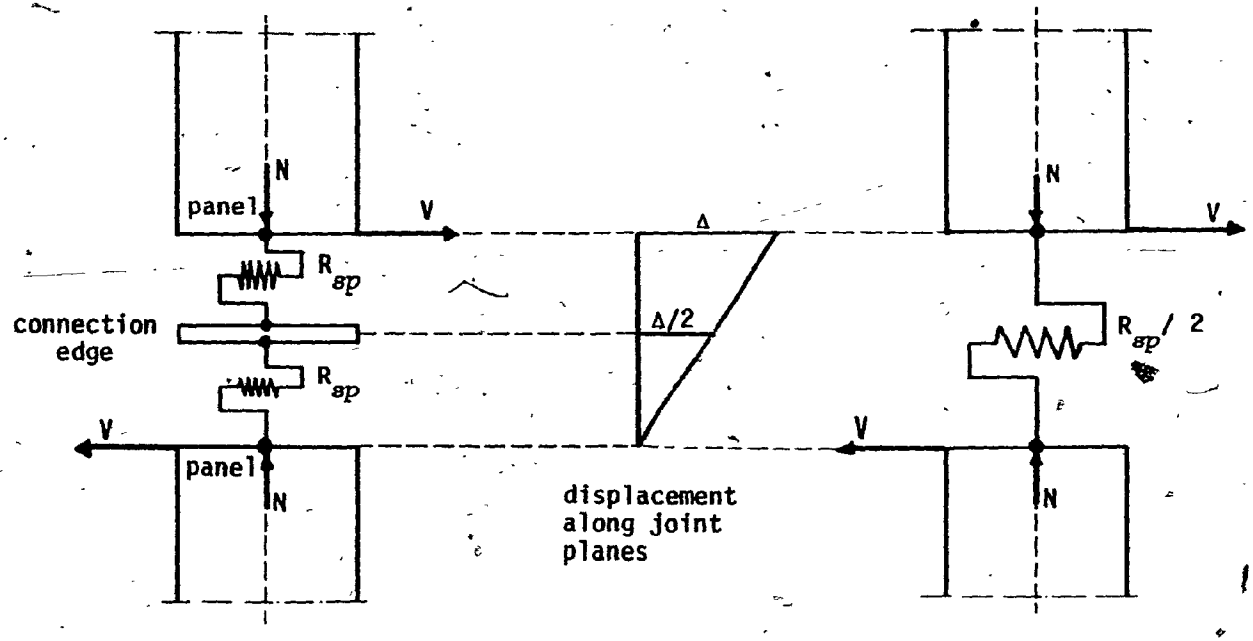

a) TRUE

b) EQUIVALENT

FIG. 6.4 - IDEALIZATION OF SPRINGS EQUIVALENT TO STAPLED JOINTS

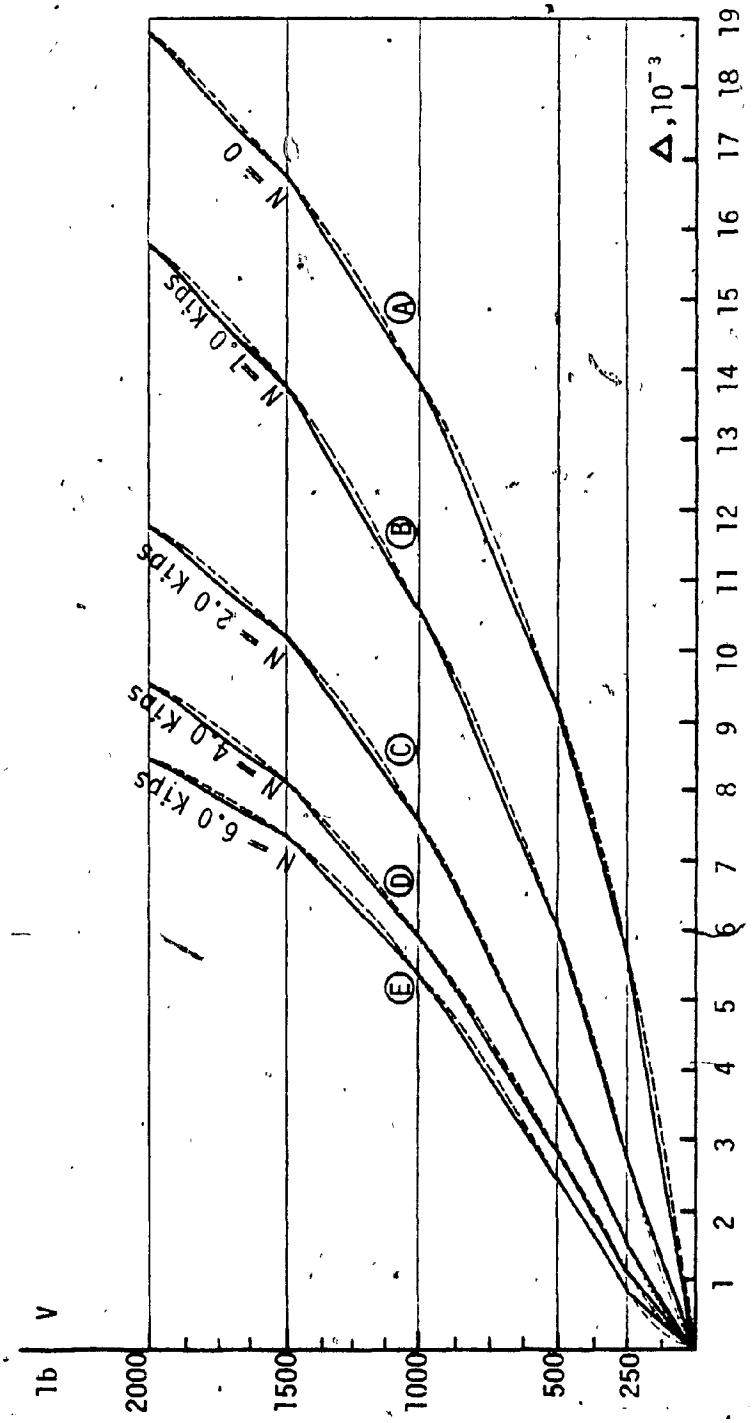

FIG. 6.5 - IDEALIZED STEPWISE SHEAR-DISPLACEMENT CURVES OF EQUIVALENT SPRINGS

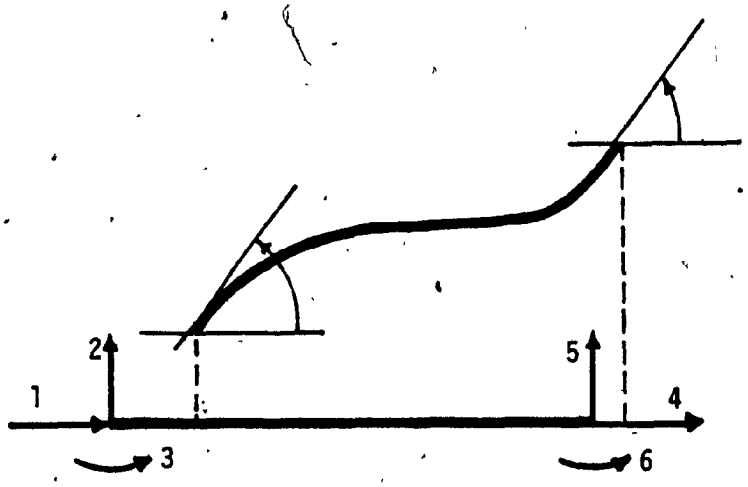

a) SLENDER 6 - D.O.F. MEMBER

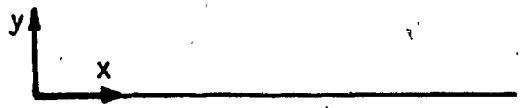

b) MEMBER AXES

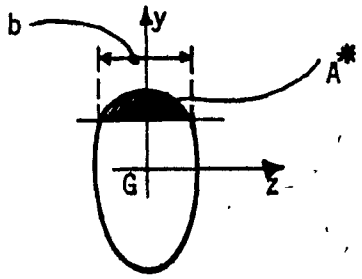

c) CROSS SECTION AXES

FIG. 6.6 - MEMBER END DISPLACEMENTS AND FORCES.
POSITIVE DIRECTIONS OF LOCAL AXES.

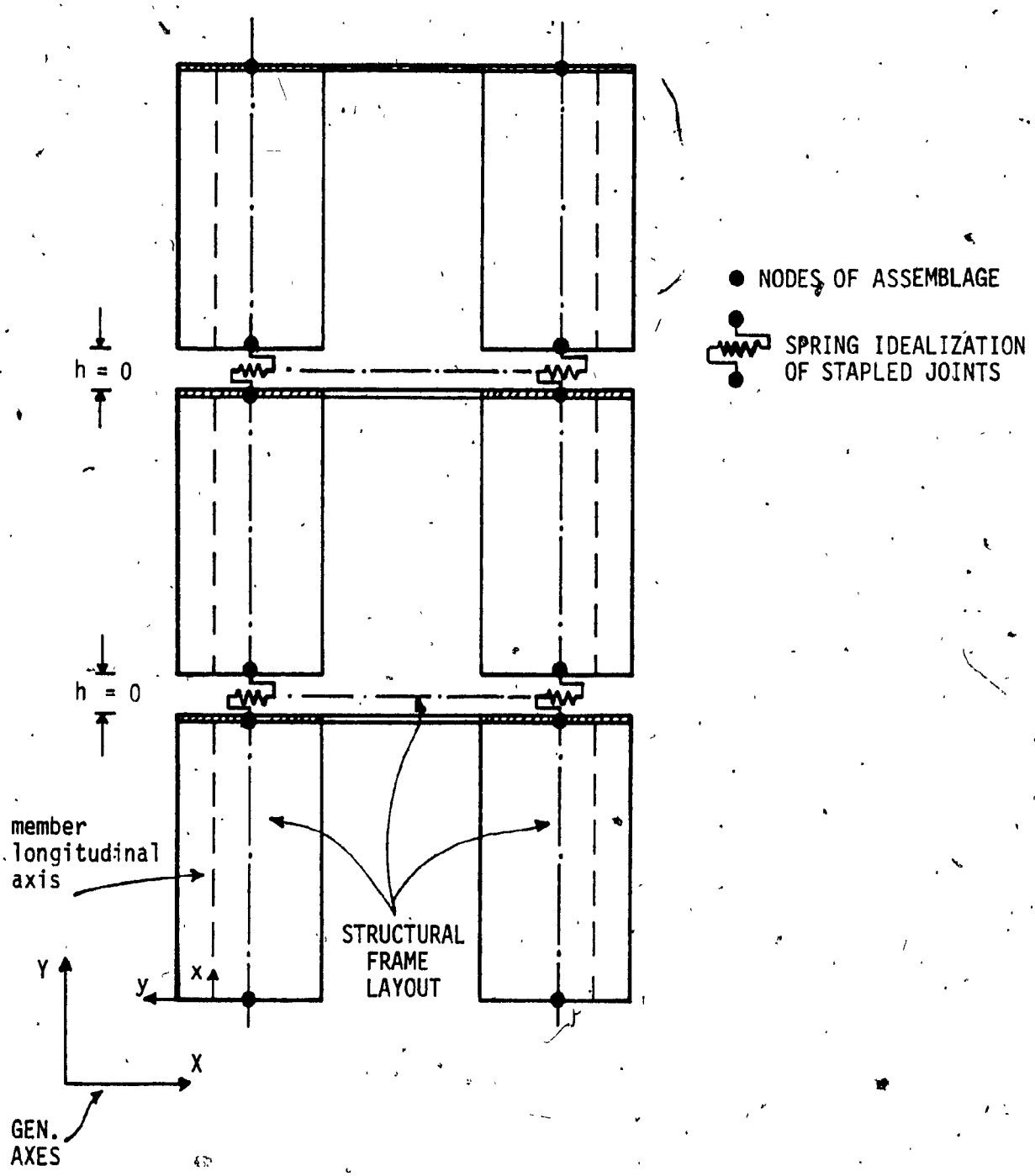

FIG. 6.7 - STRUCTURAL IDEALIZATION

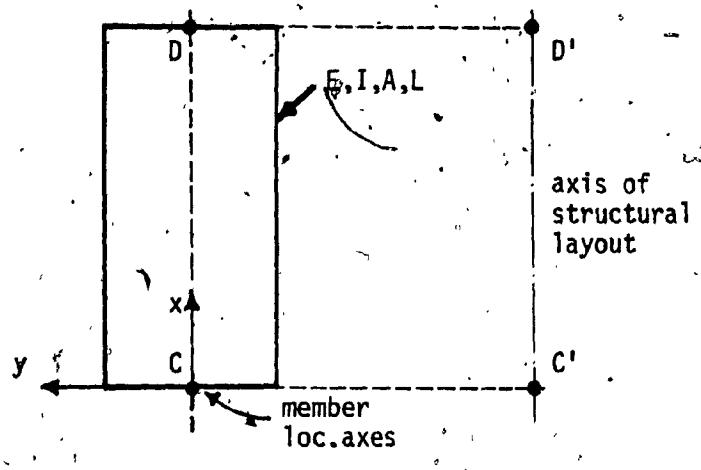

a) LINEAR TRANSFORMATION FOR PARALLEL AXES

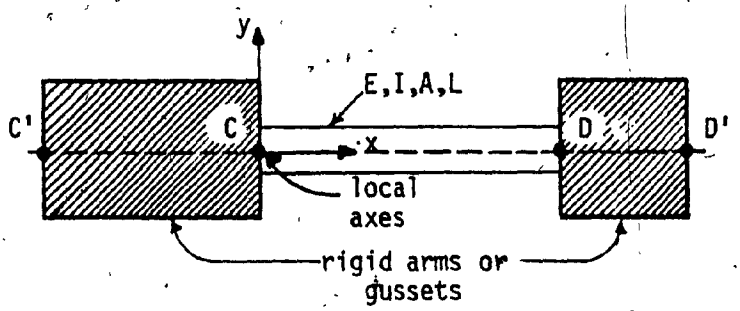

b) LINEAR TRANSFORMATION FOR GUSSETS

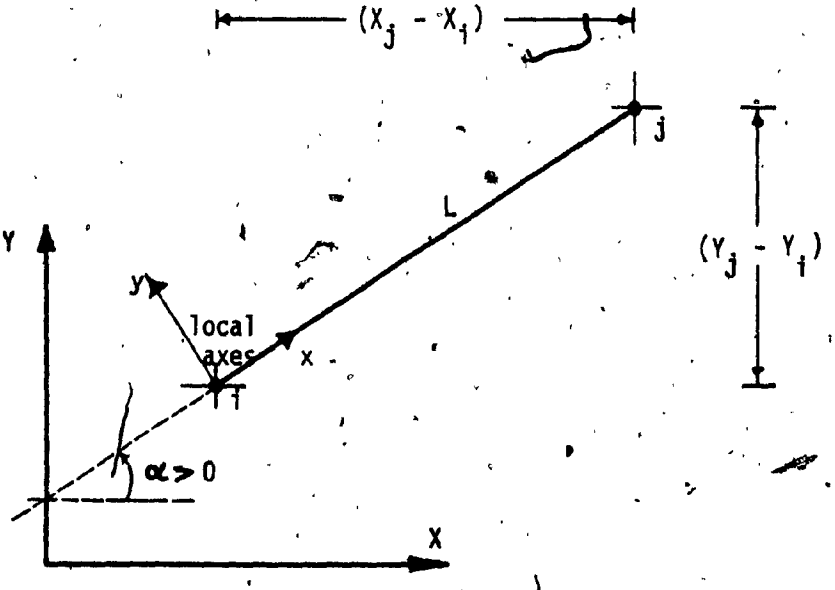

c) AXES ROTATION

FIG. 6.8 - CASES OF LINEAR TRANSFORMATION

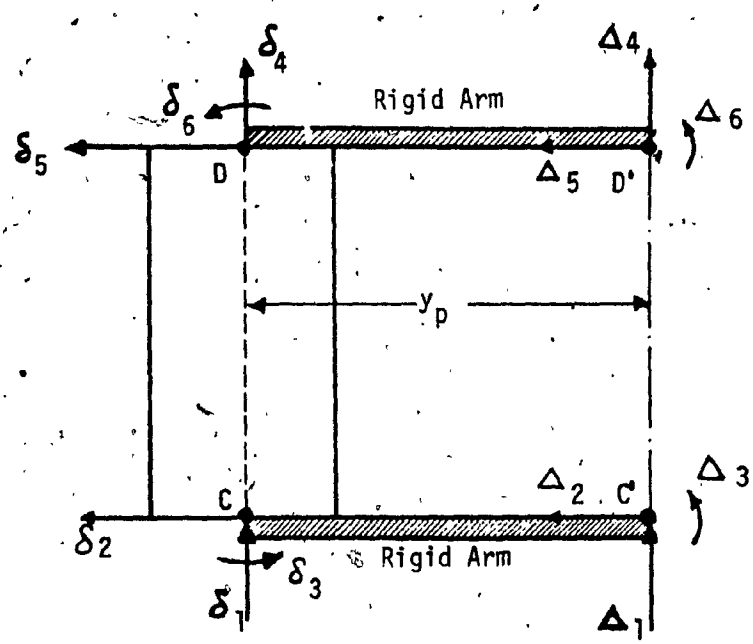

a.) PARALLEL AXES.

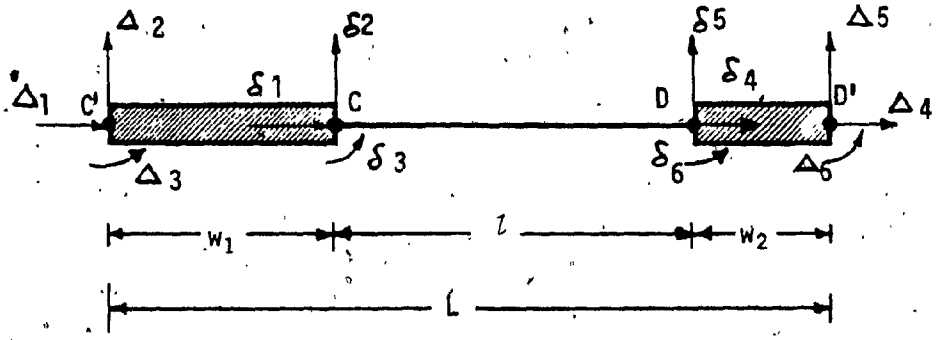

b) WIDE-COLUMN EQUIVALENT BEAM.

FIG. 6.9 -SIGN AND NUMBERING CONVENTIONS FOR DISPLACEMENTS

(δ local member displacements, Δ transformed displacements)

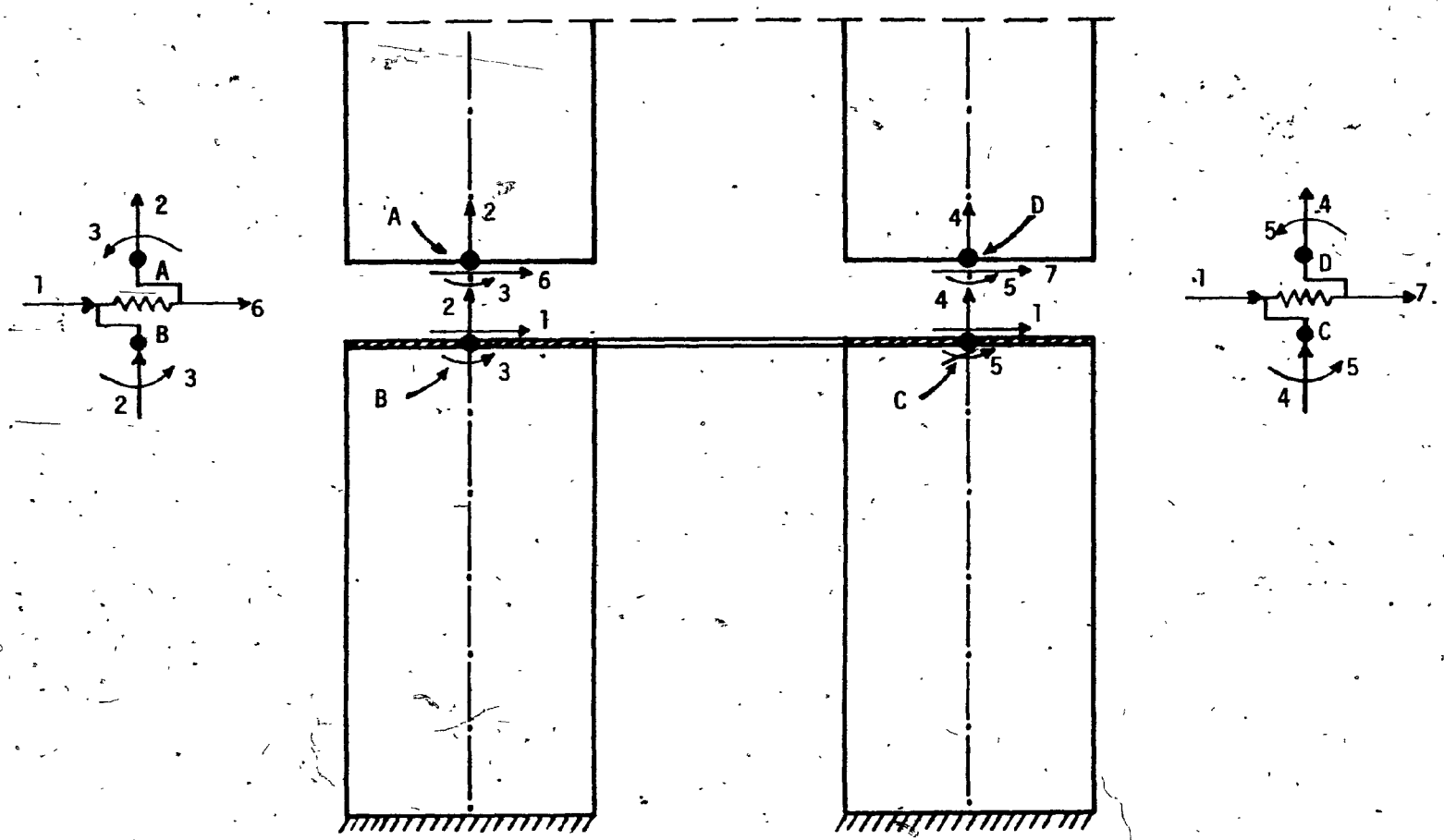

FIG. 6.10 - NUMBERING OF NODAL DISPLACEMENTS IN THE FIRST FLOOR ASSEMBLY

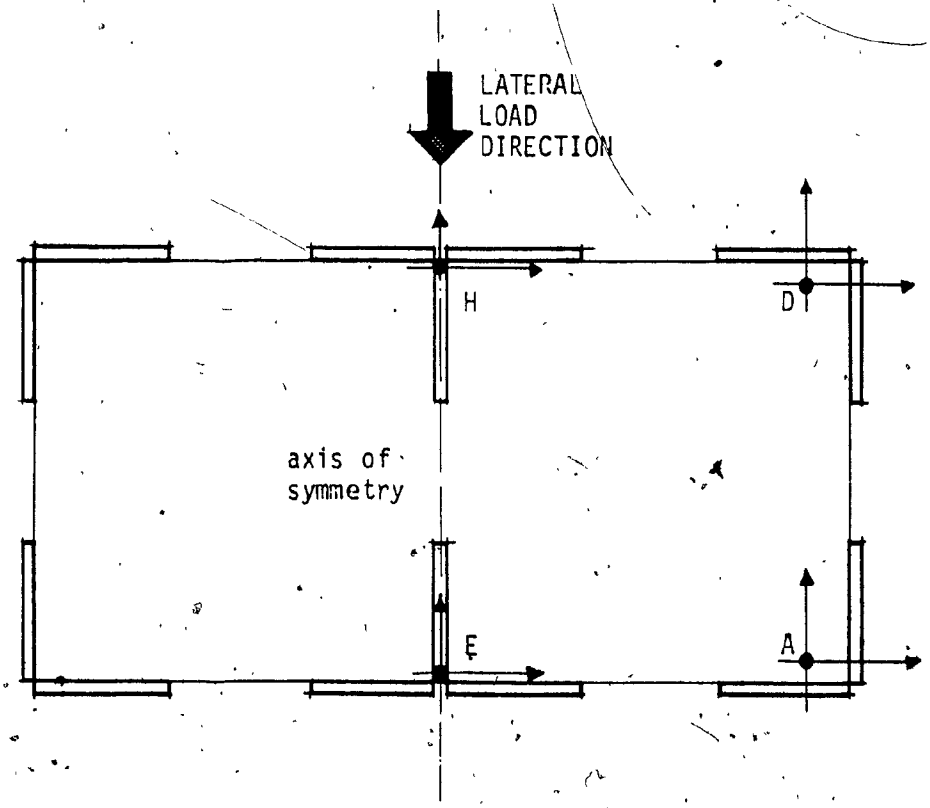

Note : The coupled shear-walls EH and AD are both lumped on the same structural frame lay-out, Fig. 6.7. The distance y_p is evaluated with respect to member axes.

FIG. 6.11 - STRUCTURAL SYMMETRY

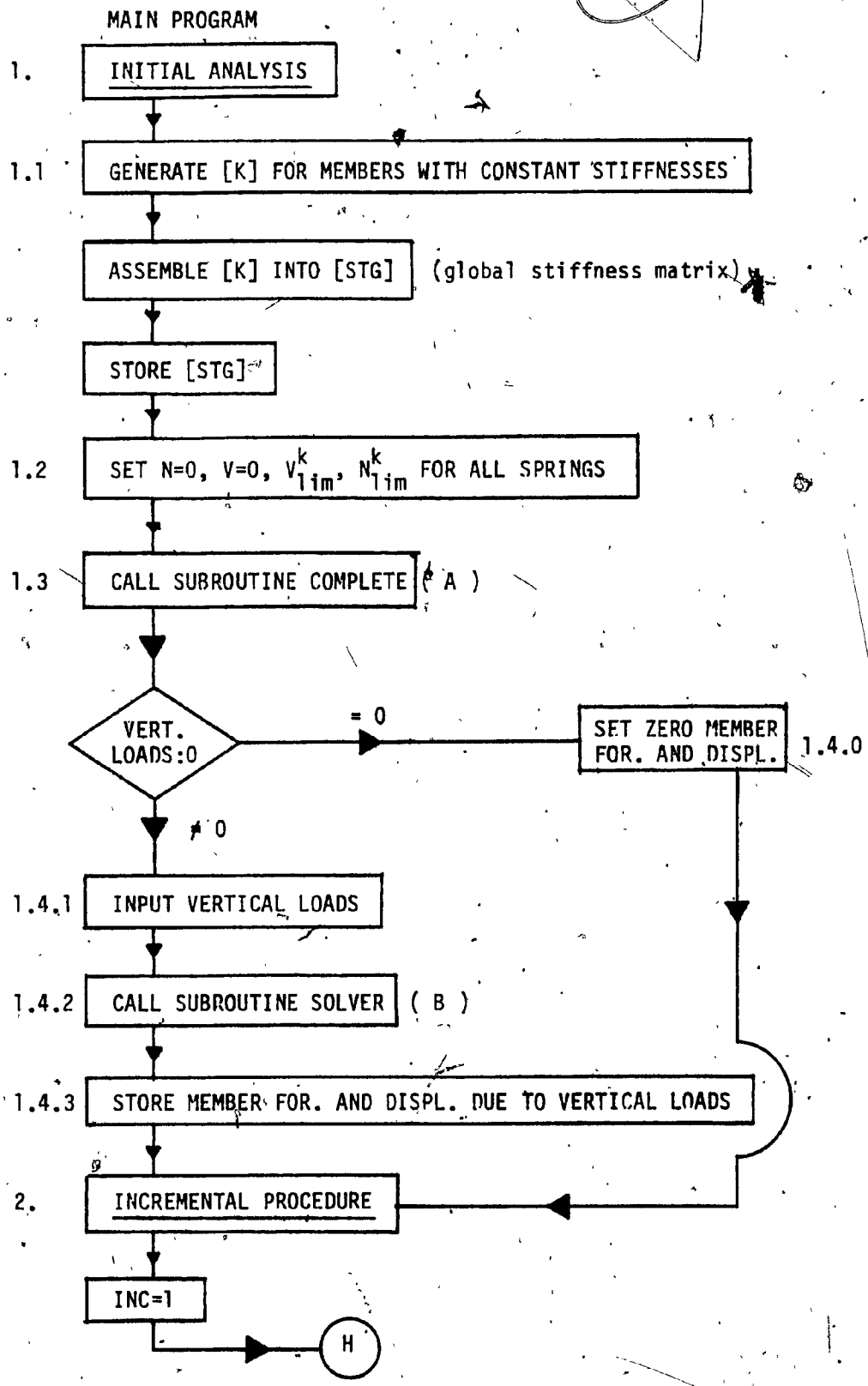

FIG. 6.12 - FLOW CHART OF NONLINEAR ANALYSIS

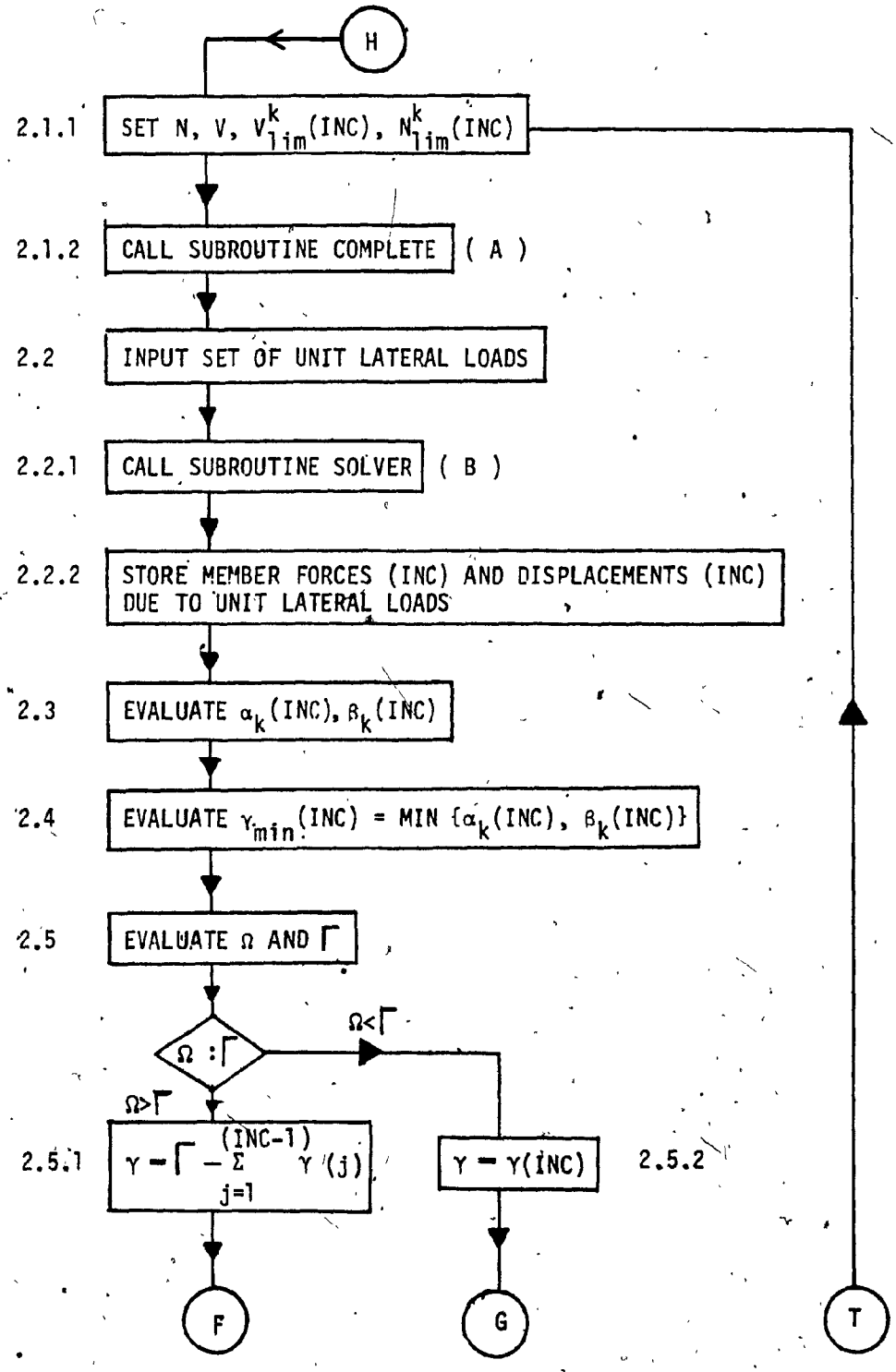

FIG. 6.12 - continued

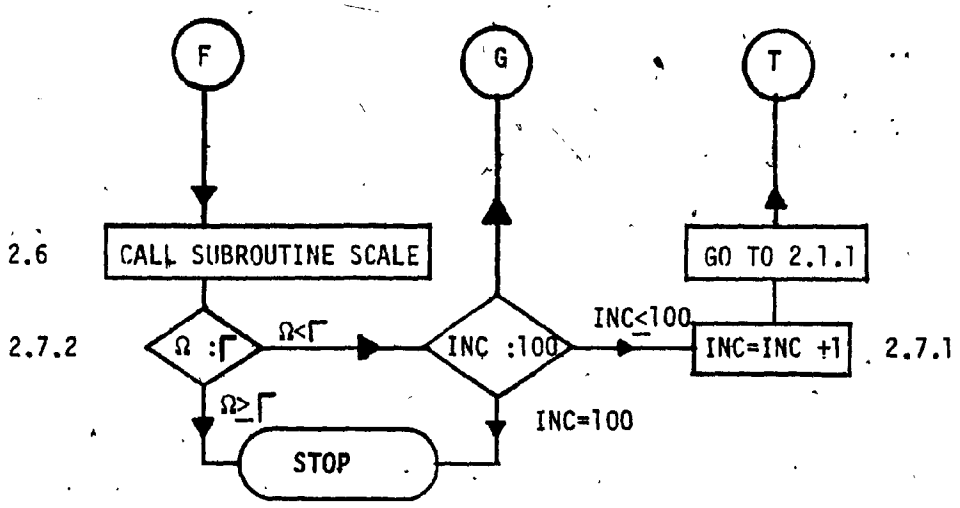

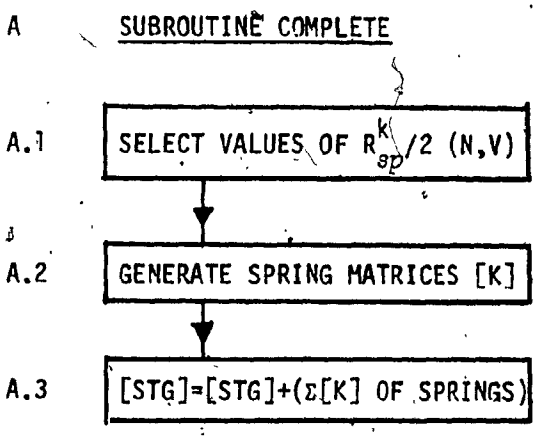

FIG. 6.12 - continued

B SUBROUTINE SOLVER

B.1 SOLVE SYSTEM OF LINEAR EQUATIONS

C SUBROUTINE SCALE

C.1 MULTIPLY RESULT OF STEP 2.2.2 BY γ

C.2 ACCUMULATE PREVIOUS AND CURRENT STEP RESULTS

C.3 STORE NEW ACCUMULATED VALUES

FIG. 6.12 - continued

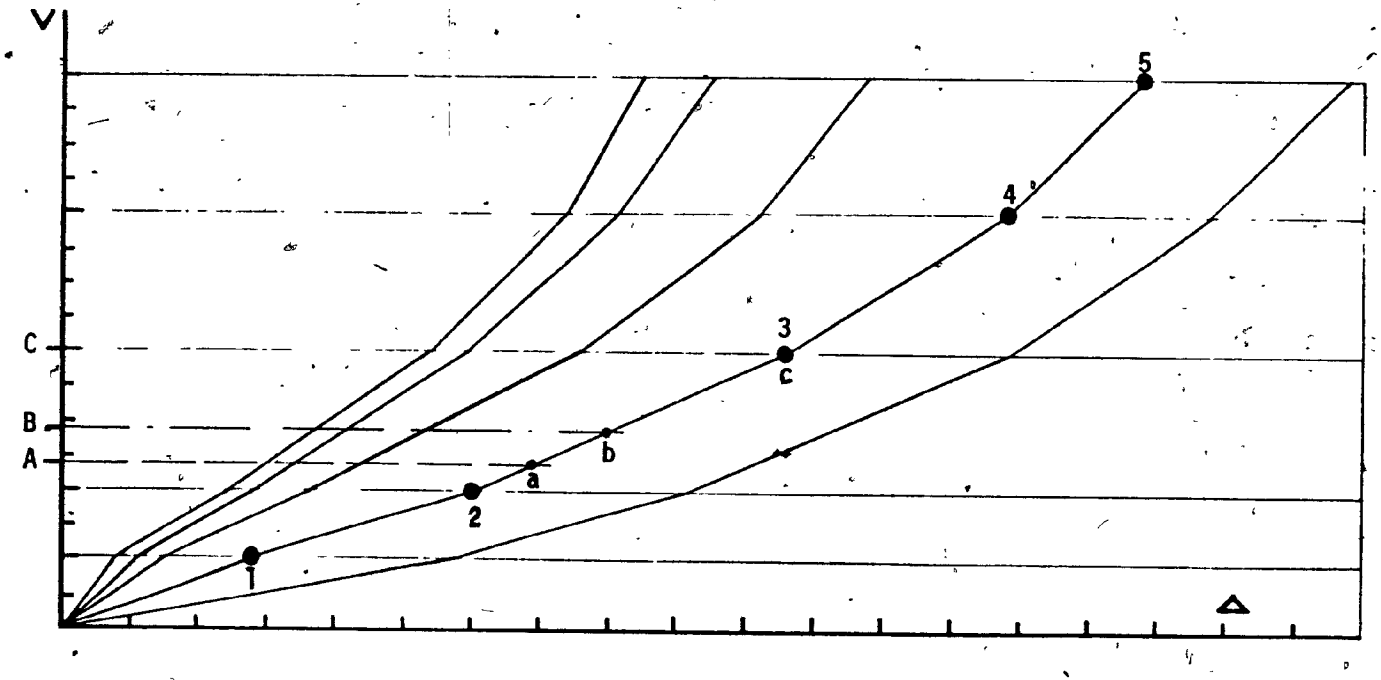

$V_A = V^k_{acc}(INC-1)$

$V_C = V^k_{lim}$

$V_B - V_A = \Delta V^k_{unit}(INC)$

$$\alpha_k(INC) = \frac{\overline{CA}}{\overline{BA}} = \frac{\overline{ca}}{\overline{ba}} = \frac{V^k_{lim} - V^k_{acc}(INC-1)}{\Delta V^k_{lim}(INC)}$$

FIG. 6.13 - GEOMETRIC REPRESENTATION OF α_k

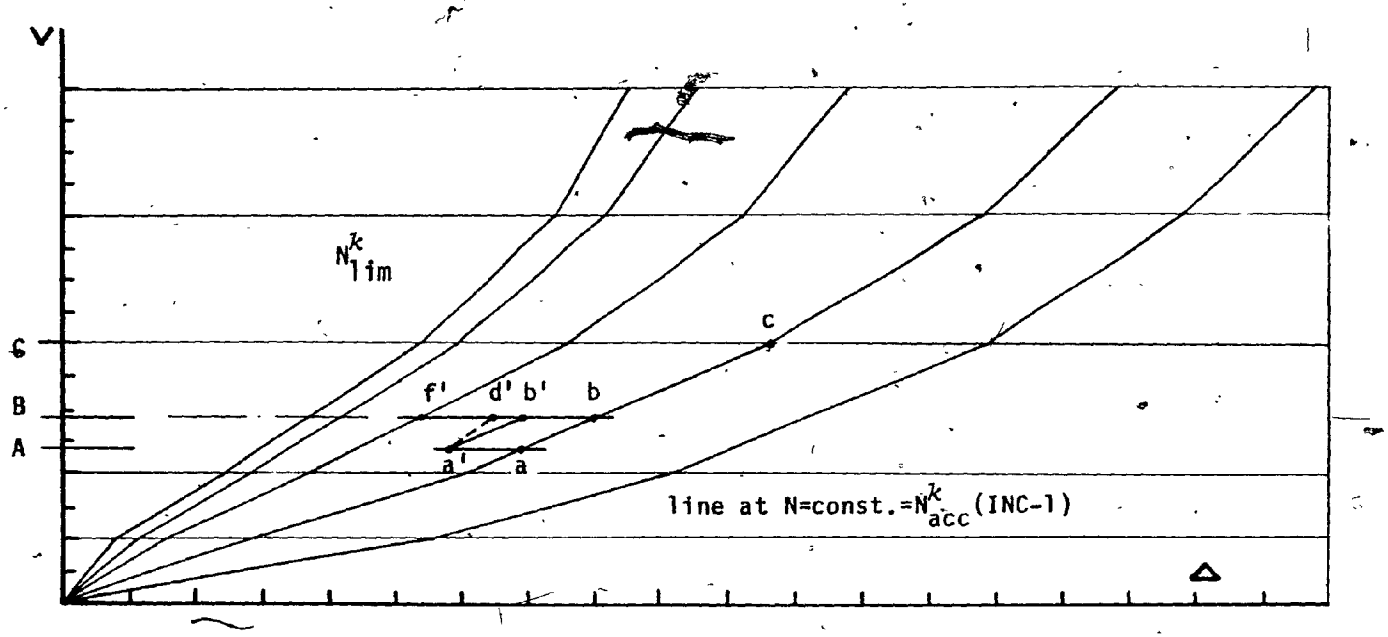

Note: During the increment (INC) from a to b , the increment $\overline{b'd'}$ of axial force ΔN^k_{unit} corresponds to the increment of shear force ΔV^k_{unit} ($\overline{a'b'}$). Let us assume the increment of shear force ($\overline{ab}=\overline{a'b'}$) is first developed along the curve $N=N_{acc}(INC-1)$; or along $\overline{a'b'}$ parallel to $\overline{ab}$, and then the $\Delta N^k_{unit} = \overline{b'd'}$ is developed along $\overline{b'f'}$ or $V'=const=V^k_{acc}(INC-1) + \Delta V^k_{unit}$. Thus

$$\beta(INC)=\frac{\overline{b'f'}}{\overline{b'd'}}=\frac{N^k_{lim} - N^k_{acc}(INC-1)}{\Delta N^k_{unit}(INC)}$$

FIG. 6.14 - GEOMETRIC REPRESENTATION OF β_k

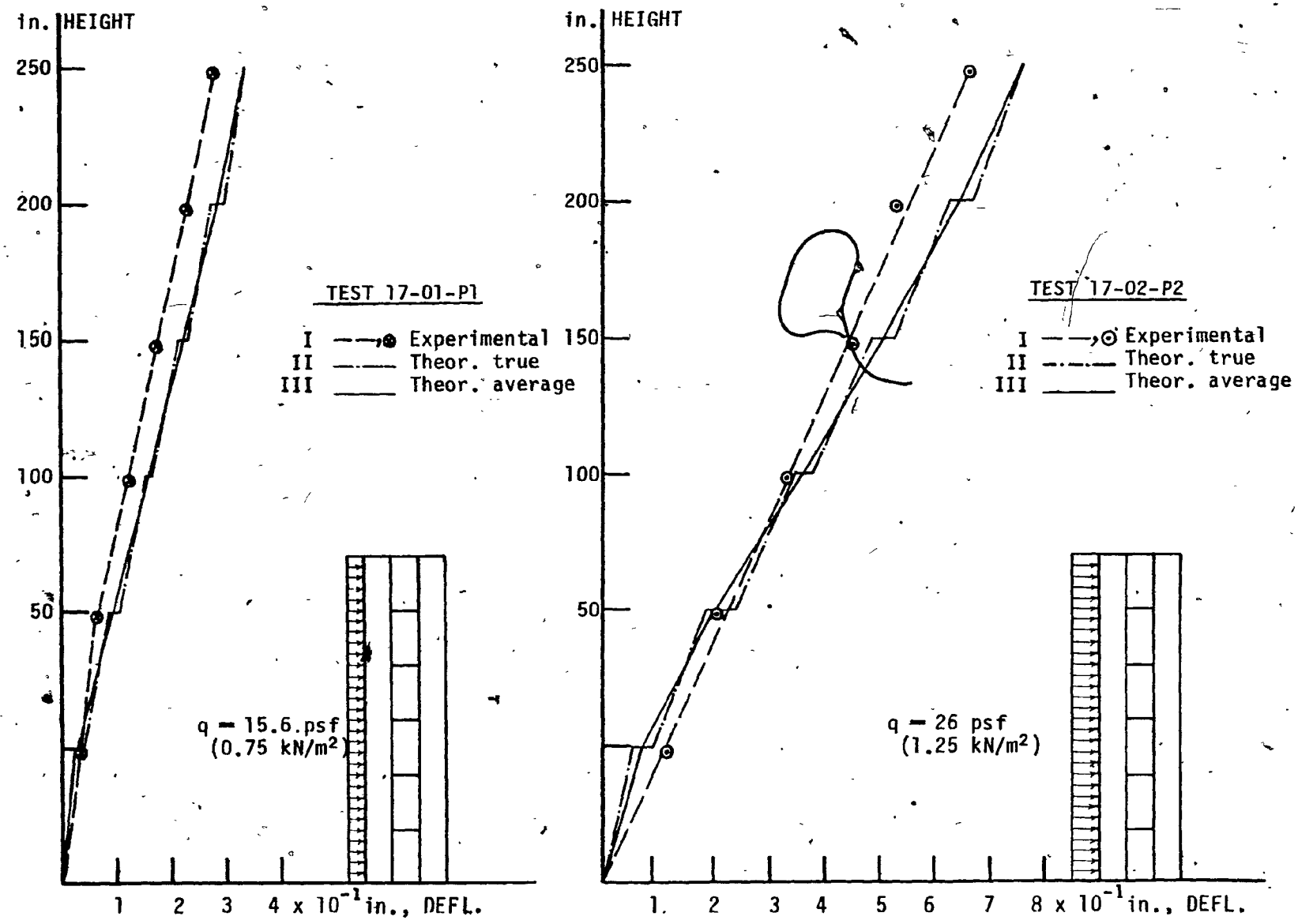

FIG. 7.1 - COMPARISON OF THEORETICAL AND EXPERIMENTAL MODEL DEFLECTIONS TESTS 17-01-P2 AND 17-02-P2

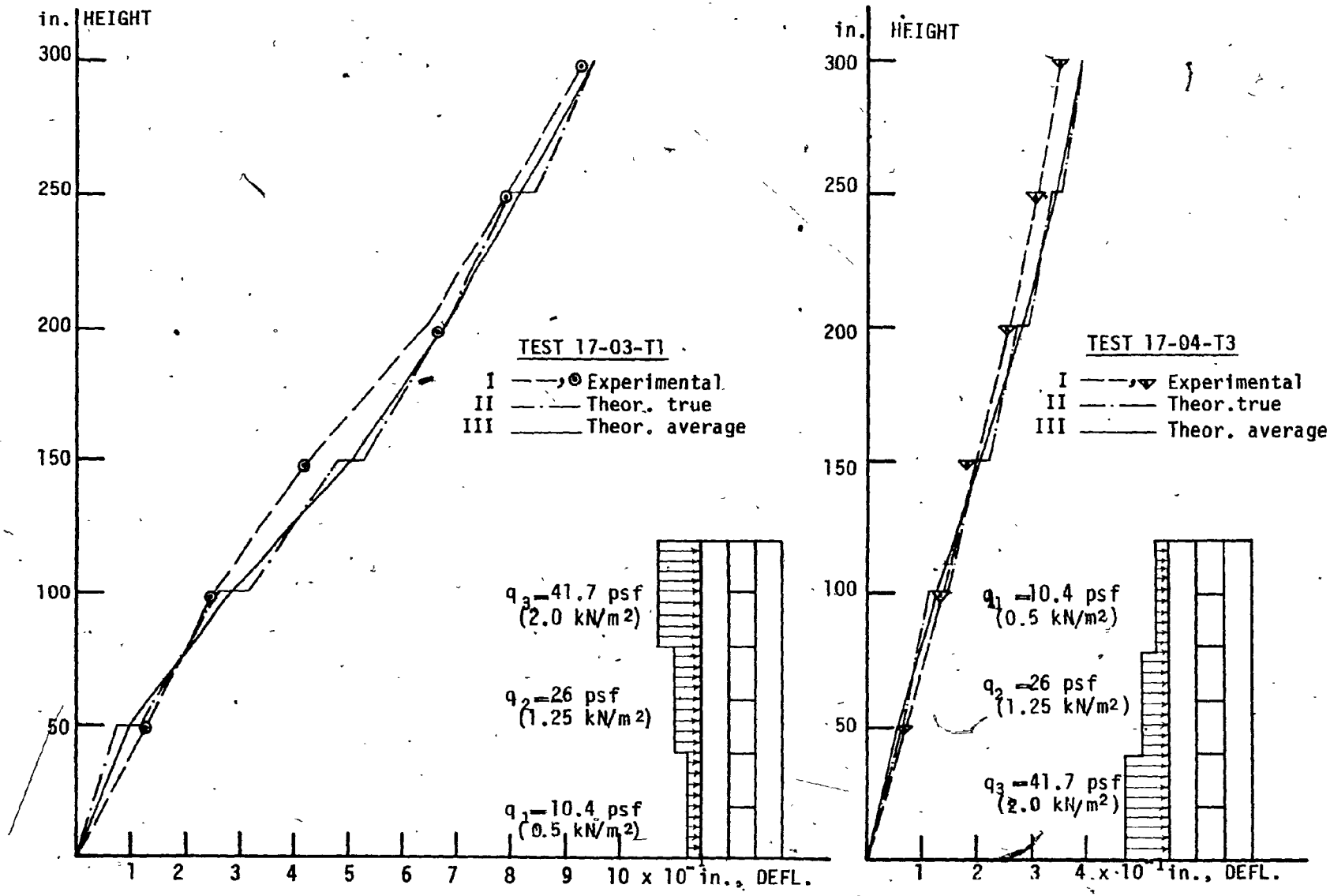

FIG. 7.2 - COMPARISON OF THEORETICAL AND EXPERIMENTAL MODEL DEFLECTIONS TESTS 17-03-T1 AND 17-04-T3

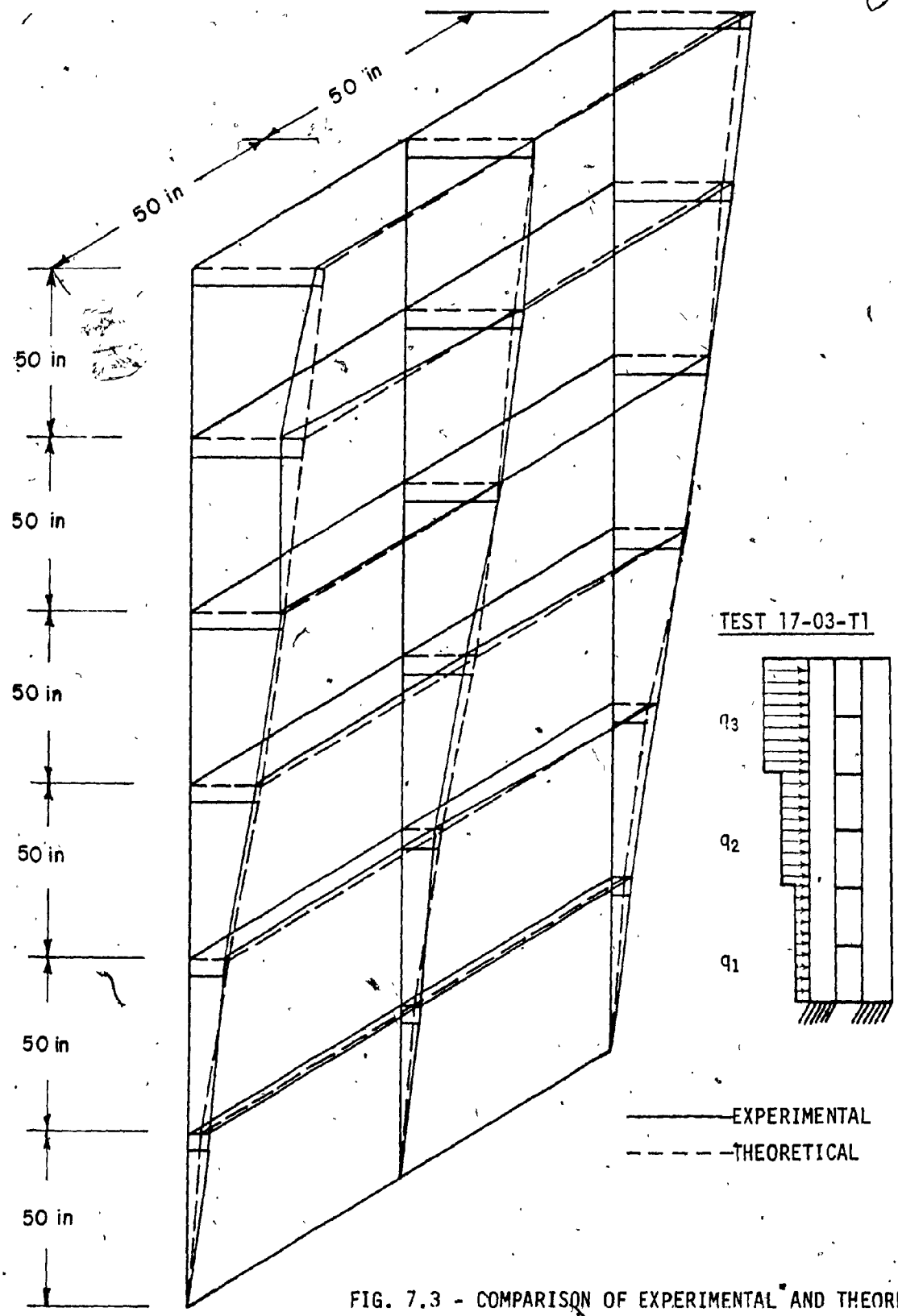

FIG. 7.3 - COMPARISON OF EXPERIMENTAL AND THEORETICAL DEFLECTIONS. 3-DIMENSIONAL PLOT.
(see also Fig. 7.2 and Table 7.1)

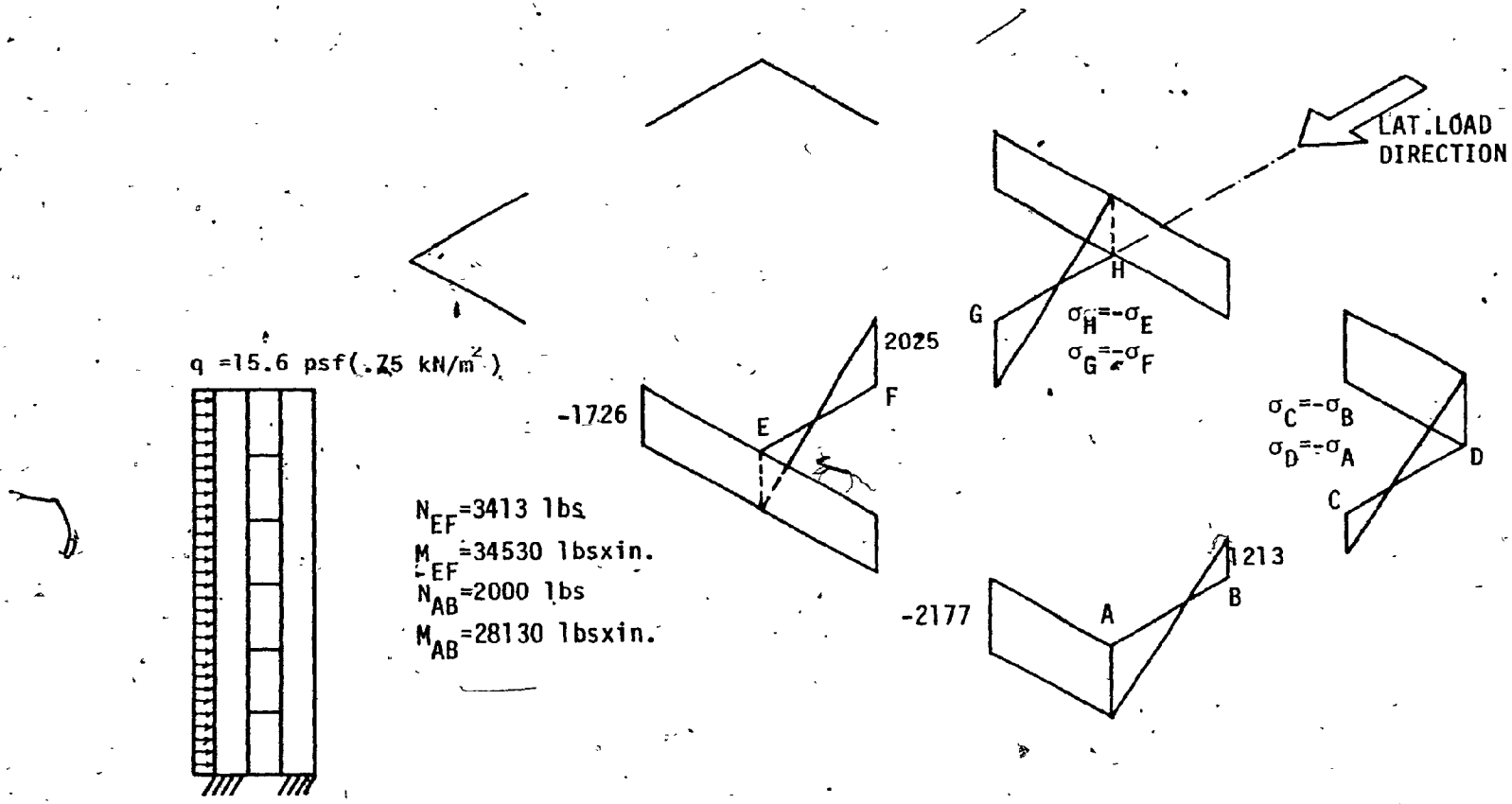

FIG. 7.4 - THEORETICAL NORMAL STRESSES IN PSI AT FOUNDATION LEVEL AND AT MAXIMUM LOAD INTENSITY - TEST 17-01-P1 (1 psi=6.9kN/m²)

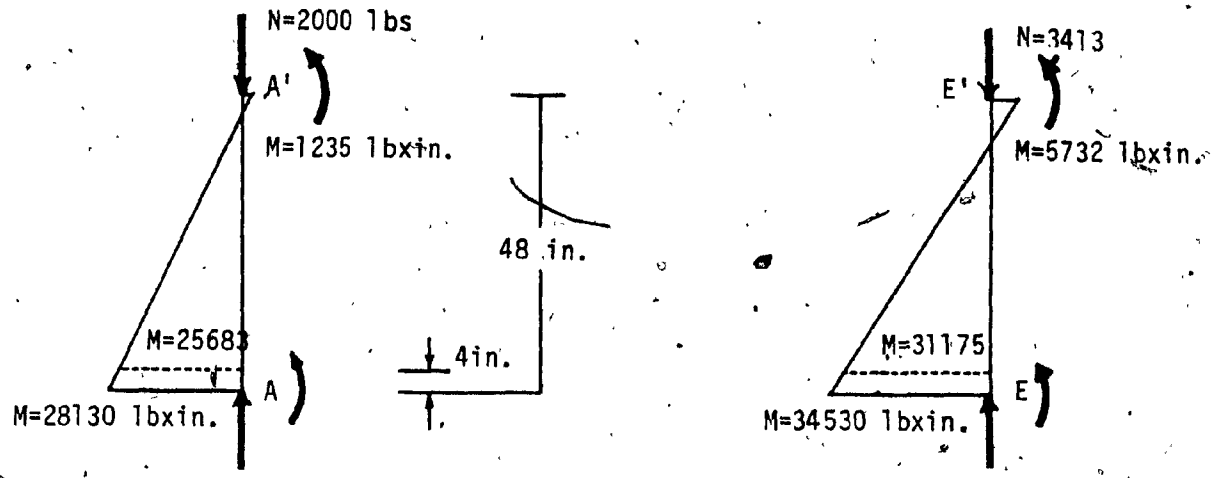

a)FORCES AT FIRST FLOORS OF WALLS AA' AND EE'(FIG. 7.4)

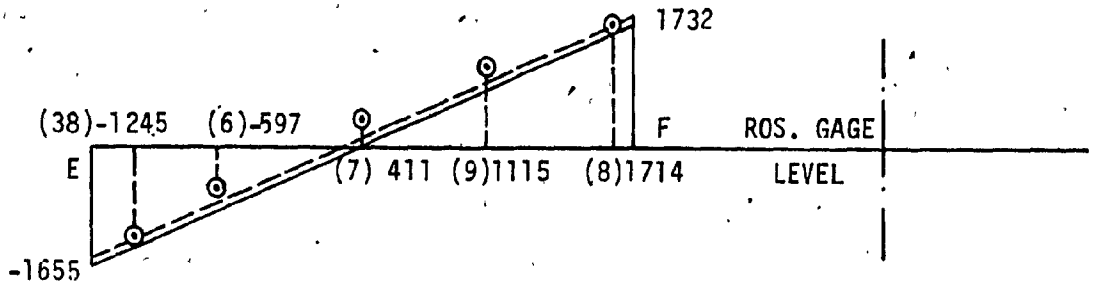

b)NORMAL STRESSES OF WALL EF (FIG.7.4)

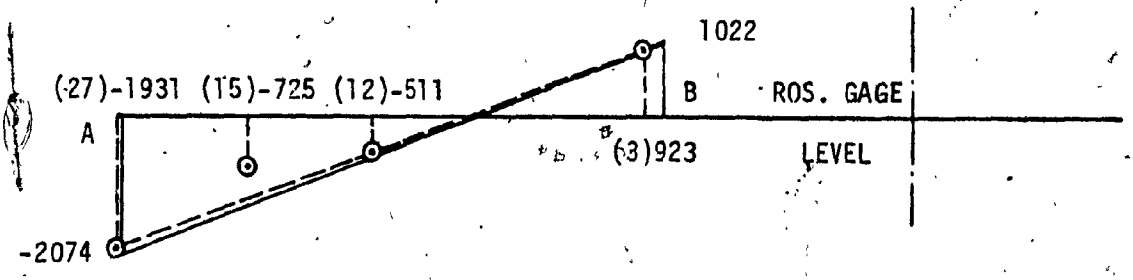

c)NORMAL STRESSES OF WALL AB (FIG.7.4)

FIG. 7.5 - COMPARISON OF THEORETICAL AND EXPERIMENTAL NORMAL STRESSES IN PSI, OF WEB PANELS AT ROSETTE GAGE LEVEL - TEST 17-01-P1
(1psf=6.9kN/m^2, 1 in.=2.54 cm)

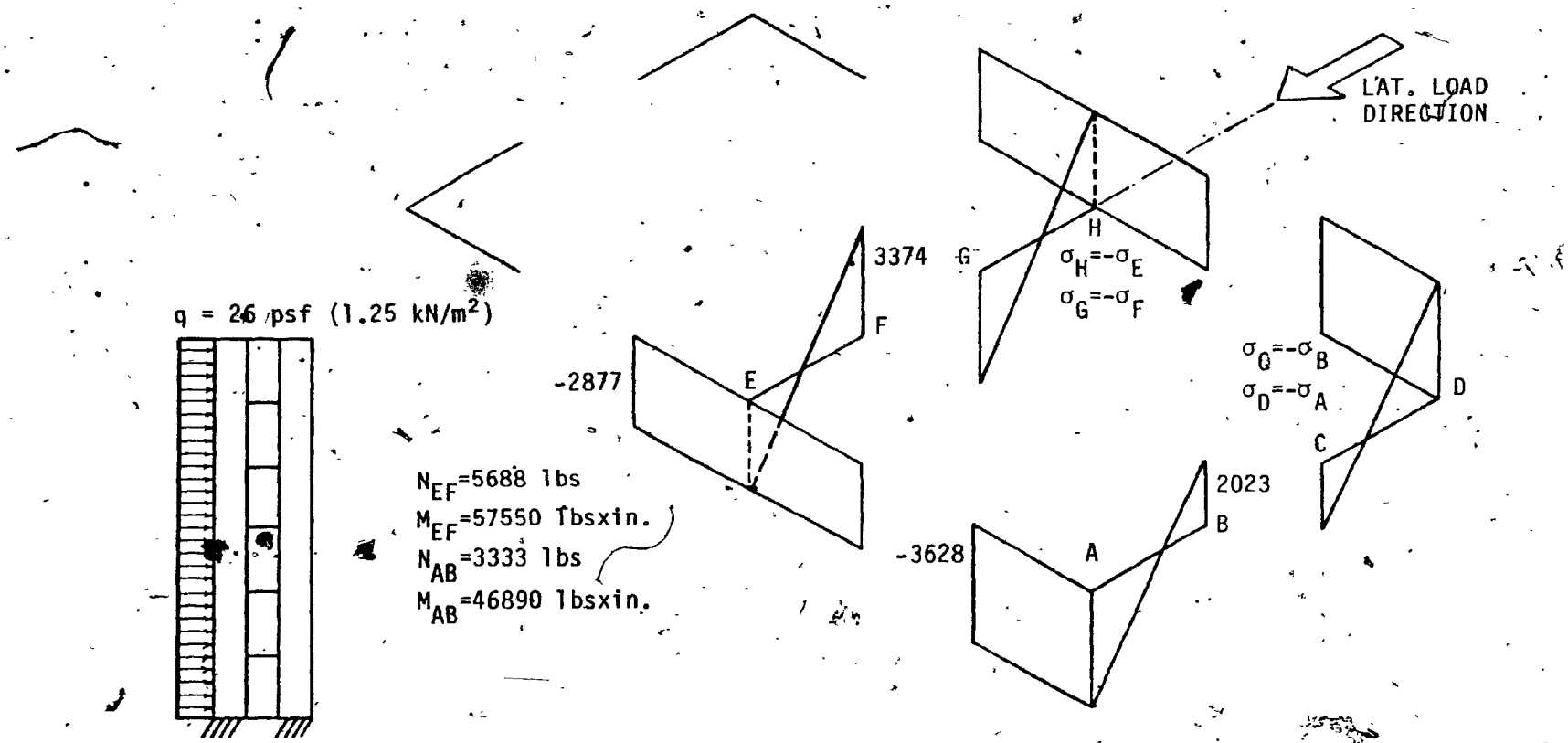

FIG. 7.6 - THEORETICAL NORMAL STRESSES IN PSI AT FOUNDATION LEVEL AND AT MAXIMUM LOAD INTENSITY - TEST 17-02-P2 (1 psi=6.9kN/m²)

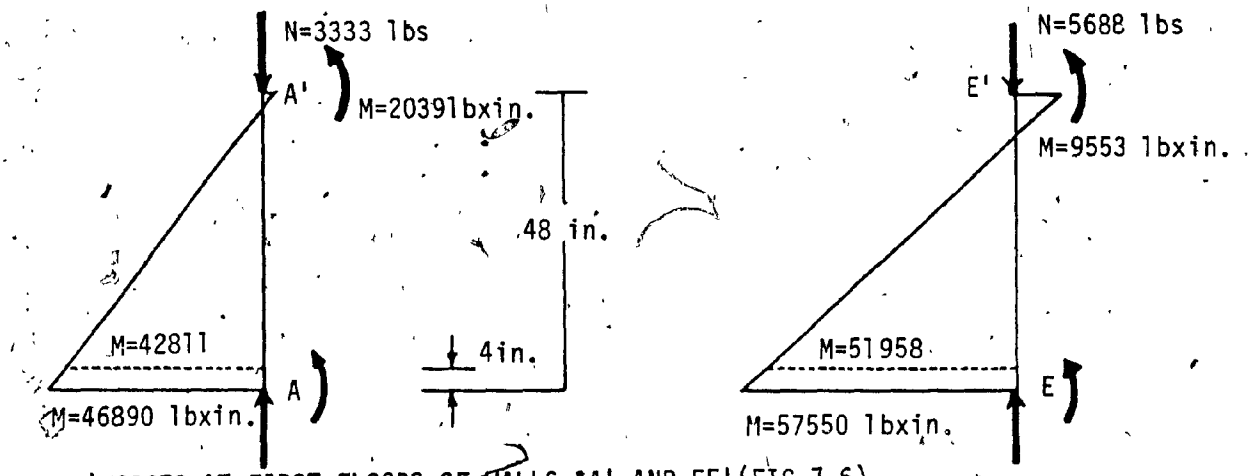

a)FORCES AT FIRST FLOORS OF WALLS AA' AND EE'(FIG.7.6)

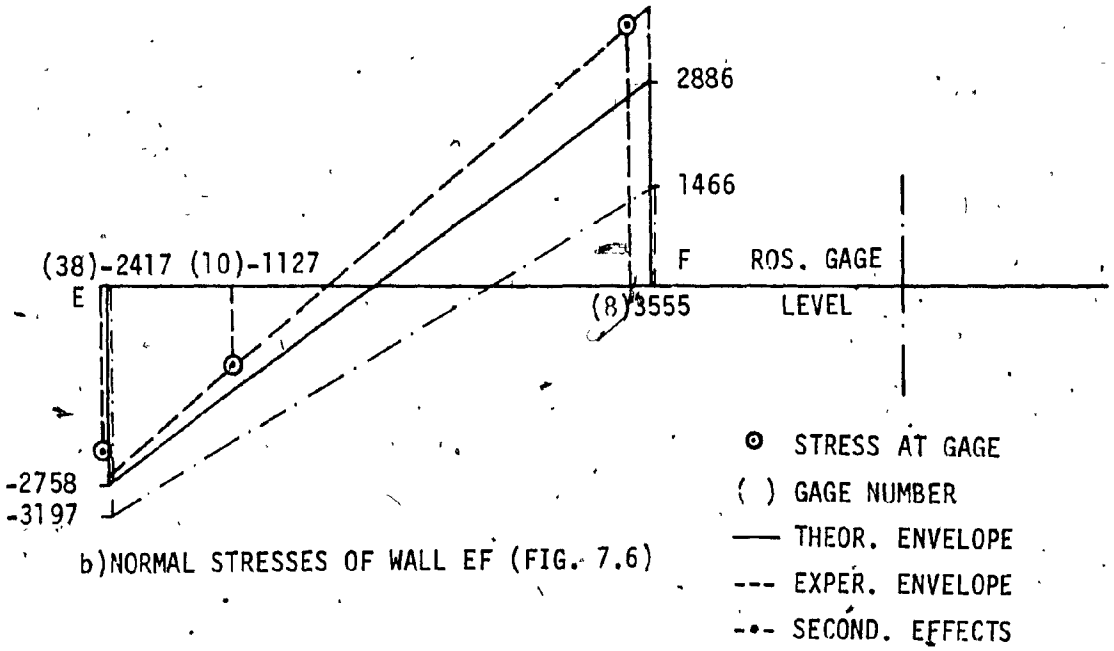

b)NORMAL STRESSES OF WALL EF (FIG. 7.6)

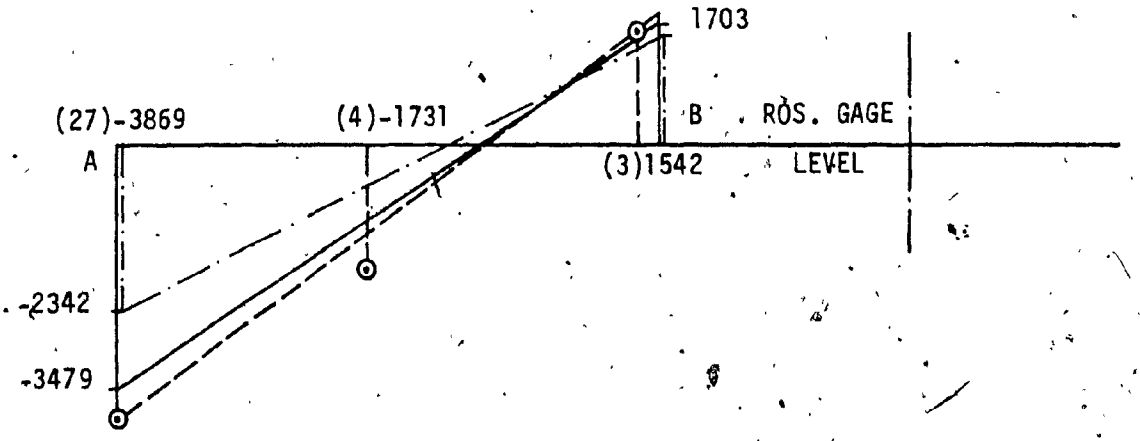

c)NORMAL STRESSES OF WALL AB (FIG. 7.6)

FIG. 7.7 - COMPARISON OF THEORETICAL AND EXPERIMENTAL NORMAL STRESSES IN PSI, OF WEB PANELS AT ROSETTE GAGE LEVEL - TEST 17-02-P2 (1psf=6.9kN/m^2, 1 in.=2.54 cm)

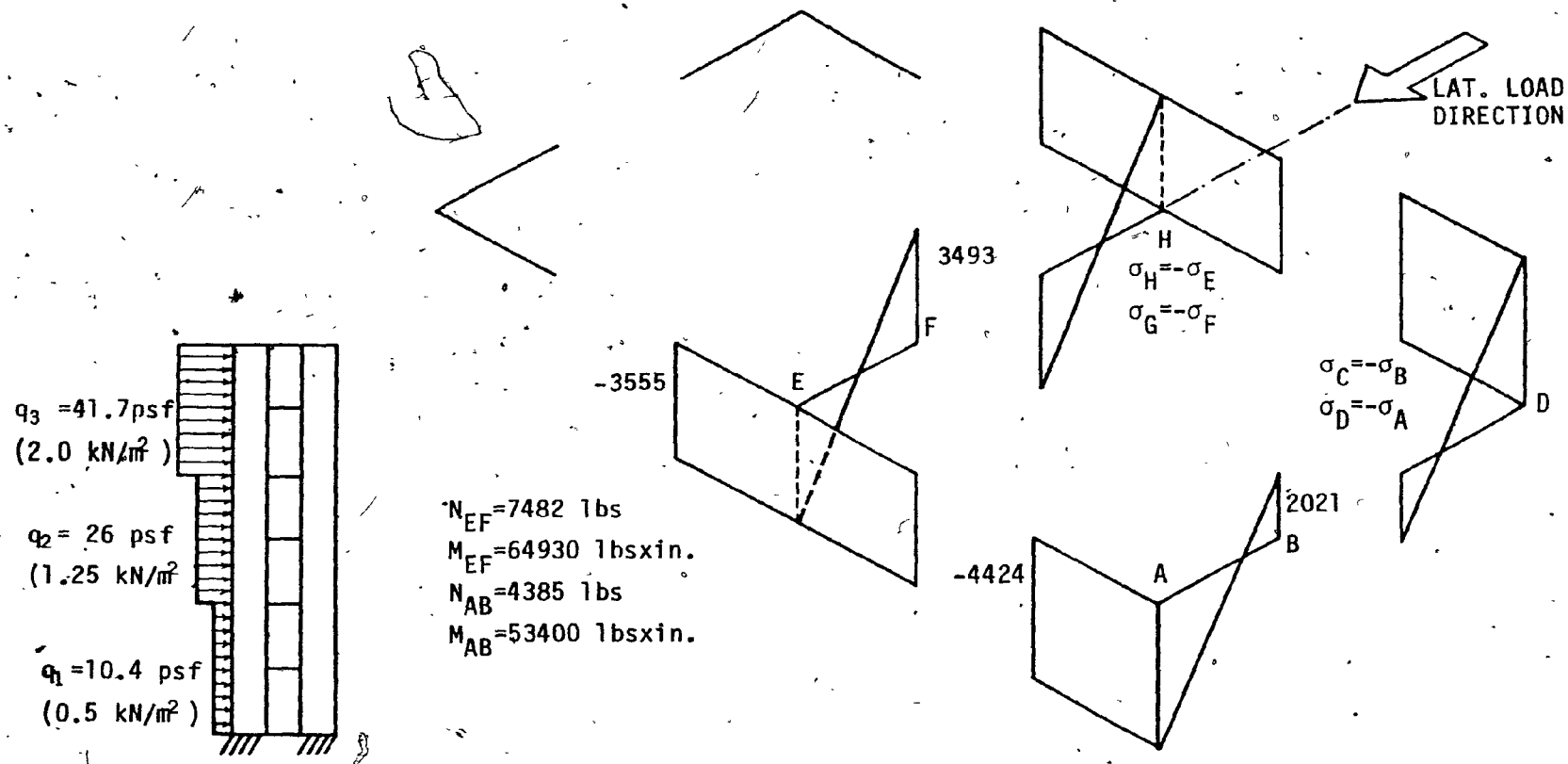

FIG. 7.8 - THEORETICAL NORMAL STRESSES IN PSI AT FOUNDATION LEVEL AND AT MAXIMUM LOAD INTENSITY - TEST 17-03-T1 (1 psi=6.9kN/m^2)

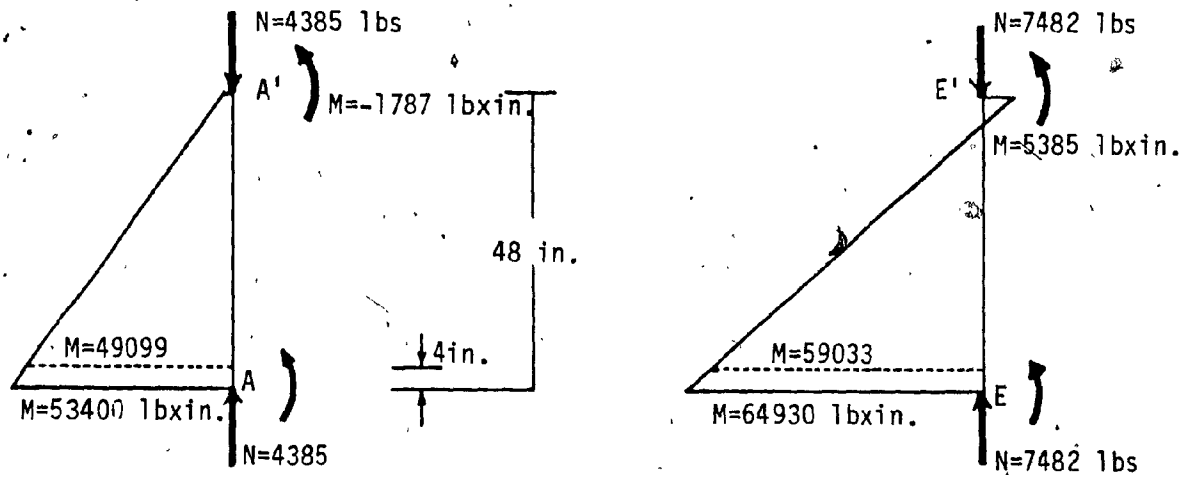

a) FORCES AT FIRST FLOORS OF WALLS AA' AND EE' (FIG.7.8)

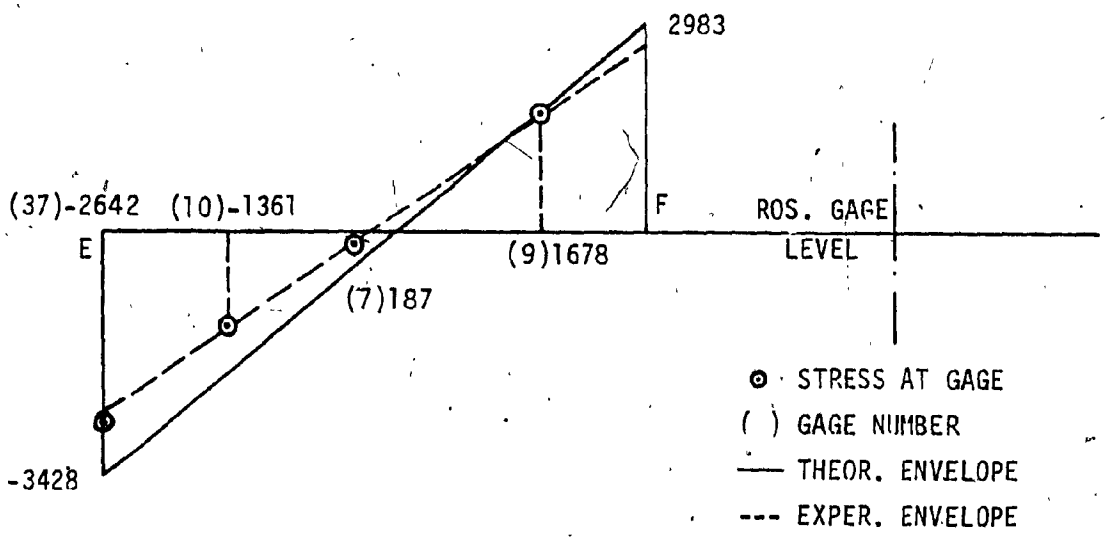

b) NORMAL STRESSES OF WALL EF (FIG.7.8)

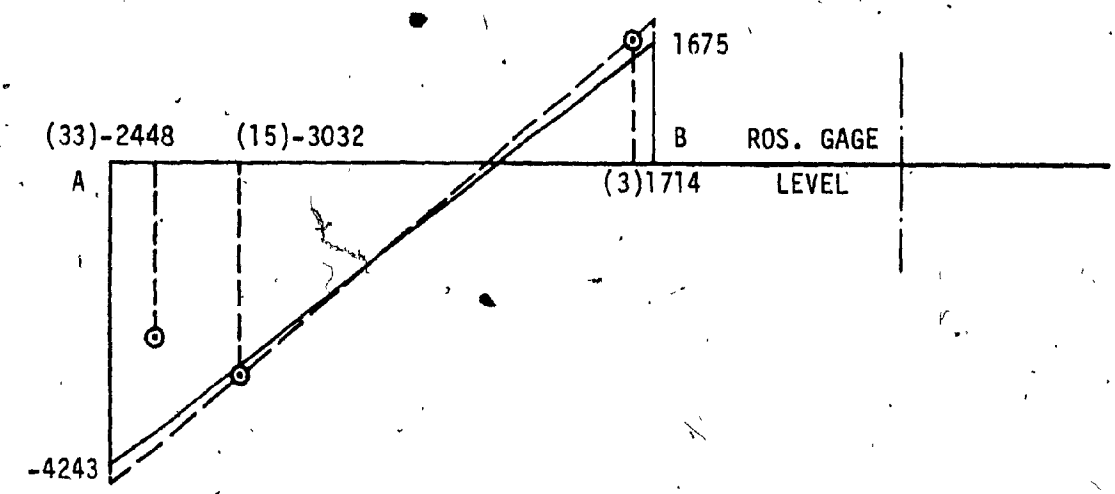

c) NORMAL STRESSES OF WALL AB (FIG.7.8)

FIG. 7.9 - COMPARISON OF THEORETICAL AND EXPERIMENTAL NORMAL STRESSES IN PSI, OF WEB PANELS AT ROSETTE GAGE LEVEL - TEST 17-03-T1 (1psf=6.9kN/m², 1 in.=2.54 cm)

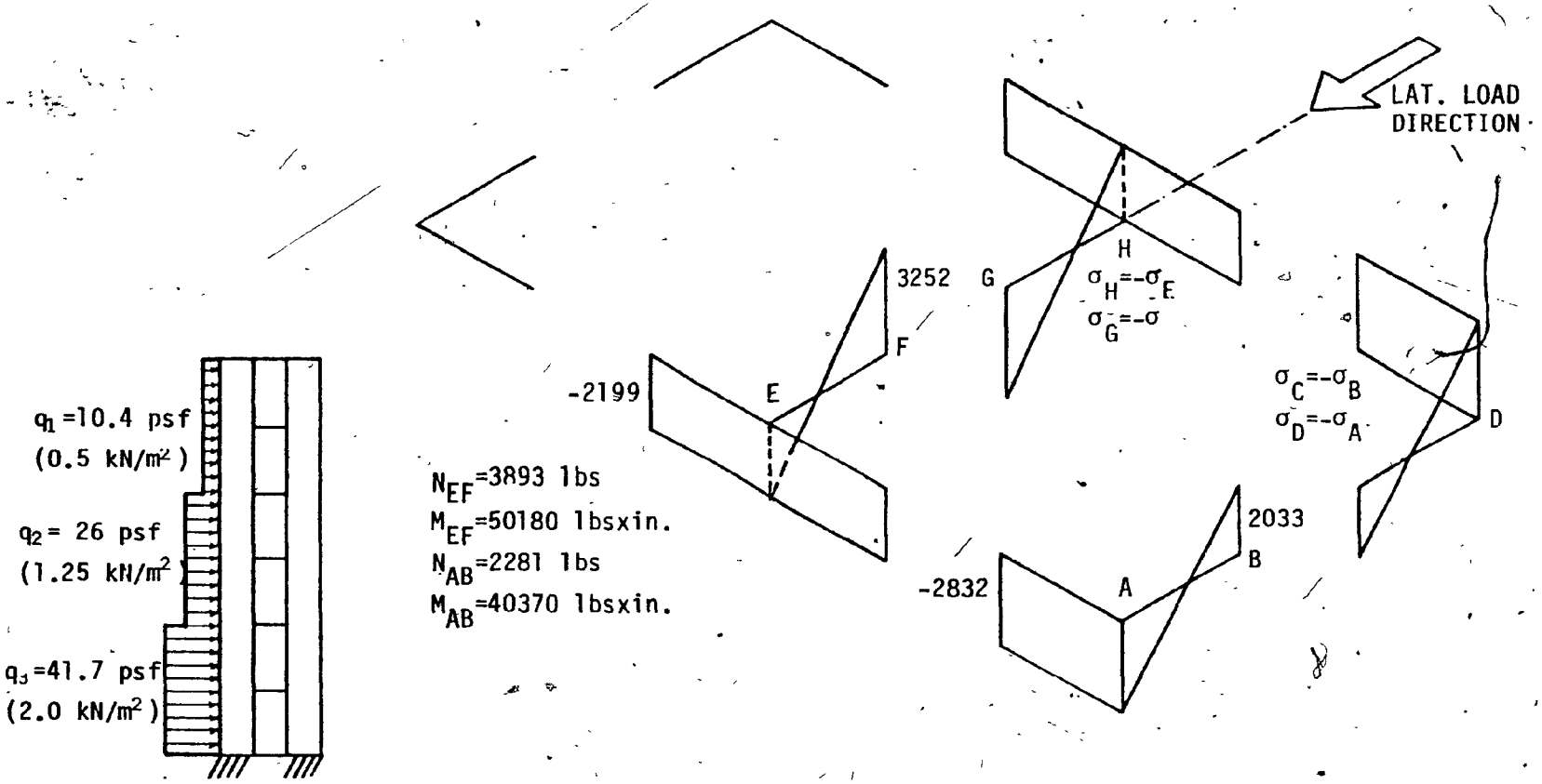

FIG. 7.10 - THEORETICAL NORMAL STRESSES IN PSI AT FOUNDATION LEVEL AND AT MAXIMUM LOAD INTENSITY - TEST 17-04-T3 (1 psi=6.9kN/m²)

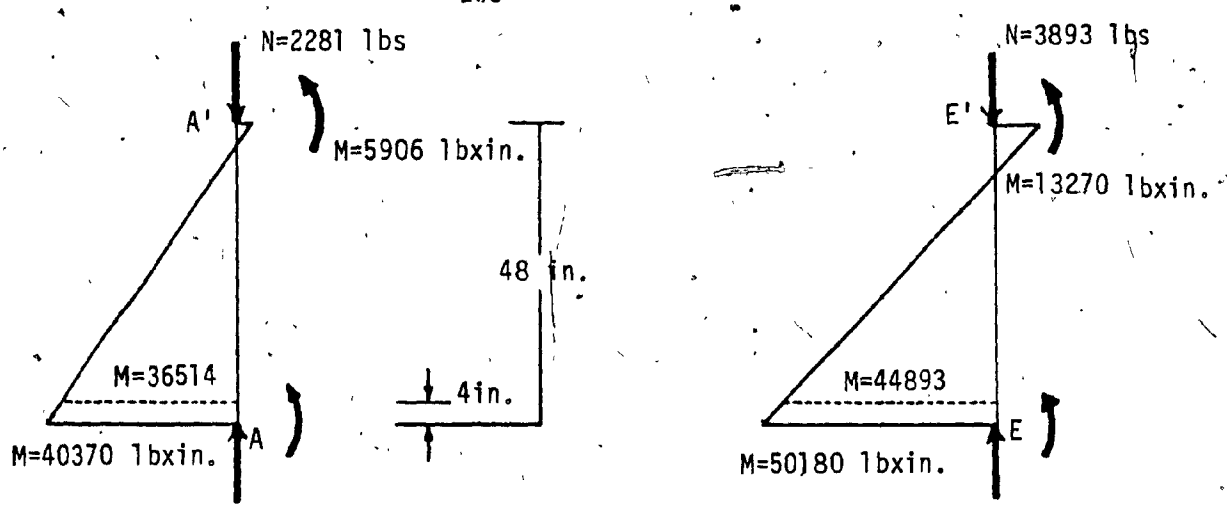

a)FORCES AT FIRST FLOOR OF WALLS AA' AND EE'(FIG.7.10).

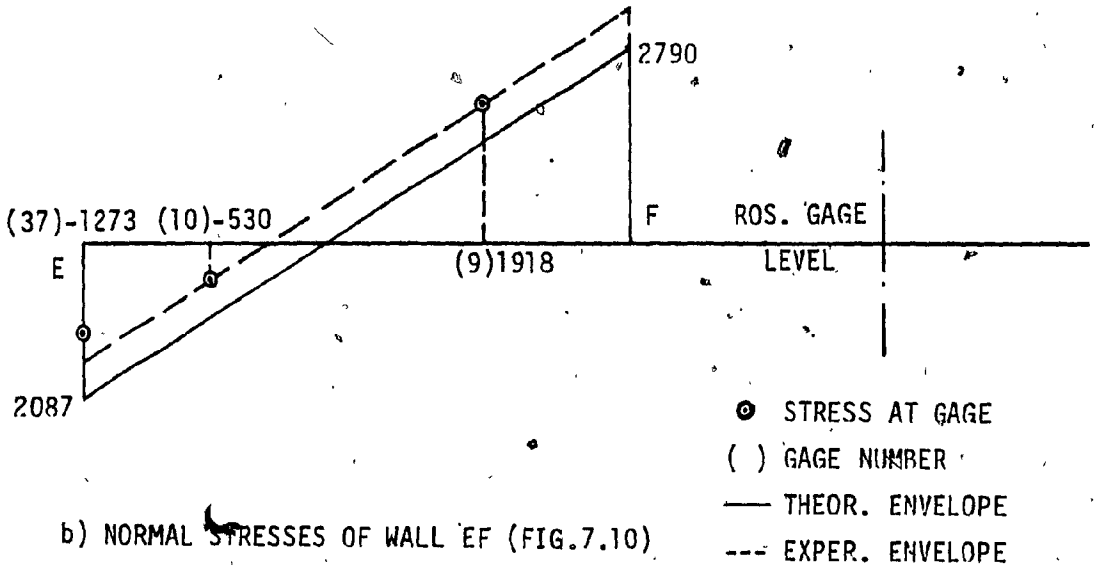

b) NORMAL STRESSES OF WALL EF (FIG.7.10)

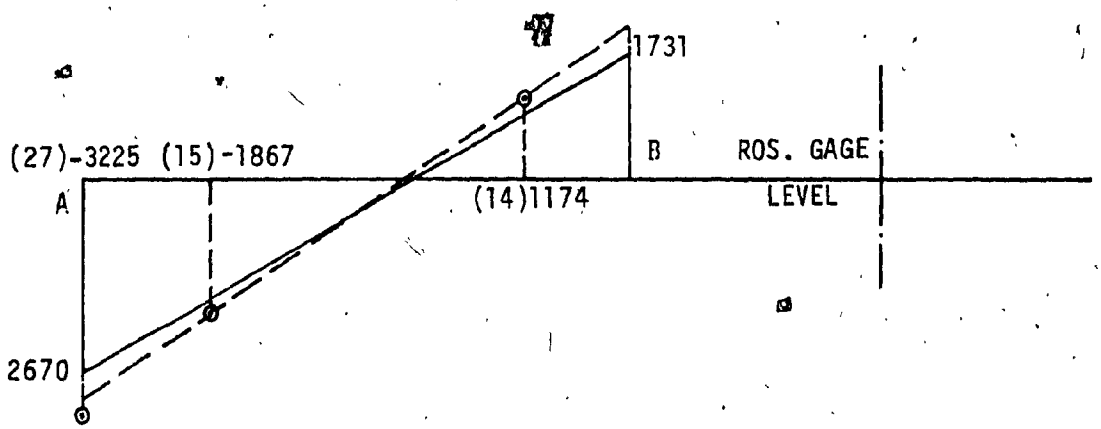

c) NORMAL STRESSES OF WALL AB (FIG.7.10)

FIG. 7.11 - COMPARISON OF THEORETICAL AND EXPERIMENTAL NORMAL STRESSES IN PSI, OF WEB PANELS AT ROSETTE GAGE LEVEL - TEST 17-04-T3
(1psf=6.9kN/m^2, 1 in.=2.54 cm)

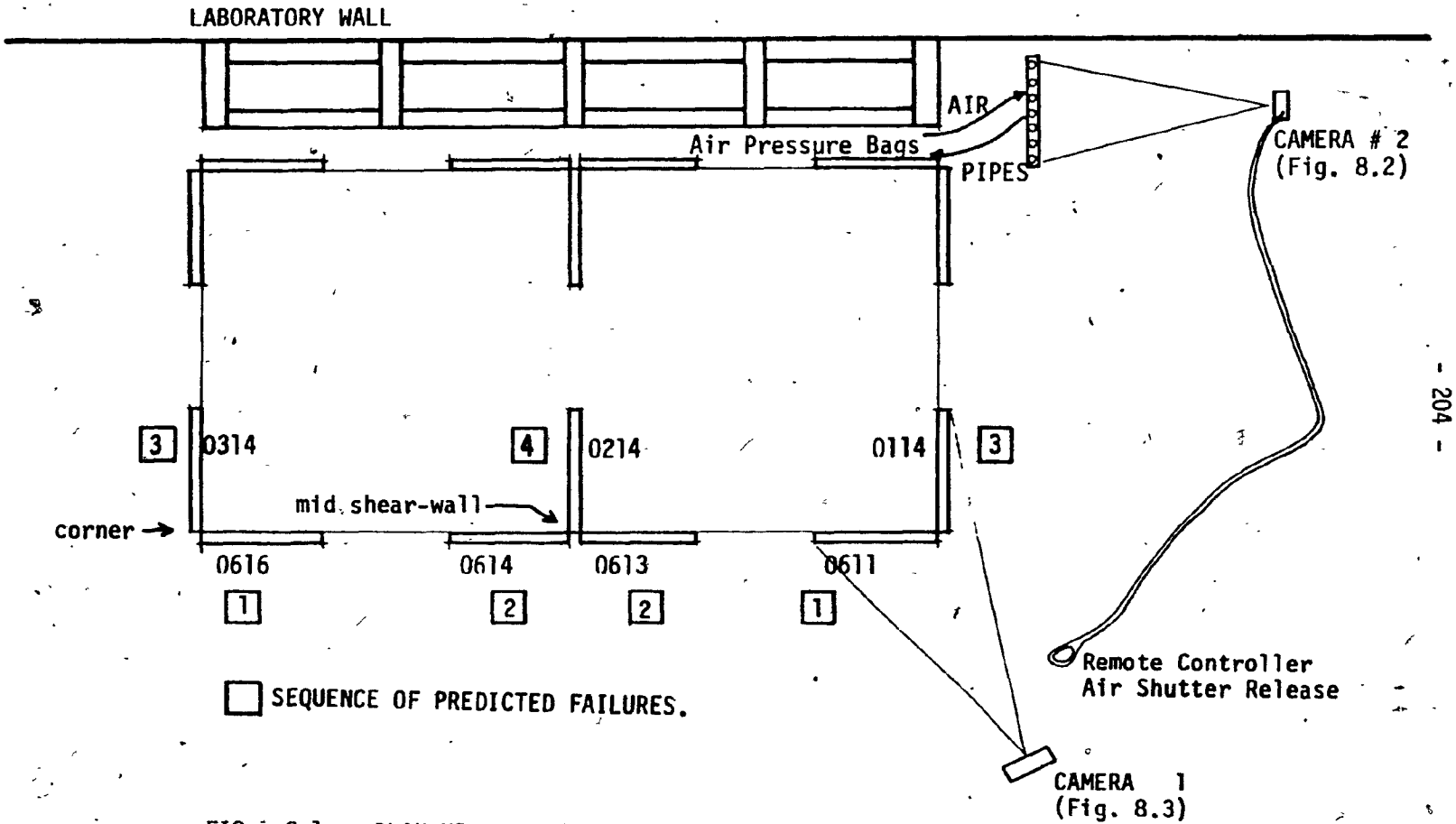

FIG. 8.1 - PLAN VIEW OF BUILDING MODEL TEST SET-UP AND PHOTOGRAPHIC SET-UP TO RECORD SIMULTANEOUS FAILURES AND CORRESPONDING LOADS

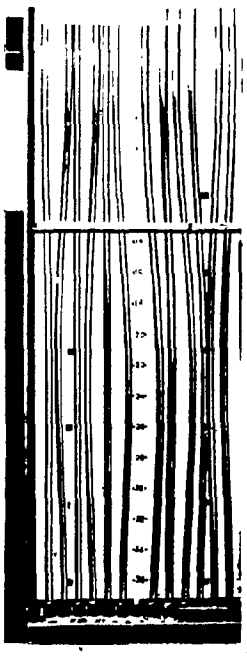

a) L.I.0

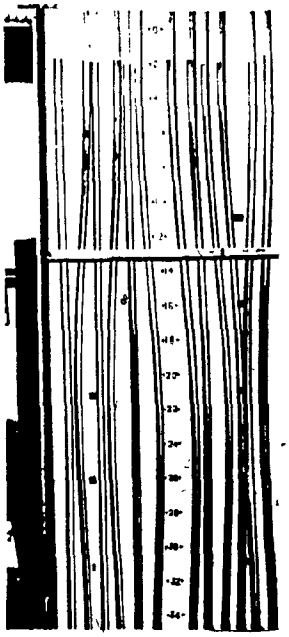

b) L.I.2
(2 in. H_2O=10.4 psf=.5 kN/m^2)

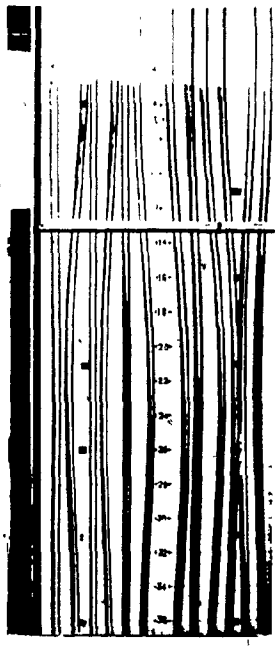

c) L.I.5
(q=26. psf=1.25 kN/m^2)

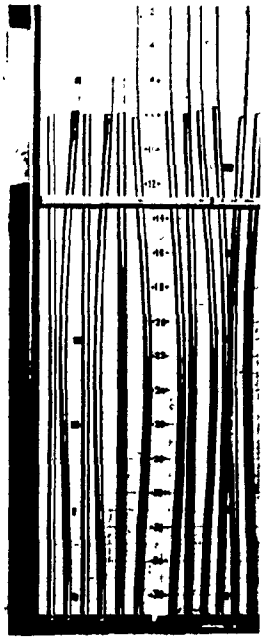

d) L.I.8
(q=41.6 psf=2. kN/m^2)

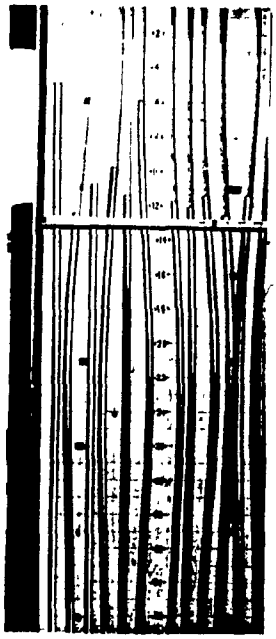

e) WRINKLING OF
FLANGE PANEL 0616

FIG. 8.2 - SEQUENCE OF LOAD INTENSITIES DURING FAILURE TEST OF BUILDING MODEL

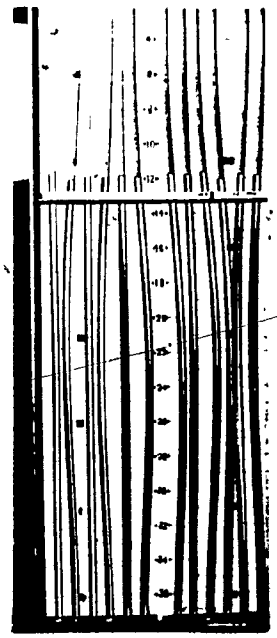

f) L.I.12 AND WRINKLING OF FLANGE PANEL 0611
(q=62.4psf=3. kN/m²)

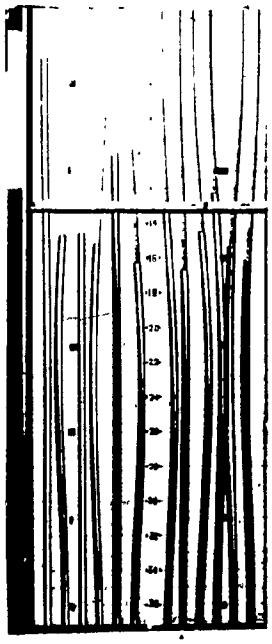

g) WRINKLING OF FLANGE PANEL 0614

h) L.I.16 AND WRINKLING OF WEB PANEL 0314
(q=83.2psf=4.kN/m²)

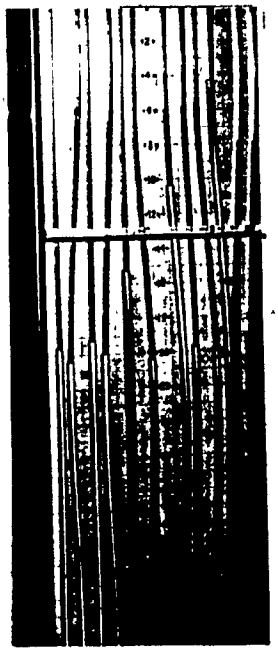

i) L.I.20 AND WRINKING OF WEB PANEL 0114
(q=104.psf=5.kN/m²)

l) L.I.24 AND WRINKLING OF FLANGE PANEL 0613
(q=125 psf=6. kN/m²)

FIG. 8.2 - continued

0616

a)

0616

b)

a) and b): FLANGE PANEL 0616 (SIDE SHEAR WALL)

0611

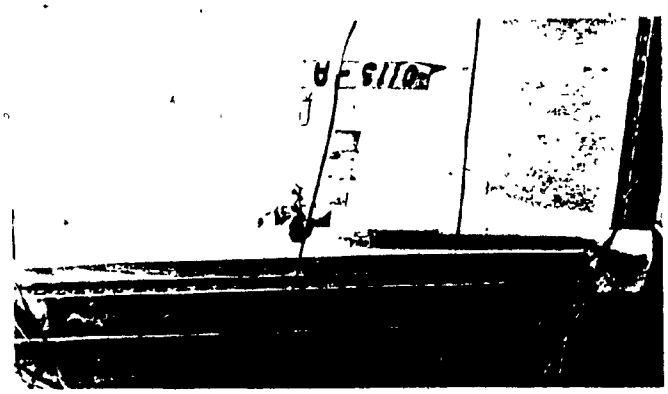

c)

0611

d)

c) and d): FLANGE PANEL 0611 (SIDE SHEAR WALL)

FIG. 8.3 - TYPICAL WRINKLING FAILURES OF LEEWARD PANELS

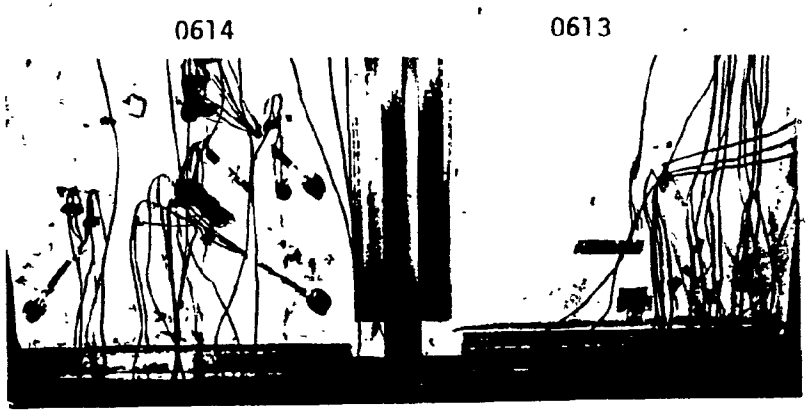

e) FLANGE PANELS 0614 AND 0613 (CENTRAL SHEAR WALL)

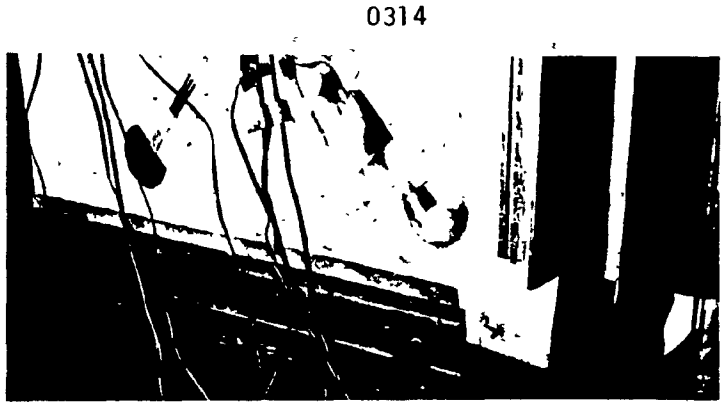

g) WEB PANEL 0314

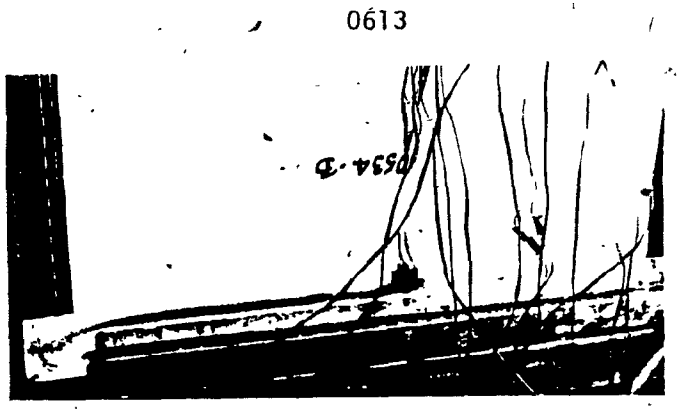

f) FLANGE PANEL 0613

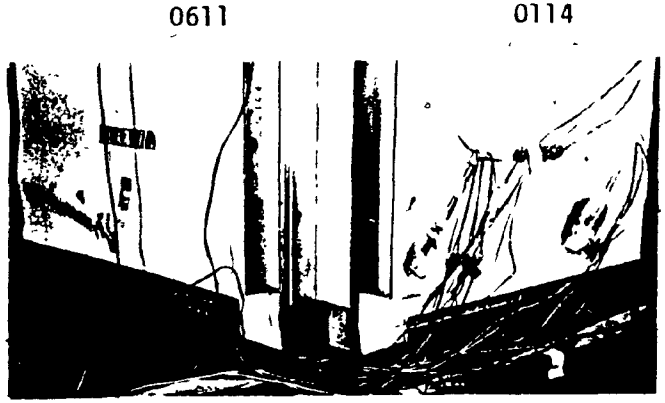

h) WEB PANEL 0114

FIG. 8.3 - continued

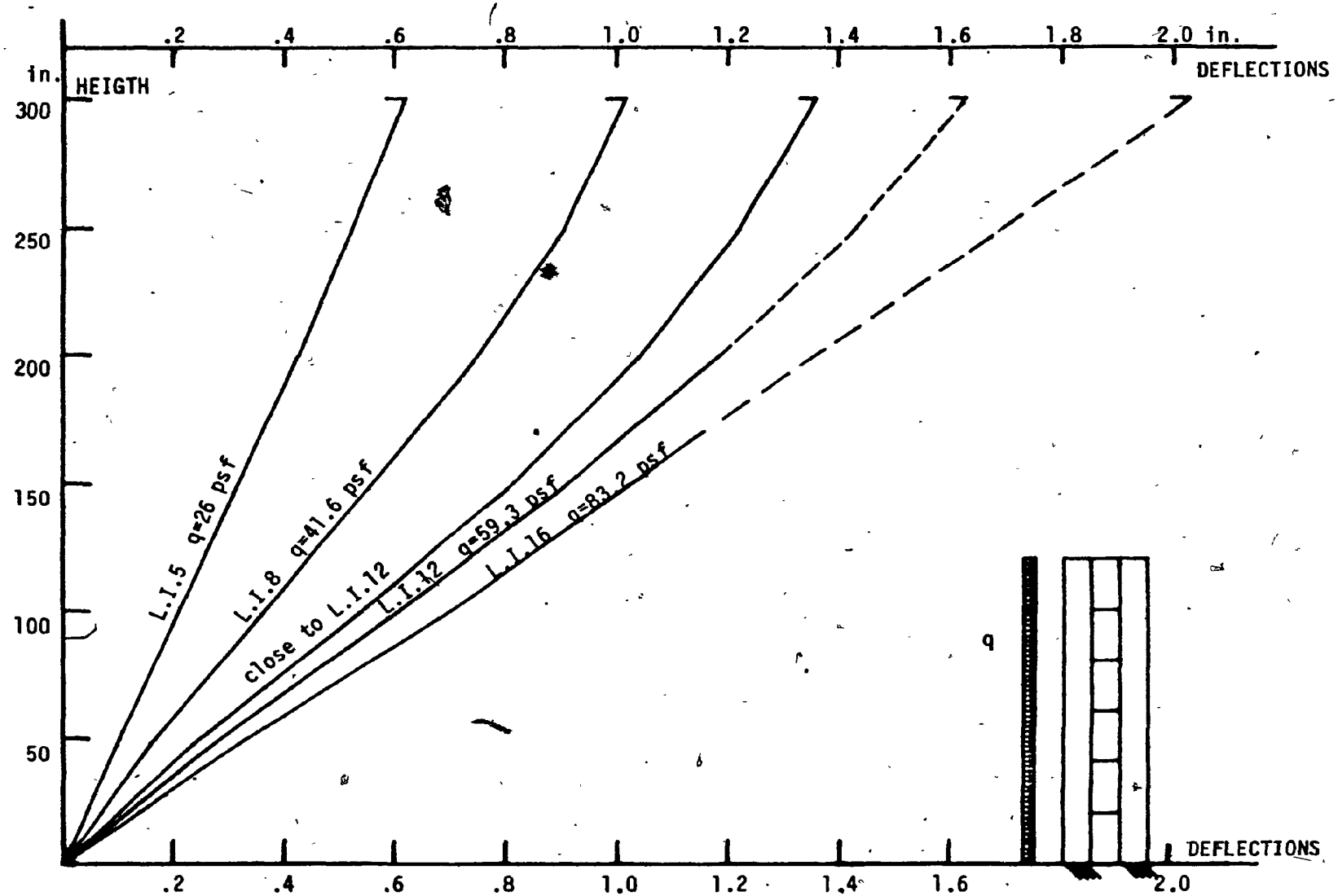

FIG. 8.4 - AVERAGE DEFLECTIONS IN INCHES OF BUILDING MODEL DURING FAILURE TEST (1in.=25.4 mm; 1psf=47.9kN/m^2)

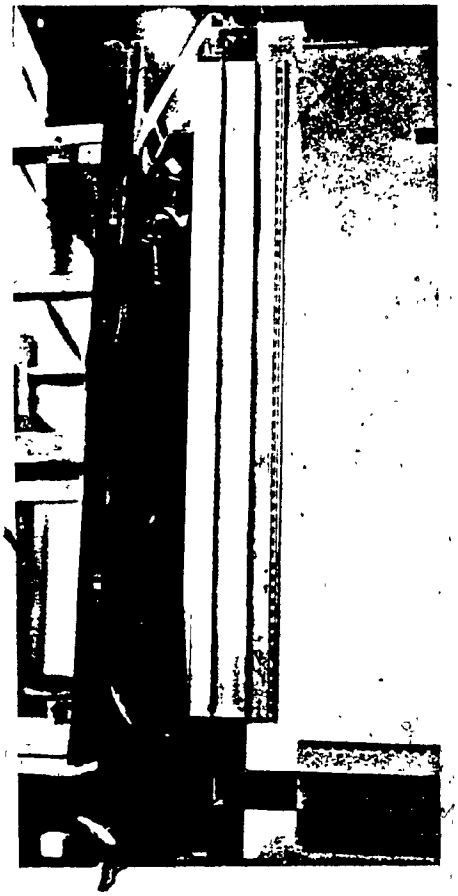

a) DISPLACEMENT OF TOP STORY

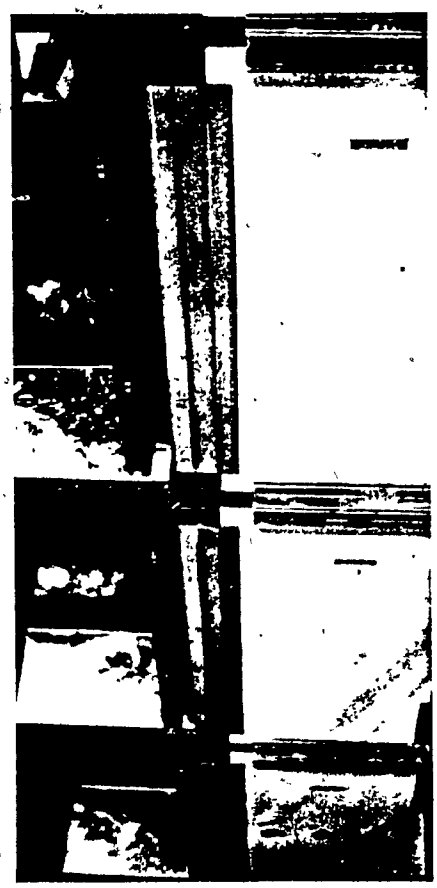

b) DEFORMED SHAPE OF MODEL

FIG. 8.5 - DEFLECTIONS AT LATERAL LOADS
q =124.9 psf (= 6 kN/m^2)

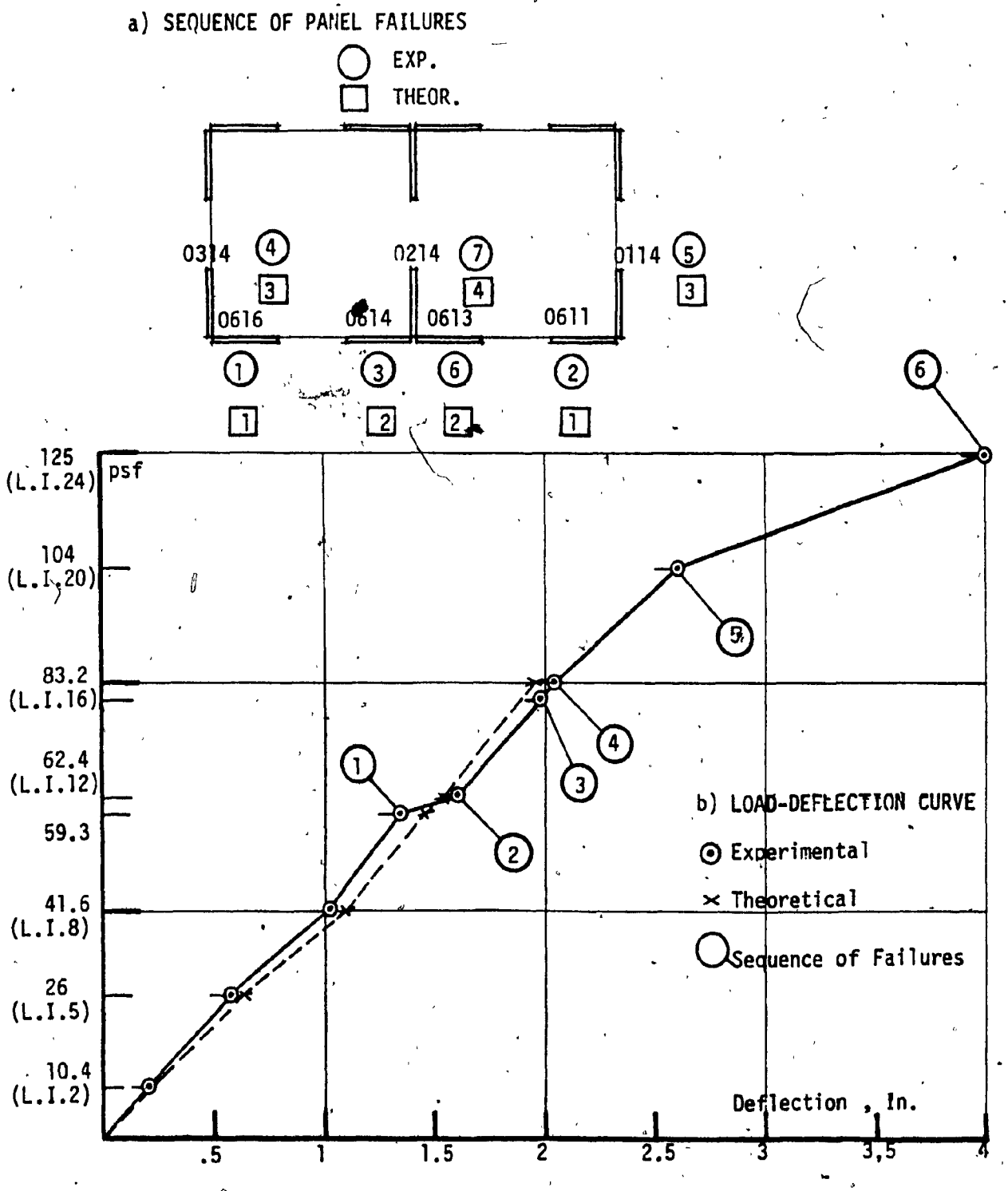

FIG.8.6- COMPARISON OF EXPERIMENTAL AND THEORETICAL BEHAVIOUR